Black Liquor Combustion
Validated Recovery Boiler Modeling
Final Year Report

Volume 1
(Main Text and Appendix I, sections 1-4)

by

T.M. Grace, W.J. Frederick, M. Salcudean, and R.A. Wessel

August 1998

A Summary Report
of the Project

Work Performed Under Contract DE-FG07-90CE40936

Prepared for

The U.S. Department of Energy
Office of Industrial Technologies
Washington, D.C.

Prepared by

The Institute of Paper Science and Technology
Atlanta, GA

Oregon State University
Corvallis, OR

University of British Columbia
Vancouver, BC, Canada

Babcock & Wilcox Company
Alliance, OH

Table of Contents
Volume 1

EXECUTIVE SUMMARY **1**

Project Objectives 1
Accomplishments 2
CFD Model Development 2
Black Liquor Combustion Modeling 3
Boiler Fouling and Plugging 6
Model Validation 7
Technology Transfer 8

INTRODUCTION **10**

Background 10
Background of Current Program 10
Context 11
Elements of Recovery Boiler Models 11
Function of Recovery Boiler Modeling Program 15

STATUS OF RECOVERY BOILER MODEL **18**

BLACK LIQUOR BURNING MODELING **21**

Black Liquor Burning Chemistry 21
Char Bed Burning 28
Radiation Heat Transfer 30

MODEL VALIDATION **32**

TECHNOLOGY TRANSFER **37**

REFERENCES..... **40**

APPENDIX I.....

UBC Reports .....

Section 1 ..... **1-69**
Modeling of Black Liquor recovery boilers
– summary report

Section 2 ..... **1-25**
Flow and Heat Transfer Modeling in the
Upper Furnace of a Kraft Recovery Boiler

Section 3 ..... **1-44**
Numerical Simulation of Black Liquor Combustion
In Kraft Recovery Furnace

Section 4 ..... **1-38**
Investigation of Turbulence Models and
Prediction of Swirling Flows for
Kraft Recovery Furnaces

EXECUTIVE SUMMARY

This project was initiated in October 1990, with the objective of developing and validating a new computer model of a recovery boiler furnace using a computational fluid dynamics (CFD) code specifically tailored to the requirements for solving recovery boiler flows, and using improved submodels for black liquor combustion based on continued laboratory fundamental studies. Many of these objectives had been accomplished at the end of the first five years and a comprehensive report on that work has been issued [1].

A critical review of recovery boiler modeling, carried out in 1995, concluded that further enhancements of the model were needed to make reliable predictions of key output variables. In addition, there was a need for sufficient understanding of fouling and plugging processes to allow model outputs to be interpreted in terms of the effect on plugging and fouling. As a result, the project was restructured. The restructured project was initiated at the end of October 1995 and completed in June 1997. The entire project is now complete. This report summarizes all of the work done on the project since it was restructured.

PROJECT OBJECTIVES

The overall objective of the restructuring was to bring closure to the project in an effective manner that maximized the usefulness of the total effort to the kraft pulp industry. The key tasks to be accomplished were as follows.

1. Complete the development of enhanced furnace models that have the capability to accurately predict carryover, emissions behavior, dust concentrations, gas temperatures, and wall heat fluxes.

2. Validate the enhanced furnace models, so that users can have confidence in the predicted results.

3. Obtain fundamental information on aerosol formation, deposition, and hardening so as to develop the knowledge base needed to relate furnace model outputs to plugging and fouling in the convective sections of the boiler.

4. Facilitate the transfer of codes, black liquor submodels, and fundamental knowledge to the US kraft pulp industry.

ACCOMPLISHMENTS

CFD Model Development

A CFD-based recovery boiler model has been developed by the team at the University of British Columbia (UBC) and is referred to in this report as the UBC model. This model is based on a new CFD code specifically tailored for solving flows typical of recovery boilers and incorporates black liquor combustion and radiant heat transfer as terms in the energy equation. The model is capable of dealing with swirling flows and includes a partial treatment of processes occurring in the convective heat transfer sections of the boiler. The UBC model provides better convergence characteristics and incorporates more realistic physical submodels than earlier CFD models.

The UBC model is capable of dealing with swirling flows. Swirling flows are characterized by extra rates of strain that are caused by rapid dilation, out of plane straining, or significant streamline curvature. These effects give rise to unequal normal Reynolds stresses that the basic eddy diffusion models of turbulence fail to capture. UBC has found that although the two-equation eddy viscosity type models apparently predicts too rapid a swirl decay rate, the standard k-ε turbulence model yields qualitatively accurate results for swirling flows and yields the same performance as other state-of-the-art two-equation models.

Heat transfer and pressure drop in the convective section (screens and superheater) of the boiler were modeled. For practical reasons, the grid used in the CFD modeling of the furnace cavity is too coarse to represent the individual tubular elements of the convective section in the upper furnace. Consequently an efficient method is needed by which the pressure loss and heat transfer due to these tube banks is realistically accounted for. The distributed resistance method was used. A model was developed that simulates the flow and heat transfer in the upper furnace section and which couples closely with the existing three-dimensional CFD model of the furnace cavity.

The hot flow model developed at UBC incorporates the energy equation and combustion modeling as well as a model of the radiation heat transfer. The hot flow CFD model solves conservation equations for momentum along the three coordinate directions, the conservation equation for mass, the conservation equations for the turbulence kinetic energy and its rate of dissipation, and one conservation equation for each chemical species included (currently O_2, CH_4, CO_2, CO, H_2O, H_2, and N_2).

The gas phase computation is coupled to a black liquor combustion model. The liquor model is based on a Lagrangian tracking of each individual drop and typically 10,000 to 20,000 drops are used in a computation. An accounting is kept for the position and speed of each individual drop during the entire duration of its flight. The liquor spray initial conditions are determined by a model of the spray system. Each computational drop is assumed to represent a number of actual liquor drops in the real spray. In the UBC model. a random method is used to specify the initial drop velocity at the point of injection.

Turbulent diffusion is taken into account in the computation of the drop trajectories, because the flow field is highly turbulent and unsteady.

The black liquor combustion model used is that developed by Frederick et al. [2]. This is a sequential treatment of drying, devolatilization, and char burning. Drying and devolatilization are taken to be heat transfer controlled processes. The char burning reaction rates are modeled as a combination of mass transfer and chemical kinetics. A more advanced black liquor combustion model has been developed and is described in detail in a separate report. Due to insufficient time, this new black liquor combustion model has not been incorporated into the UBC model.

The black liquor combustion and transport model is fully coupled to the gas phase computation through source-sink terms in the conservation equations. Combustion of the volatile gases is modeled in the gas phase program on a mixed is burned basis. The mixing model used is based on the work of Magnussen and Hjertageer [3] that takes account of the turbulent kinetic energy and its rate of dissipation in computing the rate of mixing.

The radiation heat transfer model uses the discrete ordinate method [4]. This model is implemented in a separate program which runs in parallel with the main flow computation. The radiation heat transfer in the gas phase and between the hot gas and the surrounding system is computed. The energy transfer between the radiation heat transfer model and the gas phase computation model is accounted for by source/sink terms in the energy equation.

Black Liquor Combustion Modeling

Drop Burning Model:

Black liquor burning models, more sophisticated than previous models, were required in order to deal with air emissions and issues connected with boiler fouling and plugging. These enhanced models deal with transfer of individual chemical elements between the liquor and gas phases and their subsequent reactions. Eight chemical elements (carbon, hydrogen, oxygen, sulfur, sodium, potassium, chlorine, and fuel nitrogen) can now be handled. This also requires a broader species mix.

Additional fundamental data on the release of sodium, potassium, sulfur and chloride were acquired and used to develop rate equations for the release. Data were also obtained and interpreted to provide the capability to model TRS release and oxidation to SO_2, subsequent SO_2 recapture, and NO_x formation and destruction. Rate equations for aerosol formation in the recovery furnace have also been developed.

A completely new black liquor drop burning model for incorporation into CFD-based recovery boiler models has been developed. This new model provides the basis for predicting air emissions and aerosol formation in the recovery furnace. It also eliminates

many of the empirical parameters used to describe the burning process that had led to considerable arbitrariness in older models. This new model is described in detail in a separate DOE report that is aimed directly at people developing CFD-based recovery boiler models [5].

The new model provides rate equations for the release of the eight elements mentioned above. The release of carbon and sulfur during pyrolysis is described by temperature dependent rate equations, so that the amounts converted to gases is dependent on local process conditions. Oxygen and hydrogen release is tied to carbon and sulfur release through stoichiometric algorithms. Sodium and potassium release occur both through vaporization as chlorides and by formation and subsequent vaporization of metallic sodium and potassium. Models for NO_x formation are also available.

In the new model, the processes of drying, pyrolysis, and char burning all occur in parallel. Temperature dependent rate equations determine the relative rates of these processes. This parallel treatment eliminates arbitrary designation of process transitions and also provides a basis for using the same process models to describe black liquor burning in drops and on the char bed. Swelling of black liquor drops is no longer specified in arbitrary terms, but is a natural consequence of differences in density between the char phase and the unpyrolyzed liquor solids.

A critical aspect of the new black liquor burning model is a rigorous thermodynamic treatment of the energy interactions between the liquor drops and the gas phase and of all chemical reactions occurring in either phase. This is done by defining a full set of enthalpies for the black liquor solids (based on the elemental analysis and the heating value of the liquor solids) and using only well-defined chemical species for pyrolysis gases and char components. This is necessary to insure overall energy conservation in the CFD-based recovery boiler model.

Char Bed Model:

Reactions in the char bed are significant in recovery boilers. The amount of combustion and other chemical reactions that occurs in the bed, and the production of gaseous fuels from the bed, must be accounted for in recovery boiler models. The bed is essentially impervious to gas flow and is treated as a boundary for the CFD gas flow calculations, albeit a boundary that is able to exchange mass (chemical species) and energy with the gas phase. The char bed is able to act as a fuel reservoir and for any given set of furnace operating conditions, fuel may be accumulating or depleting in the bed. The shape of the bed can also influence gas flow patterns in the lower furnace.

Heat and mass balances on the bed are inherently unsteady, in that local bed burning rates do not necessarily match the rate at which material is being supplied to that portion of the bed. One way around this problem in the model is to force the bed to operate at steady state so that all material that reaches the bed reacts and leaves. While this approach allows closure of material and energy balances, it cannot determine whether or not the

given operating state is actually obtainable. This can allow "nice-looking" simulations that are not consistent with the liquor spray and air supply conditions being used.

A new bed model has been developed in which the chemical description of the char bed processes is fully consistent with that used for the drop burning model. The model includes rate equations for handling the chemical species interchange between the bed and the gas phase. An energy balance over the bed is used to determine the bed surface temperature and the heat exchange between the gas phase and the bed. No attempt is made to force equivalence between the local burning rates and the rate of supply of material to the bed. While local inventory imbalances can be calculated, no attempt is made to use these imbalances to "reshape" the bed and ultimately obtain closure. This was considered beyond the scope of this project.

Particulate Formation:

Experimental data were obtained on the rates of formation of particulate matter during char bed burning under controlled conditions, using a laboratory char bed reactor. The experiments clearly showed that two different types of particulates were being produced. In addition to sub-micron fume particles that form by a process of vaporization and condensation, significant quantities of larger sized particles (generally in the 1-100 μm range) were also released from the bed. These latter particles were apparently formed by mechanical fragmentation and removal processes as the char burned.

Fume production during bed burning generally behaved in accordance with expectations based on existing concepts of fume forming processes. The amount of sodium released as fume varied from about 0.5% to 12% of the sodium present and was a very strong function of bed surface temperature. The sodium in the fume appears to be a composite of sodium vaporized as sodium chloride and as sodium vapor. Similar processes occur for potassium, and it appears as if potassium chloride vaporization is primarily responsible for enrichment of both potassium and chloride in the fume.

The larger particles (called ejecta) were light brown in color and 1-100 μm in diameter and were clearly produced by mechanical processes. The composition was similar to the composition of the surface layer of the char. In most experiments, the amount of sodium released as ejecta was between 3-7% of the char sodium content, which would make this a significant source of aerosol in the recovery furnace. These are the first quantitative data on ejecta formation during bed burning that have been obtained. Further work is needed to ensure that these particles are not an artifact of the experimental system used and to determine the functional dependence on process variables.

The data obtained on particulate formation during char bed burning were obtained right at the end of the project, and there hasn't yet been time to use the data to test the char bed burning model that was developed in the project.

Radiative Heat Transfer:

Measurements of radiative heat transfer properties for black liquor combustion were carried out under subcontract with Babcock & Wilcox Co. In addition, measurements of the optical constants of ash samples from kraft recovery boilers were carried out at Oregon State University [12]. These new data are expected to have a large impact on the ability to predict radiative heat transfer in recovery boilers. The most significant result is the extremely low value of the absorption index over the infrared spectrum. This confirms that suspended particles do not significantly absorb or emit radiation, that radiative scattering from fume is very significant, and porous saltcake deposits have low emissivity. Inorganic deposits are semi-transparent to radiation, and radiation is a significant component of heat transfer through deposits.

Boiler Fouling and Plugging

Recovery boilers are subject to extensive fouling and plugging. One of the most important potential uses of CFD-based recovery boiler models is to examine how designs or operation can be modified to minimize fouling and plugging (or to see how firing rates can be increased without increasing fouling rates). Thus it is necessary to link the model outputs (those variables which the model predicts) to fouling and plugging behavior. It is beyond the scope of the model to actually predict fouling and plugging rates directly. However, it is possible to interpret furnace model predictions in terms of the likely effect on fouling, particularly on a comparative or relative basis.

This project took advantage of ongoing work dealing with recovery boiler fouling and plugging at the University of Toronto and at Oregon State University and Sandia National Laboratory to obtain the necessary knowledge base. This is a very complicated subject and there is a good deal of work going on throughout the world on it. It was determined that the most effective way to pull all of this material together and make it available to the industry was to prepare a technical monograph on recovery boiler fouling and plugging. This has been done and the monograph is available as a separate report on this project [6].

Model outputs which have a direct bearing on the tendency for fouling and plugging include the gas velocity and temperature distribution leaving the furnace cavity and passing through the convective sections, the amount and composition of the carryover liquor particles from the furnace, and the fume composition. The amount of fume produced and the gas composition, particularly SO_2 concentrations, are also likely to be of significant importance.

Model Validation

Validation of recovery boiler models, by comparing model predictions against measured data, is considered essential in order to convince ultimate users that model predictions can be relied on and that models are a useful tool for improving recovery boiler design and performance. However, it is extremely difficult to do this on the full recovery boiler model. The best approach is to build up confidence in the codes systematically through assessment of the ability to predict results of simpler cases that are relevant to the actual situation. The complete, final validation is then confirmed by testing against a very limited number of "real cases". In the case of the recovery boiler model, the validation of the CFD model is first based on the ability to describe isothermal flow problems related to the types of flows expected in recovery boilers. The black liquor combustion models that are interfaced with the CFD model must first be validated against experimental data on black liquor combustion processes. Only when these have been accomplished is it meaningful to attempt to validate the predictions of the combined hot flow model with black liquor combustion.

UBC has done considerable work comparing model predictions with measured flows, and this is described in greater detail in reference 8. Most of the work focussed on isothermal flow situations including physical water models of recovery boilers and cold air flow tests in actual recovery boilers. In all cases, good qualitative agreement was found between computed and measured results. The up and down flow regions were correctly predicted and the equal upward velocity contours had similar shapes. In general, the flow prediction capabilities of the UBC model can be considered validated.

As part of this project, two field tests were carried out on actual recovery boilers to obtain data to set up and test the model. Neither of these validation exercises was that successful. The biggest problem was that the amount of quantitative data on furnace outputs was extremely limited, despite extensive efforts to acquire such data. Another problem was that certain critical model input (setup) data (such as spray initialization parameters) could not be measured directly and had to be specified in an arbitrary manner. The third problem was the inherent unsteadiness of recovery boiler flows, which resulted in uncertainty in the applicability of furnace output variables measured at a particular location and time.

In Case 1, video camera images of the liquor sprays were obtained for comparison with computed drop trajectories. The spray predictions do not appear to correspond to actuality, in that the sprays remain too wet and strike the bed with too much material. This was the case, even though spray parameters were varied. In the actual boiler, the sprays did not appear to reach the bed intact. There were no quantitative data available to compare with carryover predictions, but the mill did not consider carryover to be a problem. The amount of carryover is highly dependent on spray initialization parameters, which are quite arbitrary.

In Case 2, many different operating conditions were used during the test and data were obtained on how the furnace responded to these changes. This allowed cause and effect

relationships to be explored. However, only a single set of conditions was modeled and compared to data, because of the time and effort needed to set up, converge, and interpret a solution for a single case. Because of these factors, CFD-based recovery boiler models are very inefficient for establishing cause and effect relationships.

A benchmarking exercise was carried out in which the predictions of the UBC model were compared with those made with a FLUENT model for one isothermal flow case based on a physical water model. The benchmarking test showed that both codes did a reasonable job of predicting the flows and were in general agreement with each other.

It can be concluded that model validation must focus more intensively on smaller problems for which true answers are known. Flow predictions are most amenable to this approach and these have been rather extensively validated. A similar approach needs to be done for black liquor combustion submodels. Validating complete model predictions against data from full furnace testing is a fallacy. It is very difficult, if not impossible, to make sufficient measurements to actually test model predictions. Disagreements between model predictions and reality can also occur because of incorrect model setup conditions, some of which (such as liquor spray initialization) are not measureable directly and which must be done arbitrarily.

TECHNOLOGY TRANSFER

The codes developed in this project can and have been used to improve recovery boiler design and operation. UBC has formed a "spin-off" company, Process Simulations Ltd. (PSL) and has licensed the UBC code to PSL for industrial application. Simulations have been carried out on a number of different boilers for several different companies. The UBC code has also been licensed to IPST. Either of these organizations can be contacted for further details on how the models can be accessed.

CFD-based recovery boiler models are also available in-house at each of the major manufacturers of recovery boilers. These models are similar in nature to the model developed in this project and have drawn on much of the information developed in this project. CFD-based recovery boiler models have also been developed at the Royal Institute in Sweden, at Tampere Technical University in Finland. A simpler model has been developed at Jansen Boiler and Combustion Technologies in the United States.

These various models have been used as an effective tool over the past few years to help guide changes in recovery boiler design and operation. They are most fruitfully applied when flow patterns within the boiler are suboptimum and the boiler operating problems are directly connected to the flow patterns. They are somewhat less effective when dealing with emissions and chemical aspects of recovery boiler operation.

It still requires considerable effort, time, and computer knowledge to set up and solve a single case, so there are economic limits to the number of cases that can be done on a

given boiler. Interpretation of the model output requires considerable knowledge of boiler operation as well as computer and modeling skills. This has limited the application of the models. They are not at, and are likely to never be at, a point where they can be routinely applied in the field.

There are four separate reports resulting from the final phase of this project. These are:

1. A comprehensive final report covering all work on the project since the project was restructured [8]. A comprehensive summary report on the first five years of the project was issued recently [1] and should be consulted for information on work done during that period.

2. A report describing in detail how black liquor combustion in a recovery boiler should be modeled.[5] This report incorporates the latest information on black liquor processes and is aimed at people who are directly involved with the development of recovery boiler models.
3. A technical monograph on recovery boiler fouling and plugging, summarizing and integrating the current knowledge about recovery boiler fouling and plugging and aimed at the general technical audience involved with recovery boiler design and operation.[6]

4. A report summarizing the recovery boiler design and operating information needed for model setup and the measured output variables for the cases used for model validation in this study. The intent is to make the information available for validation of other recovery boiler models and to encourage cross-comparisons in the predictions of the different models.[7]

INTRODUCTION

BACKGROUND

Background of Current Program

This recovery boiler project started in October 1990 and was originally scheduled to run for four years. The objective of the project was to develop a computer model of a recovery boiler furnace using a CFD code specifically tailored to the requirements for solving recovery boiler flows and using improved submodels for black liquor combustion based on continued laboratory fundamental studies. There was considerable emphasis on developing accurate predictions of the physical carryover of macroscopic particles of partially burnt black liquor and smelt out of the furnace, since this was seen as the main cause of boiler plugging. This placed strong emphasis on gas flow patterns within the furnace and on mass loss rates and swelling and shrinking rates of burning black liquor drops.

The original project involved three institutions, the Institute of Paper Science & Technology (IPST), the University of British Columbia (UBC), and Oregon State University (OSU). IPST was responsible for overall project leadership, bed modeling, model simplification and application, and overall model validation. UBC was responsible for CFD code development and flow modeling and validation. OSU was responsible for fundamental data on black liquor combustion and formulation of improved black liquor burning models. In addition, T. M. Grace Company, Inc. was involved to provide technical coordination and interpretation.

When the original four year period was completed, the project was extended for an additional three years. The extension started in September 1994. By this time it had become apparent that many recovery boilers encountered serious plugging problems even when physical carryover was minimal. The objective of the extended project was to improve the utility of the models by including the black liquor chemistry relevant to air emissions predictions and aerosol formation, and by developing the knowledge base and computational tools to relate furnace model outputs to fouling and plugging of the convective sections of the boilers.

Two new members were added to the project team in the extended project. Babcock & Wilcox (B&W) became involved to provide experimentally based information on radiation heat transfer. Tran Industrial Research (TIR) was brought in to provide guidance and information relevant to boiler plugging. In January 1995, as a result of staff changes at IPST, Thomas M. Grace became a part-time employee of IPST in order to serve as principal investigator on the project. As a consequence, T. M. Grace Company, Inc. was no longer involved as as subcontractor.

Early in 1995, a critical review of recovery boiler modeling was carried out. As a result of this review and other factors, the extended project was restructured so as to bring it to closure in a manner that would maximize the value of the entire project to the pulp and

paper industry. The restructured project was initiated at the end of October 1995 and was completed in June 1997.

This report covers all of the work on the restructured project. A comprehensive report on the first five years of the project was issued in early 1997.

Context

During the course of this program, recovery boiler models have been developed at a number of different organizations. A summary of the models currently known to be in existence is given below.

1. Models (codes) developed in this study

UBC	complete model	own CFD base

2. Boiler Manufacturers

B&W	complete model	own CFD base
ABBCE	complete model	based on FLUENT
Kvaerner (Tampella)	complete model	based on PHOENICS
Kvaerner (Gotaverken)	simple model	based on FLUENT
Ahlstrom	unknown extent	based on FLUENT
Jansen (JBCT)	simple model	own base (also have KIVA)

3. Other Recovery Furnace Model Codes

Tampere Technical University	complete model	based on PHOENICS
Royal Institute of Technology	complete model	based on STAR CFD

4. Various straight CFD codes for dealing with flow problems

Elements of Recovery Boiler Models

Recovery boiler models consist of several distinct elements. The liquor and gas are treated as two separate phases. The gas phase is treated as a continuum, while the liquor is treated as distinct drops which dry and burn as they move through the gas. Liquor also burns on the bed and the walls and this is treated through reactive boundary conditions.

The CFD part of the model deals with the gas phase. The differential equations describing mass, heat, and momentum balances for the gas phase are converted to difference equations and solved numerically. The furnace volume is broken up into cells or nodes using an appropriate grid structure. Numerical solution of the equations requires specification of boundary conditions and also of sources and/or sinks of mass, energy, and momentum resulting from liquor burning. The coupling of the gas phase with the black liquor phase takes place through these source/sink terms.

The black liquor burning model consists of two distinct parts, a drop burning model and a trajectory model. The drop burning model describes how the liquor drop interacts with the surrounding gas with respect to mass and energy. It includes an appropriate chemical description of the burning drop and means for tracking state changes (composition and temperature) in the drop, and rate equations that describe the exchange of mass and energy between the liquor and the gas. The drop burning model also provides means for handling the swelling and deswelling that occurs when black liquor burns. The rate equations that describe mass and energy exchange between the liquor and the gas are the basis for the gas-phase source/sink terms needed by the CFD part of the model.

The trajectory equations come from a force balance on the burning drop as it moves through the furnace. Forces acting on the drop include gravity and drag by the gas through which it is moving. The drag force depends on the vector velocity difference between the drop and the gas and is oriented in this direction. The initial condition for the drop trajectory as it enters the furnace comes from a model for the liquor spray. Typically, this sets the initial drop size and vector velocity. The drops continue on their trajectories until they reach the bed, strike a furnace wall, or are carried up out of the furnace.

The source/sink terms apply to the gas phase. These include the masses of each of the specific chemical species entering/leaving the gas phase, the energy transferred in both directions by chemical species transfer and by heat transfer, and the momentum transfer to the gas by fluid drag from the particles. These must be specifically written for the black liquor burning process, as they are not part of the CFD codes themselves. Means of handling the source/sink terms are normally a part of CFD codes, but not the specific source/sink equations.

Models are also required to describe what happens to the liquor drops that reach the walls or land on the bed. These are referred to as wall models and bed models. The bed models usually incorporate some way of handling bed burning by interacting with the gas phase in the region directly above the bed.

Other elements involved in recovery boiler models include means for setting up the grid structure, means for setting appropriate boundary conditions, solution algorithms, and means for displaying model outputs.

The output of a CFD-based recovery boiler model includes a quantitative description of the gas velocity (three components), temperature and concentration fields, the trajectories of the liquor drops and the ultimate fate of all of the liquor drops, and heat fluxes to the bounding surfaces. It may also include information on bed burning rates, temperatures, etc. This is a tremendous amount of information. A typical grid may contain over 100,000 elements, so the output contains several million data points not including the information needed to describe drop trajectories. Graphical displays or other methods of compressing the data are required to make this amount of information manageable.

Various CFD codes can serve as a platform for a recovery boiler model. Some, such as FLUENT and PHOENICS are commercially available, while others have been developed within universities or within companies. In this program, UBC has developed computer codes that have been tailored to meet the special requirements of recovery boiler flows. Commercially available CFD codes have also undergone significant improvement since this project was initiated, and now provide a viable basis for recovery boiler models. Several boiler manufacturers are currently using such CFD codes as platforms for recovery boiler models.

Black liquor combustion models have passed through several generations. The first models focused primarily on the mass changes and diameter changes that accompanied black liquor burning, since these factors had a major influence on drop trajectories and thus on the amount of carryover. Drying and volatiles formation were treated as separate heat transfer controlled processes and char burning was treated as an oxygen mass transfer controlled process. The second generation models incorporated gasification of char carbon by reaction with CO_2 and H_2O. Gasification kinetic rate equations were developed and combined with external and internal mass transfer correlations to provide an overall rate equation for the char burning step. Rate equations for drying and devolatilization were also improved.

A third generation black liquor combustion model was developed in the course of the present work and is described in a later chapter of this report. This is a full elemental model which contains the information on sulfur release and recapture and on sodium, potassium, and chloride volatilization needed to predict air emissions and deal adequately with boiler fouling and plugging.

The char bed causes considerable complications in developing a CFD-based recovery furnace model. The CFD portion of the model is based on the gas phase and the bed acts as a boundary condition for the gas. However, it is a boundary that is able to exchange mass (chemical species), energy, and possibly momentum with the gas phase. Moreover, the bed is able to act as a fuel reservoir and for any given set of furnace operating conditions, fuel may be accumulating or depleting in the bed. This can have a pronounced effect on overall energy balances. Finally, the bed occupies space in the lower furnace that is not available for gas flow, and thus can have a pronounced effect on the gas flow patterns in the lower furnace.

Previous models of bed burning have treated it as if the chemistry involved is essentially the same as that during the char burning stage of a liquor drop. This has severe limitations. Bed models also have to deal with the inventory question. The rate of bed burning can be coupled with the rate at which combustible material reaches the bed to determine an inventory imbalance and thus an indication of bed growth or decay rates. An alternative approach is to force a steady state by assuming the bed burning rate is equal to the rate at which combustible material reaches the bed. This allows closure of furnace material and energy balances, but it begs the question of whether or not such burning rates are actually attainable for the firing conditions being simulated.

The experimental data base char bed burning is very limited. Most of the current bed models are either based on the experimental work carried out with the char bed reactor at IPC (now IPST) in 1988 [9] or on single particle char burning rate data. As a result of this deficiency, extensive experimental work on bed burning was carried out as part of this project.

A considerable part of the art of CFD-based recovery boiler model simulation is involved with setting up the problem. The geometry of the furnace must be known and the furnace volume divided up into a large number of computational cells for the CFD difference equations. A suitable grid structure to define the location of all of these cells must be set up. In order to provide for air and liquor entry into the furnace, the grid structure needs to be aligned with the air port openings and the liquor gun openings. Air entry through burner ports and other furnace openings may also need to be allowed for. Considerable compromise is often needed in setting up a problem. Requirements for computer memory and solution time have a major influence on the number of cells that can be used. Current models typically use something on the order of 100,000 cells for a simulation. This effectively prevents using enough cells to completely define the jets coming in from each individual air port. Primary air is normally modeled as a slot jet in order to accomodate the need to keep the number of cells down. Secondary air and tertiary air ports are usually modeled as individual ports. However, even for these ports, compromises may be necessary in locating the ports in the computational geometry. Ports may be arbitrarily located directly above other ports in order to be aligned with the chosen grid. Thus the computational geometry may differ from the real furnace geometry. Symmetry assumptions are often made so that only one-half or one-fourth of the furnace is actually modeled. This allows a finer mesh size on the computational grid but it also forces the flows to be symmetrical.

Problem setup also requires specification of the boundary conditions, in particular, the conditions at which air and liquor enter the unit. The simplest approach is to assume that the air at a given level entering the furnace is evenly distributed to all of the ports. This may introduce biases into the predicted flows that do not reflect reality. Pressure drops through windboxes and across dampers, etc. can result in considerable unevenness in the distribution of air between different air ports. Liquor spray specification usually involves assuming the liquor enters the furnace as discrete drops with a defined drop size distribution and vector velocity distribution. The relation between actual liquor firing variables and the specification of the sprays is often arbitrary and/or obscure.

Graphical displays or other methods of compressing the data are required to make the large amount of output information from the model manageable. Commercial CFD codes come with built-in graphic routines for displaying the data. UBC has also developed special graphical data display routines for their code. Care must be taken that the averaging processes used in displaying field information do not themselves generate artifacts.

FUNCTION OF RECOVERY BOILER MODELING PROGRAM

CFD-based recovery boiler models have the potential for being a powerful tool in optimizing recovery boiler process design and operation. They are capable of dealing with the complex flow patterns that exist in recovery boilers as well as the black liquor combustion process. Thus they can provide a means for relating firing practices and furnace design directly to furnace performance.

Boiler manufacturers are the source of most recovery boiler technology developments. The main needs of boiler manufacturers are process insight to guide design changes, increased credibility with customers to aid sales of recovery boilers, guidance in troubleshooting recovery boiler operating problems, confidence in making guarantees, and means for gaining a competitive advantage over other boiler manufacturers. All of the major recovery boiler manufacturers have CFD-based recovery boiler models within their own organizations. General benefits occur to the pulp and paper industry if these models are of high quality. The results of this project can be used by boiler manufacturers to:

- obtain necessary information on black liquor combustion and related behavior which can then be incorporated into their in-house models,
- obtain specific submodels (eg. a bed model) for incorporation in their own codes,
- keep in touch with the state-of-the-art in boiler modelling,
- evaluate methods for simplifying models,
- increase confidence in their own models through model project validation efforts,
- cross-check predictions of in-house models against other models, and
- obtain general information on boiler performance from simulations done with other models.

The second main group of potential model users are kraft pulp manufacturers. The main needs of pulp manufacturers are;

- more confidence that boiler manufacturers understand black liquor combustion and can provide equipment and operating guidance that will meet specifications,
- process insights that can guide evolutionary changes to improve recovery boiler productivity,
- specific knowledge of changes in operating procedures and/or hardware modifications that would provide incremental gains in liquor burning capacity in existing units,
- assistance in troubleshooting operating problems,
- means for increasing operator acceptance of changes in operating procedures, and
- confidence that changes in boiler design or operating procedures will not adversely affect boiler integrity.

At the current state of development, there is little need or desire to have a CFD recovery boiler model available at individual pulp mills. The mills do not have the computer or manpower resources to devote to model use, and operating problems requiring this level of capability are relatively infrequent. At the corporate level, some companies might have the computer and manpower resources and the expertise to have codes available in-house for their own utilization. However, up to the present, none have developed internal

models. Pulp manufacturers could utilize general knowledge and process insight that has been obtained as a result of model development and model simulations

Another way recovery boiler models could be used is through generic modelling and simulations to produce general results that could be interpreted and delivered as technical papers and reports. When this project was first conceived, this latter approach was considered to be one of the main ways for getting results to pulp manufacturers. As the project proceeded, the feedback from users was that the focus should be on developing a good model and validating it. The users themselves would take care of the applications.

A general furnace model could provide considerable help in dealing with boiler fouling and plugging issues if good descriptions of aerosol formation and characteristics were part of the model. The effects of variables such as gas temperature and composition and convective section geometry on deposits also needs to be understood to make maximum use of furnace model predictions. A global furnace model could also provide considerable help in understanding emissions behavior, combustion stability and bed control, and in developing operating strategies for maximizing firing rates.

There remain a number of impediments to more effective use of recovery furnace models. These include the following:

1. the high computational intensity of calculations,
2. the high degree of skill needed to set up problems and guide convergence,
3. the limited correspondence between the type of information needed to solve recovery boiler problems and the type of information a furnace model can produce,
4. the immense amount of information developed by the models that must be distilled and condensed and presented in a manner that the user can understand it,
5. the inefficiency in re-solving the entire recovery boiler furnace field to see the effects of changing a single parameter,
6. the lack of knowledge about recovery boiler design and operation on the part of the some of the institutions that have developed and are running the CFD models, and
7. the need for boiler manufacturers to preserve proprietary information obtained with their own models.

This DOE-supported program has played a four-fold role in improving recovery boiler design and operation.

1. Development of a validated CFD-based recovery furnace model specifically tailored to deal with the particular geometries and flow effects characteristic of recovery boilers and incorporating the most reliable information of the relevant burning behavior of black liquor in a recovery boiler environment.

2. Obtaining substantial fundamental information on the combustion of black liquor and on processes relevant to air emissions and aerosol formation, deposition, and removal in recovery boilers and making that information available not only for incorporation into the codes being specifically developed as part of the project but also to other developers of recovery furnace models.

3. Collecting and interpreting all available information on fouling and plugging of recovery boilers and assembling it into a comprehensive whole in the form of a technical monograph.

4. Acquiring and packaging data needed for recovery boiler model validation so as to make it generally available for model validation.

STATUS OF RECOVERY BOILER MODEL

A CFD-based recovery boiler model was developed at the University of British Columbia as a specific objective of this project, and is referred to herein as the UBC model. Other recovery boiler models have been, or are being, developed by parties who are also part of this project as well as by others, but these other models are incidental to this project. This section provides a brief summary of the UBC model. The model is described in much greater detail in Appendix 1.

The UBC model is based on a new CFD code specifically tailored for solving flows typical of recovery boilers and incorporates black liquor combustion and radiant heat transfer as terms in the energy equation. The model is capable of dealing with swirling flows and includes a partial treatment of processes occurring in the convective heat transfer sections of the boiler. The UBC model provides better convergence characteristics and incorporates more realistic physical submodels than earlier CFD models.

The UBC model is capable of dealing with swirling flows, which are characterized by extra rates of strain that are caused by rapid dilation, out of plane straining, or significant streamline curvature. These effects give rise to unequal normal Reynolds stresses which the basic eddy diffusion models of turbulence fail to capture. UBC has found that although the two-equation eddy viscosity type models apparently predicts too rapid a swirl decay rate, the standard k-ε turbulence model yields qualitatively accurate results for swirling flows and yields the same performance as other state-of-the-art, two-equation turbulence models.

The UBC model has now been extended to treat heat transfer and pressure drop in the convective section (screens and superheater) of the boiler. For practical reasons, the grid used in the CFD modeling of the furnace cavity is too coarse to represent the individual tubular elements of the convective section in the upper furnace. Consequently an efficient method is needed by which the pressure loss and heat transfer due to these tube banks is realistically accounted for. The distributed resistance method was used. A model was developed that simulates the flow and heat transfer in the upper furnace section and which couples closely with the existing three-dimensional CFD model of the furnace cavity.

The hot flow model at UBC incorporates the energy equation and combustion modeling as well as a model of the radiation heat transfer. The hot flow CFD model solves conservation equations for momentum along the three coordinate directions, the conservation equation for mass, the conservation equations for the turbulence kinetic energy and its rate of dissipation, and one conservation equation for each chemical species included (currently O_2, CH_4, CO_2, CO, H_2O, H_2, and N_2).

The gas phase computation is coupled to a black liquor combustion model. The gas phase variables (three components of velocity, pressure, temperature, the turbulence parameters k and ε, and the concentrations of each of the gas species) are solved in a fixed coordinate

system, for a steady state case, and are only a function of position. The properties of the black liquor phase are calculated in a moving frame of reference and are a function of time and location. The exchange of mass, momentum, and energy between the gas phase and the liquor phase is accounted for by source/sink terms added to the gas phase cells. The amount of thermal energy exchanged between the liquor particles and the gas phase is accounted for by source/sink terms in the gas-phase energy equation. The chemical energy is accounted for by the implicit enthalpy carried with the individual gas species transferring between the phases.

A statistical method is used to model the black liquor spray. Each computational particle (drop) is assumed to represent a number of real particles that have the same location, velocity, chemical composition and properties. A distribution function is assumed for the drop diameters. The number of computational drops is selected as an optimum between the available computer resources and the required simulation accuracy. In a typical case, 10,000 to 20,000 drops are used to model the spray. The diameter range is divided into intervals and for each interval a mean interval drop diameter is computed. Once this is done, the mass and number of real drops represented by a computational drop is determined. This does not have to be an integer. The spray is defined by the horizontal and vertical spread angles for each nozzle. A random method is used to distribute the drops among the nozzles and ranges of injection directions. Once the nozzle location and initial drop velocity magnitude and direction are known, the initial velocity components, (u, v, and w), are computed. The selected number of drops are injected at the same time and their positions, mass changes, and chemical composition are tracked and recorded until each drop/particle leaves the computational domain. The forces acting on the drop are gravity and fluid drag. As the drops move on their trajectories, they are subject to drag from a gas-drop relative velocity that includes a turbulent gas velocity component. This is determined statistically and is related to the local turbulent intensity. As a result of this, identical drops, starting with identical initial conditions do not follow the same trajectories.

The black liquor combustion model used in the current UBC code is that developed by Frederick et al. [2]. This is a sequential treatment of drying, devolatilization, and char burning. Drying and devolatilization are taken to be heat transfer controlled processes. The char burning reaction rates are modeled as a combination of mass transfer and chemical kinetics. As described elsewhere in this report, a more advanced black liquor combustion model has been developed. Due to insufficient time, this new black liquor combustion model has not yet been incorporated into the UBC model. This would need to be done if the UBC model is to have the capability of predicting air emissions and fume production.

The black liquor combustion and transport model is fully coupled to the gas phase computation through source-sink terms in the conservation equations. Combustion of the volatile gases is modeled in the gas phase program on a mixed is burned basis. The mixing model used is based on the work of Magnussen and Hjertageer [3]. It takes account of the turbulent kinetic energy and its rate of dissipation in computing the rate of mixing.

The radiation heat transfer model uses the discrete ordinate method [4]. This model is implemented in a separate program that runs in parallel with the main flow computation. The radiation heat transfer in the gas phase and between the hot gas and the surrounding system is computed. The energy transfer between the radiation heat transfer model and the gas phase computation model is accounted for by source/sink terms in the energy equation.

The bed shape is approximated by a staircase grid arrangement. A drop/particle that lands on the bed is assumed to be anchored there and to complete its remaining combustion stages on the bed surface. Mass and energy are exchanged between the bed and the gas within the cell first adjacent to the first bed gas phase cell. The bed is assumed to operate at steady state and the necessary mass and energy exchange is calculated from this assumption.

In early hot flow models with black liquor combustion, the liquor that reached the wall was assumed to stick to the wall surface and exchange mass and energy within the first neighboring gas phase cell. Later versions of the model compute the rate of combustion for the liquor that reaches the wall from the same rate equations used for the drop in-flight. If the rate of material striking the wall exceeds this rate, the excess material is moved to the bed.

It now takes 1-3 days to run a hot flow case including black liquor combustion with the UBC model. The actual CPU time to run a case is about one 24-hr day. Time is also required for setting up a case and for adjustments of boundary conditions, etc. This is a significant reduction in solution time.

For some types of problems, CFD recovery boiler models of this type are to some extent technical overkill. They provide much more information (and unverifiable information) about recovery boilers than is ever needed for practical use. They are still very computationally intensive and for practical purposes are limited to steady state predictions. Because of the amount of computation and time needed to set up and solve a single case, they are not very amenable to handling cause and effect situations.

These types of models are most suitable when applied to cases where the flow pattern in the boiler is a significant aspect of the problem. Many simulations have shown a relatively close coupling between hot flow patterns and isothermal flow patterns, as well as a similarity between upward gas velocity distributions and gas temperature distributions. Thus the models are also applicable to those plugging problems that are caused by high gas temperatures in the convective sections.

BLACK LIQUOR BURNING MODELING

Black liquor burning models are the basis for the source-sink terms in the CFD portion of the model needed to handle mass and energy coupling between the liquor phase and the gas phase. Closure of material and energy balances is a critical aspect of a valid recovery boiler model. The black liquor burning model must be constructed in such a way that it permits a rigorous energy balance in accordance with thermodynamic principles. It must also provide the appropriate chemical species transferring to the gas phase and remaining with the smelt to satisfy the model chemical requirements.

A revised black liquor burning model for use in CFD-based recovery boiler models, with the above capabilities, was developed in the restructured project. This new model is described in full detail in a separate project report [5] that is directed specifically at people who are involved with model development or enhancement.

Black Liquor Burning Chemistry

The new black liquor burning model is based on fundamental studies on black liquor combustion and the chemistry of black liquor burning which was carried out under subcontract at Oregon State University (OSU). Prior to the completion of this project, the key researchers at OSU joined IPST and the work was completed there. Much of this fundamental work on black liquor is summarized in detail in reference 1.

Researchers at Åbo Akademi University in Finland have also been active in the area of fundamental black liquor combustion behavior. Previous work on this subject was described in DOE report DOE/CE/40936-T3 (DE97050772) "Black Liquor Combustion Validated Recovery Boiler Modeling Five-Year Report" and in DOE report DOE/CE/40936-T2 (DE96006558) "Sodium and Sulfur Release and Recapture During Black Liquor Burning" [1,10].

The more sophisticated black liquor burning models are needed to deal with air emissions and issues connected with boiler fouling and plugging. These are sometimes referred to as elemental models because they deal with transfer of individual chemical elements between the liquor and gas phases.

The complete chemistry of black liquor is very complicated and the detailed composition is undefined. However, the elemental composition of the liquor solids can be measured quantitatively in the laboratory. This elemental analysis is the minimum information needed to describe the chemical reactions occurring in the furnace. In order to provide the quantitative information on liquor composition needed to describe all of the critical air emission and plugging factors, eight elements must be specified.

These elements and typical ranges of composition are:

C	carbon	30-40%
H	hydrogen	3-4%
O	oxygen	30-40%
S	sulfur	3-6%
Na	sodium	17-20%
K	potassium	0.5-4%
Cl	chloride	0-4%
N_f	fuel nitrogen.	0.05-0.25%

The carbon and hydrogen are the main constituents of the organic fuel substances in the liquor. Oxygen is a major component of both the organic fuels and the inorganic compounds in the liquor. Sulfur is present as both organic sulfur and as inorganic sulfur compounds. The sodium and potassium are present as salts of organic acids and as inorganic salts. The chloride is normally present as NaCl and KCl. The fuel nitrogen is part of the organic material in the liquor.

The overall processes modeled in the new elemental burning models are the same as those involved in simpler burning models: drying, pyrolysis (and volatiles burning), and char burning. When elements are transferred between the liquor and gas phases, they do so as specific chemical species (with defined enthalpies as functions of temperature). The essence of the elemental burning model(s) is a set of algorithms defining the element - chemical compound transformations and rate equations for each of the transferences. The individual elements in the black liquor solids are all converted to defined chemical compounds during pyrolysis, and all char burning reactions (including those that can take place when carbon is absent), occur as reactions between these defined chemical compounds.

The new model provides rate equations for the release of the eight elements mentioned above. The release of carbon and sulfur during pyrolysis is described by temperature dependent rate equations, so that the amounts converted to gases is dependent on local process conditions. Oxygen and hydrogen release are tied to carbon and sulfur release through stoichiometric algorithms. Sodium and potassium release occurs both through vaporization as chlorides and by formation and subsequent vaporization of metallic sodium and potassium. Models for NO_x formation are also available.

In the new model, the processes of drying, pyrolysis, and char burning all occur in parallel. Temperature dependent rate equations determine the relative rates of these processes. This parallel treatment eliminates arbitrary designation of process transitions and also provides a basis for using the same process models to describe black liquor burning in drops and on the char bed. Swelling of black liquor drops is no longer specified in arbitrary terms, but is a natural consequence of differences in density between the char phase and the unpyrolyzed liquor solids.

A critical aspect of the new black liquor burning model is a rigorous thermodynamic treatment of the energy interactions between the liquor drops and the gas phase and of all chemical reactions occurring in either phase. This is done by defining a full set of enthalpies for the black liquor solids (based on the measured elemental analysis and the heating value of the liquor solids and a specific heat function) and using only well-defined chemical species for pyrolysis gases and char components. This rigorous thermodynamic treatment is necessary to insure overall energy conservation in the CFD-based recovery boiler model.

As mentioned above, the new model treats drying, pyrolysis, and char burning as all occurring simultaneously. Drying is simply the loss of water from the liquor and no chemical reactions are involved. Pyrolysis involves the conversion of liquor solids into gases and char. Kobashi-type models for sulfur release and carbon release are the basis for the treatment of pyrolysis. The char produced by pyrolysis contains specific chemical compounds that can then undergo reactions in the so-called char burning step. Pyrolysis is actually a very complex sequence of reactions. We simplify this by assuming that pyrolysis simply converts liquor solids into specific gases, which come off, and char (which contains solid carbon (fixed carbon) and simple inorganic compounds). As pyrolysis proceeds, the liquor phase may contain some liquid water, some unpyrolyzed liquor solids, and the chemical compounds in char. Pyrolysis continues until all of the liquor solids have been converted to gases and char. Thus the extent of pyrolysis can be measured by one minus the ratio of unpyrolyzed liquor solids remaining to the original liquor solids.

For illustrative purposes, the treatment of pyrolysis for black liquor solids that contain the following five elements (Na, S, C, H, O) is described below. The extension to a liquor containing also K, Cl, and fuel N is straightforward, but is not shown here.

The starting point is the elemental analysis of the black liquor:

Na	a
S	b
C	c
H	d
O	e

where $a + b + c + d + e = 1$.

An initialization of the liquor solids is done where the Na and S are partitioned into pseudo-inorganic compounds "Na_2CO_3", "Na_2S" and Na_2SO_4". The fraction of the sulfur input as sulfate must be specified as an input variable, f, because the sulfate sulfur is assumed to be non-pyrolyzable. The remaining sulfur "Na_2S" is assumed to be pyrolyzable. The psuedo-inorganic compounds do not take part in any reactions. They are purely a bookkeeping device. Chemical reactions can only occur when the psuedo compounds are converted to real compounds by pyrolysis.

The next step is to calculate the pyrolyzable carbon, hydrogen, and oxygen as follows:

"C" = c - 12/106 * "Na_2CO_3"
"H" = d
"O" = e - 48/106 * "Na_2CO_3" - 64/142 * "Na_2SO_4"

Kobayashi-type rate equations are written for both carbon release and sulfur release. The pyrolysis of the carbon is assumed to follow the following path:

"C" $\rightarrow$ CO, CO_2, H_2 and H_2O (gases) + C (solid)

The relative amounts of CO, CO_2, H_2 and H_2O given off is based on conservation of elements using the ratios of "C", "H", and "O" in the unpyrolyzed liquor solids. Since there are four species and only three elements, the shift reaction equilibria can be applied to the gases coming off and used to supply a fourth equation. If for some reason there is a desire to have some CH_4 in the pyrolysis gas as well, it can be assumed that a fixed fraction of the C released comes off as CH_4 and the rest as the other gases. This would give a fifth equation for the now five unknowns.

The pyrolyzed sulfur is assumed to come off as H_2S. Since the pyrolyzable sulfur is considered to be "Na_2S", the sulfur pyrolysis can be represented as;

"Na_2S" $\rightarrow$ H_2S
$\downarrow$
Na_2S

where relative rates from the Kobayashi-type equations determine the ratio of H_2S to Na_2S in the product.

Since the released S comes off as H_2S, it is necessary to adjust the elemental balances to account for this, including the fact that the amount of Na_2CO_3 formed increases when sulfur comes off. The procedure used is to do the S pyrolysis calculation first and make an adjustment in the amount of pyrolyzable C, H, O, as needed, before doing the C pyrolysis calculation.

Thus the following procedure should be used for a given time increment.

1. Sulfur release rate equations determine Δ"Na_2S", the amount of "Na_2S" converted to H_2S and Na_2S in the given time increment. The remaining "Na_2S" is reduced by Δ "Na_2S" and it forms ΔH_2S which goes to the gas phase and ΔNa_2S which is added to the char phase.

2. An amount of Na_2CO_3 equivalent to the H_2S released is added to the char phase (= 106/34 * ΔH_2S).

3. "H" is reduced by 2/34 * ΔH_2S.
4. "C" is reduced by 12/34 * ΔH_2S

5. "O" is reduced by 48/34 * ΔH_2S.

The calculation then passes to the carbon release according to the following procedure.

1. Carbon release rate equations determine Δ"C", the amount of "C" converted to carbon-containing gases and char C in the given time increment. This gives ΔC-gas and ΔC (the char carbon formed).

2. Depending on what set of pyrolysis gases is chosen (see above), the molar ratios of "C", "H", and "O" at the start of the increment are used for determining the composition of the gas released. The conversion of "H" and "O" is the same as the "C" conversion on a percentage basis.

3. The ΔC is added to the char phase as carbon which can now undergo char reactions.

4. A proportionate amount of "Na_2CO_3" and "Na_2SO_4" are converted to Na_2CO_3 and Na_2SO_4 and added to the char phase. The amounts are Δsubstance/substance at the start of the time increment (= Δ"C"/"C" at start of increment).

5. The amounts of "C", "H", and "O" left in the unpyrolyzed liquor solids are reduced by the amounts converted.

The sulfur release calculation is continued until either "Na_2S" or "H" becomes zero. If there is still some remaining "Na_2S" when "H" becomes zero, it is immediately converted to Na_2S in the char phase. If the last increment leads to "Na_2S" becoming negative, it is set equal to zero, and the amount of Na_2S and H_2S (and associated stoichiometric adjustments) prorated.

The carbon release calculation is continued until all "C" is gone (which will also get rid of "H" and "O"). If the last increment leads to negative "C", the amount of "C" converted is set equal to that present at the start of the last increment, and all associated stoichiometric quantities prorated. At this point the devolatilization step is done.

Depending on the temperature, char gasification and other inorganic reactions can be occurring at the same time as the devolatilization. The rate equations for all of the different char reactions will determine how fast these are occurring.

Data describing the transformations of sulfur compounds during pyrolysis in a laminar entrained-flow reactor system are available (see reference 8). The available data strongly indicate that sulfur transformations and release to the gas phase during pyrolysis are dependent on the specific sulfur compounds present in the black liquor. This means that the elemental composition of black liquor composition is an insufficient description of the liquor as far as sulfur behavior in the furnace is concerned. This is a considerable complication in a CFD-based furnace model, since it increases the amount of information that has to be carried with each drop and tracked. For simplicity, we have assumed that only sulfate sulfur in black liquor is not pyrolyzable.

Sulfur can also be transferred from the liquor phase to the gas phase during char burning through reactions such as

$H_2O + CO_2 + Na_2S = H_2S + Na_2CO_3$

and

$2\ CO_2 + Na_2S = Na_2CO_3 + COS.$

The experimental data on fume composition in the char bed burning experiments (see reference 8) suggest that these reactions can occur. However, rate equations for these processes remain to be developed.

Sulfur reactions in the gas phase that lead to its ultimate capture as Na_2SO_4 fume must be included in the gas phase model. These reactions include oxidation of H_2S to SO_2 and SO_3, and the reaction of SO_2 and SO_3 with sodium and potassium compounds to form Na_2SO_4. The path by which sulfate ultimately forms is not completely understood. There are some limited data available that suggest substantial sulfur recapture occurs in the superheater region, but this is not fully accepted. Two of the sulfur reactions that can occur are

$Na_2CO_3 + SO_2 + 1/2O_2 = Na_2SO_4 + CO_2$

and

$2NaCl + SO_2 + 1/2\ O_2 + H_2O = 2HCl + Na_2SO_4$

However, there are other possible paths and algorithms and rate equations for sulfur recapture are still incomplete.

In the new black liquor combustion model, sodium release occurs only during char burning. The possibility that significant sodium release takes place during pyrolysis has now been discounted. Two "reactions" are considered to be the primary ones responsible for sodium release. These are the reduction of sodium carbonate to produce elemental sodium vapor, and the direct vaporization of NaCl. The reactions involved are generally considered to be

$Na_2CO_3 + 2C = 2Na + 3CO$

and

$NaCl_{(s,l)} = NaCl_{(v)}.$

There are algorithms and rate equations available for estimating the rates at which sodium is released by these reactions. Reduction of Na_2CO_2 is treated as a homogeneous reaction in the char phase. The kinetic rate equation equation used earlier was incomplete, since it is independent of carbon concentration and would not shut off when the char carbon was depleted. This has now been remedied. The vaporization of NaCl is treated as a purely mass transfer controlled process with the vapor pressure of the NaCl in the char determined by Raoult's Law and the pure component NaCl vapor pressure (which is a function only of temperature)

Potassium release is very similar to sodium release. It occurs during the char burning stage and takes place through the reduction of potassium carbonate by carbon and by direct vaporization of potassium chloride. The reactions involved are generally considered to be

$K_2CO_3 + 2C = 2K + 3CO$

and

$KCl_{(s,l)} = KCl_{(v)}$.

There are no data currently available on the kinetics of the C - K_2CO_3 reaction. The method currently recommended is to use the same rate equation as for Na_2CO_3 reduction and multiply it by the molar ratio of K/Na in the liquor particle. This is at best an approximation, and a better rate equation is still needed. The vaporization of KCl is treated as a purely mass transfer controlled process with the vapor pressure of the KCl in the char determined by Raoult's Law and the pure component KCl vapor pressure (which is a function only of temperature)

All chloride release from the liquor phase is considered to take place by vaporization of NaCl and KCl. Since the relevant pure component vapor pressures are only functions of temperature, and these substances are already present in the original liquor solids, some chloride release can occur during the higher temperature parts of the pyrolysis process. However, the bulk of the release takes place during char burning.

The NaCl and KCl in the dust can react with H_2O, SO_2, and O_2 in the furnace to form HCl which leaves the furnace with the other gases. A suitable algorithm and rate equation for this reaction is still needed. This reaction can be a significant chloride purge from the system and chloride contents in deposits have a large effect on recovery boiler fouling and plugging.

A good recovery boiler model must also be able to predict NO_x concentrations. It is the current consensus that NO_x in recovery boilers comes mainly from nitrogen compounds in the black liquor solids (so-called fuel NO_x); the so-called "prompt NO_X" mechanism accounts for the remainder [17,18] Thus algorithms and rate equations have been developed for the release of fuel nitrogen, and for NO_x formation and destruction in the gas phase. There has been considerable research work done on aspects of this process. The current methodology for handling fuel NO_x predictions is included as Appendix II.

One of the functions of recovery furnace models is to predict the amounts of sodium and potassium salts that may be carried with the furnace gases through the convective sections of the boiler where they can contribute to fouling and plugging. These materials cover a very wide range of sizes from millimeter-sized carryover particles to submicron fume. The amount and composition of the macroscopic carryover particles is a predicted output of the CFD-based recovery furnace models. These predictions should be reasonable if the liquor sprays are properly described.

The fume particles are assumed to form by condensation of vaporous sodium and potassium species. The main precursor species (as discussed earlier in this chapter) are assumed to be $Na_{(v)}$, $K_{(v)}$, $NaCl_{(v)}$, $KCl_{(v)}$, and possibly $NaOH_{(v)}$ and $KOH_{(v)}$. The $Na_{(v)}$ and $K_{(v)}$ are assumed to be formed by reduction of sodium and potassium carbonates by carbon. This reaction will be kinetically limited except at very high temperatures. Limited rate equations are available, but they need modification and verification before they can be relied upon. The NaCl and KCl are assumed to vaporize as the salt and to follow

Raoult's Law in relating the vapor pressure to the concentration in the smelt. There is little data on NaOH and KOH release from burning black liquor and no rate equations or models are available for these processes. All in all, there is a good deal of uncertainty in the ability to predict the rate of fume precursor release in a furnace model.

Verrill and Wessel [10] have suggested that fragmentation processes, as a black liquor drop burns, would produce tiny smelt drops (perhaps 5 - 20 microns) in the furnace and that these constitute a large fraction of the aerosols produced. Such particles would be very likely to deposit on superheater or generator bank tubes and contribute to fouling and plugging. There is little direct evidence that such particles exist in large quantities in the furnace, but there have only been very few measurements of particle size distributions of recovery furnace particulate further upstream than the generating bank outlet. It has further been suggested that these fragmentation particles are a major source of fume in recovery boilers because their very high surface area would favor vaporization. This has not been substantiated.

Experimental data on aerosol formation during char bed burning (discussed in detail in reference 8) clearly showed the production of a substantial amount of particulate in the 1 to 100 μm range apparently produced by mechanical fragmentation processes. Presumably, similar particles could be released during char burning in a liquor drop.

Cameron [12] showed that large quantities of Na_2CO_3 fume could be produced in the laboratory when sulfide in smelt was oxidized to sulfate. The importance of this process in recovery furnace fume formation has not been established.

Char Bed Burning

The char bed is a pile of partially combustible material that sits on the hearth of the furnace where it burns and releases molten smelt that drains out of the unit. The bed contains frozen and molten smelt, char (fixed carbon and inorganic compounds) and possibly unpyrolyzed liquor solids and unevaporated water.

Reactions in the char bed are significant in recovery boilers. The amount of combustion and other chemical reactions that occurs in the bed, and the production of gaseous fuels from the bed, must be accounted for in recovery boiler models. The bed is essentially impervious to gas flow and is treated as a boundary for the CFD gas flow calculations, albeit a boundary that is able to exchange mass (chemical species) and energy with the gas phase. The char bed is able to act as a fuel reservoir and for any given set of furnace operating conditions, fuel may be accumulating or depleting in the bed. The shape of the bed can also influence gas flow patterns in the lower furnace.

Heat and mass balances on the bed are inherently unsteady, in that local bed burning rates do not necessarily match the rate at which material is being supplied to that portion of the bed. One way around this problem in the model is to force the bed to operate at steady state so that all material that reaches the bed reacts and leaves. While this approach

allows closure of material and energy balances, it cannot determine whether or not the given operating state is actually obtainable. This can allow "nice-looking" simulations that are not consistent with the liquor spray and air supply conditions being used.

Material can be transferred along the surface of the bed by fluid drag from the gas flow across the surface. This can redistribute combustible material so that it does not burn at the point where it initially lands on the bed. Redistribution of char is particularly important for those firing practices that spray a large amount of liquor solids on the wall. Liquor drops that reach the wall dry, pyrolyze and burn while sticking on the wall. They accumulate on the wall until the weight becomes great enough that they slough off and fall to the hearth. This material tends to land around the perimeter of the bed and, if not redistributed, will either result in excessive bed growth right next to the wall, or very high temperatures, because of the large amount of fuel being burned in a small local area. Some sort of redistribution algorithm is needed to handle this in a bed model.

A new bed model was developed in the restructured project, and is described in detail in the separate report on black liquor combustion modeling [5]. In this new bed model, the chemical description of the char bed processes is fully consistent with that used for the drop burning model. The model includes rate equations for handling the chemical species interchange between the bed and the gas phase. An energy balance over the bed is used to determine the bed surface temperature and the heat exchange between the gas phase and the bed. No attempt is made to force equivalence between the local burning rates and the rate of supply of material to the bed. While local inventory imbalances can be calculated, no attempt is made to use these imbalances to "reshape" the bed and ultimately obtain closure. This was considered beyond the scope of this project.

As part of this project, experimental data were obtained on the rates of formation of particulate matter during char bed burning under controlled conditions, using a laboratory char bed reactor. These experiments were carried out to provide insight into bed burning processes and to provide data for testing char bed burning models.

The experiments clearly showed that two different types of particulates were being produced. In addition to sub-micron fume particles that form by a process of vaporization and condensation, significant quantities of larger sized particles (generally in the 1-100 μ m range) were also released from the bed. These latter particles, called ejecta, were apparently formed by mechanical fragmentation and removal processes as the char burned.

Fume production during bed burning generally behaved in accordance with expectations based on existing concepts of fume forming processes. The amount of sodium released as fume varied from about 0.5% to 12% of the sodium present and was a very strong function of bed surface temperature. The sodium in the fume was a composite of sodium vaporized as sodium chloride and as sodium vapor. Similar processes occur for potassium, and it appears as if potassium chloride vaporization is primarily responsible for enrichment of both potassium and chloride in the fume.

The ejecta particles were light brown in color and 1-100 μm in diameter and were clearly produced by mechanical processes. The composition was similar to the composition of the surface layer of the char. In most experiments, the amount of sodium released as ejecta was between 3-7% of the char sodium content, which would make this a significant source of aerosol in the recovery furnace. These are the first quantitative data on ejecta formation during bed burning that have been obtained. Further work is needed to ensure that they are not an artifact of the experimental system used and to determine the functional dependence on process variables.

The data obtained on particulate formation during char bed burning were obtained right at the end of the project, and there has not yet been time to use this data to test the char bed burning model that was developed in the project.

Radiation Heat Transfer

Measurements of radiative heat transfer properties for black liquor combustion were carried out under subcontract with Babcock & Wilcox Co. A complete summary report of their work is given in reference 8. In addition measurements of the optical constants of ash samples from kraft recovery boilers was carried out in a M.S. thesis at Oregon State University [12]. The results of this work are also summarized in Appendix III.

Babcock & Wilcox measured the spectral emittance of kraft black liquor and condensed phase products of combustion using two experimental techniques, one at room temperature and the other at high temperatures (450-850°C). The low temperature measurements were successful for black liquor, black liquor solids, char, and saltcake. The high temperature emittance measurements of smelt and saltcake were successful, but those for char were unsuccessful due to difficulties in heating the porous material.

Total emittance was calculated as a function of blackbody temperature for each sample. Black liquor, dried liquor solids, and char have relatively high emittances (0.8 to 1.0) that decrease with increasing temperature. Molten smelt also has a relatively high emittance (0.8 to 1.0), that is independent of the amount of sulfide oxidation. Molten smelt appears to be transparent to radiation at short wavelengths. In contrast, salt cake dust and sintered fume deposits have a very low emittance (0.2 - 0.7), that decreases significantly with increasing temperature. The highly porous nature of these materials probably contributes to the low emittance at short wavelengths due to internal scattering of transmitted radiation. Consequently, radiation properties have a large effect on furnace heat flux distribution because they are largely dependent on the physical characteristics, melting point, and temperature of recovery boiler deposits.

Engineering correlations were developed for radiation properties of black liquor, dried solids, char, molten smelt, and saltcake for temperatures from 100 to 1800°C. The correlations for total emissivity and absorptivity can be used when calculating surface radiation heat transfer. Equations for particle emission, absorption, and scattering coefficients should be used to calculate heat transfer for black liquor drop combustion.

Particle properties are valid for the large particle limit ($\pi d/\lambda >> 1$) typical of black liquor spray in recovery boilers.

Emissivity correlations were implemented into a model for heat transfer and combustion of single black liquor drops. The sensitivity of the model was tested and radiation properties were found to have a large effect on predicted burning times, both for conditions used in captive drop experiments and for combustion of 2 mm black liquor drops at simulated recovery boiler conditions. Therefore accurate radiation properties are needed to understand and interpret experimental results for black liquor combustion and to predict heat transfer in numerical models of a recovery furnace. The modeling results can be used as a benchmark for others who wish to implement the radiative properties.

The radiative properties characterized in this study provide some of the basic information needed to calculate heat transfer in recovery boilers. Additional work is needed to characterize the radiation properties of gas-entrained inorganic aerosols, particularly submicron fume particles. More detailed measurements are needed to characterize radiation properties of partially transparent materials, such as smelt and fume deposits, over a range of conditions (temperature, chemical composition, physical characteristics, layer thickness, and substrate materials).

In the Oregon State University study, the optical constants of dust samples from six kraft recovery boilers were determined by using FTIR spectroscopy to measure the composition and wavelength dependence of the optical properties. Measurements were made on the dust samples as well as pure inorganic salts. The sulfate and carbonate anions had the greatest effect on absorption while the effects of cations (Na vs K) were negligible. Both the real and the imaginary parts of the complex index of refraction were measured. At high wave numbers, the real part of the refractive index was about 1.46 for sulfates and about 1.61 for carbonates. For recovery boiler ash it ranged from 1.46 to 1.50. The imaginary part of the refractive index was found to be very low, ranging from 0.001 to 0.2.

These new data are expected to have a large impact on the ability to predict radiative heat transfer in recovery boilers. The most significant result is the extremely low value of the absorption index over the infrared spectrum. This confirms that suspended particles do not significantly absorb or emit radiation, that radiative scattering from fume is very significant, and porous saltcake deposits have low emissivity. Inorganic deposits are semi-transparent to radiation, and radiation is a significant component of heat transfer through deposits.

MODEL VALIDATION

Validation of recovery boiler models, by comparing model predictions against measured data, is considered essential in order to convince ultimate users that model predictions can be relied on and that models are a useful tool for improving recovery boiler design and performance. However, this is extremely difficult to do on the full recovery boiler model. The main reason for this is the difficulty of obtaining a sufficient amount of reliable data on an operating recovery boiler to set up the model properly as well as to compare with model predictions.

The only feasible approach is to build up confidence in the codes systematically through assessment of the ability to predict results of simpler cases that are relevant to the actual situation. The complete, final validation is then confirmed by testing against a very limited number of predictions of key variables in a few "real cases".

Because of the extensive use of CFD in the aerospace industry, NASA has recently developed a systematic procedure and criteria for assessing CFD codes. The four-phase validation procedure is described in detail in NASA Tech Briefs MFS-29972 [13]. This procedure can be used with any computational code and can be customized for any application of interest. The level of validation may be incrementally upgraded as the need exists and time and funding permit. The application of this procedure to recovery boiler model validation is discussed in the summary report on the first five years of this project [1].

In the case of the recovery boiler model, the validation of the CFD part of the model is first based on the ability to describe isothermal flow problems related to the types of flows expected in recovery boilers. The black liquor combustion models that are interfaced with the CFD model must first be validated against experimental data on black liquor combustion processes. Only when these have been accomplished is it meaningful to attempt to validate the predictions of the combined hot flow model with black liquor combustion.

Validation has been and is an on-going part of the current model development effort. Numerous validation exercises for the UBC CFD model have been carried out at UBC using isothermal flow. In these cases, velocity distributions obtained from numerical modeling were compared against experimental data. These validation exercises were carried out simultaneously with the development of numerical algorithms. This ensured adequate program robustness in early stages of code development.

UBC has done considerable work comparing model predictions with measured flows in real and simulated recovery boilers. This work is described in greater detail in the summary report for this project [8]. Most of the work dealt with isothermal flows including physical water models of recovery boilers and cold air flow tests in actual recovery boilers. In the recovery boiler air cold flow tests, there were many similarities between measured and computed flow fields. The locations of upward flow, downward

flow, and zero velocity regions were well predicted as were the peak values of the upward and downward velocities. In all cases, good qualitative agreement was found between computed and measured results. The up and down flow regions were correctly predicted and the equal upward velocity contours had similar shapes. In general, the flow prediction capabilities of the UBC model can be considered validated. Since cold flow velocity distributions are similar to hot flow velocity distributions, the flow predictions in operating recovery boilers have a high probability of being valid.

Validation of the black liquor combustion models is not as far advanced, but there has been some validation against single-drop black liquor burning data as well as data from other laboratory systems. Black liquor drop combustion models have been mainly derived from experimental data from laboratory single-drop muffle furnace systems and laminar entrained flow reactors. Some fundamental kinetic rate expressions have been obtained using TGA systems.

In the single-drop muffle furnace systems, a single drop of black liquor is suspended inside a muffle furnace and observed as it burns. The composition of the gas atmosphere inside the furnace can be controlled. The primary mode of heat transfer to the drop is initially by radiant heating from the walls of the muffle furnace. Most of the data have been obtained with furnace temperatures of 700-900°C, although there is some data at higher temperatures. Once volatile gases ignite, the drop is surrounded by a flame of burning gases and the radiation from these hot gases can be the dominant mode of heat transfer. Mass transfer is by natural convection that accelerates once a flame is established. The geometry changes as the liquor dries, pyrolyzes and burns can be followed with a camera system, and these geometry changes and the presence of a visible flame are used to mark the different burning stages. Most of the data on burning rates under heat and mass transfer controlled conditions have been obtained with this system.

However, there are some critical differences between this type of system and the furnace. In the furnace, the drops/particles are moving at a high velocity relative to the gas (at least in comparison to the stagnant gas environment that exists in the muffle furnace). This means that forced convection heat and mass transfer is important, and natural convection minimal. The combustible gases coming off the particle will tend to be stripped away and not form a localized flame around the particles. Radiation from the hot surrounding furnace gases as opposed to the walls will be the dominant heat transfer mechanism.

The laminar entrained flow reactor uses tiny particles of black liquor solids as feed. It can be a useful system for defining the relevant chemistry, but the very small particles make it impossible to get at heat and mass transfer effects and rates.

Thus, although the black liquor drop models are all based on experimental data, there are enough differences between real furnaces and the laboratory systems to raise questions about the quantitative validity of the rate equations.

There has been very little validation of char bed models. The only experimental data that had been available for validating char bed burning models is that of Grace et al [14]. This is a very limited data set.

In the present study, experimental data were obtained on the rates of bed burning and the formation of particulate matter during char bed burning under controlled conditions, using a laboratory char bed reactor. These data were obtained right at the end of the project, and there hasn't yet been time to use the data to test the char bed burning model that was developed in the project.

IPST undertook three activities regarding model validation in the final phase of the project. Two of these were field tests on recovery boilers to acquire data to set up and test the model by comparing computer model predictions with measured values. The third was a benchmarking exercise comparing prediction of the UBC model and FLUENT model against each other and against water model data for an isothermal flow case. These are described in detail in Appendix IV.

There are three basic elements in each validation exercise:

1. experimental data are acquired to define the operating and setup conditions for the case as well as output performance data,

2. one or more simulations are run on the case in question,

3. model predictions are compared to the actual data and judgements made with regard to the degree that predictions conform to reality.

The information required is as follows:

1. Geometry data on the boiler in question giving furnace dimensions, locations and size of air ports and liquor gun openings, nose arch shape, etc. that are needed to set up the model grids.

2. Data describing furnace operating conditions including liquor flows, composition and heating value, liquor spray characteristics, and air flows, pressures, and temperatures. Liquor spray characteristics may have to be inferred from the location, angle, and types of liquor guns, and the liquor temperature and pressure.

3. Data describing the furnace performance. Ideally this would be the gas velocity, temperature and compositions at many locations within the furnace cavity along with data on the state and fate of the liquor as it burns in the furnace. In practice, this would be a much more limited set of data, mainly near the furnace boundaries.

As mentioned above, two field tests were carried out on actual recovery boilers to obtain data to set up and test the model. These data are presented in detail in a separate report.[7] Neither of these validation exercises was as successful as hoped. The biggest problem

was that the amount of quantitative data on furnace outputs was extremely limited, despite extensive efforts to acquire such data. Another problem was that certain critical model input (setup) data (such as spray initialization parameters) could not be measured directly and had to be specified in an arbitrary manner. The third problem was the inherent unsteadiness of recovery boiler flows, that resulted in uncertainty in the applicability of furnace output variables measured at a particular location and time.

The model set up conditions, simulation results and comparisons for the two field tests (referred to as Case 1 and Case 2) are described in detail in reference 8. UBC also carried out a simulation of Case 1 and their results are described in reference 8.

In Case 1, video camera images of the liquor sprays were obtained for comparison with computed drop trajectories. The spray predictions do not appear to correspond to actuality, in that the sprays remain too wet and strike the bed with too much material. This was the case, even though spray parameters were varied. In the actual boiler, the sprays did not appear to reach the bed intact.

There were no quantitative measured data available to compare with carryover predictions, but the mill did not consider carryover to be a problem. The amount of carryover is highly dependent on spray initialization parameters, which as mentioned above, were quite arbitrary.

UBC found that gas temperatures from the calculated temperature field compared very well to experimental data at the bullnose, primary superheater, and the boiler bank inlet in Case 1. In the simulation of this case carried out at IPST, the gas temperatures leaving the furnace ahead of the superheater were too high and those entering the generating bank were too low.

In Case 2, many different operating conditions were used during the test and data were obtained on how the furnace responded to these changes. This allowed cause and effect relationships to be explored. However, only a single set of conditions was modeled and compared to data, because of the time and effort needed to set up, converge, and interpret a solution for a single case. A limited amount of gas temperature data was predicted reasonably well.

A benchmarking exercise was also carried out in which the predictions of the UBC model were compared with those made with a FLUENT model for one isothermal flow case based on a physical water model. The details of this benchmarking exercise are given in Appendix IV; see also reference 8. The benchmarking test showed that both codes did a reasonable job of predicting the flows and were in general agreement with each other. It appears that CFD models, properly set up, can, when applied to isothermal flows, do a reasonably good job of predicting the flows.

The model predicts gas temperatures in a small region in the lower furnace above the bed that are unreasonably high. This is not unique to the UBC model. Similar behavior has

been seen in most published temperature fields produced by simulations using other recovery boiler models. The cause of these excessive temperatures is not known.

It is now very apparent that future validation efforts must focus on more intense validation of smaller problems for which true answers are known. The flow predictions are amenable to this approach and have been rather extensively validated. A similar approach needs to be done for black liquor combustion, where the model should be used to examine simple setups. By comparison between prediction and data, there should be an increased acceptance of the validity of the model.

Validating complete model predictions against data from full furnace testing is a fallacy. It is very difficult to make sufficient measurements to actually test model predictions. The measurements tend to be made locally and be time dependent, as the flow patterns are not completely steady. It is extremely expensive to acquire the amount of data to really compare predictions with reality. Disagreements between model predictions and reality can also occur because of incorrect model setup conditions, some of which (such as liquor spray initialization) are not measurable directly and which must be done arbitrarily.

TECHNOLOGY TRANSFER

Recovery boiler models are tools for improving recovery boiler design and operation and not ends in themselves. The overall objective of this restructured project was to bring closure in an effective manner that maximized the usefulness of the total effort to the kraft pulp industry. This has been achieved. This DOE-supported program played a four-fold role in improving recovery boiler design and operation.

1. Development of a validated CFD-based recovery furnace model specifically tailored to deal with the particular geometries and flow effects characteristic of recovery boilers and incorporating the most reliable information of the relevant burning behavior of black liquor in a recovery boiler environment.

2. Obtaining substantial fundamental information on the combustion of black liquor and on processes relevant to air emissions and aerosol formation, deposition, and removal in recovery boilers and making that information available not only for incorporation into the codes being specifically developed as part of the project but also to other developers of recovery furnace models.

3. Collecting and interpreting all available information on fouling and plugging of recovery boilers and assembling it into a comprehensive whole in the form of a technical monograph.

4. Acquiring and packaging data needed for recovery boiler model validation so as to make it generally available for model validation.

For the industry to gain maximum benefit from this work, there is a need to have simulations of recovery boilers carried out. This can be done with the computer codes developed directly as part of this project or to use other codes that have been enhanced because of the information and submodels developed and supplied from this effort. The industry has also benefited from the general knowledge about recovery boilers that has been obtained as a result of this project.

The code developed as part of this project was developed at UBC and is referred to as the UBC code. UBC's technology transfer plan is summarized in reference 8. Basic model development work will continue to be done at UBC and UBC will retain ownership of the code and the models. UBC has formed a spin-off company, Process Simulations Ltd. (PSL), and has licensed the code to PSL for industrial application. Potential users should contact PSL directly to obtain further information on how simulations and other services can be obtained.

UBC has granted a royalty free license to IPST to use the code. IPST is free to use the code and apply it to industrial problems, however it does not have the right to sub-license the code to third parties. Interested potential users should contact IPST directly for further information.

There are now a considerable number of CFD-based recovery boiler models in use throughout the world. These models are generally similar in nature to the models developed in this project. A listing of available models is given below.

Babcock & Wilcox (B&W)	in-house CFD code
ABB	FLUENT CFD code
Kvaerner (old Tampella)	Phoenics CFD code
(old Gotaverken model)	
Ahlstrom	FLUENT CFD code
Jansen Boiler & Combustion Technologies	KIVA CFD code
UBC model (PSL and IPST)	new CFD code
Royal Institute (Sweden)	STAR CFD code
Tampere Technical University	Phoenics CFD code

The pulp and paper industry benefits from improved recovery boiler models regardless of where they are located. In particular recovery boiler manufacturers have the experience and know how to interpret model predictions in an effective manner and to acquire the field data that increases confidence in model predictions. One of the significant technology transfer mechanisms on this project was to make black liquor combustion information as well as information on modeling per se available to the boiler manufacturers in order to improve their own models.

These various models have been used as an effective tool over the past few years to help guide changes in recovery boiler design and operation. They are most fruitfully applied when flow patterns within the boiler are sub-optimum and the boiler operating problems are directly connected to the flow patterns. In some cases, only the flow problem needs to be solved to gain considerable benefit. The models are somewhat less effective when dealing with emissions and chemical aspects of recovery boiler operation, and this is the area where the greatest improvements are likely to occur.

It still requires considerable effort, time, and computer knowledge to set up and solve a single case, so there are economic limits to the number of cases that can be done on a given boiler. Interpretation of the model output requires considerable knowledge of boiler operation as well as computer and modeling skills. This has limited the application of the models. They are not at, and are likely to never be at, a point where they can be routinely applied in the field.

There are four separate reports that will result from this final phase of the project. These are:

1. A comprehensive final report covering all work on the project since the project was restructured [8]. A comprehensive summary report on the first five years of the project was issued recently [1]. It should be consulted for information on work done during that period.

2. A report describing in detail how black liquor combustion in a recovery boiler should be modeled [5]. This report incorporates the latest information on black liquor processes and is aimed at people who are directly involved with the development of recovery boiler models.

3. A technical monograph on recovery boiler fouling and plugging, summarizing and integrating the current knowledge about recovery boiler fouling and plugging and aimed at the general technical audience involved with recovery boiler design and operation [6].

4. A report summarizing the recovery boiler design and operating information needed for model setup and the measured output variables for the cases used for model validation in this study [7]. The intent is to make the information available for validation of other recovery boiler models and to encourage cross-comparisons in the predictions of the different models.

In addition, a considerable number of technical papers have been published as a result of the work on this project. A listing of earlier papers was included in the previous report on the first five years work on this project [1]. More recent publications are listed in the references that accompany the various Appendices to this report.

REFERENCES

1. Grace, Frederick, Salcudean & Wessel "Black Liquor Combustion Validated Recovery Boiler Modeling - Five-Year Report", DOE/CE/40936-T3 (DE97050772), (1996).

2. Frederick, W.J., Noopila, T., and Hupa, M.,"Swelling of spent pulping liquor droplets during combustion" JPPS 17,5:164-170 (1991).

3. Magnussen, B.F. and Hjertager, B.H., "On mathematical models of turbulent combustion with special emphasis on soot formation and combustion", 16th International Symposium on Combustion, Cambridge, MA (1976).

4. Fiveland, W.A., "Three-dimensional radiative heat transfer solutions by the discrete-ordinates method", J. Thermophysics and Heat Transfer, vol.2, J309-J316 (1988).

5. Separate DOE report on this project on Black Liquor Combustion Model

6. Tran and Grace, "Monograph on Recovery Boiler Fouling and Plugging" separate DOE report on this project

7. Separate DOE report on this project on Data from Model Validation Field Tests

8. Brown, C., Grace, T., Lien, S., and Clay, D., "Char bed burning rates – experimental results", Tappi J. 72 (10)' 175-181 (1989).

9. Frederick, Iisa, Wag, Reis, Boonsongsup, Forssen and Hupa, "Sodium and Sulfur Release and Recapture During Blank Liquor Burning" SOE/CE/40936-T2 (DE96006558) (1995).

10. Verrill, C. and Wessel, R., "Validation of combustion and fume formation models for an operating kraft recovery boiler" Proceedings of 1996 Tappi Engineering conference, pp 775-792, Chicago, (1996)

11. Cameron, J. Clay, D., and Grace, T., "OxidVerrill, C. and Wessel, R., "Validation of combustion and fume formation models for an operating kraft recovery boiler" Proceedings of 1996 TAPPI Engineering Conference, pp775-792, Chicago, (1996).

12. Samretvanich, A., "Determination of the Optical Constants of Ash Samples from Kraft Recovery Boilers" M.S. Thesis, Oregon State University, Corvallis, OR (April 1997

13. "Procedure and Criteria for Assessing CFD Codes", NASA Tech Briefs MFS-29972.

14. Clay, Lien, Grace, Brown, Empie, Macek, Amin, and Rao Charandgundla, "Fundamental Studies of Black Liquor Combustion, Final Report for the Period December 1987 -December 1989" DOE/CE/40637-T9 (DE91018580), (1990).

APPENDIX I

Reports from the University of British Columbia

Section 1

Modeling of Black Liquor Recovery Boilers – Summary Report (69 pages)

Section 2

Flow and Heat Transfer Modeling in the
Upper Furnace of a Kraft Recovery Boiler (25 pages)

Section 3

Numerical Simulation of Black Liquor Combustion
In a Kraft Recovery Furnace (44 pages)

Section 4

Investigation of Turbulence Models and Prediction of
Swirling Flows for Kraft Recovery Furnaces (38 pages)

Section 5

Radiative Heat Transfer in Kraft Recovery Boilers (62 pages)

Modeling of Black Liquor Recovery Boilers

Summary Report to DOE

M. Salcudean, I. Gartshore, Z. Abdullah, P. Nowak, P. Sabhapathy,

D. Tse, P. Matys, M. Savage, Z. Xiao, K. Zhang

Department of Mechanical Engineering
University of British Columbia
Vancouver, B.C.

April 30, 1997

Contents

1 Introduction **2**

2 Development of Enhanced Furnace Models **4**

2.1 Implementation of convergence acceleration in smoothers for the Navier-Stokes equations 4

2.2 Investigation of rotational or swirling flows 5

2.3 Implementation of variable gas properties on the radiation heat transfer and prediction of the wall radiant heat flux 7

2.4 Implementation of simplified heat/mass transfer between the char bed and the gas flow 8

2.5 Implementation of the enhanced chemistry and char combustion models developed in program 9

2.6 Modeling of pressure drop and heat transfer in the convective sections . 10

2.7 Summary description of the UBC hot flow model 11

3 Establish Validity of Furnace Models **14**

3.1 Summary of available comparison between CFD predictions and measured isothermal flows 14

3.2 An isothermal flow case - benchmarking exercise 15

3.2.1 Detailed Geometry 16

3.2.2 Experimental conditions and flow measurements 16

3.2.3 Comparison between experimental and numerical results 18

3.3 Validation of hot flow model 18

4 Technology Transfer **21**

References **23**

Figures **26**

Introduction

This report describes the work completed at the Department of Mechanical Engineering, UBC, for the project entitled 'Modeling of Black Liquor Recovery Boilers'. This project was funded by the U.S. Department of Energy and leadership was provided by the Institute of Paper Science & Technology (IPST), Atlanta, GA. The overall objective of the work at UBC was to develop a comprehensive mathematical model of recovery boilers using computational fluid dynamics (CFD) and to carry out model validation.

Knowledge of gas flow and combustion in recovery boilers is difficult to obtain because of the large dimensions of the unit, the high temperature, and the extremely corrosive environment. Prior to the commencement of this project, the mathematical models developed for recovery boilers were mainly 'one-dimensional' type models (Shiang (1986)) – spatial variation of the flow fields was usually ignored. These models had only limited usefulness as they did not deal realistically with flow and combustion asymmetry of the complex gas flow patterns, and the effects of the positions of the combustion air entry ports.

The numerical modeling work carried out at IPST was a pioneering effort in the use of CFD methodology to model recovery boilers (Grace et al. (1989)). However, this earlier effort has limited utility due to uncertainties both in the solution efficiency and in the accuracy of physical sub-models.

The CFD model developed at UBC simulates the gas flow patterns and combustion in recovery boilers. This model is an improvement over earlier CFD models since it provides better convergence characteristics and it incorporates more realistic physical sub-models developed in the recent years. As a result, the model can be used as a tool to optimize the efficiency and environmental impact of new boiler designs and modifications to existing boilers as well as developing the beet operating regimes for

existing boilers. The following list outlines the tasks completed by UBC:

1. Development of Enhanced Furnace Models:
   (a) Implementation of convergence acceleration in smoothers for the Navier-Stokes equations,
   (b) Investigation of swirling flow,
   (c) Implementation of variable gas properties (based on composition, temperature and fume) on the radiation heat transfer and prediction of the wall radiant heat flux,
   (d) Implementation of simplified heat/mass transfer from the char bed into the gas flow,
   (e) Implementation of the enhanced chemistry and char bed models developed in program,
   (f) Modeling of pressure drop and heat transfer in the convective sections to determine the extent that these affect flow and temperature fields in the furnace proper.
2. Establish Validity of Furnace Models:
   (a) Summarize available comparisons between CFD flow predictions and measured flows in water models of recovery boilers and cold air flow tests in full-scale boilers
   (b) Provide one set of boundary conditions and isothermal flow field measurements for benchmarking and validation,
   (c) Simulate one case of hot flow in recovery boilers for use in comparison with data collected in an actual boiler.
3. Technology transfer of UBC codes to IPST to facilitate application of models to US recovery boilers.

All of the above objectives have been accomplished. The results of code development have been presented in numerous technical reports and papers published during the course of this project. The following chapters summarize the contribution made.

Chapter 2

Development of Enhanced Furnace Models

2.1 Implementation of convergence acceleration in smoothers for the Navier-Stokes equations

Numerical simulations of recovery boilers require very extensive computational resources. There is a large variation in geometric dimensions: the dimensions of the furnace is two to three orders of magnitude greater than those of an individual air port. Consequently the discretization of the entire recovery boiler domain requires the use of a large number of control volume cells. Thus, efficiency in the numerical solution scheme is important for the overall success of the numerical simulation exercises.

The robustness and efficiency of our numerical algorithms were first established for the case of cold flow or isothermal flow modeling. The study of isothermal flow in the initial stages has the following advantages: First, isothermal flows can be simulated with a smaller set of dependent variables and hence are more suitable in the testing and development of numerical algorithms. Second, the cold flow velocity distribution is very representative of the gas flow velocity distribution in an operating recovery boiler. This is because the flow patterns are determined mainly by the interaction of high momentum air jets entering the furnace. Our numerical studies revealed that a non-linear multigrid method originally formulated by Hackbusch (1992) returned fast convergence performance when the symmetrically coupled Gauss-Seidel solution scheme proposed by Vanka (1986) was used in conjunction. These earlier results are reported in Salcudean et al. (1993).

For non-isothermal flows which include the effects of combustion, the solution procedure becomes more complicated as the variable density of the fluid causes difficulties in establishing mass conservation during computation. The standard SCGS solver alone

is usually not efficient in solving the system of modeling equations. A new sectional pressure correction (SPC) procedure was introduced to help enforce a given mass flow through a section of the domain. In this procedure, a pressure correction is defined based on the mass flow imbalance across a computational plane. This pressure correction is then used to either accelerate or decelerate the flow with a mass force which depends on the error in the mass flow through the plane. This gives a stable and rapid reduction of the residue of the continuity equation at negligible computational cost. Details of this method are given in Nowak and Salcudean (1996).

Figure 1 shows the convergence results of various numerical schemes tested in Nowak and Salcudean (1996). Eight tests were conducted: Test 1 was for the use of the alternating line Gauss-Seidel (ALGS) solver on a single grid. Test 2 was ALGS solver plus the new SPC procedure on a single grid. Tests 3, 5 and 7 were for ALGS solver used with a non-linear multigrid method formulated by Hackbusch (1992). The three tests were differed in the number of smoothings carried out at different grid levels. Tests 4, 6 and 8 were similar to Tests 3, 5 and 7 above except that the SPC procedure was employed. The superiority of the SPC procedure is evident from the results shown.

2.2 Investigation of rotational or swirling flows

Swirling flows are frequently generated in recovery boilers to increase the residence time of the combustibles in the furnace. These swirling flows are usually created by a specific air admission practice for which the windboxes at the secondary or tertiary elevation are injecting air in specific directions so as to impart a rotation pattern for the flow within the furnace cavity. In many operations, this practice has demonstrated to achieve good mixing and high combustion efficiencies at moderate jet velocities and low fan power requirements (see Lefebvre and Burelle (1988)). However, it may contribute to unacceptable gas side temperature variations at the furnace outlet plane. As a result, accurate predictions of such swirling flows in a recovery furnace can enable the optimization of the air system.

Swirling flows are characterized by extra rates of strain that are caused by rapid dilation, out of plane straining, or significant streamline curvature. These effects give rise to unequal normal Reynolds stresses which the basic eddy viscosity models of

turbulence fail to capture. A study was carried out at UBC to investigate the use of various turbulence models to predict swirling flows.

The numerical study was based on an experiment carried out at UBC. The experiment was conducted in an isothermal scale water model of a CE recovery boiler design (Figure 2). Particle image velocimetry (PIV) was used as a quantitative flow visualization technique to provide two-dimensional velocity information on the liquid flow field through optical recording and analysis of motion of small tracer particles added to the flow. A laser light sheet was used to illuminate a two-dimensional region within the experimental apparatus, in which the motion of the particles was recorded using digital videotape for high resolution. The recordings were then analyzed using correlation techniques to obtain a time series of two-dimensional velocity vectors. Details of the experiment and description of the recovery boiler model can be found in Ketler et al. (1994).

There are four starting burners located just above the primary orifices in the front and rear faces at an elevation 0.05 m from the base of the boiler model. The burners are angled in a horizontal plane towards the center at 25° from the perpendicular. Jets from these burners cause a swirling flow in the model. In the experiment, jets from the primary elevation, the starting burners, the secondary elevation, and load burners were in operation. The resulting flow field was examined by particle image velocimetry at three horizontal levels: level 1 was 0.26 m above the base, while levels 2 and 3 were respectively at the height of 0.55 m and 0.70 m.

Numerical predictions of the furnace flow field were carried out using three variants of the two-equation turbulence models: the standard $k-\epsilon$, RNG $k-\epsilon$ and Wilcox's $k-\omega$ models. For the two $k-\epsilon$ models, the wall function was used to simulate the viscous damping effect due to the presence of solid walls. Zero gradient condition was imposed for all flow variables at the furnace model's exit. Comparison between the numerical and experimental results is presented next.

Figures 3, 4 and 5 display the computed and measured flow fields in the three elevations mentioned earlier. The empty areas in the experimental PIV results were caused by the blockage of the bullnose of the model to laser light. The predictions by the RNG $k-\epsilon$ model are visually almost indistinguishable from those by the standard

$k-\epsilon$ model. With proper tuning of empirical parameters, The predictions by the $k-\omega$ model are also very similar to the standard $k-\epsilon$ results for both the magnitude of the velocity vectors around the swirl core and the position of the core. The overall impression is that the numerical results appear to predict the position of the swirling core at each elevation quite well.

It is significant to note that the magnitudes of the velocity vectors around the swirl core predicted by any of the three models are generally higher than the experimental values at level 1, while the opposite is true at the two higher levels. This observation confirms the suspicion that two-equation eddy viscosity type models predict too rapid a swirl decay rate (Sloan et al. (1986)) and are unable to produce quantitatively accurate results for swirling flows.

Details of the above study are given in the report by Tse (1996a). It was concluded in the report that the main attractiveness of eddy viscosity based two-equation turbulence models is their efficient and robust numerical performance, and that the standard $k-\epsilon$ model yields the same performance as two other state-of-the-art two-equation models, the RNG $k-\epsilon$ and Wilcox's $k-\omega$ models, for the prediction of complex flows that are found in recovery furnaces. In view of the uncertainty in the modeling of the many other physical and chemical processes in a kraft recovery furnace, the standard $k-\epsilon$ model is recommended for use for general simulation purposes. Despite its noted weaknesses, the model yields qualitatively accurate results as shown in our study of furnace swirling flows. The results are therefore useful in guiding design development.

2.3 Implementation of variable gas properties on the radiation heat transfer and prediction of the wall radiant heat flux

Gases such as water vapor (H_2O), carbon dioxide (CO_2) and sulfur dioxide (SO_2) are present in recovery furnaces and their asymmetric molecular structures cause them to emit and absorb radiation strongly in certain narrow wavelength bands associated with their molecular energy levels. The amount of radiation absorbed or emitted by a gas at any wavelength depends on the molecular composition, pressure, temperature and total path length of propagation of the radiation in the gas. Estimates of the radiative

properties of those gases can be made using values of the concentrations of the gases. The exponential wide-band model by Edwards (1981) is a good compromise in terms of levels of accuracy and computational efficiency.

In this wide-band model, the profile of band absorption by a polar gas is approximated by an effective bandwidth, which is made a function of the gaseous density, temperature, and pressure. Empirical correlations for gases such as H_2O and CO_2 are available to fit this effective bandwidth to available experimental data. Details of the model is given in Sabhapathy (1996).

The radiant heat flux to the wall is an important quantity to be determined in a recovery boiler simulation study. Its value gives information about the surface temperature of the wall tubes on the side walls of the furnace and the extent of heat transfer to the water running within those tubes. In the radiation modeling program, the amount of radiation heat transfer from an elemental volume of flue gas to an area of furnace wall is computed. The contribution from all such elemental volumes that make up the entire furnace domain is then added up, and the procedure is repeated for the entire surface area of the furnace. This yields the total wall radiant heat flux which is computed to be between 200 and 500 MW for an average boiler.

2.4 Implementation of simplified heat/mass transfer between the char bed and the gas flow

The char bed is made up of fallen black liquor droplets. Pyrolysis of the droplets may still continue when the droplets land on the bed. As a result, the char content in the bed is increased while heat energy and chemical species are released into the gas phase, and part of this energy released is used to convert sulfate salts to sulfides within the bed.

In the present model, only the gasification reactions at the surface layer of the bed are considered while the chemical reactions happening within the bed are ignored. The reactions of interest are

$$C + O_2 \rightleftharpoons CO_2$$

$$C + CO_2 \rightleftharpoons 2CO$$

$$C + H_2O \rightleftharpoons H_2 + CO$$

After a particle lands on the bed surface it is assumed that the evaporation of water and pyrolysis produce mass sources which are released into the gas phase in the layer of cells directly above the bed surface. The energy sources due to the evaporation and pyrolysis can be used in subsequent calculation of bed temperature.

The bed char combustion rate is computed based on the mass transfer rates of the reactants (O_2, CO_2, H_2O) to the bed surface. The mass transfer rates are correlated with the local flow conditions and the concentration of the species; the formulae used are those developed originally for a flat plate. If the char combustion rate is smaller than the char deposition rate than there is a net accumulation of unburned carbon in a given cell. Once the char reaction rate is known, the source terms for all the involved species are updated. The mass sources are provided directly to the gas phase and the energy sources are used in the bed model energy balance.

2.5 Implementation of the enhanced chemistry and char combustion models developed in program

The calculation of char combustion rate is based on the theory developed at IPST. The char combustion rate is defined as the rate of removal of carbon in char particles. In the determination of this carbon removal rate, the mass transfer rates of O_2, H_2O and CO_2 from the surrounding flue gas to the surface of the char particle are needed. Then the char combustion rate is assumed to be dependent on the mass transfer rate of these gases. With known molar carbon loss rate, the mass loss of the char particle can be estimated.

For char combustion with reduction of sodium sulfate, the rate equations governing the generation or depletion of CO_2, H_2O and SO_4 are needed. Empirical expressions from Grace et al. (1994) are used to express these rate equations in terms of the concentration of the chemical species as well as the temperature of the gas. Details are given in Matys (1996).

2.6 Modeling of pressure drop and heat transfer in the convective sections

Slender tubes of planer and tubular designs occupy the upper portion of a recovery furnace. The steam inside these tubes is superheated by radiation and convection due to the hot flue gas from the lower furnace. For practical consideration, the grid used in the CFD modeling of the furnace cavity is too coarse to represent the individual tubular elements in the upper furnace. Consequently, in the combined simulation of flow and heat transfer processes in both the lower and upper furnace, an efficient method is needed whereby the pressure loss and heat transfer due to these tube banks can be realistically accounted for.

The distributed resistance method developed by Patankar and Spalding (1974) can be applied to the calculation of thermal-hydraulic flow through tube banks. The method acknowledges the fact that fine geometrical details of the tube banks cannot be captured by the grid commonly used in the CFD simulation of the device. Instead, modifications applying the porosity and distributed resistance concepts are introduced to the governing equations to simulate the effects due to the tube banks. Source terms in the momentum equations are modified to simulate the pressure loss due to the tube bank obstructions. This approach has the following major advantages:

1. The grid used can be much coarser than the dimensions of individual tubes.

2. Since only the terms in the governing equation system are modified, the same CFD solution algorithm can be applied in the entire domain comprising regions that contain tube banks and regions that do not.

3. The method provides a means of using extensive experimental data on the pressure drop through tube banks.

Heat sources and sinks can also be distributed in a manner akin to the distributed resistance method to simulate the heat loss/gain by the flue gas due to heat transfer with the tube banks. The extent of heat transfer is affected by many geometric and physical factors. Examples of geometric factors are the arrangements, locations, and dimensions of the tube banks. Physical factors include the velocity and temperature

of the gas flow and steam flow, composition of the flue gas, and the amount of fouling deposits on the tube surfaces. Analytical and empirical formulae are available to explicitly state the influence of these factors on heat transfer.

A model was developed that simulates the flow and heat transfer in the upper furnace heat exchanger section. The model couples closely with an existing three-dimensional CFD furnace model to allow for a comprehensive simulation of the flow and heat transfer phenomena both in the furnace cavity and in the heat exchanger section. Figure 6 shows the results of temperature distribution when this tube bank model is applied to a generic boiler. The temperature in the upper furnace region is reduced when the tube bank model is applied as expected. Details of the model can be found in Tse et al. (1996b).

2.7 Summary description of the UBC hot flow model

The hot flow model developed at UBC incorporates the energy equation and combustion modeling, as well as a model to compute radiation heat transfer. The hot flow CFD model solves conservation equations for momentum along the three coordinate directions, the conservation equation for the mass, the conservation equations for the turbulence kinetic energy and its rate of dissipation, and one conservation equation each for various chemical species included in the model. Our model presently includes oxygen (O_2), methane (CH_4), carbon dioxide (CO_2), carbon monoxide (CO), water (H_2O), hydrogen (H_2) and nitrogen (N_2).

The gas phase computation is coupled to a model which computes the trajectory of individual liquor droplet. This black liquor combustion model is based on a Lagrangian tracking of each individual droplet and typically 10,000 to 20,000 droplets are used in a computation. An accounting is kept for the position and speed of each individual droplet during the entire duration of its flight.

The black liquor spray computation starts from a model of the spray system. The spray system simulates either the splash plate nozzles or the conical nozzles that are typically used in recovery boilers. A log-normal distribution is used to represent the droplet diameters. In reality there are millions of liquor droplets that are suspended in a recovery boiler at any particular instance. In our model, each computational droplet

is assumed to represent a number of actual liquor droplets that share very similar location, velocity, chemical composition and physical properties. A random method is used to specify the droplet velocity at the injection port. The range of the possible injection direction and the initial injection velocity depend on the type of liquor spray system that is being modeled. After injection, each droplet goes through a number of phases as specified in the chemical combustion model developed by Frederick et al. (1991).

A typical black liquor droplet contains about 30% of its mass as water. Drying of the droplet occurs immediately after injection. The rate of drying is assumed to be controlled by the transfer of energy from the hot gas phase to the droplet. Devolatilization starts after the droplet drying is completed. During devolatilization the droplet releases any remaining water and the volatile gases which include methane, carbon monoxide and hydrogen. After devolatilization is completed the droplet consists of char which contains organic compounds carbon and inorganic smelts. These organic compounds are then burned through gasification processes that produce water and carbon dioxide.

Turbulent dispersion is taken into account in the computation of the droplet trajectory because the flow field is highly turbulent and unsteady. The black liquor combustion and transport model is fully coupled to the gas phase computation via source/sink terms in the conservation equations for momentum, energy, and in species mass. Combustion of the volatile gases is modeled in the gas phase program. It is presently assumed that methane, carbon monoxide and hydrogen are the combustible gases that react with oxygen in the gas phase. The average temperature in the furnace is 1000°C which implies that the combustion rate is dependent not on the chemical kinetics but on the mixing rate between oxygen and the combustible gases. The model presently used is based on the study by Magnussen and Hjertageer (1977). This model takes into account the turbulent kinetic energy and its rate of dissipation to compute the rate of mixing. Details of the UBC black liquor combustion model are given in Matys (1996).

The radiation heat transfer model uses the discrete ordinate method (Fiveland (1988)). This model has been implemented in a separate program which runs in parallel with the main gas flow calculation. The radiation heat transfer in the gas phase and

between the hot gas and the surrounding surfaces is computed. The energy transfer between the radiation heat transfer model and the gas phase computation model is accounted for by the source/sink term in the energy equation. The radiation heat transfer is the dominant mode of energy transfer in the lower furnace and is significant in the upper furnace. Further details of the radiation heat transfer model can be found in Sabhapathy (1995).

Chapter 3

Establish Validity of Furnace Models

3.1 Summary of available comparison between CFD predictions and measured isothermal flows

Numerous validation exercises for the UBC CFD model had been carried out using isothermal flows. In these exercises, cold flow velocity distributions obtained from numerical modeling were compared against experimental data. Such isothermal studies are valuable for the following reasons:

- numerical simulations are more easily carried out due to the smaller set of equations for modeling the problem,
- reliable experimental data are more readily obtainable,
- cold flow velocity distribution is representative of the gas flow velocity distribution in an operating recovery boiler.

Consequently, cold flow modeling allowed for more extensive comparison with experimental data and substantially aids the development of the numerical algorithm. Hence, adequate program robustness was ensured in early stages of code development.

Cold flow measurements have been done in the form of air flow tests in full-scale boilers and in water models of recovery boilers. Velocity data are usually collected at elevations where measurements could be taken conveniently. Measurements techniques included the use of hot-wire anemometer probes for air tests in full-scale boilers and laser Doppler velocimetry (LDV) and particle image velocimetry (PIV) for water model tests. Pressure or flow rate measurements were made at inlet ports to calculate the flow velocity through these ports. This information was necessary to establish the boundary conditions of the CFD model.

Comparison of these results with CFD predictions have been presented in technical papers (Abdullah et al. (1994a,1994b)) and in an earlier report by the UBC group (Abdullah et al. (1995)). Examples of such comparison are presented in Figures 7 and 8, which are taken from Abdullah et al. (1994a). The results were for a series of cold flow air test studies carried out at a recovery boiler at the Weyerhaeuser mill in Kamloops, BC. The figures display the contours for the vertical velocity component, with positive values indicate upward flow and negative values for downward flow.

Figure 7 shows the results where there was air flow through both primary and secondary ports, while Figure 8 shows the results where only the secondary ports were open. There are many similarities between the measured and the computed flow fields. The locations of upward flow, downward flow, and zero velocity regions were very well predicted, so were the peak values of the upward and downward velocities.

The report by Abdullah et al. (1995) contained additional comparison for isothermal flow modeling of recovery boilers. It was observed for all cases that qualitative agreement was obtained between the computed and the measured results. The upward flow and downward flow regions were correctly predicted, and the zero upward velocity contours have a similar shape across most of the cross-section, both for the physical measurement results and the numerical modeling results.

A water model test case is presented in details in the next section. The flow conditions will be thoroughly described to provide as a benchmarking exercise for other CFD modeling studies.

3.2 An isothermal flow case - benchmarking exercise

The case chosen for this benchmarking exercise is the isothermal flow experiment carried out in a recovery boiler model of Babcock & Wilcox design. Details of the experimental set-up can be found in Ajersch (1995).

The model is a 1:28 scale model of a recovery boiler located in a Weyerhaeuser mill in Kamloops, British Columbia. The model walls are constructed of 16 mm thick plexiglass, so that laser light can be transmitted freely through to the measurement locations. The three elevations of air injection are included in the model, as well as the sloped furnace floor. The upper section of the furnace model includes the bullnose and

the heat exchangers. A schematic drawing of the model is given in Figure 9. Detailed drawings of the boiler are presented next which are suitable for use in a CFD modeling exercise.

3.2.1 Detailed Geometry

Figure 10 displays a profile of the recovery boiler model showing the positions of different elevations of injection ports, the dimensions of the bullnose, and the locations of the three levels (#1, #2, #3) where LDV measurements were taken. The model boiler has a sloping floor and the primary injection ports are inclined from the front to the back of the model.

Figures 11, 12 and 13 show positions and dimensions of the primary, secondary and tertiary injection ports, respectively. Due to the numerous primary ports that are present, their positions can only be schematically illustrated in Figure 11. Detailed locations of individual ports can be found in Figures 14(a) and (b), which are drawings of the aluminum templates used for crafting the orifices.

The 174 primary air ports are nearly evenly distributed around the perimeter of the furnace. At the secondary air elevation, four ports are located on the front and back walls, and five on the left and right. Also included at this elevation are the two large starter burners on each of the front, left and right walls. The tertiary air is distributed in an interlaced fashion, with four ports on the front wall and five on the back.

3.2.2 Experimental conditions and flow measurements

The experiment considered was as follows: the total volume flow rate through the model was set to 570 L/min, and the flow was through primary and secondary ports only. Approximately 40% of the flow is diverted to the primary ports and the rest to the secondary ports; there was no tertiary injection.

The flow system for the model was designed such that at the secondary elevation, water is supplied to each port by its own line. At the primary elevation, however, flow to the 174 ports was supplied by only 24 lines, each of which fed a group of 7 or 8 ports. Figure 15 shows the volume flow rates and the momentum fluxes at the primary and secondary levels. From the flow rate figures and the dimensions of each individual

port, a velocity value can be calculated for the flow leaving each port.

Measurements were acquired in three horizontal planes. Each plane was divided into a 6×6 grid of rectangular cells with the measurement locations corresponding to the cell centers. The lower plane was located at the liquor gun elevation, or 175 mm above the secondary ports. The middle plane was located approximately the same distance (177 mm) above the tertiary ports. The upper plane was located 445 mm above the tertiary ports, so as to evenly space the three planes along the boiler's vertical axis. These three planes are referred to as levels 1, 2 and 3, respectively (shown earlier in Figure 10).

As a first order verification of the LDV measurements, the total flow through a horizontal cross-section was calculated by summing the individual measured flows through each cell in the 6×6 grid. A volume flow rate was calculated for each of the measurement levels with the results summarized in Table 3.1.

Location	Set bulk flow across the level [L/min]	Measured bulk flow [L/min]	Percent error in measurement
Level 1	570	754	+32%
Level 2	570	641	+12%
Level 3	570	656	+15%

Table 3.1: Measured vs. set bulk volume flow rate

The general disagreement may be attributed to the following factors:

1. The measurement grid is rather coarse and may not well represent some of the lower velocity regions.

2. Turbulence levels, in particular at level 1, are high, and may lead to significant errors in flow statistics.

3. Operation of the LDV data acquisition equipment with less than extreme care may have led to a systematic filtering of signals corresponding to low velocity measurements.

At higher elevations, the error is not as significant, and probably has little effect on the information retrieved from the data with respect to the observed trends and large-scale patterns in the flow field.

3.2.3 Comparison between experimental and numerical results

Measurements made for the flow field reveals the following general flow feature: there is a strong upward flow core, mostly in the central region, but deflected somewhat towards the rear-left corner. A fairly strong downward flow region exists along the right wall. The downward flow is more pronounced in the front right corner. Weak downward flow was also measured in the front left corner.

Figure 16 shows the distribution of the upward velocity component at level 1, above the secondary elevation. There is upward flow close to the left side wall, and downward flow along the right wall, closer to the front wall. The small circles on the left image indicate the 6 by 6 measurement grid. The upward flow core closer to the left side can be seen. The computed and the measured fields are quite similar. Figure 17 shows the vertical velocity distribution at level 2. Similar features in the flow fields can be seen; that is, upward flow in the rear left half of the model, and downward flow in the front right half. Figure 18 shows the velocity distribution at level 3, under the bullnose. Similar velocity fields are found for both cases, with upward flow in the rear left side and downward flow in the front right side.

3.3 Validation of hot flow model

The UBC hot flow model is validated against the experimental data collected by IPST for an operating recovery boiler of ABB-CE design. This case is designated as hot flow case 1 and information on furnace geometry and the operating condition during the test is presented in the Appendix. The chief sources of air were through the lower primary ports and the secondary ports. A small amount of air was leaking into the furnace through the liquor gun ports while the upper primary ports were permanently sealed off.

From the given data on furnace geometry, jet velocity and black liquor characteristics, a CFD model for the boiler operation was constructed. Individual primary jets

were not modeled while equivalent slot representation was used. The char bed was modeled as having a parabolic shape symmetrically located in the boiler with a maximum height of one meter. Bed chemistry and fume production were ignored in the modeling study. The tube banks constituting the superheaters and steam generator located in the upper furnace were modeled by the distributed resistance and heat sink method mentioned earlier. In this study, the changes in steam side temperature were not calculated. Instead, the fluid inside the superheater and steam generator tubes were assumed to have a constant temperature of 680 K.

Figure 19 shows the velocity field in the vertical plane 4 m from the left side of the boiler. The velocity distribution shows a strong upward flow core formed through the deflection of primary jets by the bed. This core was however disrupted by the secondary jets which were injected diagonally from the four corners. Above the secondary elevation an upward flow core was formed again and the flow was biased towards the front side of the boiler. The flow at the bullnose elevation and above was quite uniform.

Figure 20 shows the temperature distribution in the same vertical cross-section. The highest temperature is in the vicinity above the bed. As the flow progresses upward towards the upper heat exchanger section, the temperature gradually reduces due to the lower tube bank temperature specified in the study. The temperature values listed in Table 3.2 were estimated from the calculated temperature field and compared very well to the experimental data obtained.

Location	Measured Ave. Temp., °C	Computed Temp., °C
Bullnose (near tip)	985	1000
Primary Superheater (at 36.3 m elevation)	714	800
Boiler Bank Inlet (at 36.3 m elevation)	595	640

Table 3.2: Upper furnace gas temperatures

Figure 21 shows the oxygen concentration in the same vertical plane. The average concentration of O_2 in the upper furnace is seen to be between 7% and 12%. This compares favorably with the measured O_2 concentration of 8.6% at the boiler stack.

Figures 22, 23 and 24 show the detailed flow patterns at the liquor gun elevation, secondary elevation, and below bullnose elevation, respectively. The small amount of air leaking into the boiler through the liquor guns is seen in Figure 22, where the upward flowing core is also apparent. At the secondary elevation, the flow field is dominated by the injection of four strong corner jets aiming towards the center of the furnace. The result of this injection scheme is that the high velocity center core is temporarily eliminated. The upward velocity value in the center at the secondary elevation is quite moderate at about 5 m/s. The effect of the secondary injection scheme causes a counter-rotating flow pattern in horizontal planes higher up in the furnace as seen in Figure 24. The vertical velocity component increases gradually from the perimeter to the center of the furnace.

The CFD model also gives the distribution of carryover particles as shown in Figure 25. The figure shows the carryover distribution at the superheater entry plane. Each open circle on the graph represents a computational particle that was entrained by the upward flow to enter the superheater region. The size of the symbols is proportional to the average diameter of the computational particle. A high concentration of these carryover particles indicate the location where plugging of the convective section is likely to occur. In this case, the particles are quite evenly distributed across the plane, with larger particles concentrated more in the lower half and smaller particles in the upper half.

Many additional flow tests had been carried out by the UBC group for the hot flow modeling of recovery boilers. The technical paper by Matys et al. (1995) presents a numerical study on different air input configurations for a generic recovery boiler model. The results showed that modifying the secondary and tertiary air inputs can change significantly the temperature and mechanical carryover distributions which affect the plugging rate of a boiler. Many other variations are possible and are currently being investigated by the UBC group.

Chapter 4

Technology Transfer

A number of considerations were taken into account in the development of a technology transfer plan for the UBC recovery boiler model. Some of these include:

1. The model has been developed under significant funding from a number of different agencies (including the US DOE, CANMET NRCan, Industry Canada, NSERC, BC Science Council, UBC internal funding and Weyerhaeuser) and therefore ownership of the model cannot simply and easily be transferred to any single external funding agency.

2. The model requires continuous development as new and better CFD methods and sub-models become available.

3. The model is very complex and requires the attention of knowledgeable and experienced users both to obtain converged solutions, and to interpret the solutions.

4. The size of a single output file can be of the order of 100 megabytes, and hence post processing and possible animation of the results is not a trivial task.

5. The modeling expertise of the potential users covers a wide range. Potential users may include CFD modeling specialists who would like to use the code themselves and only require limited assistance. There are also potential users who may have an engineering background but no CFD modeling expertise. These users would like to use the final results, with somebody else doing the modeling work.

6. Confidentiality is an important issue to some industrial clients.

UBC, as an educational institution, is not suitable for providing confidential consulting and code maintenance services to industry. UBC has a strong group in the area of mathematical model research and development, and would like to continue to

incorporate state of the art solution techniques and sub-models into the code. These fundamental research activities are suited to an educational institution. Many industrial clients do not have large R&D departments, and in order to get this segment of the industry to use the new technology it is necessary to take a pro-active role in its use. In order to address these difficulties UBC has decided to use the following technology transfer mechanism:

1. The basic model development work is being done and will continue to be done at UBC.

2. UBC will retain ownership of the code and the models.

3. UBC has granted a royalty free license to IPST to use the code. As a deliverable of the DOE contract extension, this license will also be extended to include the hot flow code and the global model. IPST will be free to use the code and apply it to industrial problems, however it will not have the right to sub- license the code to third parties.

4. UBC has formed a spin-off company, Process Simulations Ltd. (PSL), and has licensed the code to PSL for industrial application.

Arrangement had already been made for the transfer of code to IPST. A research engineer from UBC spent two months in 1996 at IPST to show the engineers there the techniques involved to carrying out simulations using the code. The hot flow simulation case 1 was the result of the collaboration between UBC and IPST.

References

Abdullah, Z., Salcudean, M., Nowak, P., Xiao, Z., Savage, M., Markovic, C., Uloth, V., and Thorn, P. (1994a), "Initial Validation of a Mathematical Model of Cold Flow in a Recovery Boiler", TAPPI Journal, Vol.77, No.5, pp.149-157.

Abdullah, Z. (1994b), "On the Validation of the Cold Flow Recovery Boiler Model", Presentation at the Weyerhaeuser Yosemite Colloquium on Recovery Boiler Modeling, September 25-29.

Abdullah, Z., Salcudean, M., Gartshore, I. et al. (1995), "Black Liquor Combustion Validated Recovery Boiler Modeling", 1990-1994 Contract Report to DOE.

Ajersch, P. (1995), "Detailed Measurements on a Row of Jets in a Crossflow - with applications", M.A.Sc. Thesis, Department of Mechanical Engineering, University of British Columbia.

Edwards, D.K. (1981), Radiative Transfer Notes, Hemisphere Publishing Co., New York.

Fiveland, W.A. (1988), "Three-Dimensional Radiative Heat Transfer Solutions by the Discrete-Ordinates Method", *J. Thermophysics and Heat Transfer*, Vol.2, pp.J309-J316.

Frederick, W.J., Noopila, T. and Hupa, M. (1991), "Swelling of spent pulping liquor droplets during combustion", *Journal of Pulp and Paper Science*, Vol.17, No.5, pp.164-170.

Grace, T.M., Walsh, A., Jones, A. and Dumnicht, D. (1989), "A Three Dimensional Model of the Kraft Recovery Furnace", Proceedings of the International Chemical Recovery Conference, pp.1-8.

Grace, T.M., Wag, K.J., Horton, R.R. and Frederick, W.J. (1994), "Recovery Boiler Modeling: An Improved Char Burning Model Including Sulfate Reduction and

Carbon Removal", Proceedings of the 16th National Industrial Energy Technology Conference, Houston, Texas.

Hackbusch, W. (1992), "Comparison of Different Multigrid Variants for Nonlinear Equations", *Z. angew. Math. Mech.*, Vol.72, No.2, pp.148-151.

Ketler, S.P., Ajersch, P. and Gartshore, I.S. (1994), "Particle Image Velocimetry Investigation of Recovery Boiler Flows", Proceedings TAPPI Engineering Conference, pp.215-224.

Lefebvre, B.E. and Burelle, R. (1988), "The Chemical Recovery Boiler Optimized Air System", TAPPI Notes, Kraft Recovery Operations Seminar, pp.237-244.

Magnussen, B.F. and Hjertager, B.H. (1976), "On Mathematical Models of Turbulent Combustion with Special Emphasis on Soot Formation and Combustion", 16th Symp. (Int'l.) on Combustion, Cambridge, MA.

Matys, P., Sabhapathy, P., Nowak, P., Abdullah, Z. and Salcudean, M. (1995), "Effects of Air and Liquor Delivery on Carryover in a Kraft Recovery Furnace", Canadian Pulp and Paper Association Conference, Parksville, B.C.

Matys, P. (1996), "Numerical Simulation of Black Liquor Combustion in a Kraft Recovery Boiler", Research Report, Department of Mechanical Engineering, University of British Columbia.

Nowak, Z.P. and Salcudean, M. (1996), "Turbulent Flow Calculations by the Nonlinear Multi-Grid Method", *Z. angew. Math. Mech.*, Vol.76, No.8, pp.463-469.

Patankar, S.V. and Spalding, D.B. (1974), "Heat Exchangers: Design and Theory Sourcebook", Scripta Book Co., Washington, DC., pp.155-176.

Sabhapathy, P. (1995), "Radiative Heat Transfer in Kraft Recovery Boilers", Research Report, Department of Mechanical Engineering.

Salcudean, M., Nowak, P. and Abdullah, Z. (1993), "Cold Flow Computational Model of a Recovery Boiler", *Journal of Pulp and Paper Science*, Vol.19, No.5, pp.J186-J194.

Sloan, D.G., Smith, P.J. and Smoot, L.D. (1986), "Modeling of Swirl in Turbulent Flow Systems", *Prog. Energy Combust. Sci.*, Vol.12, pp.163-250.

Tse, D. (1996a), "Investigation of Turbulence Models and Prediction of Swirling Flows for Kraft Recovery Furnaces", Research Report, Department of Mechanical Engineering.

Tse, D., Matys, P., Nowak, P., Abdullah, Z., Salcudean, M. and Gartshore, I. (1996b), "Flow and Heat Transfer Modeling in the Upper Furnace of a Kraft Recovery Boiler", Paper 17a02, Combustion and Heat Transfer in the Forest Products Industry, AIChE Annual Meeting in Chicago.

Vanka, S.P. (1986), "Block Implicit Multigrid Solution of Navier-Stokes Equations in Primitive Variables", *Journal of Computational Physics*, Vol.65, pp.138-158.

Figures

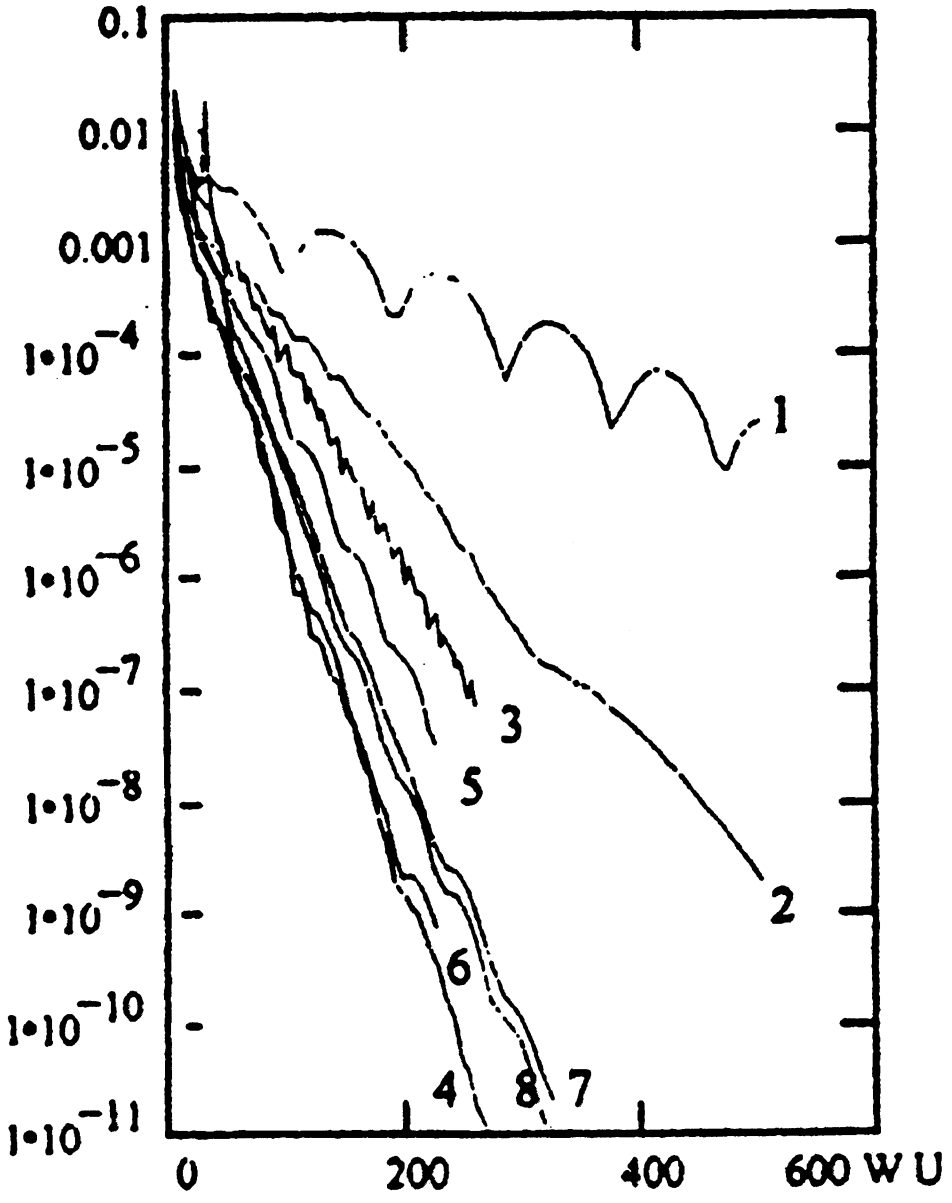

Figure 1: Residues of the continuity equation in various tests (from Nowak and Salcudean (1996)).

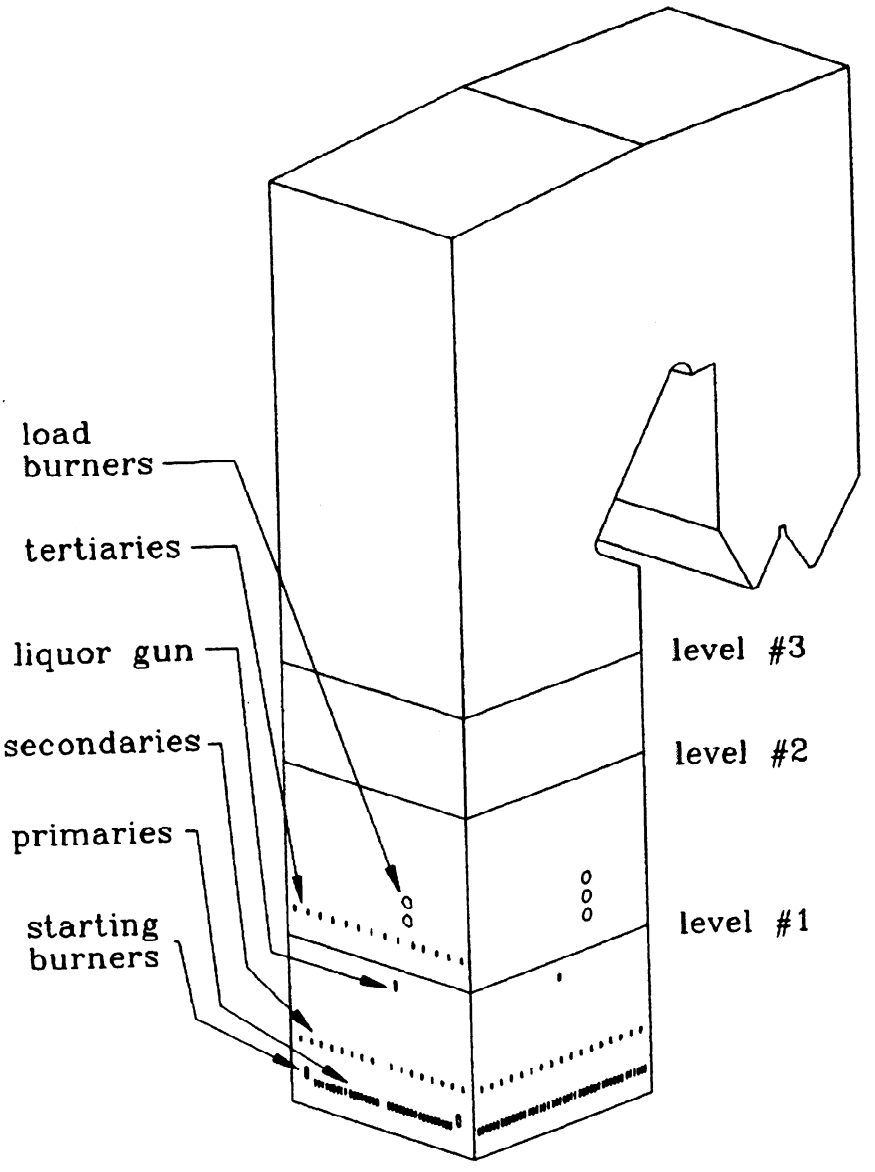

Figure 2: Drawing of the CE recovery boiler model used in the swirling flow experiment.

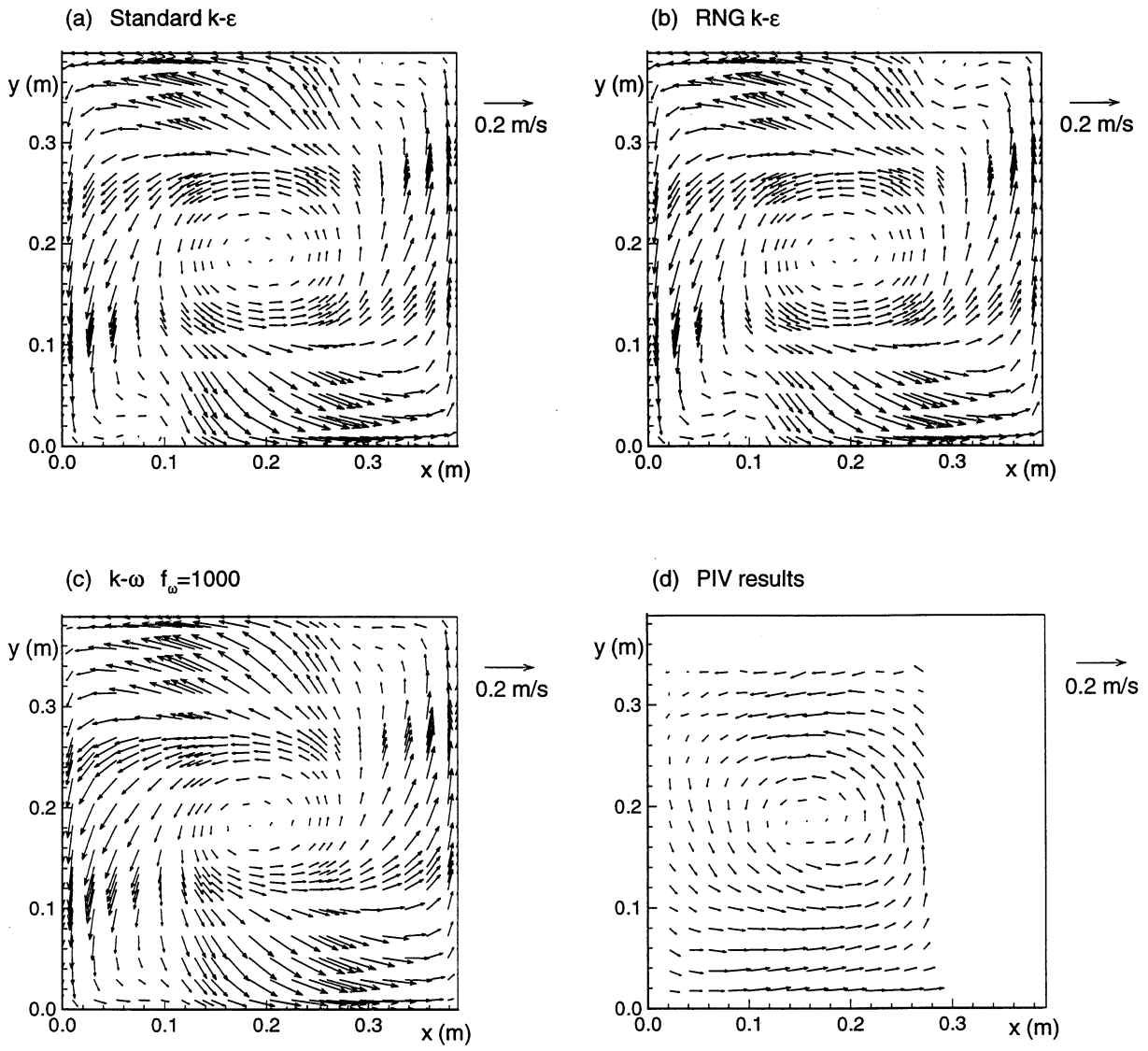

Figure 3: Swirling flow study: velocity distribution at level 1, numerical and experimental results (from Tse (1996a)).

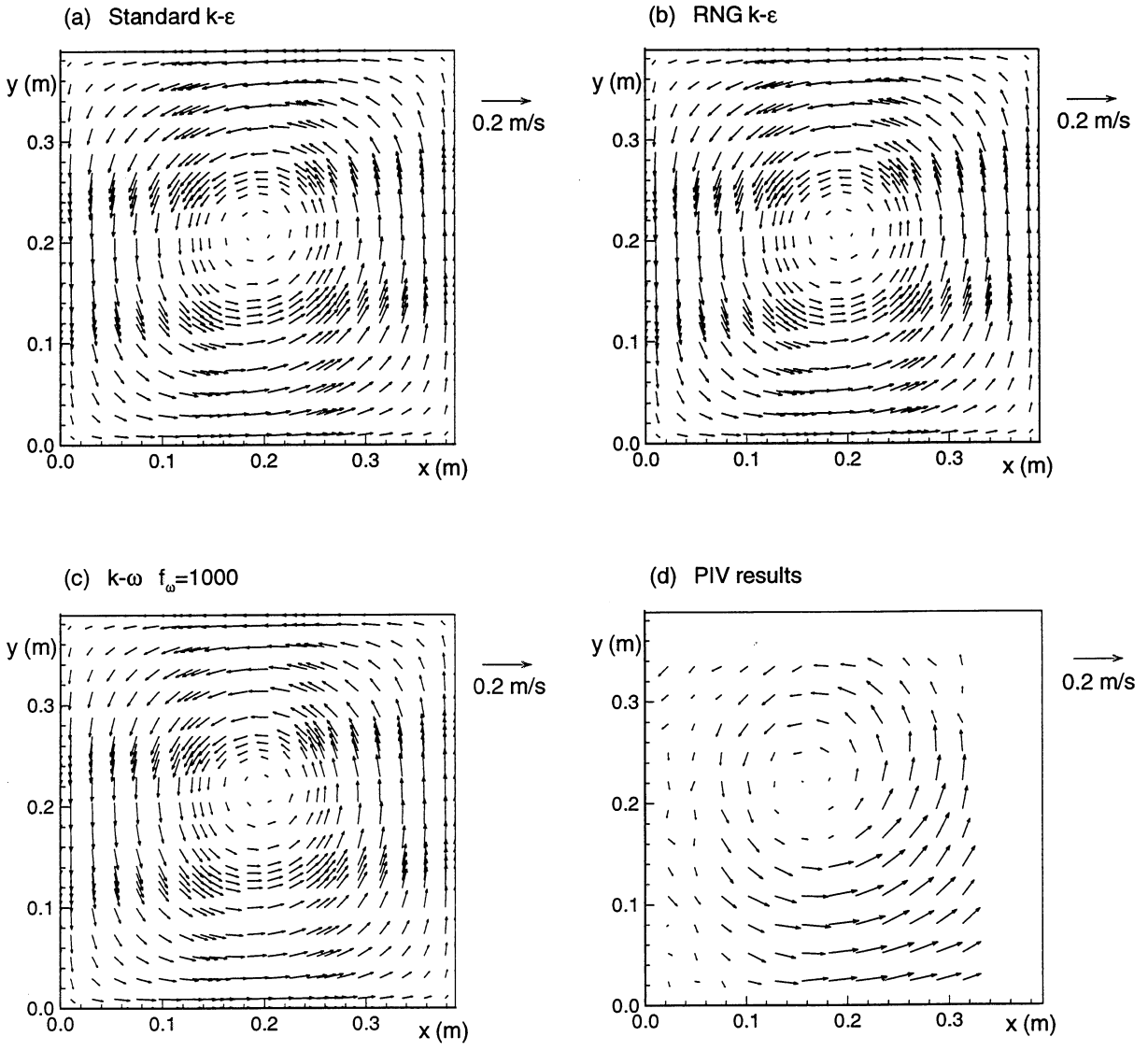

Figure 4: Swirling flow study: velocity distribution at level 2, numerical and experimental results (from Tse (1996a)).

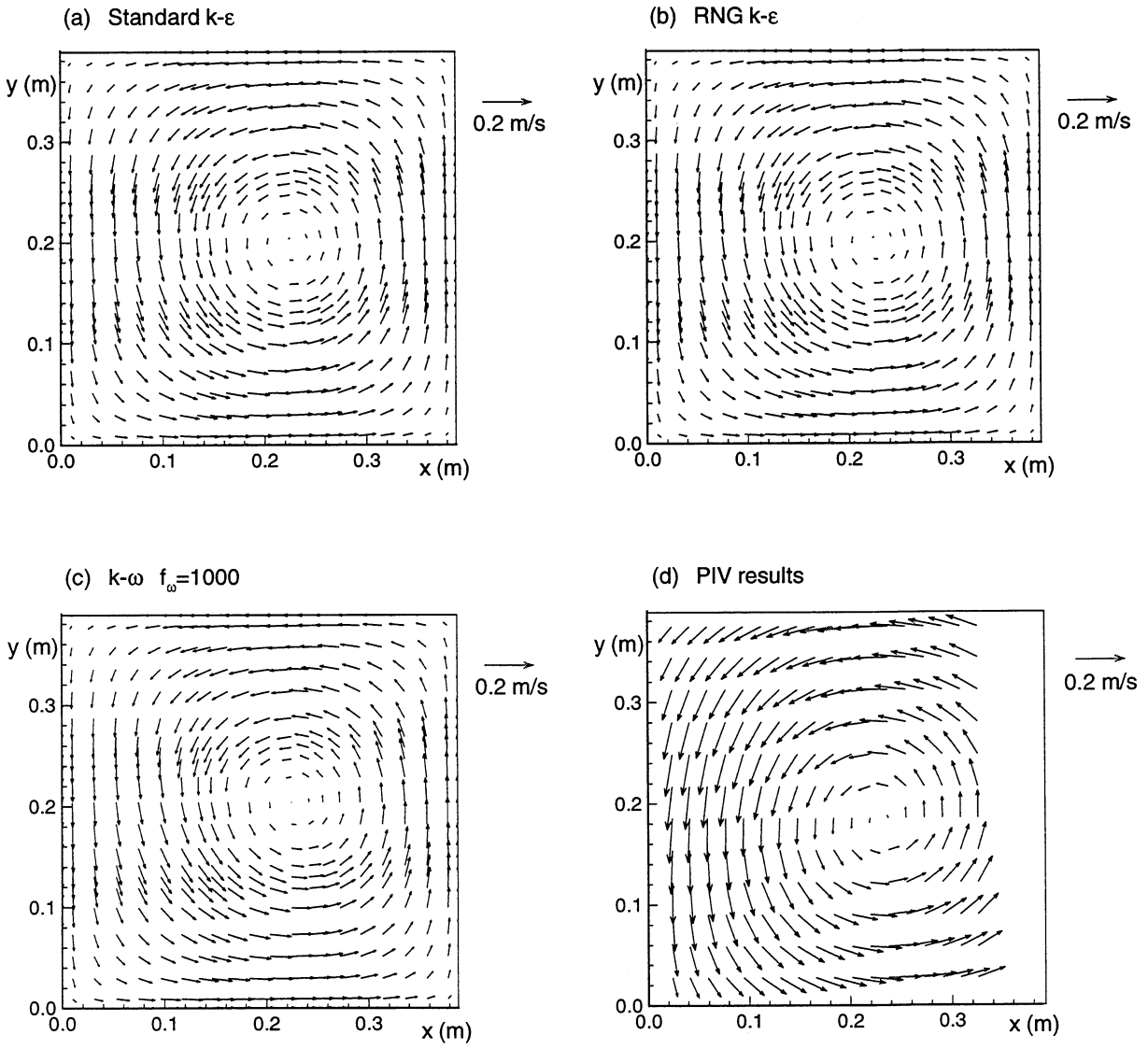

Figure 5: Swirling flow study: velocity distribution at level 3, numerical and experimental results (from Tse (1996a)).

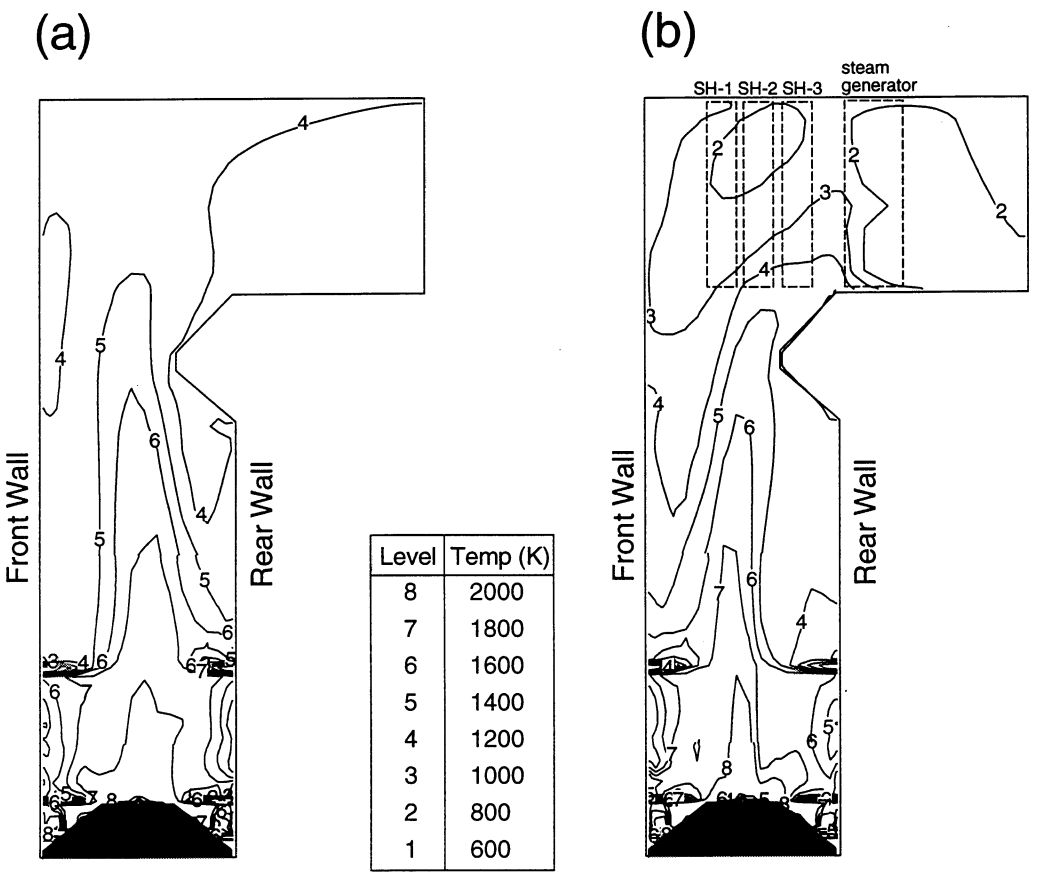

Figure 6: Temperature contours in the front-rear vertical central plane: (a) No tube banks, (b) With tube banks. Locations of tube banks are shown in dashed lines in graph (b) (from Tse et al. (1996b)).

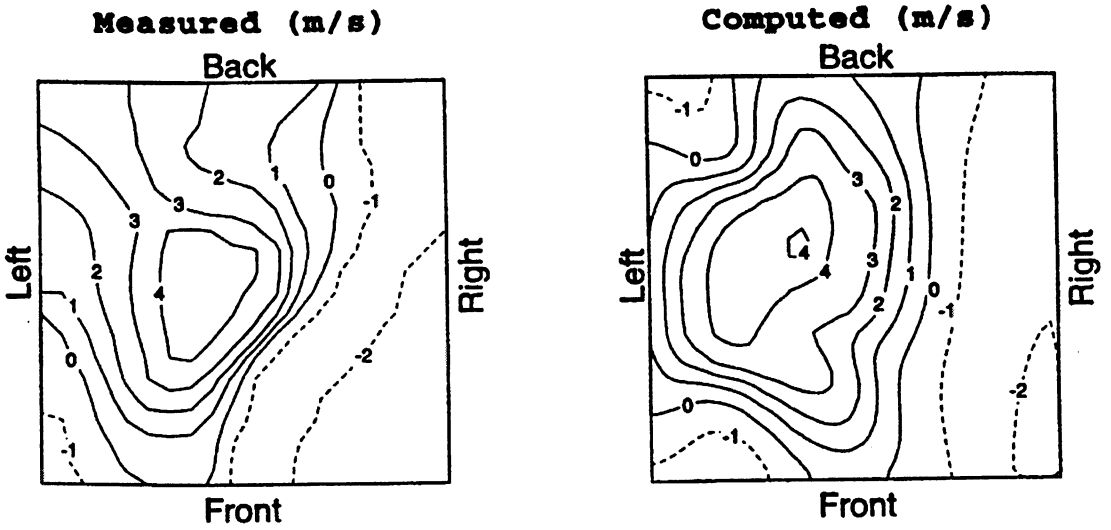

Figure 7: Measured and computed vertical flow (in m/s) at the liquor gun elevation for the recovery boiler at Kamloops. Both primary and secondary ports are open (from Abdullah et al. (1995)).

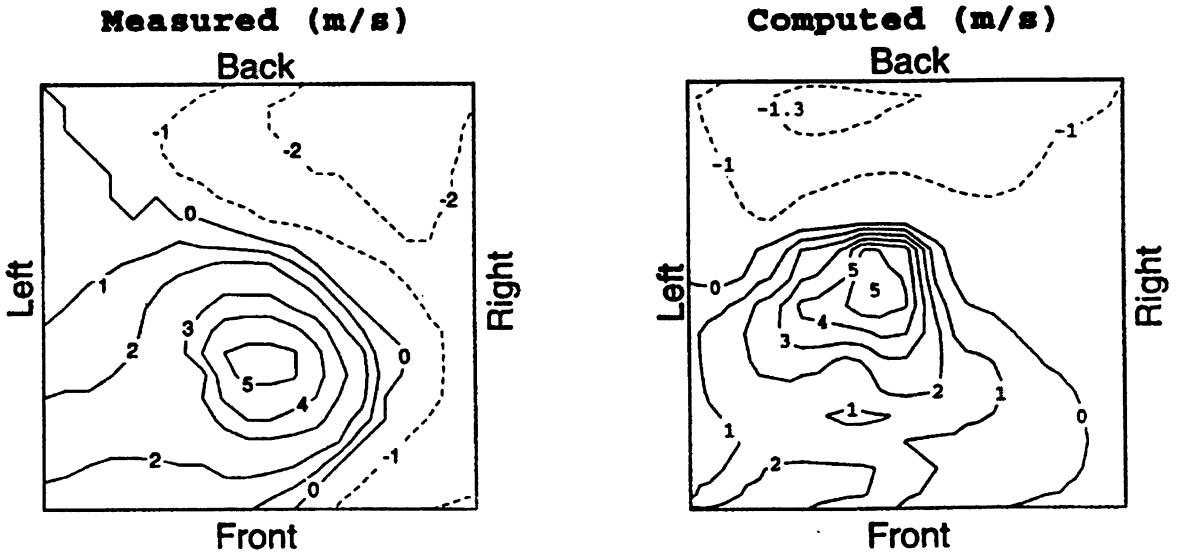

Figure 8: Measured and computed vertical flow (in m/s) at the liquor gun elevation for the recovery boiler at Kamloops. Only secondary ports are open (from Abdullah et al. (1995)).

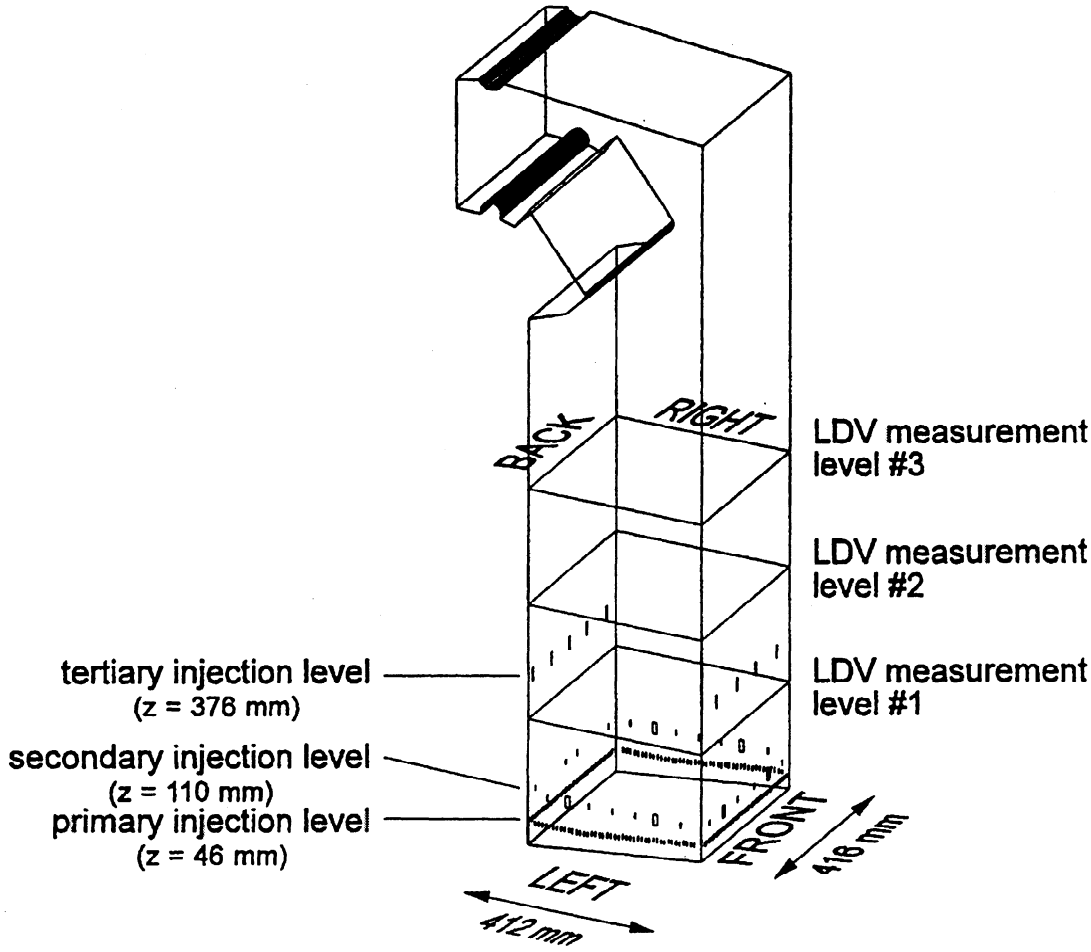

Figure 9: Schematic drawing of the Kamloops recovery boiler water model.

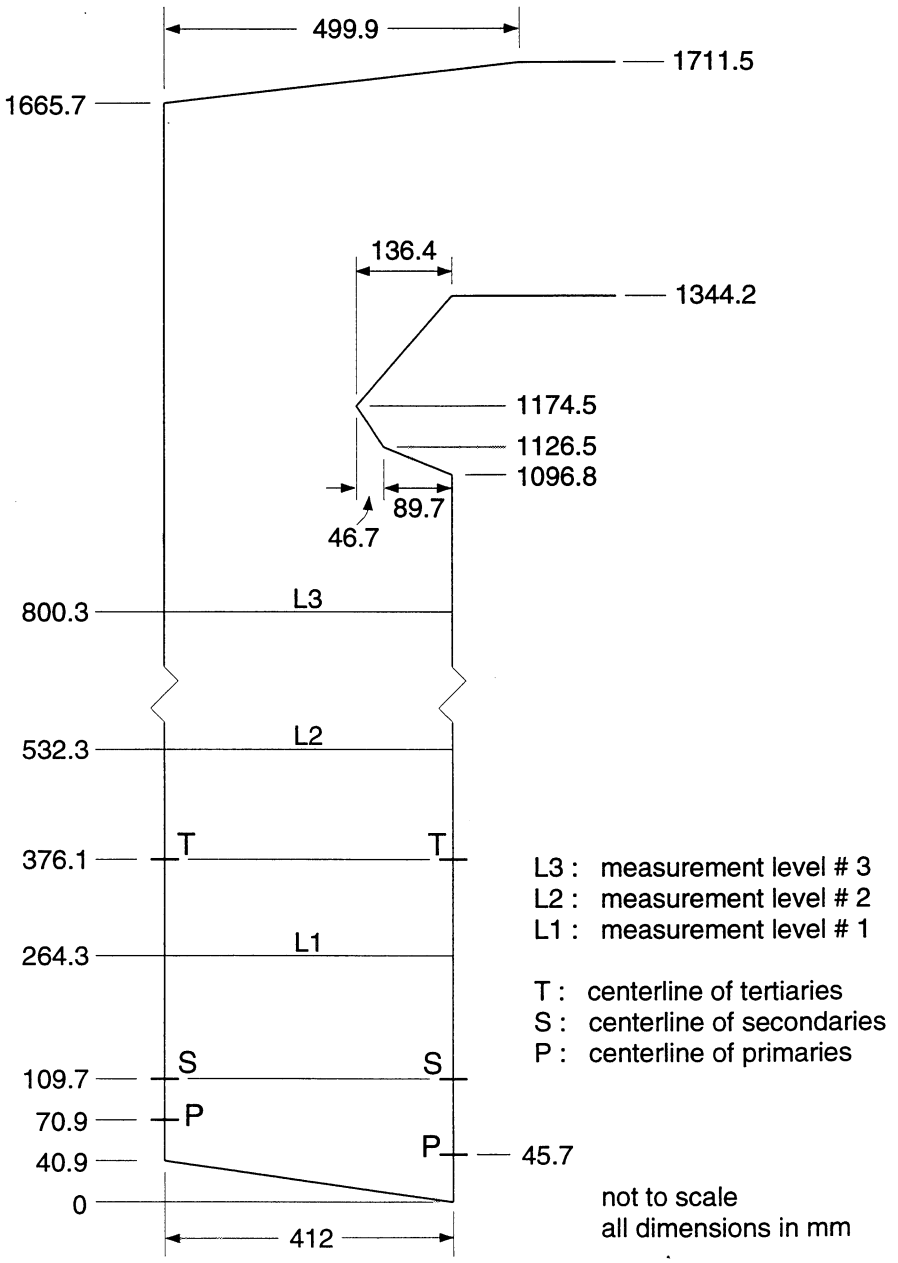

Figure 10: Kamloops boiler water model: vertical cross-sectional profile.

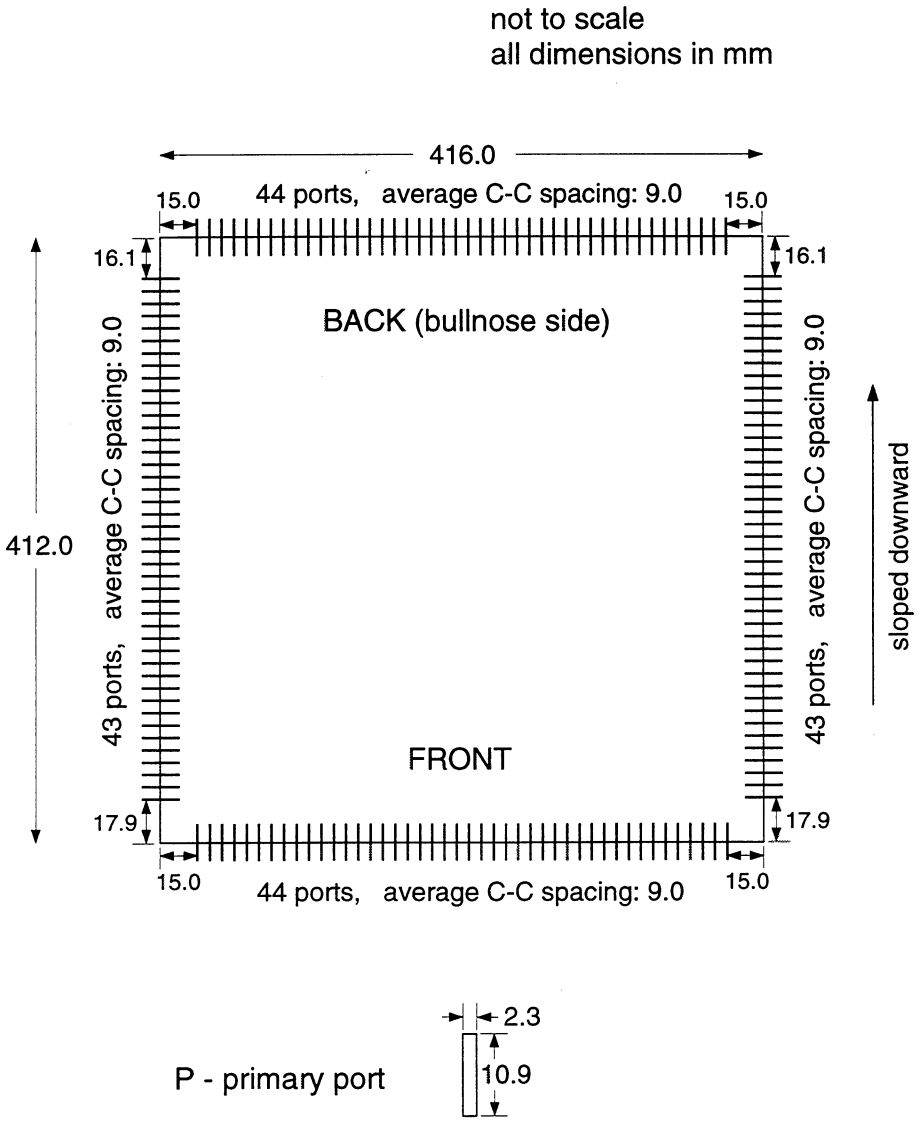

Figure 11: Kamloops boiler water model: locations of primary ports.

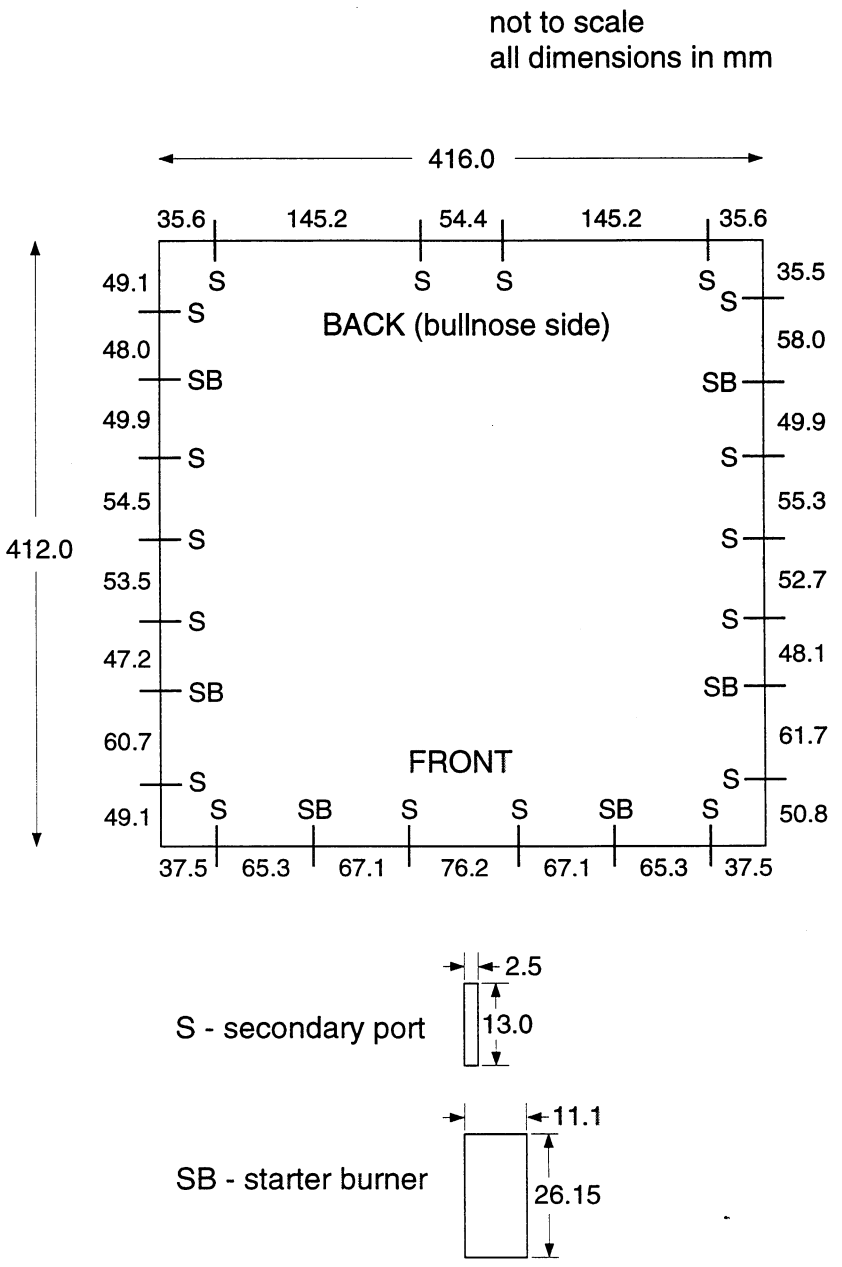

Figure 12: Kamloops boiler water model: locations of secondary ports.

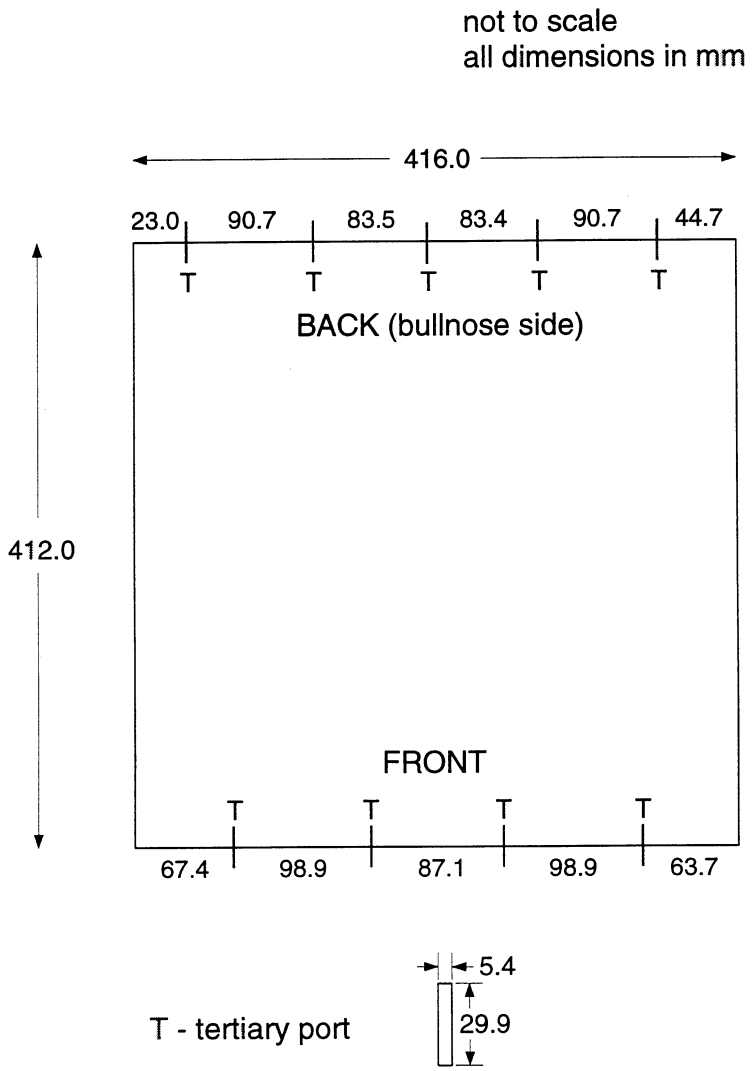

Figure 13: Kamloops boiler water model: locations of tertiary ports (closed in the benchmark experiment).

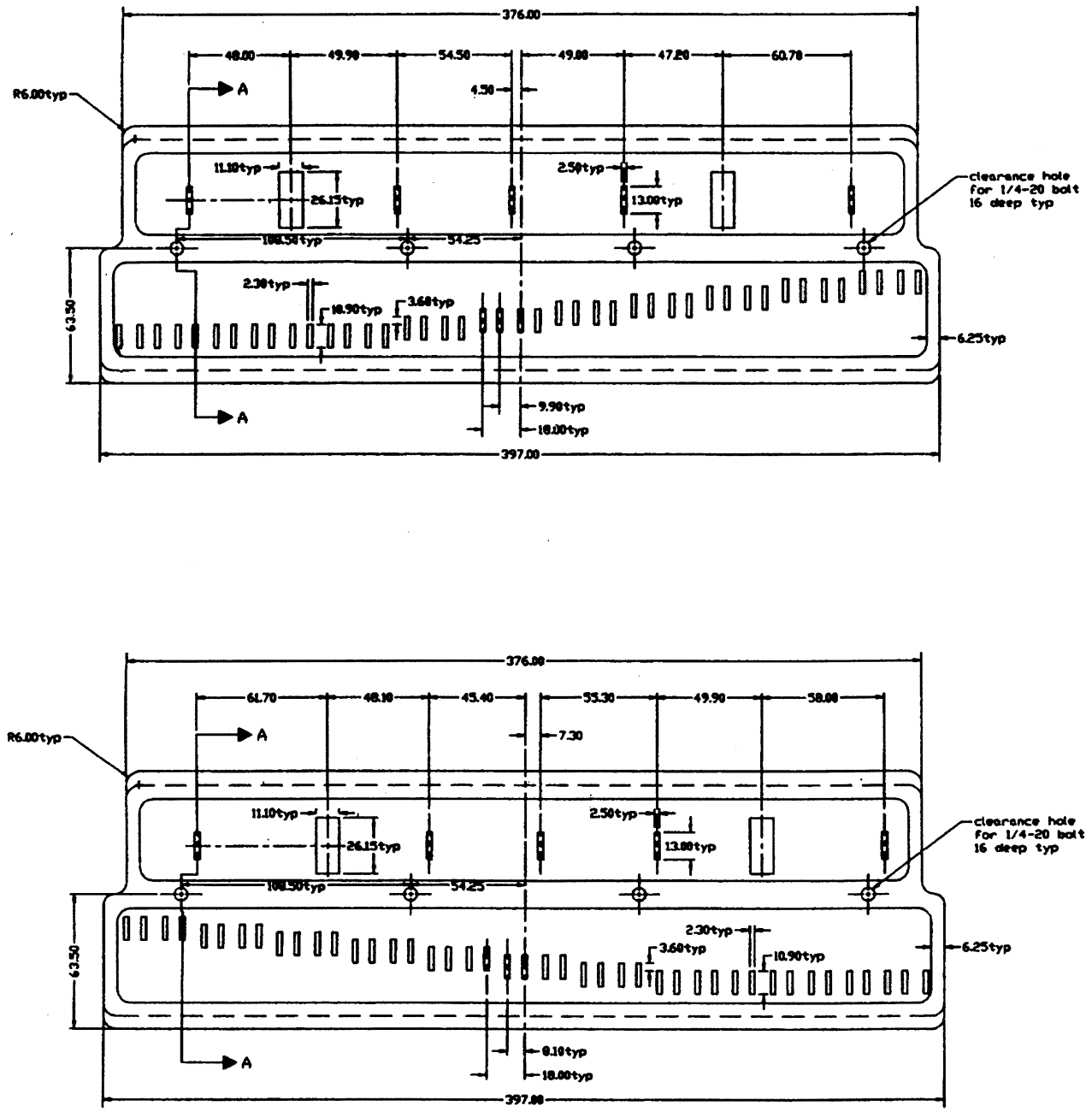

Figure 14(a): Templates used for primary and secondary ports for the Kamloops model. Top: left side; Bottom: right side.

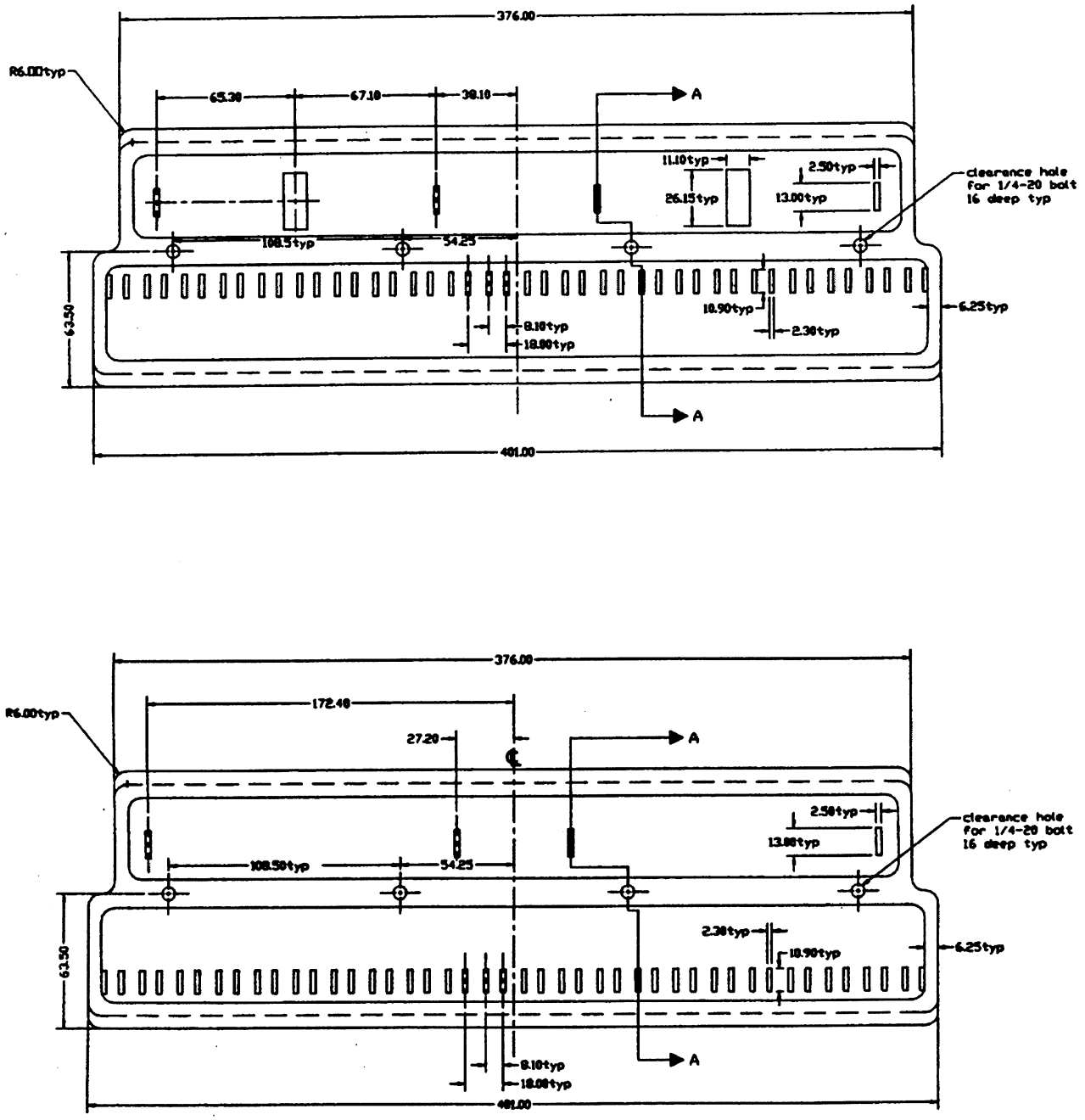

Figure 14(b): Templates used for primary and secondary ports for the Kamloops model. Top: front side; Bottom: back side.

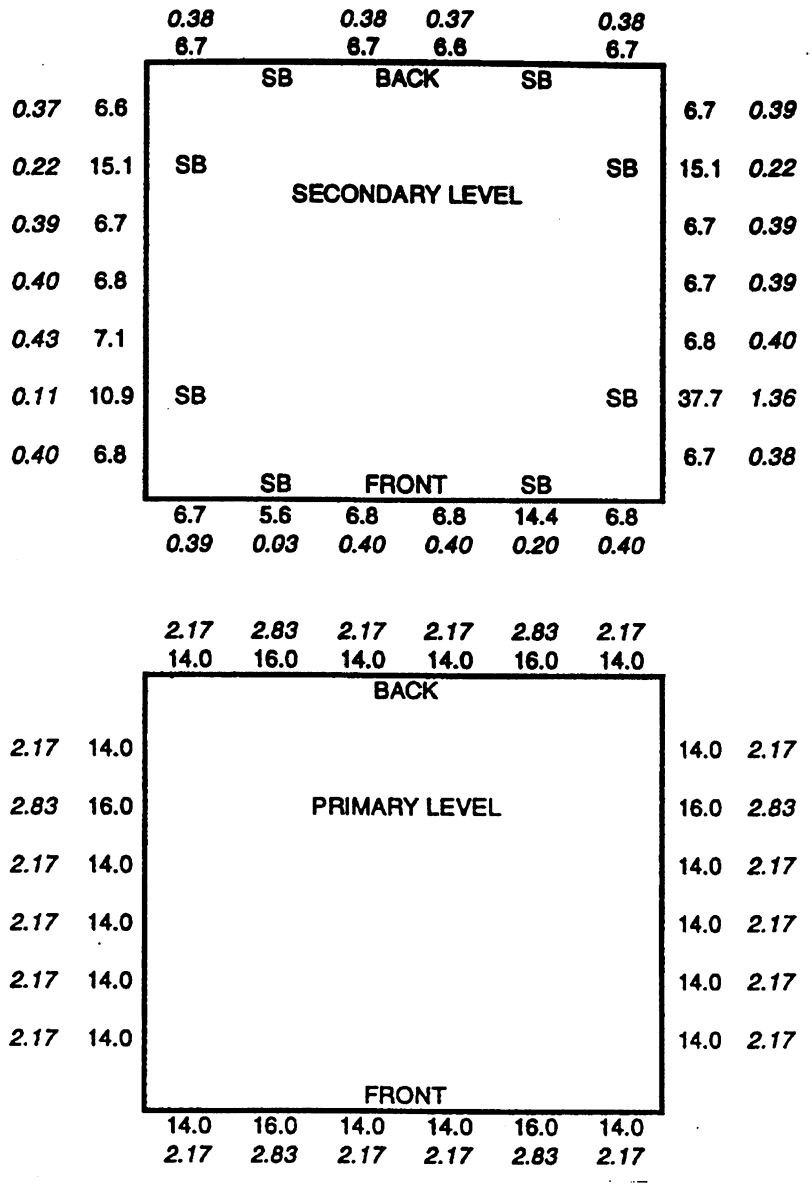

Figure 15: Experimental volume flow rates (normal text) and momentum fluxes (italic text) at the primary and secondary elevations. SB denotes 'starter burner'.

Figure 16: Measured and computed vertical velocity contours at level 1 for the Kamloops water model.

Figure 17: Measured and computed vertical velocity contours at level 2 for the Kamloops water model.

Figure 18: Measured and computed vertical velocity contours at level 3 for the Kamloops water model.

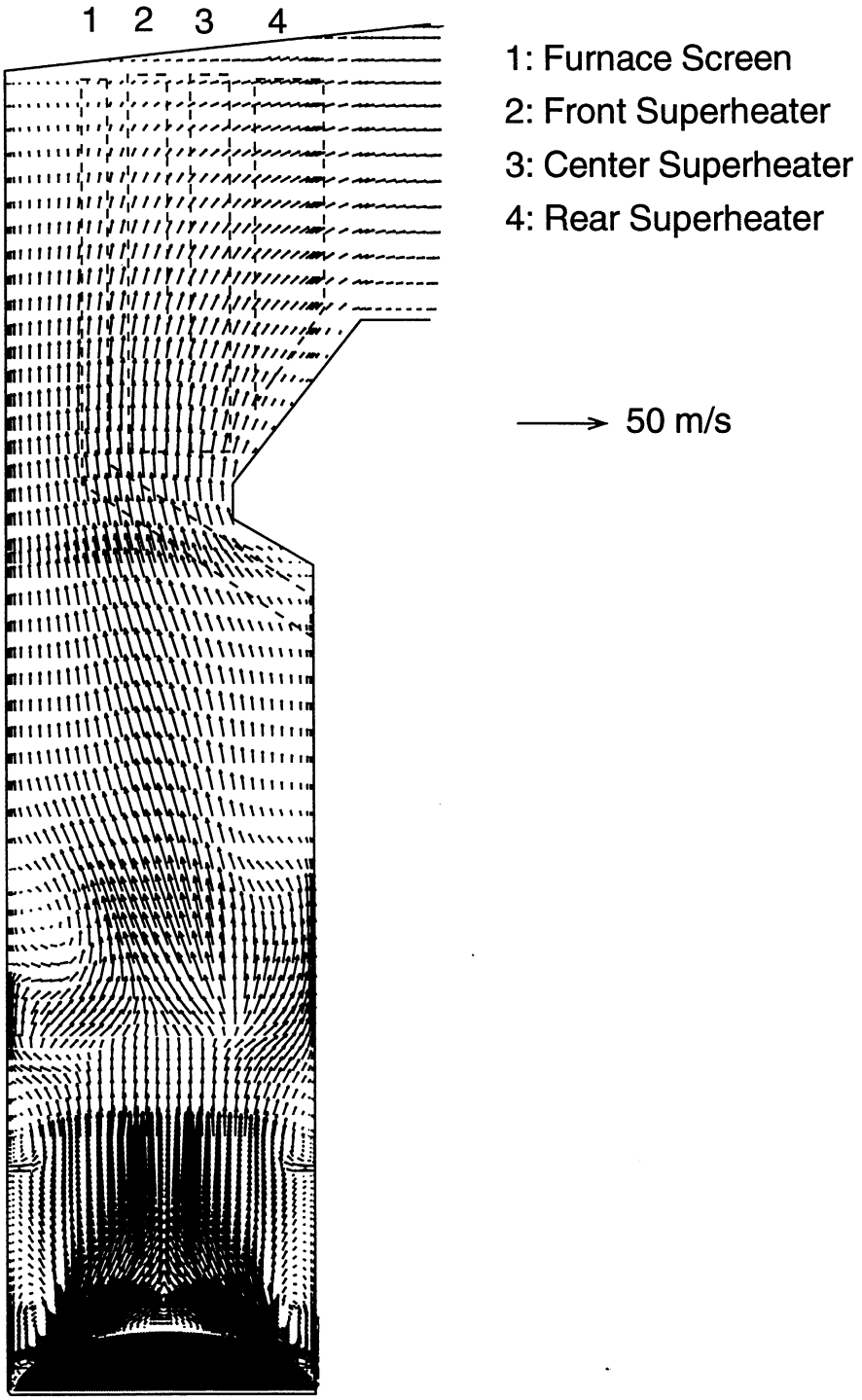

Figure 19: Hot flow case 1: Velocity vector field in the front-rear vertical plane 4 m from the left wall. Locations of tube banks are shown in dashed lines.

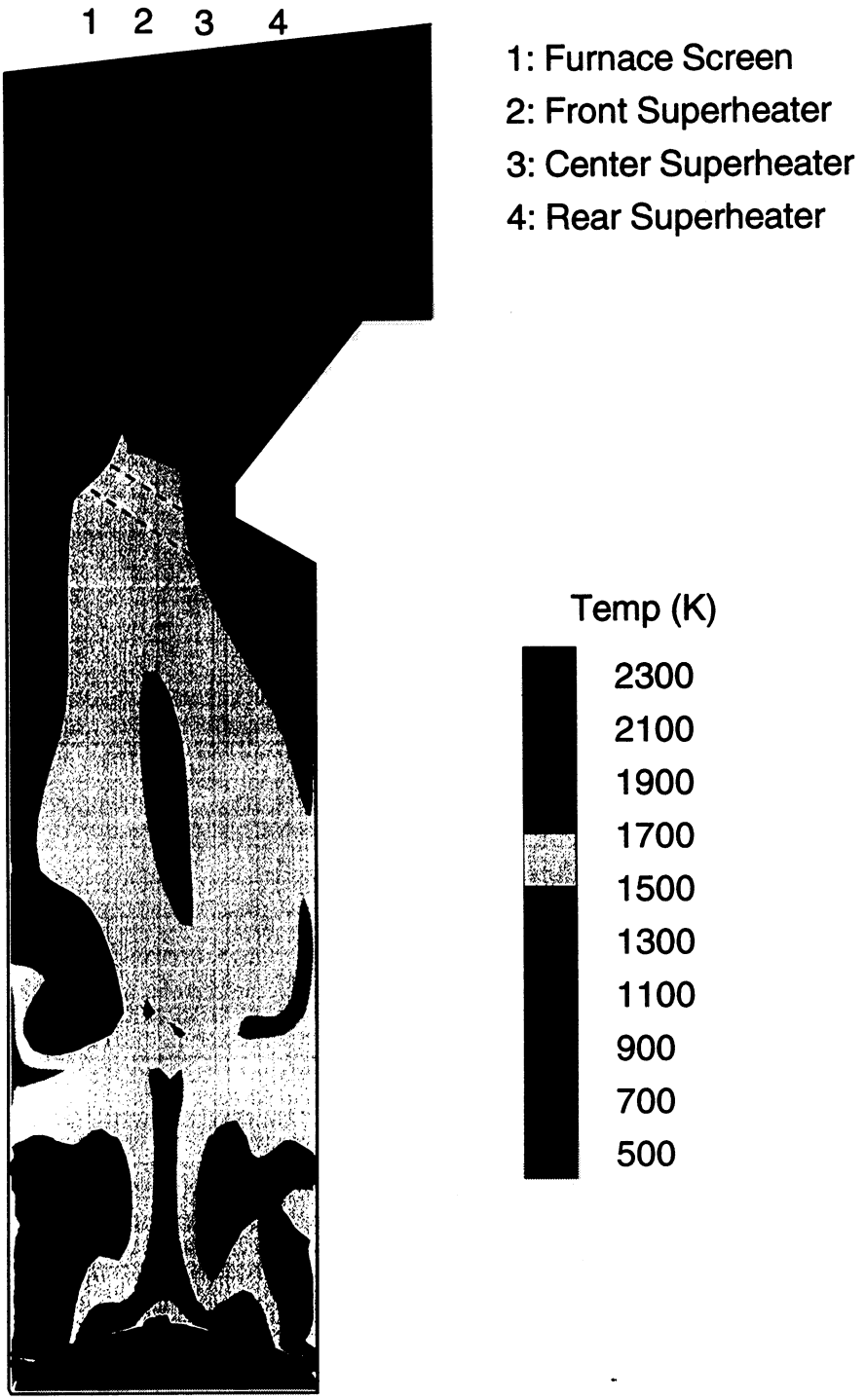

Figure 20: Hot flow case 1: Temperature contours in the front-rear vertical plane 4 m from the left wall. Locations of tube banks are shown in dashed lines.

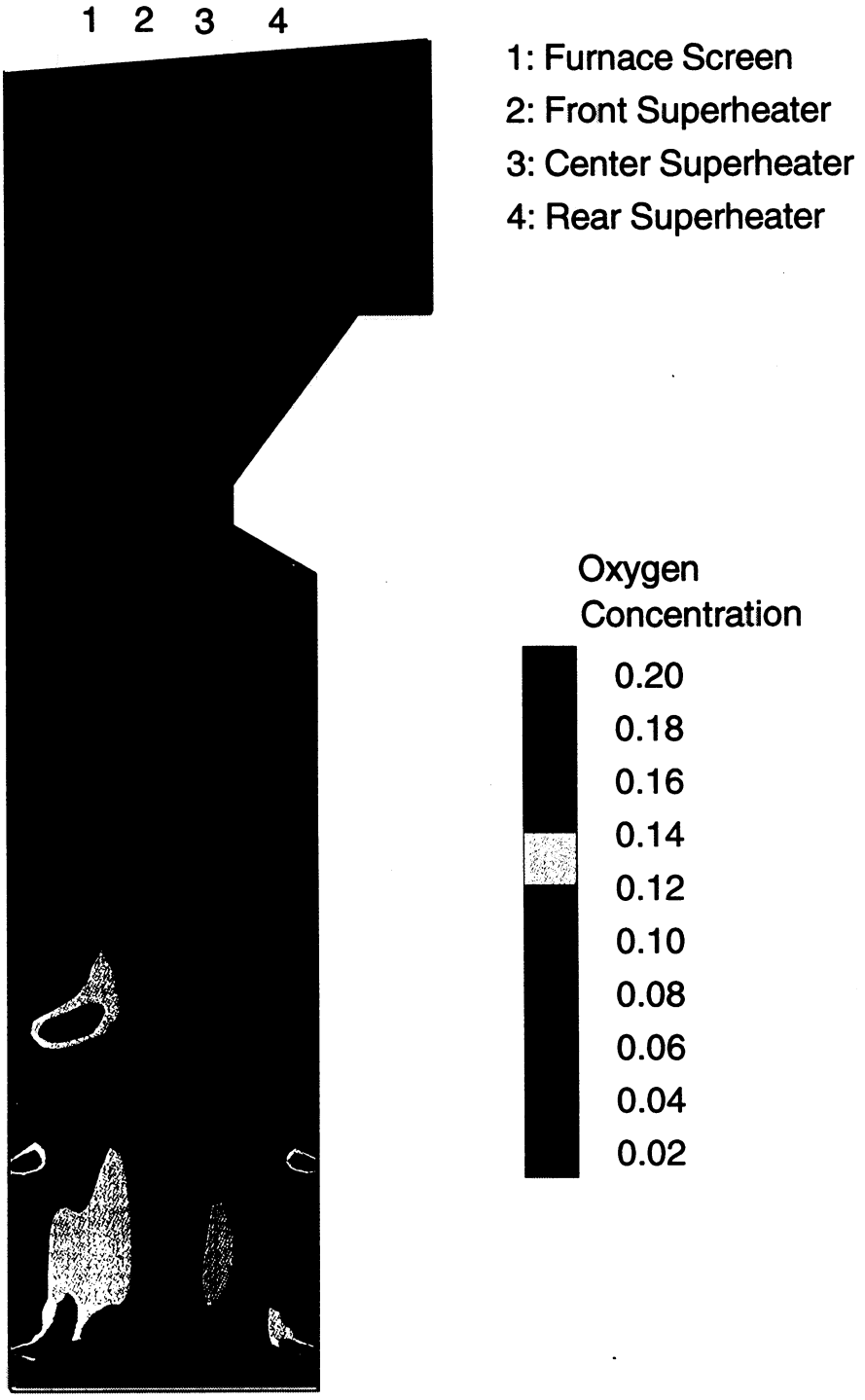

Figure 21: Hot flow case 1: Oxygen concentration contours in the front-rear vertical plane 4 m from the left wall. Locations of tube banks are shown in dashed lines.

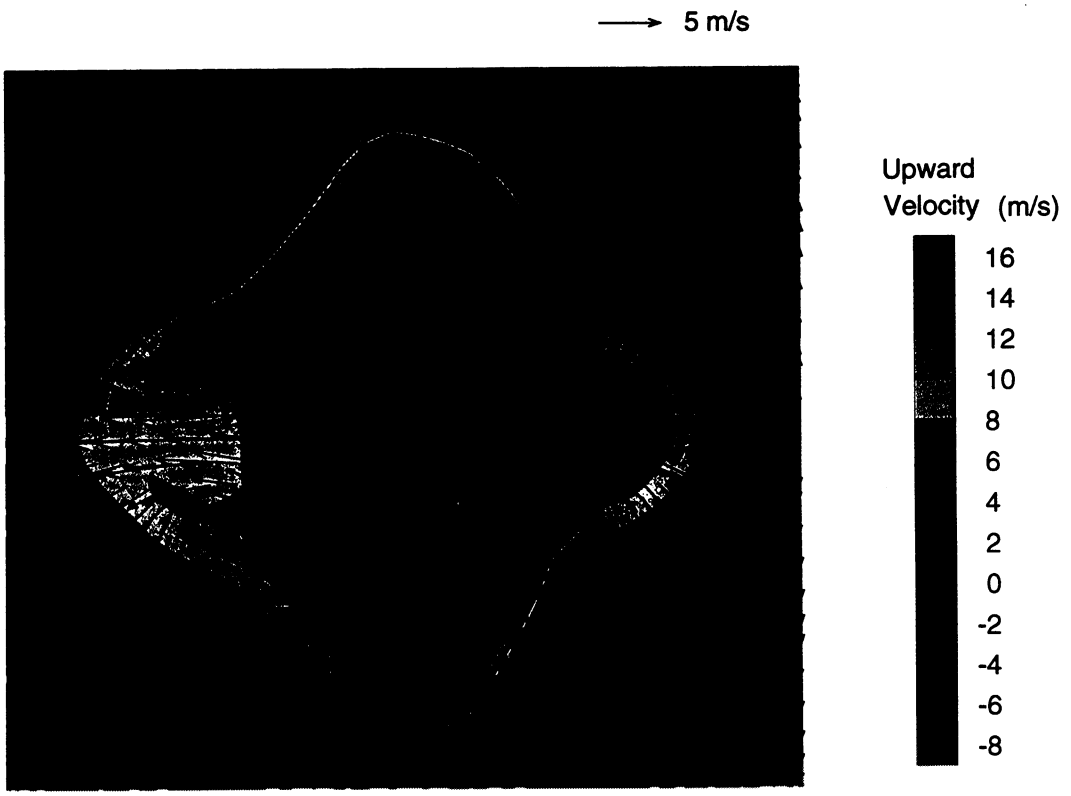

Figure 22: Hot flow case 1: Velocity distribution at the liquor gun elevation.

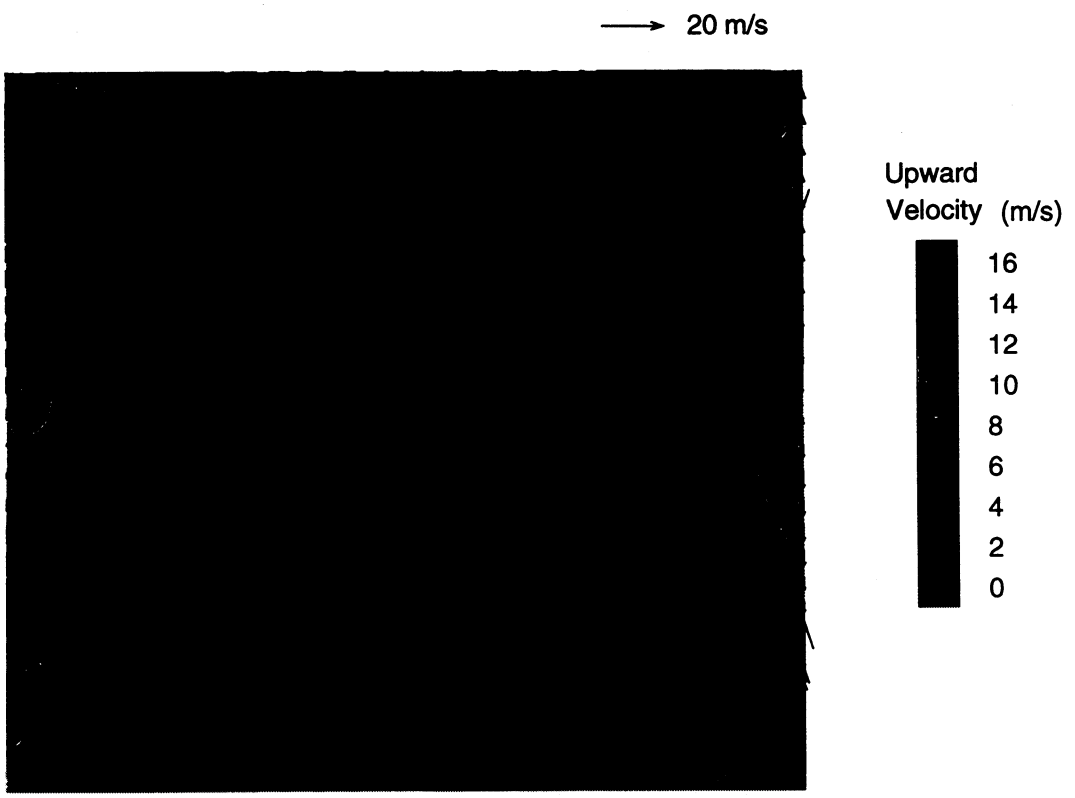

Figure 23: Hot flow case 1: Velocity distribution at the secondary elevation.

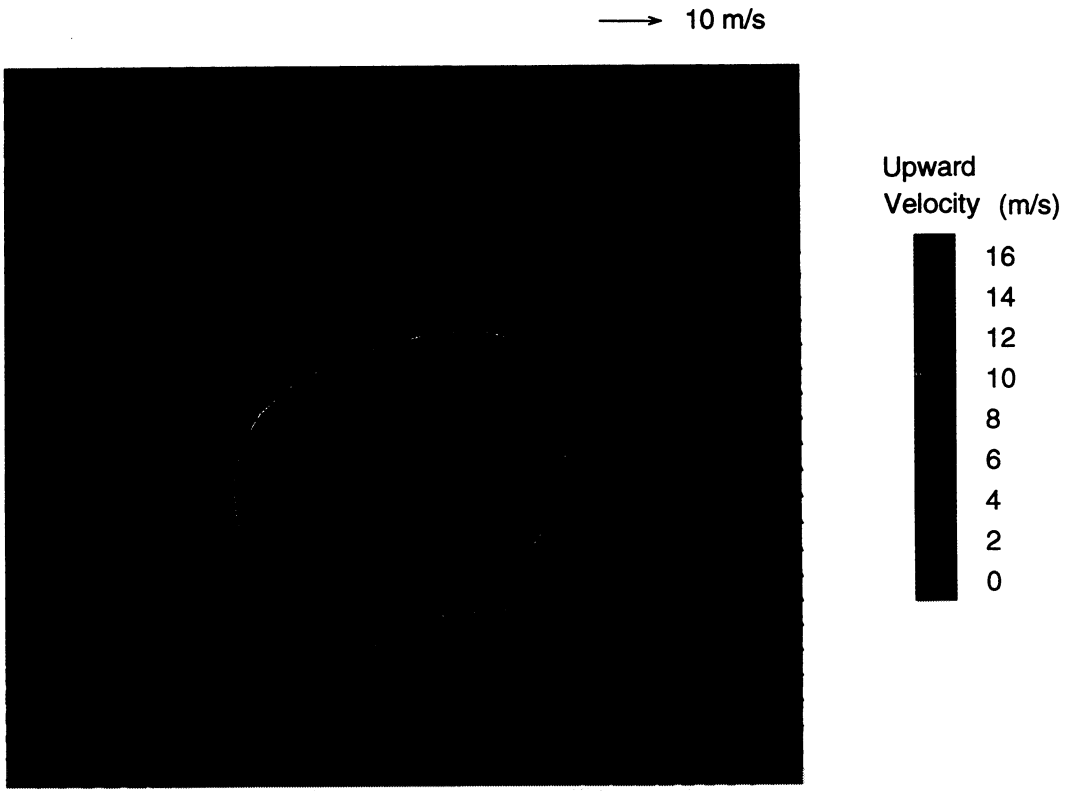

Figure 24: Hot flow case 1: Velocity distribution at the elevation just beneath the bull-nose.

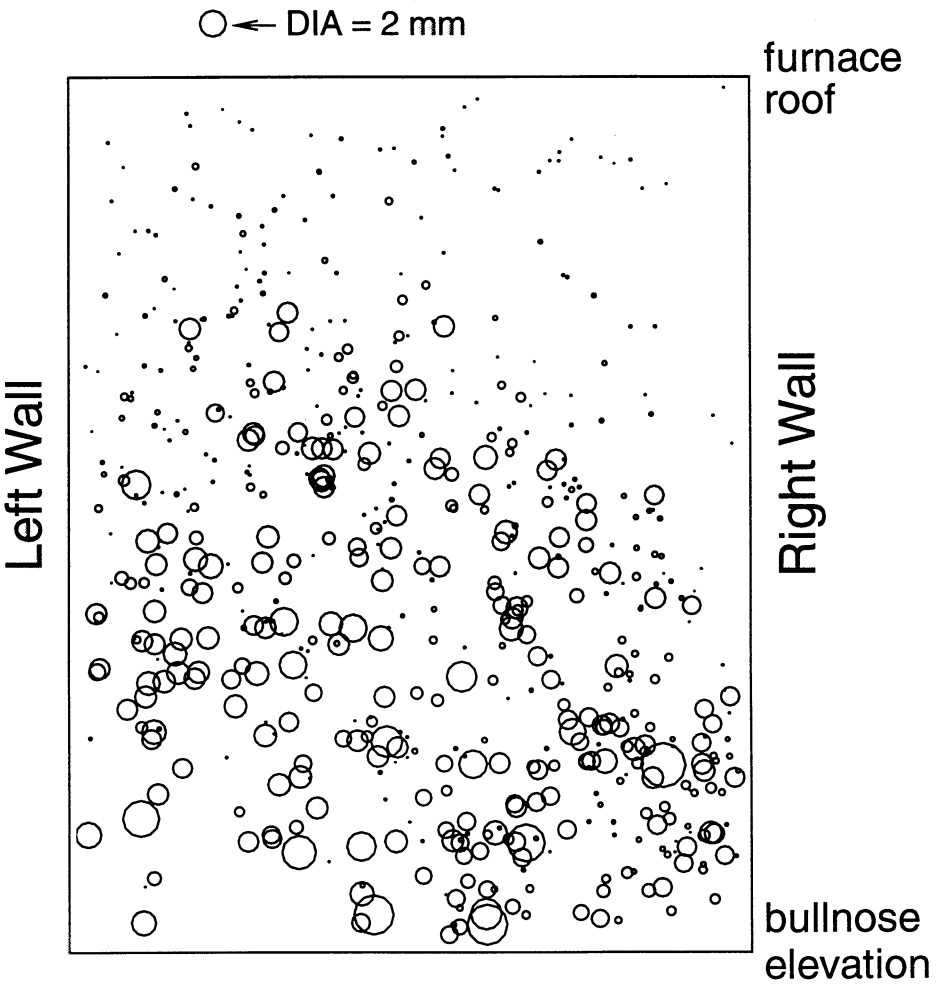

Figure 25: Hot flow case 1: Carryover distribution at the superheater entry plane (vertical plane from the tip of the bullnose to the top).

Appendix

Data for Hot Flow Simulation Case 1

Furnace Geometry Information

Drawings depicting the furnace geometry, and data on the items listed below, are provided in Appendix I, and a summary of the overall furnace dimensions is provided in Table I.

- Nose arch geometry--full definition of shape and dimensions.
- Location and dimensions of primary and secondary air ports.
- Windbox arrangement and air port damper assembly.
- Locations and dimensions of liquor gun ports, burner openings, and other furnace openings where spurious air can enter.
- Furnace screen and superheater tube arrangements, dimensions, geometry, and locations.

Note: the upper primary air ports were not in use during the validation study (the dampers were closed), but they are not permanently sealed off. Since this testing was conducted towards the end of an operating cycle, it is assumed that these ports were completely slagged over.

Table I. Furnace Dimensions

Parameter	Value	Comments
Furnace Orientation	Front = South, Rear = North, Left = West, and Right = East	
(x, y, z) Coordinate System Origin	(0, 0, 0)=Front/Left/Floor corner	Floor elevation = 693' 0"
Overall Dimensions	Distance, in. (m)	
Width	x = 395 (10.03)	
Depth	y = 359 (9.119)	
Height to Roof	z = 1,568 (39.83)	
Height to Nose Arch (bottom/top)	z = 1,025 / 1,064 (26.04 / 27.03)	
Nose Arch Protrusion into Furnace	y = 88 (2.235)	
Port Locations (No. of walls x No. per wall)	Centerline Elevations above Floor, in. (m)	Dimensions (width x height), in.; Total Area, in.^{2}
Smelt Spouts (2x4)	z = 15.63 (0.397)	8 x 12, elliptical; 603
Lower Primary Air Ports (114)	z = 42 (1.067)	1.88 x 6.69; 1,434
Char Bed Cameras; Gas Burners	z = 66.4 (1.686)	Camera angle = 5° downward
Upper Primary Air Ports (4x9)	z = 72 (1.829)	1.88 x 6.0; 406; Not used
Black Liquor Gun Ports (4x4)	z = 262 (6.655)	4.5 x 12; 864
Secondary Air Ports (4x1)	z = 405 (10.29)	See Appendix I; 1,230

Operating Information To Set Up A Simulation

Air

Complete mean values for process data are provided in Appendix II. A summary is provided below.

Table II. Operating Information--Air

Parameter	Value	Comments
Primary air flow	366.0 klbm/hr	
Secondary air flow	304.1 klbm/hr	
Total air flow	670.2 klbm/hr	
Primary air velocities		Data provided in Appendix II.
Secondary air velocities	Not measured	Calculated values given in Appendix II.
Primary & secondary port dampers	Consistently set wide open	Upper primary windboxes permanently blocked off.
Static pressures in windbox	Not measured	Calculated values based on measured velocities given in Appendix II.
Primary air port temperatures	129-133 °C	Range for 9 ports tested (2 or 3 per wall).
Secondary air port temperatures	119-128 °C	Range for all four secondary ports.
Leakage air through burner ports	Not measured	Calculated value given in Appendix II.
Furnace draft	-0.1 in. water	Two taps located on front/east wall, one tap located on front/west wall.

Liquor Firing Conditions

Complete mean values for process data are provided in Appendix II. A summary is provided below.

Table III. Operating Information--Liquor Firing Conditions

Parameter	Value	Comments
Number, location, and type of liquor guns	16 guns (four on each wall); 1.5" Sch. 40 straight pipe	Exact location of gun openings given in furnace drawings in Appendix I.
Nozzle size	ID = 1.61 in.	
Gun tilt angle	15°	
Flow rate to furnace	358.7 gpm	
Temperature	130.3 °C	
Pressure to nozzles	15 psig	Measured from main line before split to individual nozzles.
Solids content (as-fired)	71.3 %	Mean of Computrac off-line values; on-line measurements unreliable.
Initial Drop Velocity	4 m/sec	Guesstimate accounting for liquor flashing
Mean drop diameter	3.25-4.5 mm	Estimated from spraying correlations for V-jet nozzles.
Spray expansion angle	12° total angle of spray cone	Estimated from videos.
Spray distance into furnace		Estimated from videos.
Spread of spray into furnace		Estimated from videos.

Liquor Properties

Table IV. Black Liquor Elemental Analysis

Analyte	Concentration, Wt. %
Total Carbon	35.72
Organic Carbon	35.36
Inorganic Carbon	0.36
Hydrogen	4.15
Oxygen	34.59
Sulfur	4.86
Sodium	17.70
Potassium	3.34
Total	100.35
Higher Heating Value	6,456 Btu/lbm

Table V. Single Particle Combustion Tests

Combustion Phase	Time
Drying (Start to Ignition)	1.9 sec
Pyrolysis (Ignition to Max Volume)	1.5 sec
Char Burning (Max Vol to Smelt Bead)	10.5 sec
Total Combustion	12.0 sec
Swelling Measurements	
Swelling at Ignition	17.39 cc/g
Maximum Swelling	34.38 cc/g
Drop Diameter Ratio	
Diam. at Ignition/Initial Diam.	2.87
Diam. at Maximum/Initial Diam.	3.60

Performance Data to Compare with Simulation Predictions

Steam-side Information

Mean values and plots of hourly averages for: feedwater flow rate and temperature, sootblower flow rate, final steam flow rate, temperature, and pressure, exit temperature for SH#2, inlet temperature for SH#3, inlet pressure for SH#1, outlet pressure for SH#2, and boiler and economizer exit temperatures are presented in Appendix II. A summary is presented in Table IV.

Table VI. Performance Data--Steam Side

Parameter	Value	Comments
Final steam flow rate	535.0 klbm/hr	
Final steam temperature	422.2 °C	
Final steam pressure	899.1 psig	
Superheater #1 inlet pressure	956.2 psig	
Superheater #2 exit temperature	426.3 °C	
Superheater #2 outlet pressure	861.2 psig	
Superheater #3 inlet temperature	389.0 °C	
Sootblower steam flow rate	56.25 klbm/hr	Drawn from the final steam line.
Feedwater flow rate	594.3 klbm/hr	
Feedwater temperature	138.9 °C	
Boiler drum pressure	Not measured	
Boiler exit temperature	378.2 °C	
Economizer exit temperature	217.7 °C	
Attemporator flow rate	Not recorded	
Attemporator temperature	Not recorded	
Heat absorption in furnace waterwalls	No data yet	Still waiting on Alarick

Gas Information (Combustion side)

Table VII. Upper Furnace Gas Temperatures

Location	Low Temp., °C	High Temp., °C	Ave. Temp., °C
Bullnose	970	992	985
Primary Superheater	703	740	714
Boiler Bank Inlet	575	623	595
Boiler Bank Exit	370	388	379
Economizer Exit	199	233	218

From University of Toronto thermoprobe measurements.

Table VIII. Combustion Gas Analysis (Mill Data)

Gas	Concentration	Comments
CO	600-650 ppm	Measured in the stack.
O_2	8.6%	Measured in the stack.
Excess O_2	2.69%	Overall mean value, measured at precipitator inlet; plot of hourly average values in Appendix II.
SO_2, TRS	Not provided	

Gas velocity indications and flow patterns, based on paths taken by suspended particles, must still be determined from the videos.

Upper Furnace Deposit Information

Table IX. Upper Furnace Deposits

Parameter	Value	Comments
Total Dust Production Rate	6,400-8,000 kg/hr	Estimated by Univ. of Toronto to equal internal dust recycle rate: 8 to 10 % kg dust/kg as fired BLS.
Entrained Particle Detector Readings	Not measured	
Deposit Buildups	No data	Mill does not have a fouling problem.

Table X. Upper Furnace Fume Composition

Sampling Location	Na, wt. %	K, wt. %	Cl, wt. %	SO_4, wt. %	CO_3, wt. %
6th Floor--before Screen Tubes	29.6	4.8	1.8	60.1	3.7
6th Floor--after Screen Tubes	28.3	6.4	4.8	57.7	2.8
8th Floor--between Primary & Sec. SH	29.3	6.8	2.2	54.3	7.4
8th Floor--at Generating Bank Inlet	29.3	6.8	2.2	54.3	7.4
Precipitator Dust	29.1	6.8	1.4	56.7	6.0

Char Bed Information

1. Information on bed shape and temperature profile from the Diamond bed cameras.
   We must still determine this from the videos.

2. Thermocouple probe measurements of the bed surface and subsurface temperatures.
   Temperature profiles from thermocouple probe measurements are presented in Appendix III.

3. Composition of material taken from bed surface and/or interior.
   No samples were successfully collected; they burned up during sampling.

4. Smelt composition and temperature data.
   The smelt composition is presented in Table XI. The smelt temperature was not measured.

Table XI. Smelt Composition

Analyte	Concentration, Wt. %
Total Carbon	7.97
Organic Carbon	0.16
Inorganic Carbon	7.81
Hydrogen	0.54
Oxygen	38.52
Sulfur	9.23
Sodium	36.98
Potassium	5.40
Total	98.65

5. Smelt residence time distribution (RTD) from the zinc tracer experiment.
Results of the smelt RTD experiment are plotted in Appendix III and summarized in Table XII.

Table XII. Smelt Bed Residence Time Distribution

Parameter	Value	Comments
Time Constant: East Side/West Side/Mean Value	76 / 63 / 70 min.	Na reference
Composite Time Constant: East+West Sides	78 min.	Na reference
Smelt Bed Depth	8 in.	Na ref.; est. using mean time constant
Zinc Recovery	88% / 107%	Na reference / K reference

6. Reduced digital bed temperature information obtained with the Diamond cameras from Alarick's data acquisition system.
Temperature data for the 48 hour time period of 3/27 through 3/28/96 from the Diamond cameras' Fireside Advisory System (FAS) are plotted in Appendix III. Included below in Table XIII is a summary of the mean char bed surface temperatures for this time period which are based on the "Average" pyrometer readings.

Table XIII. Char Bed Surface Temperatures

Char Bed Camera	Mean Bed Surface Temperature, °C
One: Front/Right (SE) corner	1,087
Two: Rear/Left (NW) corner	1,136

APPENDIX I
Furnace Drawings

Overall Furnace Dim.

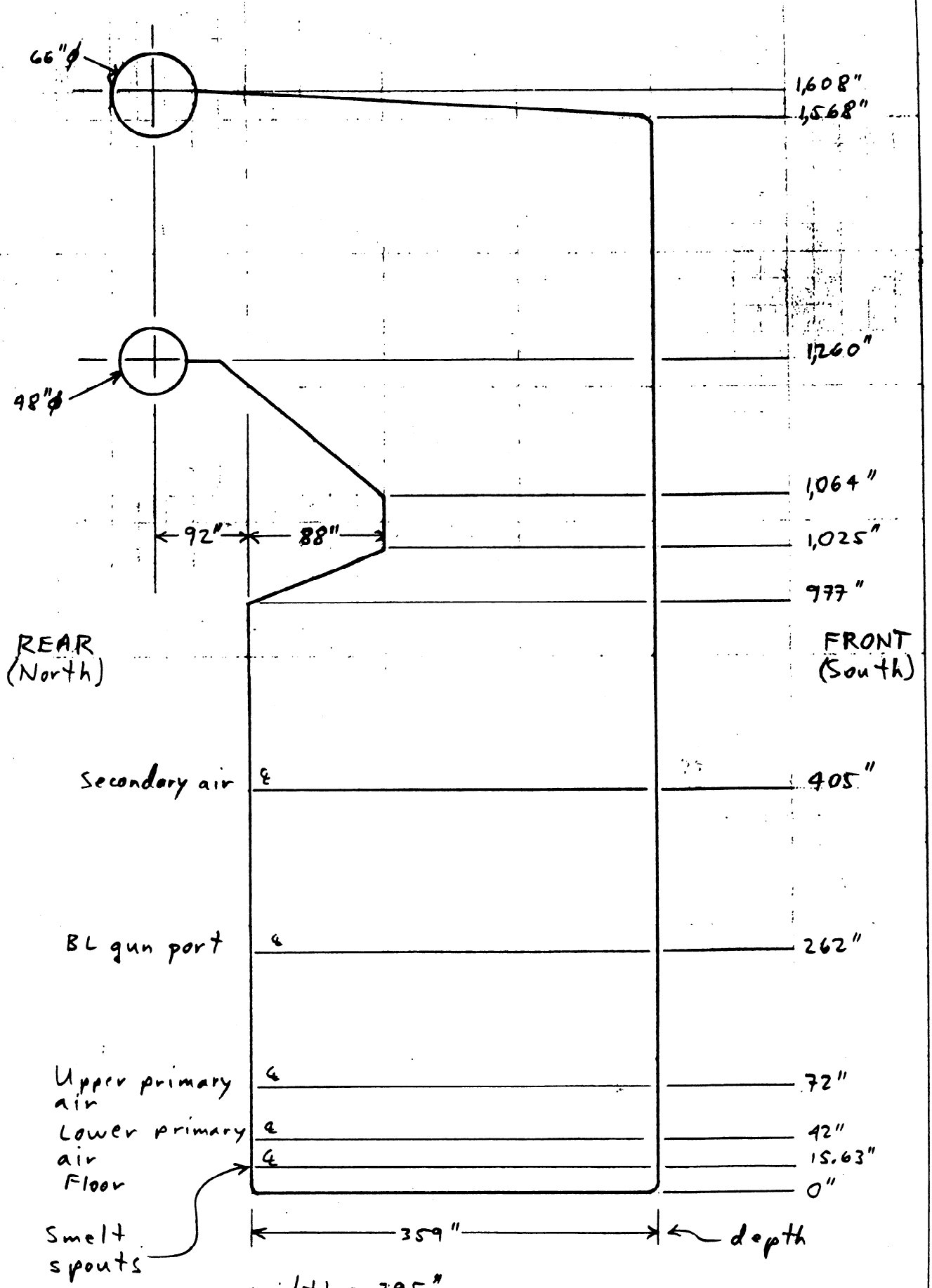

Furnace Screen + Superheater Tube Banks

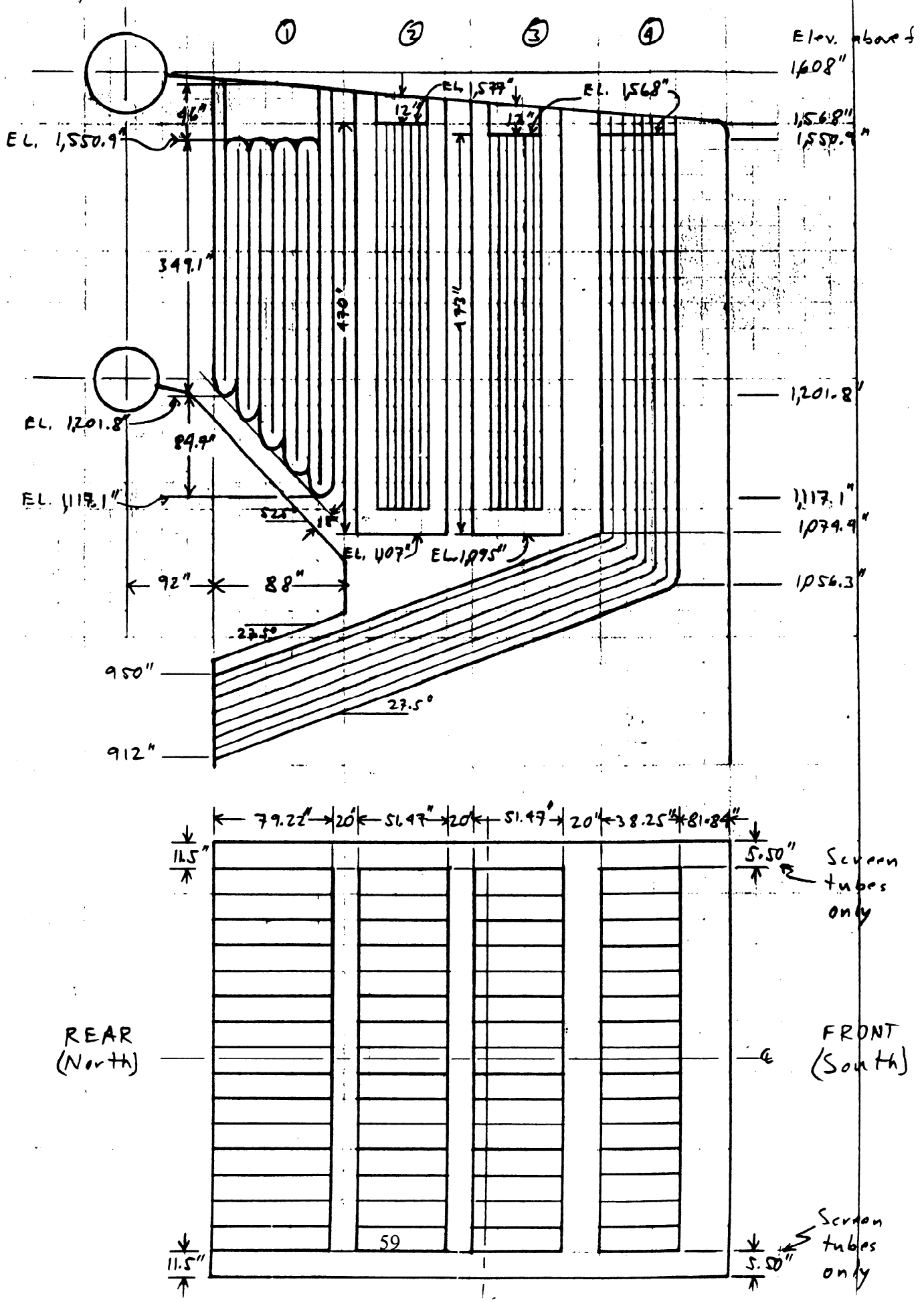

① Rear Superheater

- 2.0" OD tubes, 30 per row
- platen arrangement, 0.03" gap between tubes
- 32 rows, 12" center-to-center spacing

② Center Superheater

- 1.875" OD tubes, 22 per row
- platen arrangement, 0.03" gap between tubes
- 32 rows, 12" center-to-center spacing

③ Front Superheater

- same as ②

④ Furnace Screen

- 2.25" OD tubes, 17 per row
- platen arrangement, tangent tube design
- 17 rows, 24" center-to-center spacing

13-782 500 SHEETS FILLER 5 SQUARE
42-381 500 SHEETS EYE-EASE® 5 SQUARE
42-382 100 SHEETS EYE-EASE® 5 SQUARE
42-389 200 SHEETS EYE-EASE® 5 SQUARE
42-392 100 RECYCLED WHITE 5 SQUARE
42-399 200 RECYCLED WHITE 5 SQUARE
Made in U.S.A.
National Brand

BL Gun Layout

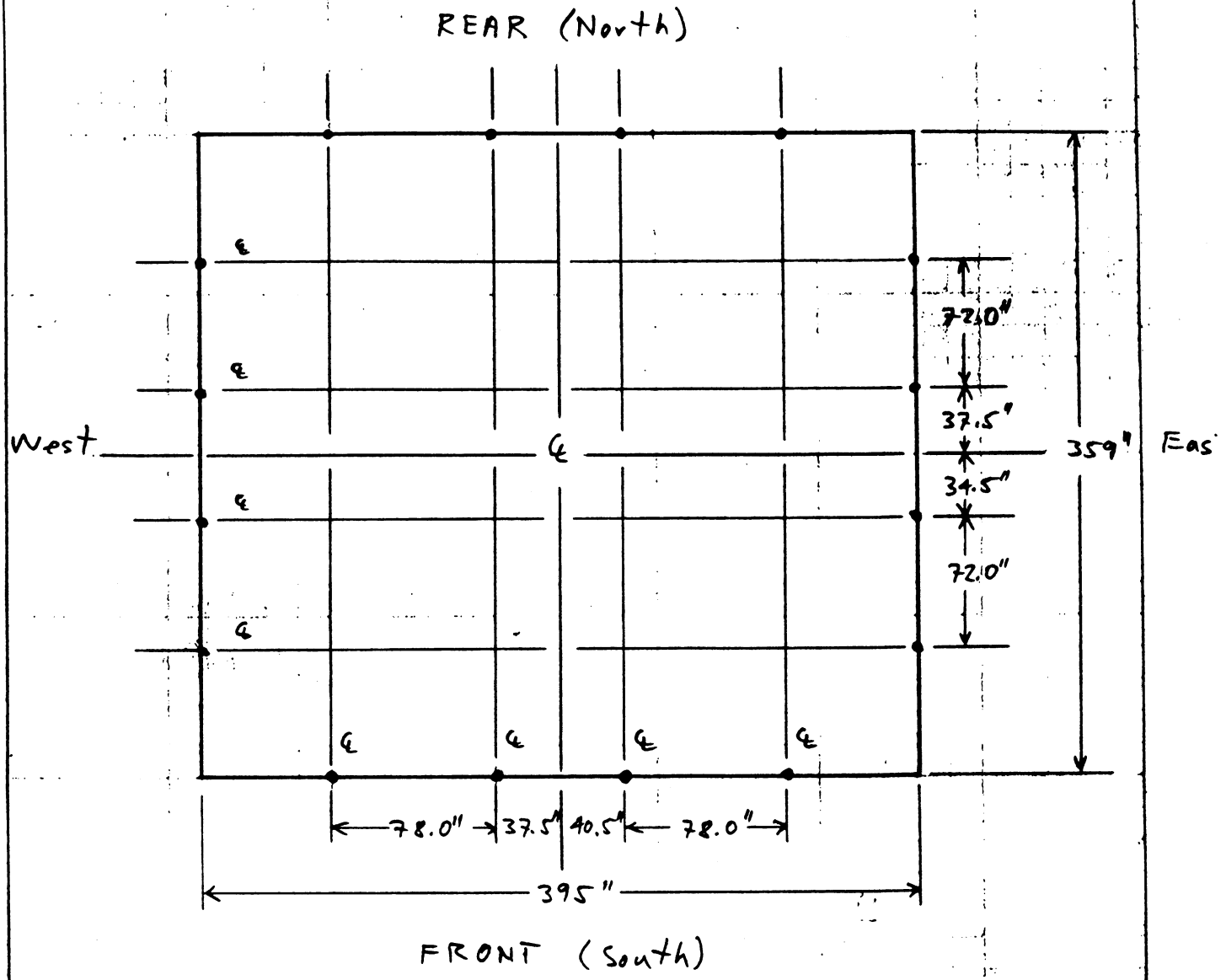

16 guns total

Liquor gun openings

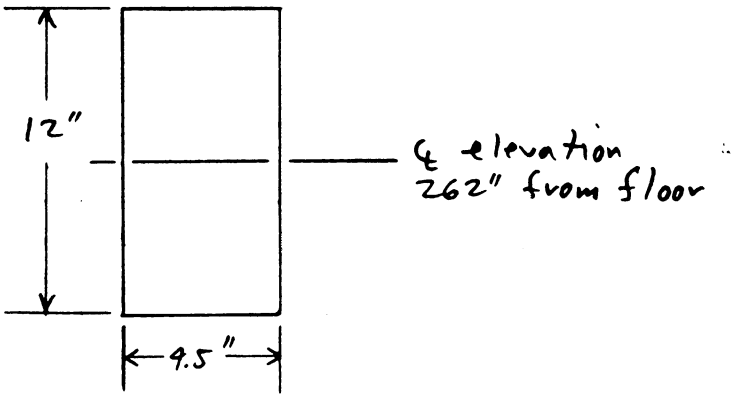

Lower Primary Air Ports

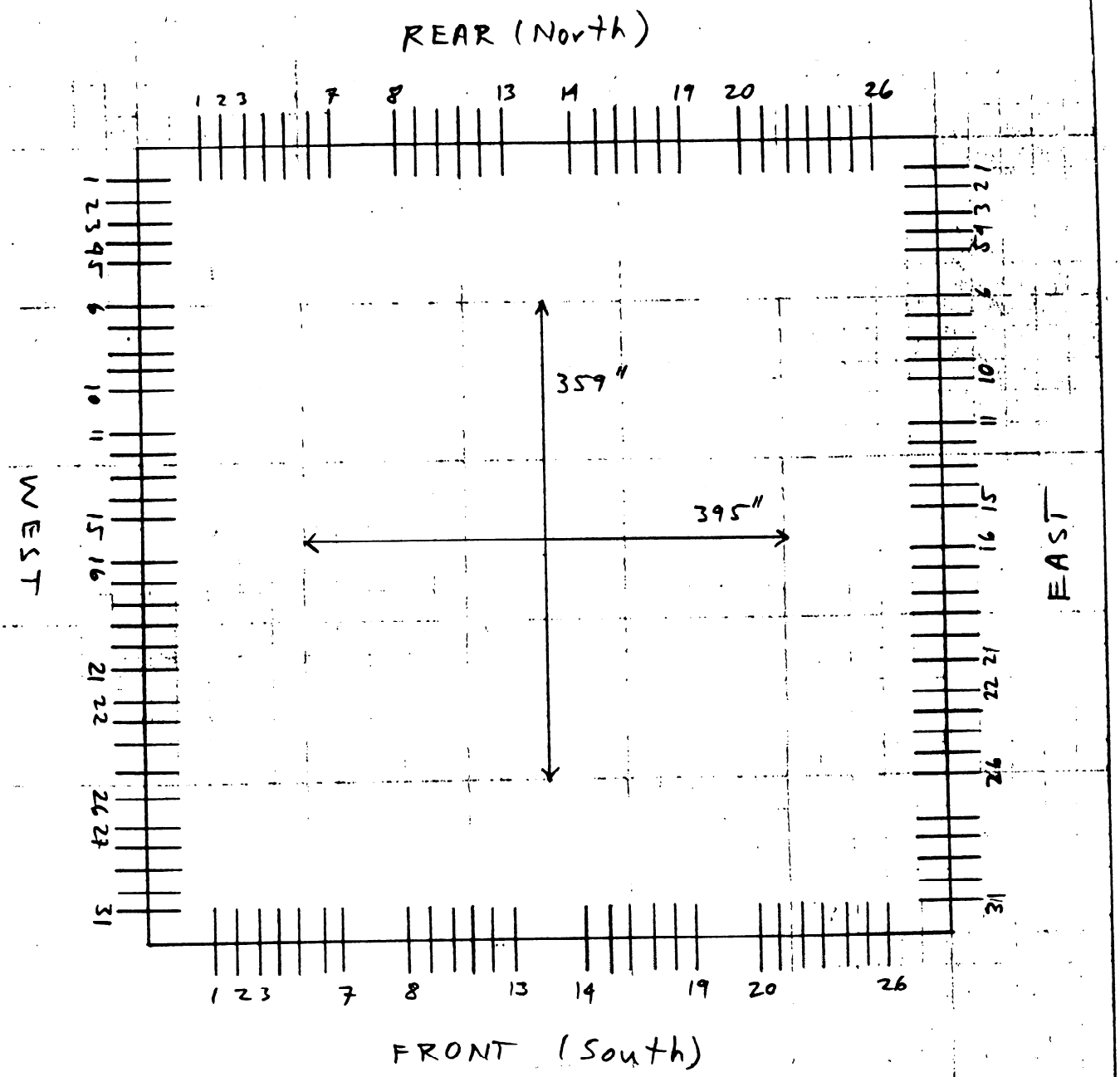

Lower primary air port

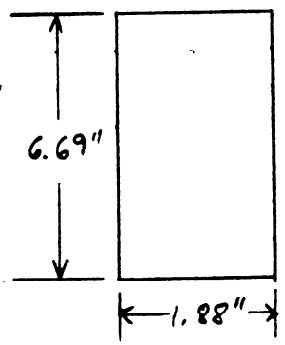

Typical spacing:
9.0" center-to-center

114 ports total

Total lower primary port area = 1,434 in.²

Lower Primary Air Ports

FRONT & REAR Ports

Port No.	Distance from WEST wall to port center (in)
WEST wall	0
1	71
2	80
3	89
4	98
5	107
6	116
7	125
8	142.5
9	151.5
10	160.5
11	169.5
12	178.5
13	187.5
14	197.5
15	205.5
16	214.5
17	223.5
18	232.5
19	241.5
20	250.5
21	269
22	278
23	287
24	296
25	305
26	314
EAST wall	323
	395

EAST & WEST Ports

Port No.	Distance from REAR wall to port center (in.)
REAR wall	0
1	26
2	35
3	44
4	53
5	62
6	71
7	83
8	92
9	101
10	110
11	128
12	137
13	146
14	155
15	164
16	179.5
17	190.5
18	199.5
19	208.5
20	217.5
21	226.5
22	235.5
23	255
24	264
25	273
26	282
27	291
28	302.5
29	311.5
30	320.5
31	329.5
FRONT wall	338.5
	359

13-782 500 SHEETS FILLER 5 SQUARE
42-381 50 SHEETS EYE-EASE 5 SQUARE
42-382 100 SHEETS EYE-EASE 5 SQUARE
42-388 150 RECYCLED WHITE 5 SQUARE
42-389 200 RECYCLED WHITE 5 SQUARE
Made in U.S.A.
National Brand

Upper Primary Air Ports

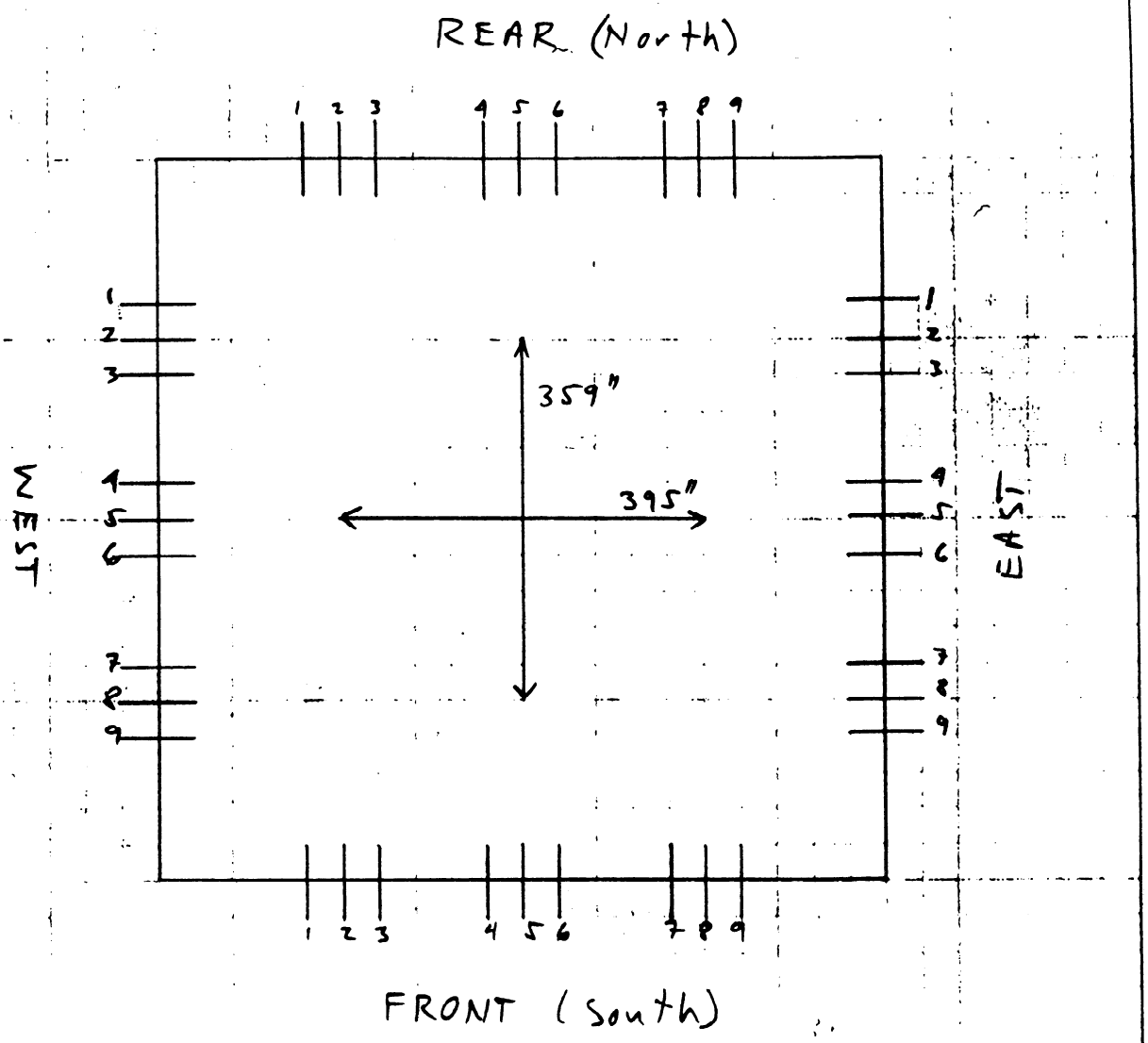

Upper primary air port

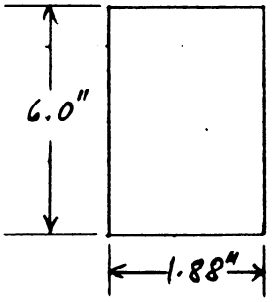

Typical spacing:
9.0" center-to-center within group

36 ports total

Total upper primary port area = 406.1 $in.^2$

Note: upper primary ports are permanently blocked off.

Upper Primary Air Ports

FRONT & REAR Ports

Port No.	Distance from WEST wall to port center (in.)
WEST wall	0
1	125
2	134
3	143
4	188
5	197
℄	197.5
6	206
7	251.5
8	260.5
9	269.5
EAST wall	395

EAST & WEST Ports

Port No.	Distance from REAR wall to port center (in.)
REAR wall	0
1	110
2	119
3	128
4	173
℄	179.5
5	182
6	191
7	236.5
8	245.5
9	254.5
FRONT wall	359

500 SHEETS, FILLER 5 SQUARE
500 SHEETS EYE EASE 5 SQUARE
500 SHEETS EYE EASE 5 SQUARE
200 RECYCLED WHITE 5 SQUARE
200 RECYCLED WHITE 5 SQUARE
13-782
42-381
42-382
42-383
42-386
Made in U.S.A.

Secondary Air Ports

REAR (North)

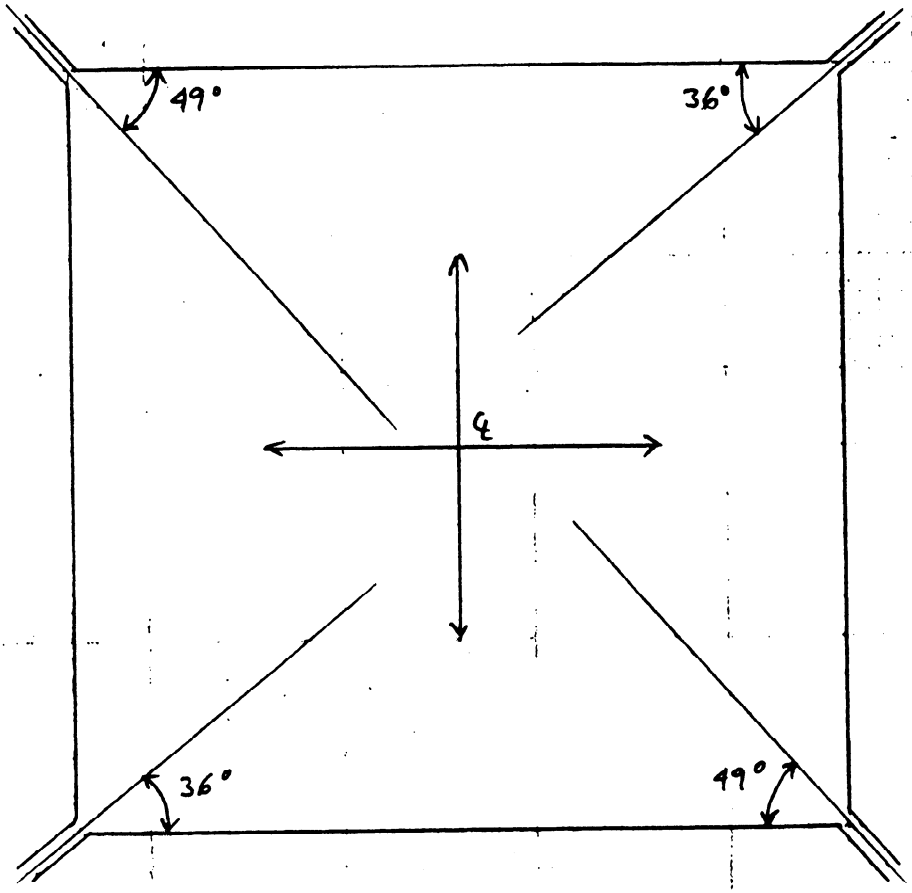

FRONT (South)

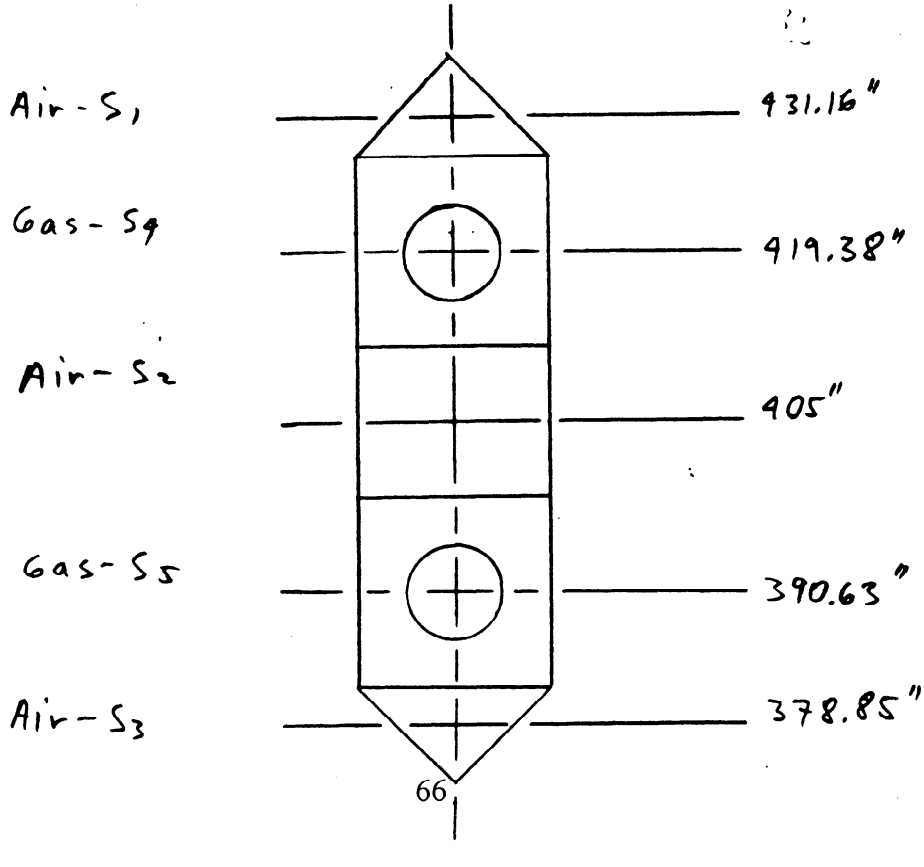

Smelt Spouts

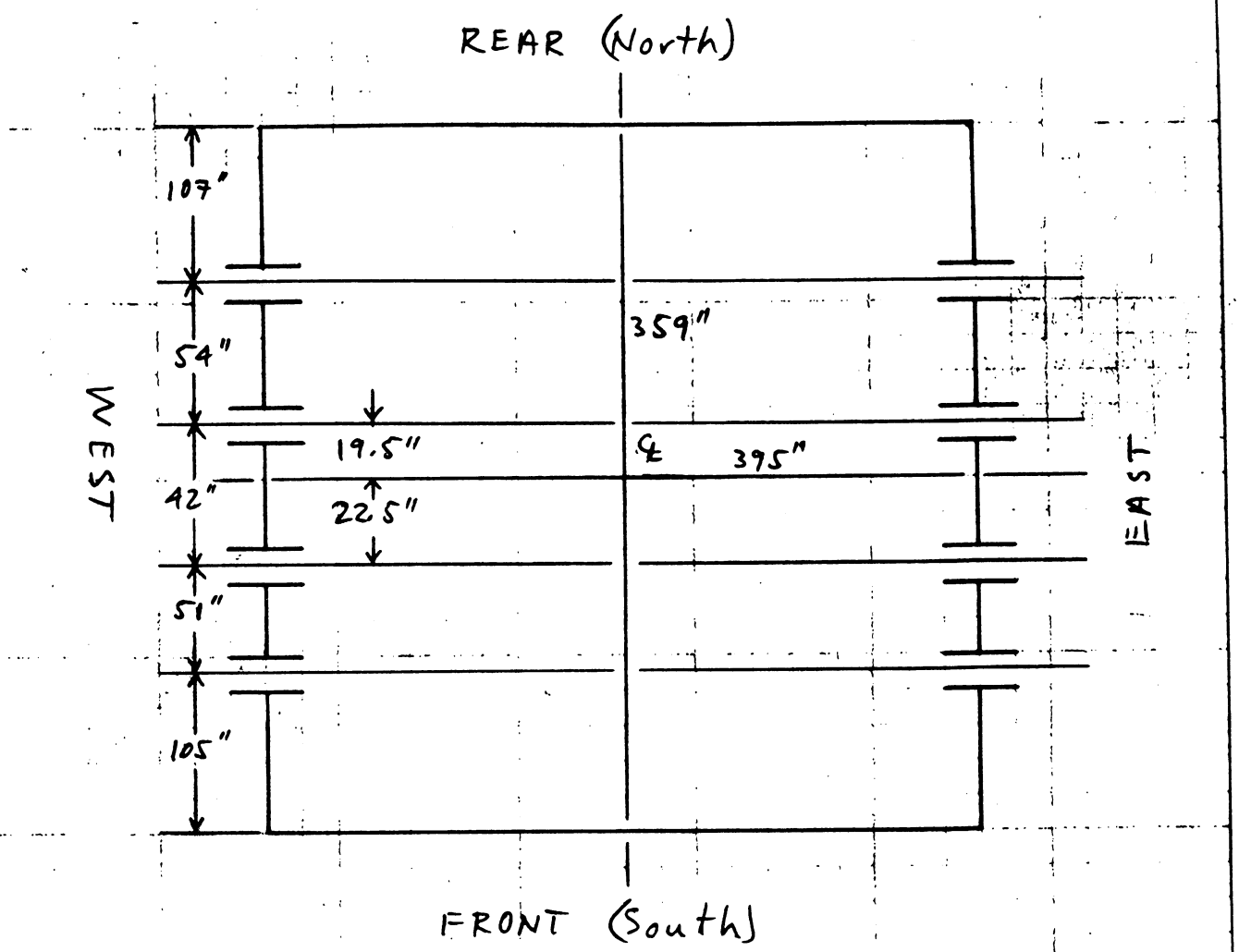

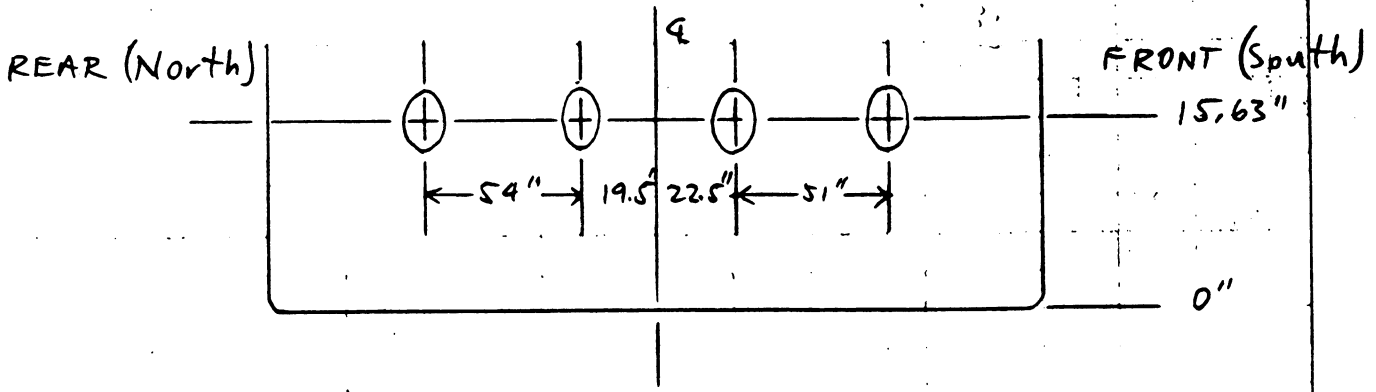

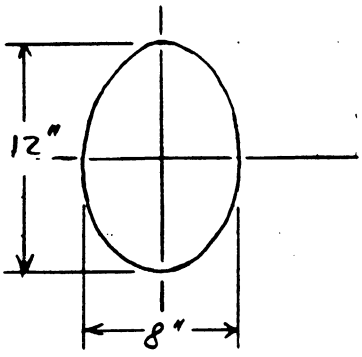

℄ Elevation 15.63" from floor

8 spouts total

Total smelt spout area ≈ 610 in.²

APPENDIX II
Process Data

Air Port Inlet Conditions for EB Eddy Recovery Boiler

Inlet Velocities			Measured Conditions						Calculated Conditions				
				Port	Total								
		No.	Temp	Area	Area	Vel	Flow	% of Total	M Flow	Temp	Vel	Windbox
		Ports	(K)	(cm^2)	(m^2)	(m/sec)	(kg/s)	Design L	(kg/s)	(K)	(m/sec)	(in H2O)
Normal Load		100%										
Primary		114	403	73	0.8360	61.92	45.38	54.8%	46.12	403.192	62.94	6.98
	Front	26	406	73	0.1907	62.94	10.45	12.5%	10.52	403.2	62.94	6.98
	Rear	26	402	73	0.1907	64.70	10.84	12.5%	10.52	403.2	62.94	6.98
	Right	31	402	73	0.2273	61.78	12.34	14.9%	12.54	403.2	62.94	6.98
	Left	31	403	73	0.2273	53.42	10.66	14.9%	12.54	403.2	62.94	6.98
BL Gun Leaks		16		232	0.3716			4.8%	4.01	298	9.09	0.20
Secondary		20		3555	1.3361			45.2%	38.04	397.1	31.99	1.83
	Top Air	4		429	0.1716			12.5%	10.55	397.1	69.09	8.54
	Hi Gas	4		897	0.3587			2.0%	1.68	397.1	5.27	0.05
	Mid Air	4		903	0.3613			26.4%	22.22	397.1	69.09	8.54
	Lo Gas	4		897	0.3587			2.0%	1.68	397.1	5.27	0.05
	Low Air	4		429	0.0858			6.3%	5.28	397.1	69.09	8.54
							Total Gas Flow =		84.2			

Flow and Heat Transfer Modeling in the Upper Furnace of a Kraft Recovery Boiler

Daniel Tse, Paul Matys, Paul Nowak, Zia Abdullah, Martha Salcudean and Ian Gartshore

Department of Mechanical Engineering
University of British Columbia
Vancouver, B.C., Canada, V6T 1Z4

November 1996

Contents

Abstract 1

1 Introduction 2

2 Fluid Flow Modeling 4

2.1 Mathemetical Model for Fluid Flow in a Porous Medium 4

2.2 Empirical Correlations for Pressure Drops Past Tube Banks 6

2.3 Numerical implementation of Pressure Loss Correlations 7

3 Heat Transfer Modeling 8

3.1 Combination of Heat Transfer Mechanisms 9

3.2 Calculation of Heat Transfer Coefficients 10

3.2.1 Conduction heat transfer across cylindrical tubes 10
3.2.2 Convection heat transfer for turbulent flows inside tubes 11
3.2.3 Convection heat transfer for gas flows over tube banks 11
3.2.4 Intertube radiation heat transfer 12

3.3 Numerical Implementation of Heat Transfer in Tube Banks 14

4 Capabilities of the Modeling Program 14

5 Application to a Full Scale Recovery boiler Simulation 15

5.1 Description of the Steam Generating Tube Banks 15

5.2 Cases Investigated 16

6 Results and Discussion 17

7 Conclusion 18

References 19

Figures 22

Abstract

A computer simulation of gas flow and heat transfer that includes the upper furnace of a kraft recovery boiler is presented. This upper furnace model applies the concepts of porosity and distributed resistance to simulate the hydrodynamics of gas flows past the superheater and steam generator tube banks. The heat transfer portion of the model captures the detailed superheater geometry, and the steam flow through the superheater sections and tubes is followed closely. This upper furnace model is coupled with a three-dimensional furnace model and together they can be used to study the flow and heat transfer phenomena in a recovery boiler. The overall model is applied to predict the flow field and steam temperature of a generic boiler under typical operating conditions. Different superheater routing schemes are examined to highlight the performance of the model.

1 Introduction

The upper furnace sections of many industrial boilers contain heat exchanger units such as superheaters and steam generators. Superheaters receive heat energy through radiation from the flame in the furnace and through convection from the passing flue gas. The mechanical arrangement of superheaters is dictated by furnace design, fuel characteristics, the degree of superheat, and past practice of the manufacturer. Radiant superheaters are closely spaced to receive the maximum radiant energy, while convective superheaters are more widely spaced. In-line arrangement of superheaters are commonly used for ease of tube cleaning and lower gas-pressure drops across the tube bundles.

Kraft recovery boilers are used in pulp mills for recovering valuable chemicals such as sodium sulfide from chemical wastes due to the kraft pulping process and for producing heat energy through combustion of organic residual matters. The goal of comprehensive modeling of a recovery boiler is to model the flow and heat transfer processes in both the lower furnace region and in the upper heat exchanger section. Available results of numerical simulations for industrial boilers tend to focus on the physical and chemical processes in the lower furnace region only. Examples of such progresses can be found in Fiveland and Wessel (1988), Karvinen et al. (1990), Coelho and Carvalho (1993), Hill and Smoot (1993), Smith et al. (1993), Coimbra et al. (1994), and Nowak et al. (1995). Many advances have been claimed: the establishment of better numerical techniques and the use of more sophisticated mathematical models to describe the complex physical and chemical processes that take place in the furnace region.

In comparison, modeling of fluid flow and heat transfer through boiler tube banks is discussed less often despite the importance of such a task. Accurate predictions of superheater steam temperature is important both for evaluating the performance of a boiler unit and for estimating the possibility of fouling and corrosion of the superheater. The small size of the constitutive components that made up a boiler tube bank causes difficulties for the numerical modeling of the upper furnace region. The grid employed in the computational analysis of flow dynamics is usually much coarser than the dimensions of individual tubes in the upper furnace to allow for any substantial resolution of geometric features. Consequently, in the combined simulation of flow and heat transfer processes in both the lower and upper furnace, it is necessary to have a methodology whereby the pressure loss and heat transfer due to these

tube banks can be realistically accounted for. Wessel et al. (1993) applied flow resistance and heat transfer conditions in the upper furnace in their calculation of recovery boiler flows. Realistic results were obtained for the flue gas flow field, but the steam temperature distribution within the superheater was not predicted.

The distributed resistance method developed by Patankar and Spalding (1974) can be applied to the calculation of thermal-hydraulic flow through tube banks. The method acknowledges the fact that fine geometrical details of the tube banks cannot be captured by the grid commonly used in the CFD simulation of the device. Instead, modifications applying the porosity and distributed resistance concepts are introduced to the governing equations to simulate the effects due to the tube banks. In this method, a porosity factor based on the amount of flow blockage is introduced to allow for flow acceleration through obstructed passages. Distributed resistances are introduced as source terms in the momentum equations to simulate the pressure loss due to the tube bank obstructions. This approach has the following major advantages:

1. The grid used can be much coarser than the dimensions of individual tubes.

2. Since only the terms in the governing equation system are modified, the same CFD solution algorithm can be applied in the entire domain comprising regions that contain tube banks and regions that do not.

3. The method provides a means of using extensive experimental data on the pressure drop through tube banks.

Examples of applications of such methods to heat exchanger tube banks can be found in Chang et al. (1994) and Ormiston et al. (1995).

Heat sources and sinks can in principle be distributed in a manner akin to the distributed resistance method to simulate the heat loss/gain by the flue gas due to heat transfer with the tube banks. A methodology was presented by Esaki et al. (1993), Kawaji et al. (1995) and Shen et al. (1995) to study the heat transfer between the flue gas and the steam flowing inside superheater platen tubes. Their model was two-dimensional: only the flow channel bounded between two parallel platens was considered. In addition, their procedure appeared to be distincted from the CFD calculation for the boiler. An averaged flow field of the flue gas in the superheater region was used for their superheater heat transfer model. The computed

temperature distribution in the platens was then fed back as boundary conditions for a subsequent CFD calculation of the flow field, and the procedure was repeated. Although realistic results can be obtained with this method, the coupling of such a method with a three-dimensional CFD furnace model can be cumbersome.

The goal of the present research is to develop a model that simulates the flow and heat transfer in the upper furnace heat exchanger section. The model should couple closely with an existing three-dimensional CFD furnace model to allow for a comprehensive simulation of the flow and heat transfer phenomena both in the furnace cavity and in the heat exchanger section. The combined model is applied to investigate the dependence of the steam temperature on different superheater routing schemes.

2 Fluid Flow Modeling

For large tube bundles such as those found in recovery boiler heat exchangers, the porosity and distributed resistance approach is currently the only viable numerical method for thermal-hydraulic analysis. The prediction of overall flow patterns in tube banks is facilitated but at the expense of losing the detailed flow characteristics.

2.1 Mathematical Model for Fluid Flow in a Porous Medium

The mathematical model that describes subsonic turbulent flows is commonly used to study flows in a kraft recovery boiler. The model consists of equations for the conservation of mass, momentum, specific enthalpy h, turbulent kinetic energy k, and the dissipation rate of turbulent kinetic energy ϵ. Using Cartesian tensor notations, the system of equations can be written in terms of a general variable Ψ, its diffusivity Γ_Ψ, and an associated source term S_Ψ as follows (Table 1):

$$\frac{\partial}{\partial x_j}(\rho U_j \Psi) = \frac{\partial}{\partial x_j}\left(\Gamma_\Psi \frac{\partial \Psi}{\partial x_j}\right) + S_\Psi \tag{1}$$

For flows in a porous continuum, the conservation equations are modified to account for the effect of porosity in the medium and become (Sha (1979), Spalding (1986))

$$\frac{\partial}{\partial x_j}(\beta \rho U_j \Psi) = \frac{\partial}{\partial x_j}\left(\beta \Gamma_\Psi \frac{\partial \Psi}{\partial x_j}\right) + S'_\Psi \tag{2}$$

where β, defined as the porosity of the medium, represents the local fraction of the volume

Ψ	Γ_Ψ	S_Ψ
1	0	0
U_i, $i = 1,2,3$	μ_{eff}	$-\partial P/\partial x_i + \partial/\partial x_j[\mu_{eff}(\partial U_j/\partial x_i)]$
h	μ_{eff}/σ_h	heat of reaction + radiation + interphase transport
k	μ_{eff}/σ_k	$G - \rho\epsilon$
ϵ	$\mu_{eff}/\sigma_\epsilon$	$(\epsilon/k)(C_1 G - C_2\rho\epsilon)$

$P = p + \frac{2}{3}\rho k$
$G = \mu_{eff}[(\partial U_i/\partial x_j) + (\partial U_j/\partial x_i)](\partial U_i/\partial x_j)$
$\mu_{eff} = \mu + \mu_t, \qquad \mu_t = C_\mu\, \rho k^2/\epsilon$
$C_\mu = 0.09$, $C_1 = 1.44$, $C_2 = 1.92$, $\sigma_k = 1.0$, $\sigma_\epsilon = 1.2$, $\sigma_h = 1.0$

Table 1: Terms representing the time-averaged Navier-Stokes equations, the enthalpy equation and the $k - \epsilon$ turbulence model.

of space that is occupied by the fluid. For the tube bank arrangement shown in Figure 1,

$$\beta = 1 - \frac{\pi D^2}{4 S_L S_T} \tag{3}$$

where D is the tube diameter, S_L is the longitudinal tube separation and S_T is the transverse separation.

In essence, the introduction of this porosity factor β causes the density ρ to take on its effective value $\beta \cdot \rho$. Shown in Table 2 are the modified source terms S'_Ψ which account for the effect due to distributed flow resistance for the case of momentum equations, and heat transfer to the tube banks for the case of the enthalpy equation. The term F_i represents the

Ψ	S'_Ψ
U_i, $i = 1,2,3$	$-\beta \cdot \partial P/\partial x_i + \partial/\partial x_j[\beta\mu_{eff}(\partial U_j/\partial x_i)] + F_i$
h	$S_h + \tilde{Q}$

Table 2: Modified source terms for the tube bank model.

extra flow resistance caused by the porous medium and is usually modeled by empirically based law, while $\tilde{Q}$ is the heat energy per unit volume exchanged between the flue gas and the tube banks.

The additional momentum sink term F_i is modeled as follows:

$$F_i = \alpha_1^i U_i + \alpha_2^i |\mathbf{V}| \cdot U_i \qquad i = 1,2,3 \tag{4}$$

where α_1^i and α_2^i are permeability coefficients whose values depend on the flow as well as physical properties of the porous medium and the fluid. Empirical correlations based on one-dimensional flow tests exist that relate this flow resistance F_i to pressure loss coefficients. These correlations are useful for calculating pressure drop for each component of the flow in three dimensions.

2.2 Empirical Correlations for Pressure Drops Past Tube Banks

The correlation by Grimison (1937) is still commonly used to determine the drag across tube bundles. Grimison's correlation gives the following functional dependence for the pressure drop:

$$\Delta p = 2N f' \rho U_{max}^2 \tag{5}$$

where

U_{max} = velocity at minimum flow area, m/s

ρ = density evaluated at free-stream conditions, kg/m^3

N = number of transverse rows

The empirical friction factor f' is given by Jakob (1938) as

$$f' = \left\{ 0.044 + \frac{0.08 S_L/D}{[(S_T - D)/D]^{[0.43+1.13D/S_L]}} \right\} \mathrm{Re}_{D,max}^{-0.15} \tag{6}$$

for in-line arrangements, with $\mathrm{Re}_{D,max} = \rho U_{max} D/\mu$ being a characteristic Reynolds number. Grimison's correlation is expected to be accurate to within 20% for $5000 < \mathrm{Re}_{D,max} < 40000$.

In terms of the free stream velocity component U_f, the maximum velocity is

$$U_{max} = \frac{S_T}{S_T - D} \cdot U_f \tag{7}$$

Then Eq.(5) for pressure loss can be written as

$$\Delta p = 2N f' \rho \left(\frac{S_T}{S_T - D} \right)^2 \cdot U_f^2 \tag{8}$$

The pressure gradient $\Delta p/\Delta x$ is obtained from Eq.(8) by noting that

$$\frac{\Delta p}{\Delta x} \approx \frac{\Delta p}{N \cdot S_L} = \frac{2 f' \rho}{S_L} \cdot \left(\frac{S_T}{S_T - D} \right)^2 \cdot U_f^2 \tag{9}$$

The flow resistance term shown in Eq.(4) can be interpreted as the negative pressure gradient $-\Delta p/\Delta x$. A comparison between Eqs.(4) and (9) yields

$$\alpha_1^i = 0 \tag{10}$$

$$\alpha_2^i = -\frac{2f'\rho}{S_L}\cdot\left(\frac{S_T}{S_T-D}\right)^2 \tag{11}$$

with $i = 1, 2$ denotes the two cross-flow directions past the tube bank, and the definitions for S_L and S_T need to be interchanged according to which direction is under consideration.

The correlation by Knudsen and Katz (1958) as referenced in Tierney (1992) gives expressions for the permeability coefficients for determining the drag when the flow is directed along the tube bundles. Let x_3 be the axial direction of the tube bundles, then the permeability coefficients are given as follows:

$$\alpha_1^3 = 0 \tag{12}$$

$$\alpha_2^3 = -0.092\cdot\rho \mathrm{Re}_{L_H}^{-0.2}/L_H \tag{13}$$

where $\mathrm{Re}_{L_H} = \rho|U_3|L_H/\mu$ is the Reynolds number based on the hydraulic diameter L_H for axial flow. This hydraulic diameter is given by the following formula for the tube bank configuration shown in Figure 1:

$$L_H = \frac{4}{\pi}\cdot\frac{S_T S_L - \pi D^2/4}{D} \tag{14}$$

The correlation stated in Eq.(13) was obtained for the following range of Re_{L_H}: $3000 < \mathrm{Re}_{L_H} < 1\times 10^6$.

2.3 Numerical Implementation of Pressure Loss Correlations

The conservation equations are discretized by the finite volume integration procedure over small control volumes surrounding nodal points. The standard staggered treatment is made to distribute velocity and scalar variables, and the power-law discretization scheme is used to approximate the convective-diffusive flux terms. The resulting difference equations and the constitutive coefficients are given in Patankar (1980).

The discretized momentum equations are of special interest since they contain the terms for hydraulic resistance. To describe the numerical implementation of these hydraulic resistance terms, the discretized momentum equation in the x_1 direction is written explicitly. The treatment for other momentum equations is similar.

Referring to the grid node notations about the control volume cell for the U_1 velocity component shown in Figure 2, the discretized momentum equation has the following form:

$$a_P^{U_1} \cdot U_{1,P} = \sum_{nb} a_{nb}^{U_1} \cdot U_{1,nb} - \beta(p_e - p_w) \cdot \Delta A_{ew} + B_P + F_1|_P \cdot \Delta V \tag{15}$$

where $nb = \{E, W, N, S, T, B\}$ denotes the neighboring grid nodes of P, ΔA_{ew} is the cross-sectional cell area on which the pressure difference $(p_e - p_w)$ is applied, B_P represents the discretized source term of $\partial/\partial x_j[\beta\mu_{eff}(\partial U_j/\partial x_i)]$ which arises from turbulence modeling, and $F_1|_P \cdot \Delta V$ is the volume integrated value of F_1, with $F_1|_P$ denotes the value of F_1 computed at P, and ΔV the volume of the control volume cell.

From Eqs.(4) and (11),

$$F_1|_P \cdot \Delta V = -\frac{2f'\rho}{S_L} \cdot \left(\frac{S_T}{S_T - D}\right)^2 \cdot |\mathbf{V}_P| \cdot U_{1,P} \cdot \Delta V \tag{16}$$

Define

$$C_{F_1} = \frac{2f'\rho}{S_L} \cdot \left(\frac{S_T}{S_T - D}\right)^2 \cdot |\mathbf{V}_P| \cdot \Delta V \tag{17}$$

then C_{F_1} is non-negative and the discretized momentum source term due to hydraulic resistance from the tube bank is

$$F_1|_P \cdot \Delta V = -C_{F_1} \cdot U_{1,P} \tag{18}$$

This momentum source contribution is most effectively accounted for by combination with the principal term $a_P^{U_1} \cdot U_{1,P}$ to give

$$(a_P^{U_1} + C_{F_1}) \cdot U_{1,P} = \sum_{nb} a_{nb}^{U_1} \cdot U_{1,nb} - \beta(p_e - p_w) \cdot \Delta A_{ew} + B_P \tag{19}$$

This practice has the important advantage of augmenting the magnitude of the principal coefficient term (coefficient of $U_{1,P}$) and consequently better numerical stability characteristics when the system of finite difference equations is to be solved by an iterative procedure.

3 Heat Transfer Modeling

The determination of heat transfer in the tube bank region is complicated due to the intricate geometry involved and the presence of all three modes of heat transfer: conduction, convection and radiation. For those parts of the screen tubes and superheaters that are exposed to the flame in the lower furnace, heat energy is received through radiation from the flame. For

those parts that are shielded, heat energy is transmitted from the flue gas to the steam or boiling water in the tubes by mainly convection and intertube radiation.

The superheater and steam generator are modeled as a series of tube banks with each bank having particular values of tube dimensions and spacings. The routing of steam through the superheater tube circuit can be specified arbitrarily so that the performance of different routing strategies can be studied and compared. Each tube within the tube bank is divided into a number of tube elements which permits the evaluation of steam temperature as the steam proceeds around the circuit. Usually several tube elements are embedded in a single control volume cell for the flue gas as illustrated in Figure 3.

For a tube element with steam temperature T_s embedded in a gas cell with temperature T_g, the temperature difference driving the heat transfer is $\Delta T = T_g - T_s$ if $T_g > T_s$. The amount of heat transfer per unit time from the flue gas to the steam in the tube element is

$$Q_{elem} = h_{elem} \cdot A \cdot \Delta T \tag{20}$$

where h_{elem} is the cumulative or overall heat transfer coefficient for the tube element of interest and A is the surface area of the element.

The extent of heat transfer is affected by many geometric and physical factors. Examples of geometric factors are the arrangements, locations, and dimensions of the tube banks. Physical factors include the velocity and temperature of the gas flow and steam flow, composition of the flue gas, and the amount of fouling deposits on the tube surfaces. The influence of these factors on heat transfer is made explicit through the analytical formulae discussed in the following sections.

3.1 Combination of Heat Transfer Mechanisms

For heat to transfer from a gas outside a tube that is made up of composite materials to a fluid inside the tube, a typical temperature distribution is shown in Figure 4, which illustrates a condition found in a superheater tube. The composite wall is comprised of the metal tube material and fouling deposits on the metal surface. Heat is transferred in tube banks by radiation and convection from the flue gas to the tube surface, by conduction across the thickness of the tube materials, and by forced convection to the steam and boiling water within the tube.

Using the inner surface area of a tube element as reference, and noting that the gaseous

radiation and convection are occurring in parallel while the rest of the heat transfer processes occurs in series, the overall heat transfer coefficient h_{elem} can be computed as

$$\frac{1}{h_{elem}} = \frac{1}{h_{cs}} + \frac{1}{h_{tw}} + \frac{D_i}{D_o}\frac{1}{h_{cg} + h_{rg}} \tag{21}$$

where

h_{cs} = heat transfer coefficient for convection heat flow inside the tube

h_{tw} = heat transfer coefficient for conduction heat flow through tube wall

h_{cg} = heat transfer coefficient for convection heat flow past the tube bank

h_{rg} = heat transfer coefficient for radiation heat flow within the tube bank

D_i = inner tube diameter

D_o = outer tube diameter

Analytical expressions for the individual heat transfer coefficients obtained through theoretical analysis and experimental correlations are presented next.

3.2 Calculation of Heat Transfer Coefficients

For simple geometries, the heat transfer coefficients for conduction heat transfer can often be obtained analytically. However, empirical correlations are necessary for convection and radiation heat transfer due to the turbulent nature of fluid motion and complicated boundary conditions. The use of empirical correlations to model heat transfer in the tube bank region is also important practically, not only because limitations with grid resolution to resolve individual components, but also the limitations of current turbulence models to give accurate predictions of heat transfer close to wall surfaces where most of the resistance to heat transfer occurs.

3.2.1 Conduction heat transfer across cylindrical tubes

The thermal resistance for a long cylinder subjected to radial heat flow is

$$\frac{1}{h_{tw}} = \frac{D_i \ln(D_o/D_i)}{2k} \tag{22}$$

where k is the thermal conductivity of the material. For a tube that has a composite wall, the individual thermal resistances can be added in series to obtain the overall resistance. The thermal conductivity for carbon steel has a typical value of 30 W/m-K at 1000°C, while for

smelt deposits found on the outer tube surface, a typical value for k is about 0.3 W/m-K as quoted in Adams and Frederick (1988), p.222.

3.2.2 Convection heat transfer for turbulent flows inside tubes

The flow of steam in superheater and boiler tubes is turbulent. One of the simplest correlations for fully developed turbulent flow in smooth tubes is the Dittus and Boelter correlation:

$$\frac{h_{cs} D_i}{k_s} = 0.023 \, \mathrm{Re}_{D_i}^{0.8} \, \mathrm{Pr}^{0.4} \tag{23}$$

where k_s and Pr are thermal conductivity and Prandtl number for the steam. The properties in Eq.(23) are evaluated at the fluid bulk temperature, and the correlation is valid for fluids with Prandtl numbers ranging from 0.6 to 100 and with moderate temperature differences between wall and fluid conditions. More elaborate correlations that account for a wider range of conditions such as the difference between film temperature and bulk temperature can be found in Babcock & Wilcox (1978) (hereafter B & W), Chapter 4.

According to the calculation done in B & W Chapter 4, for a typical boiler design, the water-film thermal resistance is about two orders of magnitude lower than the combined gas-side resistance (convection plus intertube radiation). Hence, in the calculation of overall heat transfer coefficient, the water-film resistance can be neglected in the calculation of resistance to heat flow. This condition applies to those parts of the tube banks where boiling water is expected to present (screen tubes and boiler tubes).

3.2.3 Convection heat transfer for gas flows over tube banks

Experimental data have been collected for convection heat transfer for gas flows past tube bundles by Babcock & Wilcox and by Zukauskas (1972). The data show the heat transfer correlation has the following form:

$$\frac{h_{cg} D_o}{k_g} = F_a \cdot C \cdot \mathrm{Re}_{D_o,max}^{n} \, \mathrm{Pr}^{0.33} \tag{24}$$

where k_g is the thermal conductivity of the flue gas, and all properties are evaluated at the bulk temperature of the cross-flow. Values for F_a, C and n are dependent on the arrangement of the tube bank and suitable values are tabulated in Holman (1986).

Properties of the flue gas in the upper furnace region are needed for the evaluation of flue gas characteristics such as the thermal conductivity and the Prandtl number. For a flue gas

that has n gaseous components, the following semi-empirical formulae given in Bird et al. (1960) are applicable:

$$\mu_m = \sum_{i=1}^{n} \frac{x_i \mu_i}{\sum_{j=1}^{n} x_j \Phi_{ij}} \tag{25}$$

$$k_m = \sum_{i=1}^{n} \frac{x_i k_i}{\sum_{j=1}^{n} x_j \Phi_{ij}} \tag{26}$$

with

$$\Phi_{ij} = \frac{1}{\sqrt{8}} \left(1 + \frac{M_i}{M_j}\right)^{-1/2} \left\{1 + \left(\frac{\mu_i}{\mu_j}\right)^{1/2} \left(\frac{M_j}{M_i}\right)^{1/4}\right\}^2 \tag{27}$$

and

$$C_{pm} = \sum_{i=1}^{n} w_i C_{pi} \tag{28}$$

The symbols displayed above have the following meaning:

μ_m = viscosity of the flue gas mixture

k_m = thermal conductivity of the flue gas mixture

C_{pm} = specific heat capacity of the flue gas mixture

x_i,x_j = mole fractions of components i and j, respectively

μ_i, μ_j = viscosities of components i and j at the flue gas temperature and pressure

M_i, M_j = molecular weights of components i and j

k_i = thermal conductivity of a pure component i

w_i = weight ratio of component i

C_{pi} = specific heat capacity of the pure gas component i

3.2.4 Intertube radiation heat transfer

The prediction of radiation heat transfer is more difficult due to the more complex physical processes involved. In the present heat exchanger model, only radiation from the flue gas to the surrounding tube bank is considered. The following method for estimating the extent of intertube radiation is adopted from Welty (1978) and Ganapathy (1982). The main source of radiation heat transfer is the electromagnetic radiation emanating from polar gases such as CO_2, H_2O and SO_2, which are formed during combustion of black liquor.

The net interchange of radiation between the flue gas mixture at temperature T_g and tube banks of surface area A at the deposit temperature T_d (refer to Figure 4) is written as

$$Q_{rad} = \epsilon_s \cdot \sigma \cdot A \cdot (\epsilon_g T_g^4 - \alpha_g T_d^4) \tag{29}$$

where ϵ_s is the effective surface emissivity with value taken to be 0.7, σ is the Stefan-Boltzmann constant, ϵ_g is the emissivity of gases at T_g, and α_g is the absorptivity at T_d.

A radiative heat transfer coefficient h_{rg} is defined to be

$$h_{rg} = \epsilon_s \cdot \sigma \cdot (\epsilon_g T_g^4 - \alpha_g T_d^4)/(T_g - T_d) \tag{30}$$

Then Eq.(29) can be expressed as

$$Q_{rad} = h_{rg} \cdot A \cdot (T_g - T_d) \tag{31}$$

This form of expression is parallel to that for convective heat transfer so that the two modes of heat transfer mechanism can be summed conveniently.

To determine h_{rg}, values of ϵ_g and α_g are needed for all the polar gases present in the gaseous mixture. Hottel and Sarofim (1967) developed an approximate method for estimating the values of ϵ_g and α_g for both CO_2 and H_2O. In the present study, occurrence of SO_2 is neglected.

In Hottel and Sarofim's procedure, the partial pressure for each gaseous component as well as a characteristic mean beam length L_{bl} are needed for the determination of ϵ_g. The value of L_{bl} characterizes the configuration and dimensions of the tube bundle, and may be taken to have the same value as the hydraulic diameter L_H given in Eq.(14). In the present model, the partial pressure for each of the gases is obtained through the ideal gas equation of state. With values for the mean beam length and partial pressures known, the emissivities of CO_2 and H_2O can be obtained from the graphs presented in Holman (1986, pp.416-419). Determination of α_g follows a similar procedure.

A remark was made earlier that the screen tubes and the front part of the superheater tubes may receive direct radiation from the furnace flame. The effect of this source of radiation is to reduce the amount of effective heating surfaces that are available for intertube radiation heat transfer. Empirical estimates of this reduction are presented in B & W Chapter 14. However, this reduction in effective area has been estimated to be insignificant for superheater banks ($\approx$ 2%), and only moderately significant for the screen tubes ($\approx$ 30%).

Since the screen tubes constitute only a small portion of the overall area for heat transfer in the upper furnace, in the present consideration, intertube radiation is assumed to take place for the entire surface areas of all the tube banks.

3.3 Numerical Implementation of Heat Transfer in Tube Banks

After h_{elem} and Q_{elem} are computed respectively by Eqs.(21) and (20), the steam temperature is calculated based on a simple enthalpy balance:

$$\Delta T_s = Q_{elem}/(C_{ps} \cdot W_s) \tag{32}$$

where ΔT_s is the change in steam temperature between the entry and exit ends of the tube element, C_{ps} is the specific heat capacity of the steam and W_s is the mass flow rate of the steam.

For the flue gas, the enthalpy lost is calculated by summing up the heat transfer to tube elements within each control volume cell. Referring to Figure 3, enthalpy balance gives

$$Q_{cell} = - \sum_{elem \in cell} Q_{elem} \tag{33}$$

where the summation is over all the tube elements embedded in the cell under consideration. This heat sink per unit volume $\tilde{Q} = Q_{cell}/\Delta V$ where ΔV is the volume of the computational cell will be added to the source term of the enthalpy equation as shown in Table 2. Although the above discussion specifies that heat is lost by the flue gas and gained by the superheater steam, the formulation works equally well if the heat transfer were reversed.

4 Capabilities of the Modeling Program

The modeling program developed at the University of British Columbia for recovery boiler simulations accepts the specification of an arbitrary number of tube banks in the upper furnace heat exchanger section. The properties of each tube bank are described by tube diameters, longitudinal and lateral tube spacings, and the thickness of fouling deposits. A temperature is specified for the superheated boiling water in the steam generator. The heat absorbed by the fluid inside the steam generator tube bank is assumed to cause phase change only and hence the tube-side fluid assumes a constant temperature equals to the specified value. The steam is then piped to the superheater tube banks and the tube circuit can be specified in an arbitrary manner.

Parametric studies of the heat transfer characteristics in the tube bank region can be carried out. For example, the effect on heat loss by the flue gas due to fouling deposits on the tube banks can be studied by varying the thickness and thermal conductivity of the deposits on the screen and superheater tubes. Variation of the thickness of the fouling deposits causes the overall thermal resistance to change as well as the effective diameter of an individual tube. The superheater circuit can also be changed so as to determine an optimal sequence for highest steam temperature output.

An iterative procedure is applied to solve the governing equations for the flow field (Salcudean et al. (1993)). During every iteration, the steam temperature distribution is calculated throughout the superheater banks. The residues of the governing conservation equations and the differences in the steam temperature between successive iteration are monitored. Convergence is deemed to have achieved when both the residues and the steam temperature variations are small.

5 Application to a Full Scale Recovery Boiler Simulation

A generic recovery boiler is considered for testing the utility of the computer model developed. The boiler has a 10 m square base, and is 40 m high. The tip of the bullnose is located 26.5 m from the floor. There are three levels of air: four wall primary (1.2 m above the floor), four wall secondary (3 m above the floor) and two wall tertiary (10 m above the floor). The boiler operates at a load of 17.67 kg/s (3.37×10^6 lbs/day) of black liquor solids with four liquor guns, one at the center of each wall and at 7 m above the floor.

The following air and black liquor injection scheme is considered: the boiler operates with an air split of 48% primary, 32% secondary and 20% tertiary; the black liquor spray has a mean droplet diameter of 2.8 mm and a horizontal spray angle of 150°, and the nozzles oscillate vertically from 0° to $-30°$. A comprehensive parametric study on different air and liquor injection systems is presented in Nowak et al. (1995), which also provides a detailed description of the CFD furnace model. The present study focuses on the flow and heat transfer in the upper furnace section.

5.1 Description of the Steam Generating Tube Banks

The heat exchanger section is assumed to be made up of three superheater tube banks (SH-1, SH-2 and SH-3) and a steam generator tube bank. Each superheater tube bank has the

following simple arrangements:

Superheater bank (each of the three banks)

- 26 platens evenly spaced at 0.28 m (11 in.)
- height of each platen = 3.8 m (12.5 ft.)
- 4 tubes in a platen each making 6 passes
- average tube spacing = 0.074 m (2.9 in.)
- tube outer diameter = 0.0635 m (2.5 in.), tube thickness = 0.0035 m (0.14 in.)

The steam generator or boiler tube bank has the following characteristics:

Steam generator bank

- 78 columns by 26 rows
- height of tube bank = 3.8 m (12.5 ft.)
- average longitudinal and transverse tube spacing = 0.114 m (4.5 in.)
- tube outer diameter = 0.0635 m (2.5 in.), tube thickness = 0.0035 m (0.14 in.)

The unit is expected to generate 556 klbs/hr (70 kg/s) of steam at approximately 700°F and 800 Psi (644 K and 5500 kPa).

Boiling water at the saturation temperature of 523 K is assumed to occupy the steam generator bank and later passes to the superheater. The boiling water is then transformed into superheated steam, which is assumed to have a constant heat capacity at 2.6 kJ/kg-K. In the simulation, each vertical segment of tubes in the superheaters is divided evenly into seven tube elements. The centers of the tube elements for the middle set of platens for SH-1, SH-2 and SH-3 are shown in Figure 5. The tubes of the steam generator are discretized in a similar fashion. The vertical dashed lines shown in Figure 5 illustrate the orientation of the tubings.

5.2 Cases Investigated

The following three cases are studied:

Case 1 - Tube bank model not applied

Case 2 - Steam is piped successively through SH-1, SH-2, and then SH-3

- Steam flow is parallel to the flue gas flow in all three superheater banks
- Tubes are covered with 0.5 cm thick fouling deposits

Case 3 - Steam is piped successively through SH-1, SH-3, and then SH-2
- Steam flow is parallel to the flue gas flow in SH-1 and SH-2
- Steam flow is counter to the flue gas flow in SH-3
- Fouling deposition as in Case 2

Figure 6 presents a schematic description of the steam routing scheme. The operation mode depicted in Case 3 is usual to many superheaters. Transient calculations are performed with a time step of 1 second. Convergence is achieved readily for each case simulated. The results show only minor variations between successive time steps.

6 Results and Discussion

The effect of the tube bank model on the velocity field is shown in Figure 7, which displays the velocity fields in the front-rear vertical central plane bisecting the entire height of the boiler. The velocity fields of Cases 2 and 3 are similar; hence, only the results of Cases 1 and 2 are shown. For Case 2, it is seen that an extensive recirculation region is formed in the top region near the front wall. The additional flow resistance specified by the tube bank model causes the flow near the top to bend downward before it exits the furnace.

Figure 8 compares the temperature distributions for Cases 1 and 2 in the same vertical plane. The temperature field of Case 3 is not shown since it is similar to Case 2. The temperature is reduced in the upper furnace as expected when the heat exchanger model is applied. The reduction in flue gas temperature is about 400 K, which is significant. This observation illustrates the importance of using an accurate upper furnace model to predict the temperature field in an industrial boiler.

Figure 9 shows the steam temperature distribution for Case 2 within the platens across the width of the furnace in a plane parallel to the front wall. The platens belong to the superheater SH-2, and the tube elements shown are located about 5 m from the front wall. The graph on the right shows the corresponding flue gas temperature distribution. The steam temperature in the platen tubes varies in the same way as the flue gas temperature distribution: cooler in the middle and hotter away from the center.

Figure 10 compares the steam temperature distributions between Cases 2 and 3 for the middle set of platens of all three superheater units. These platens are located approximately in the vertical central plane as shown previously in Figures 7 and 8. The results show that the counter-flow strategy employed by Case 3 yields higher steam temperature at the outlet. Thus, this study confirms the practice of using counter-flow routing scheme in enhancing the final steam temperature.

7 Conclusion

A methodology using the concepts of porosity, distributed flow resistance, and cumulative heat transfer is presented for modeling the heat exchanger tube banks found in a kraft recovery boiler. Each tube in the heat exchanger section is divided into a number of tube elements for computing the heat transfer between the steam or boiling water inside the tube with the flue gas. Consequently, the progressive changes in the steam temperature through the superheater can be calculated. The model allows for different routing of steam through the superheater and hence the performance of different superheater circuits can be compared.

This heat exchanger model is fully coupled with a three-dimensional CFD furnace model to effect a straight-forward comprehensive simulation of boiler performance. In future studies, the model will be used to predict surface temperature of the tube banks for fouling and corrosion analysis.

References

Adams, T.N. and Frederick, W.J., Kraft Recovery Boiler Physical and Chemical Processes, The American Paper Institute, Inc., New York, 1988.

Babcock & Wilcox, Steam / its generation and use, Thirty-ninth edition, The Babcock & Wilcox Company, New York, 1978.

Bird, R.B., Stewart, W.E. and Lightfoot, E.N., Transport Phenomena, John Wiley & Sons, New York, 1960.

Chang, P.S., Nesbitt, D.G., and LaRose, J.A., "TVA Colbert Unit 3 Upper Furnace Flow Distribution Study", Proceedings of the 56th Annual American Power Conference, Vol.56, Pt.2, pp.1766-1771, 1994.

Coelho, P.J. and Carvalho, M.G., "Application of a Domain Decomposition Technique to the Mathematical Modelling of a Utility Boiler", *International Journal for Numerical Methods in Engineering*, Vol.36, pp.3401-3419, 1993.

Coimbra, C.F.M., Azevedo, J.L.T., and Carvalho, M.G., "3-D Numerical Model for Predicting NO_x Emissions from an Industrial Pulverized Coal Combustor", *Fuel*, Vol.73, No.7, pp.1128-1134, 1994.

Esaki, S., Dees, C., Kawaji, M. and Tran, H., "A Heat Transfer Model for Predicting Superheater Tube Temperatures in Kraft Recovery Boilers", ASME HTD-Vol.250, Heat Transfer in Fire and Combustion Systems, pp.235-242, 1993.

Fiveland, W.A. and Wessel, R.A., "Numerical Model for Predicting Performance of Three-Dimensional Pulverized-Fuel Fired Furnaces", *Journal of Engineering for Gas Turbines and Power*, Vol.110, pp.117-126, 1988.

Ganapathy, V., Applied Heat Transfer, PennWell Publishing Company, Tulsa, Oklahoma, 1982.

Grimison, E.D., "Correlation and Utilization of New Data on Flow Resistance and Heat Transfer for Cross Flow of Gases over Tube Banks", *Trans. ASME*, Vol.59, pp.583-594, 1937.

Hill, S.C. and Smoot, L.D., "A Comprehensive Three-Dimensional Model for Simulation of Combustion Systems: PCGC-3", *Energy & Fuel*, Vol.7, pp.874-883, 1993.

Holman, J.P., Heat Transfer, Sixth Edition, McGraw-Hill Books Company, New York, 1986.

Hottel, H.C. and Sarofim, A.F., Radiative Transfer, McGraw-Hill Book Company, New York, 1967.

Jakob, M., "Heat Transfer and Flow Resistance in Cross Flow of Gases over Tube Banks", *Trans. ASME*, Vol.60, p.384, 1938.

Karvinen, R., Siiskonen, P., and Hyoty, P., "Role of Combustion Simulation during the Operation and in the Design of a Modern Recovery Boiler", Mathematical Modeling and Computer Simulation of Processes in Energy Systems, edited by Kemel Hanjali, Hemisphere Pub. Corp., New York, pp.287-297, 1990.

Kawaji, M., Shen, X.H., Tran, H., Esaki, S., and Dees, C., "Prediction of heat transfer in the kraft recovery boiler superheater region", *Tappi Journal*, Vol.78, No.10, pp.214-221, 1995.

Knudsen, J.G. and Katz, D.L., Fluid Dynamics and Heat Transfer, McGraw-Hill Book Company, New York, 1958.

Nowak, P., Matys, P., Sabhapathy, P., Abdullah, Z., and Salcudean, M., "Numerical Study of a Kraft Recovery Furnace", TAPPI International Chemical Recovery Conference, Toronto, pp.A149-A159, 1995.

Ormiston, S.J., Raithby, G.D., and Carlucci, L.N., "Numerical Modeling of Power Station Steam Condensers - Part 1: Convergence Behavior of a Finite-Volume Model", *Numerical Heat Transfer*, Part B, Vol.27, pp.81-102, 1995.

Patankar, S.V., Numerical Heat Transfer and Fluid Flow, Hemisphere Publishing Corporation, McGraw-Hill Book Company, New York, 1980.

Patankar, S.V. and Spalding, D.B., "Heat Exchangers: Design and Theory Sourcebook", Scripta Book Co., Washington, DC., pp.155-176, 1974.

Salcudean, M., Nowak, P. and Abdullah, Z., "Cold Flow Computational Model of a Recovery Boiler", *Journal of Pulp and Paper Science*, Vol.19, No.5, pp.J186-J194, 1993.

Sha, W.T., "Summary of Methods Used in Rod-Bundle Thermal-Hydraulic Analysis", in: Kakac, S. and Spalding, D.B. (eds.): Turbulent Forced Convection in Channels and Bundles, Vol.1, pp.279-299, New York: Hemisphere, 1979.

Shen, X.H., Kuhn, D.C.S., Tran, H.N., Mostaghimi, J., and Dees, C., "Simulation of Flue Gas Flow in the Upper Furnace of a Recovery Boiler", *Pulp & Paper Canada*, Vol.96, No.5, pp.T171-T175, 1995.

Smith, P.J., Eddings, E.G., Adams, B.R., and Heap, M.P., "Application of Combustion Computations to Industrial Problems", ASME Engineering Foundation Conference on "Coal-Blending and Switching of Low-Sulfur Western Coals", Snowbird, Utah, pp.441-452, 1993.

Spalding, D.B., Heat Exchanger Theory, Chapter 1 of Heat Exchanger Design Handbook, Hemisphere Publishing Corporation, London, 1986.

Tierney, M., "CFD Predictions of the Hydraulic Performance of Heat Exchangers", Institution of Chemical Engineers (ICHEME) Symposium Series, No.129, pp.397-408, 1992.

Welty, J.R., Engineering Heat Transfer, SI version, John Wiley & Sons, New York, 1978.

Wessel, R.A., Parker, K.L., and Aniefiok, A.-E., "Three-Dimensional Flow and Combustion Model of a Kraft Recovery Furnace", TAPPI Proceedings, Engineering Conference, pp.651-664, 1993.

Zukauskas, A., "Heat Transfer from Tubes in Cross Flow", *Adv. Heat Transfer*, Vol.8, pp.93-160, 1972.

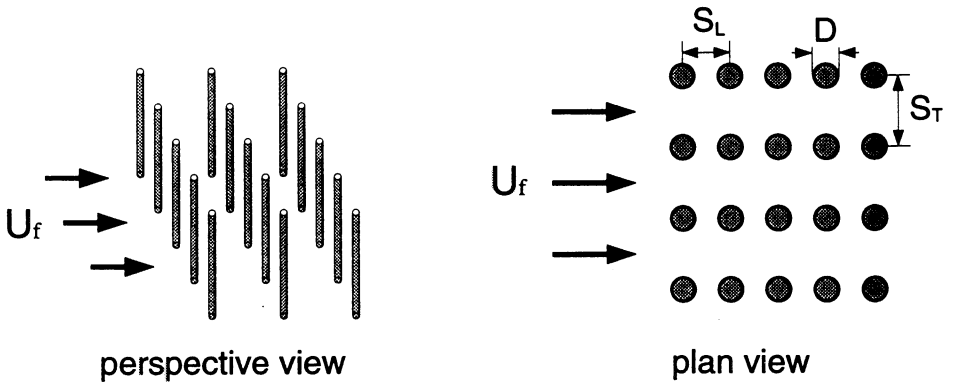

Figure 1: Flow past a tube bank.

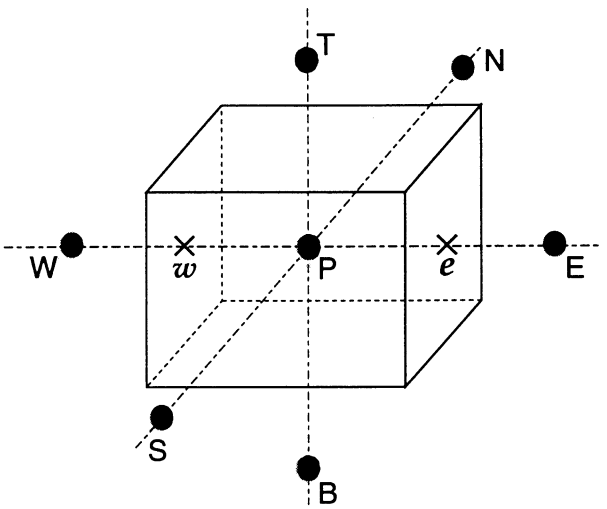

Figure 2: Control volume for the U_1 velocity component showing grid nodes and their locations.

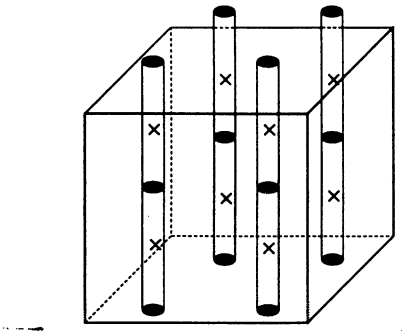

Figure 3: Schematic drawing showing tube elements (marked by X) embedded in a computational cell.

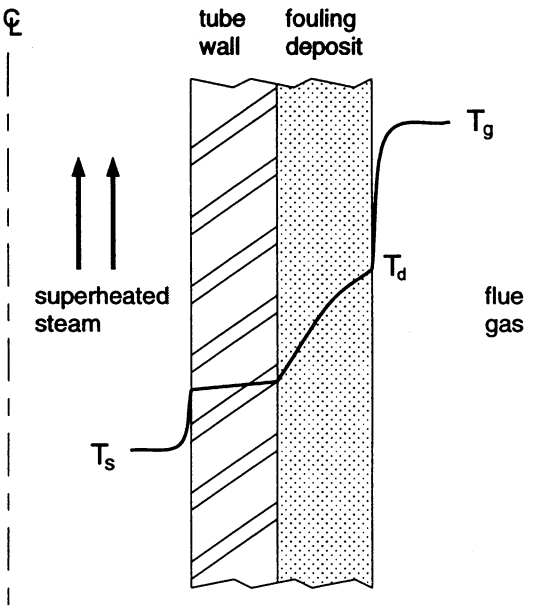

Figure 4: Temperature distribution in composite wall (fluid films included).

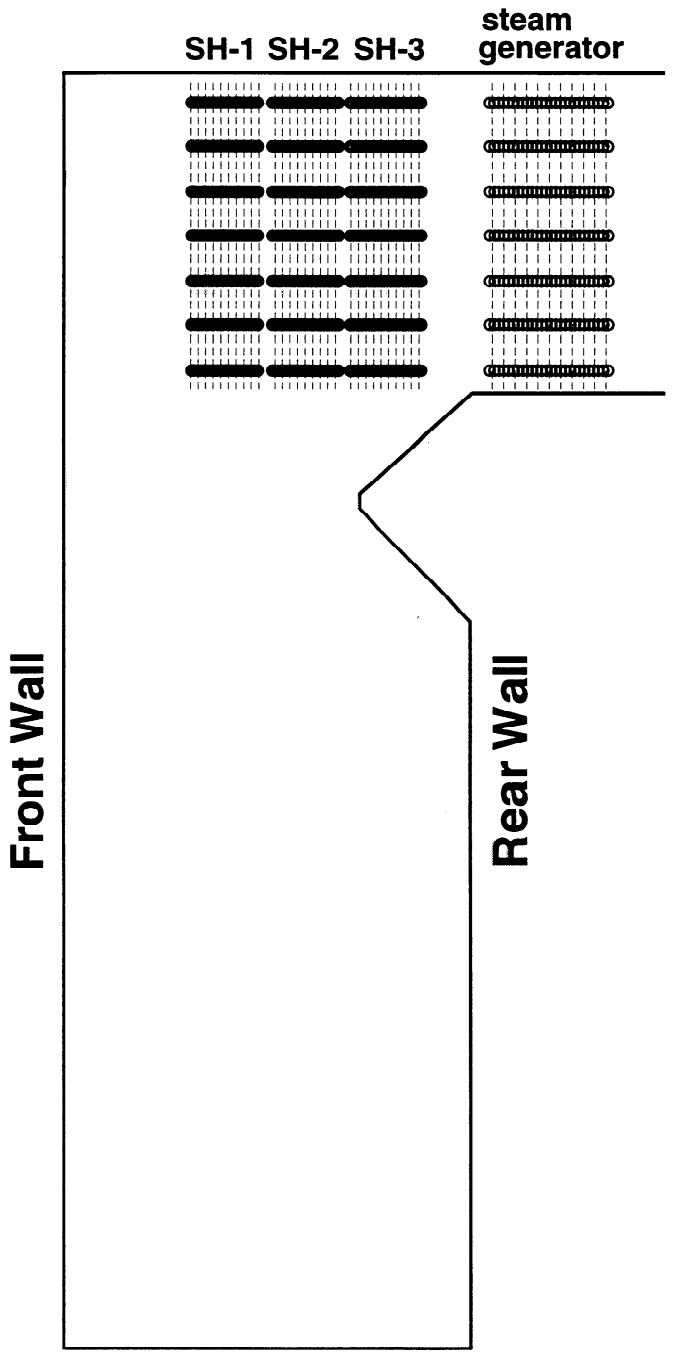

Figure 5: Locations of tube elements used in the heat exchanger model.

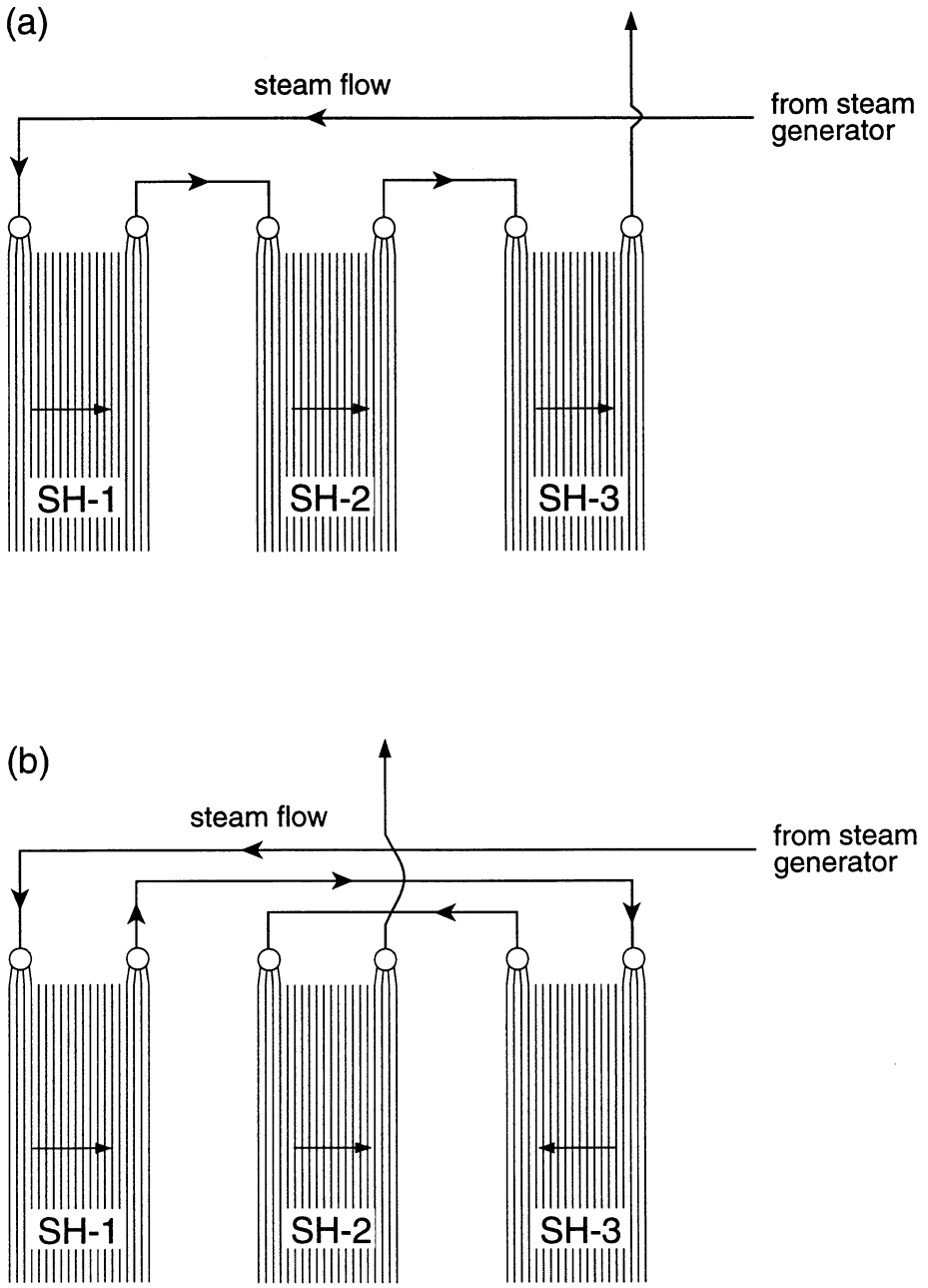

Figure 6: Steam routing schemes: (a) Case 2, (b) Case 3.

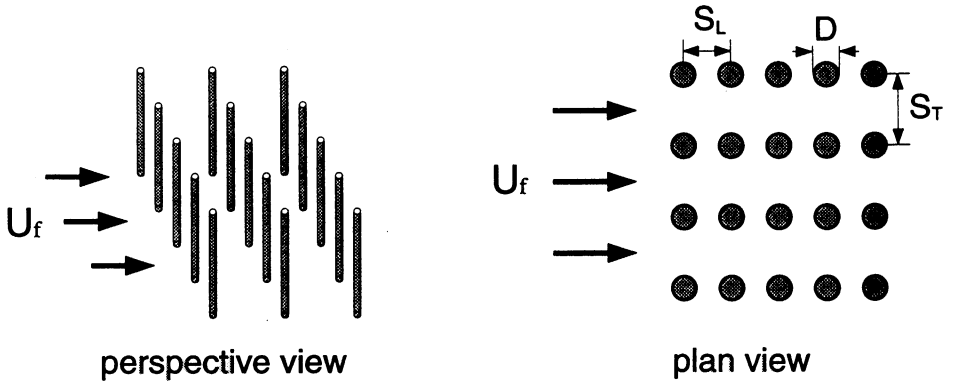

Figure 1: Flow past a tube bank.

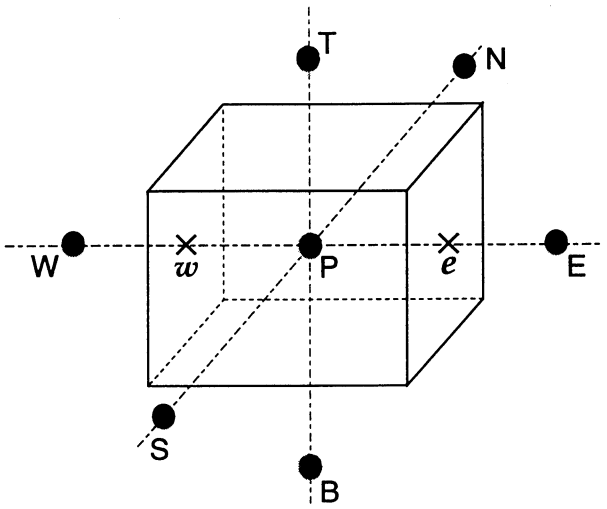

Figure 2: Control volume for the U_1 velocity component showing grid nodes and their locations.

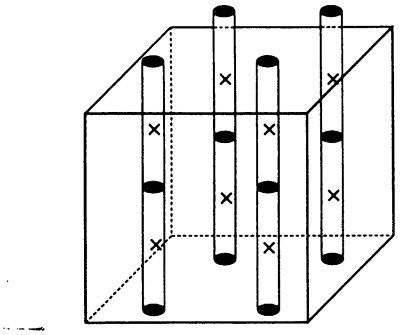

Figure 3: Schematic drawing showing tube elements (marked by X) embedded in a computational cell.

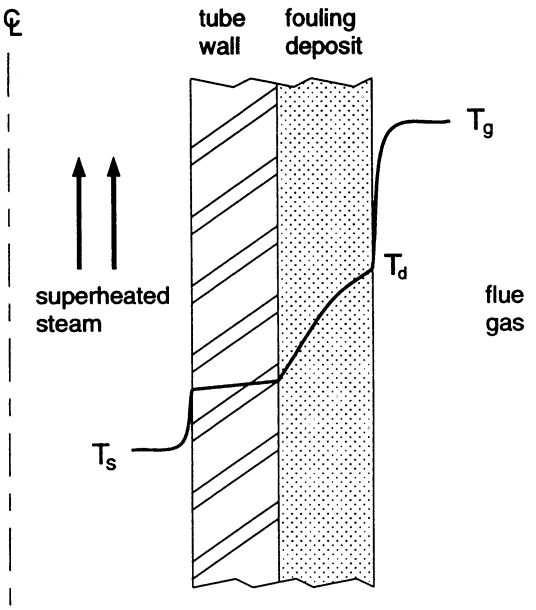

Figure 4: Temperature distribution in composite wall (fluid films included).

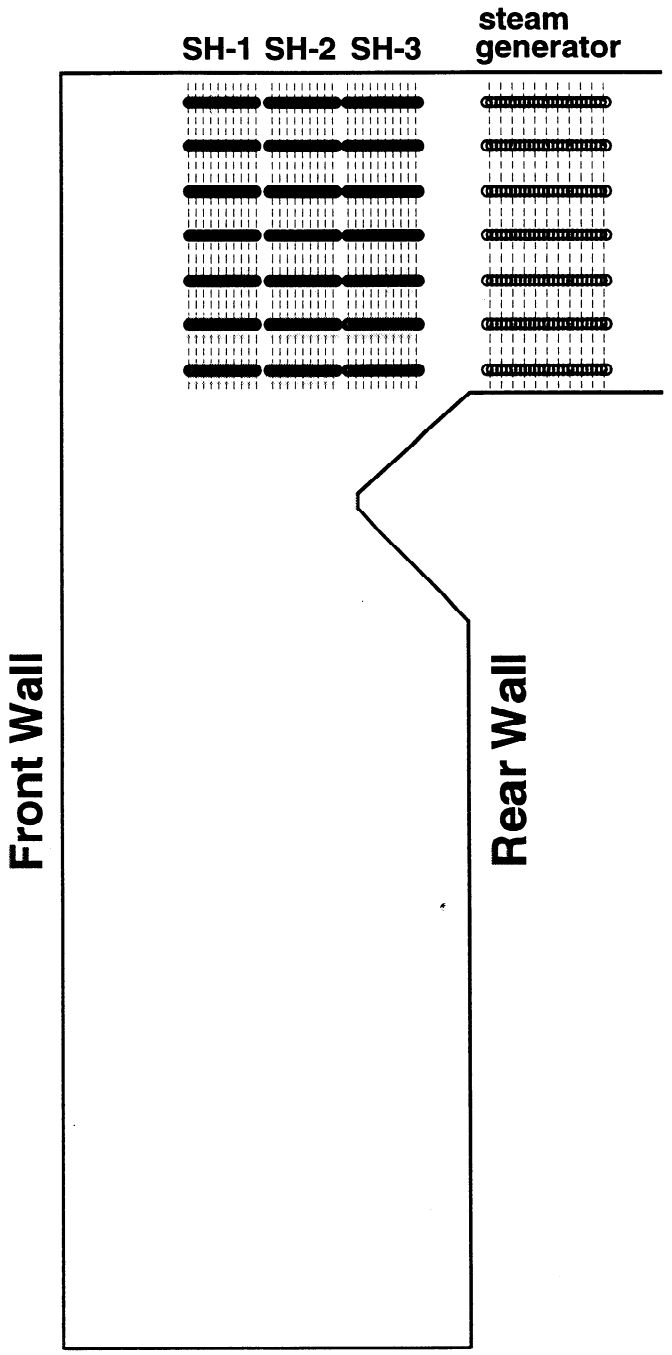

Figure 5: Locations of tube elements used in the heat exchanger model.

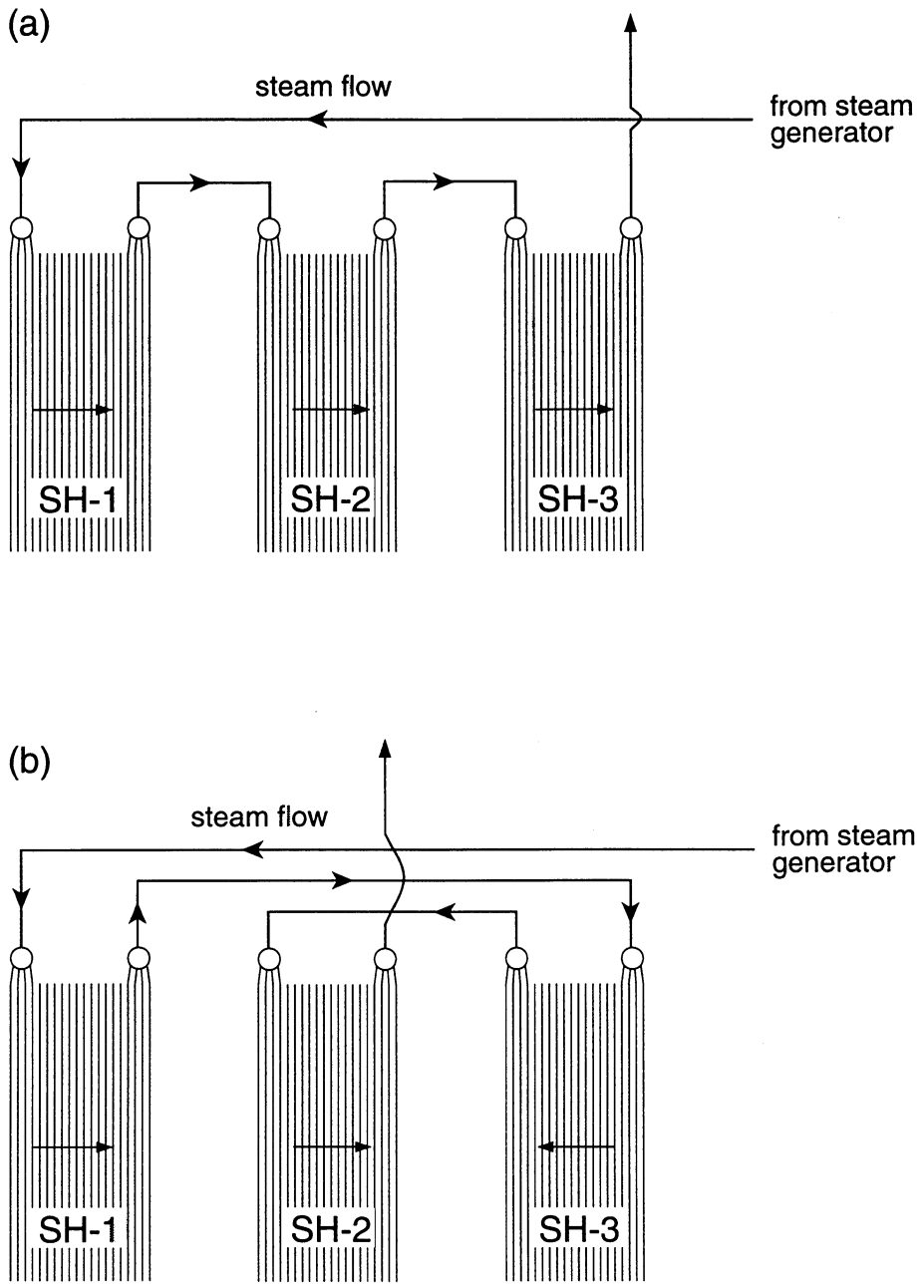

Figure 6: Steam routing schemes: (a) Case 2, (b) Case 3.

Numerical Simulation of Black Liquor Combustion in a Kraft Recovery Furnace

by

Paul Matys

The University of British Columbia
Department of Mechanical Engineering
March 1996

Abstract

The objective of this study is to develop a computer model simulating the combustion of black liquor in a kraft recovery boiler. The physical and chemical processes occurring in the boiler are represented in the form of the conservation equations of the mass, momentum, energy and gas species concentration. The turbulent flow is modeled using the k-ϵ model [14]. The black liquor spray is simulated using a statistical method; each computational droplet represents number of real droplets that have the same diameter, velocity, physical properties and chemical composition. Droplets are tracked from the time of injection until they land on the bed or are carried over. The exchange of mass and energy between the droplet phase and the gas phase is accounted for by the source terms. The gas combustion rate is computed using the Magnussen model [9]. The gas radiation heat transfer is calculated using the discrete-ordinates method [10].

A generic kraft recovery boiler is chosen to illustrate the capability of the model. The results for a number of cases are presented, and the effects of relevant parameters are discussed.

The present three-dimensional computer model of black liquor combustion contributes to the better understanding of the furnace operation. It allows to study the dependence between the main design parameters, e.g. black liquor physical properties, spray system, air delivery system, and the boiler's performance parameters, e.g. reduction efficiency, combustion efficiency, carryover/fouling, pollution, furnace capacity. This study demonstrates that mathematical modeling can be used as a predictive tool to improve the operation of the recovery boiler.

Contents

Abstract i

List of Tables iv

List of Figures v

Nomenclature vi

1 Introduction 1

2 Black Liquor Combustion 3

2.1 Mathematical Model 3

2.2 Elemental Analysis 4

2.3 Spray System 5

2.4 Black Liquor Combustion Stages 7

2.4.1 Drying 7

2.4.2 Devolatilization 9

2.4.3 Char Combustion 10

2.4.4 Char Combustion with Reduction 12

2.5 Droplet Trajectory 13

2.6 Turbulent Dispersion 13

2.7 Volatiles Combustion Model 15

2.8 Spray and Gas Phase Coupling 17

3 Results 20
3.1 Boundary Conditions 21
3.1.1 Air Systems 21
3.1.2 Liquor Systems 21
3.2 Discussion of Results 22

4 Conclusions 35

Appendix A 38

Appendix B 41

Bibliography 43

List of Tables

2.1 Elemental composition of black liquor solids. 5

3.1 Summary of black liquor combustion 26

List of Figures

2.1 Typical particle trajectories in a recovery boiler: a) based on the mean flow data only b) with turbulent dispersion 19

3.1 Air systems: (a) Base Case, (b) Two Wall Secondary, and (c) Interlaced Tertiary 27
3.2 Liquor Systems 28
3.3 Upward velocity contours (in m/s) in the front-rear vertical central plane: (a) Base Case, (b) Two Wall Secondary, (c) Interlaced Tertiary 29
3.4 Isotherms (in C) in the front-rear vertical central plane: (a) Base Case, (b) Two Wall Secondary, and (c) Interlaced Tertiary 30
3.5 Flow field in a horizontal plane at the secondary level: (a) Base Case, (b) Two Wall Secondary, and (c) Interlaced Tertiary 31
3.6 Flow field in a horizontal plane at the tertiary level: (a) Base Case, (b) Two Wall Secondary, and (c) Interlaced Tertiary 32
3.7 Upward velocity contours in a horizontal plane 6.5 m below the bullnose: (a) Base Case, (b) Two Wall Secondary, and (c) Interlaced Tertiary 33
3.8 Carryover distribution at the superheater entry plane (vertical plane from the tip of the bullnose to the top): (a) Base Case, (b) Two Wall Secondary, and (c) Interlaced Tertiary 34

Nomenclature

k	turbulent kinetic energy
q	heat flux
r	radius
u, v w	x, y, z -direction velocity component
A	area
P	pressure
R	reaction rate
Pr	Prandtl number
Re	Reynolds number
T	temperature
V	volume

Greek Symbols

ϵ	dissipation rate of k, emission coefficient
μ	dynamic viscosity
ν	kinematic viscosity
ρ	density
σ	Stefan-Boltzmann constant

Chapter 1

Introduction

Kraft recovery boilers are large combustion units used in the pulp and paper industry. A recovery boiler burns black liquor, recovers pulping chemicals and generates hot steam. Black liquor is a by-product from chemical pulping process. It is a mixture of water, volatile hydrocarbons, fixed carbon and inorganics. Black liquor is sprayed into the furnace through a number of liquor guns. The droplets are relatively coarse, most of them are from 0.5mm to 5.0mm. The droplets exposed to the high temperature of the furnace evaporate water, volatile gases are released, fixed carbon burns and inorganics undergo chemical reactions.

Physical modeling is usually limited to cold water models of a furnace that provides qualitative information about the flow patterns. Numerical modeling can provide a better insight into the complex physical and chemical phenomena occuring in a kraft recovery furnace, and combined with experimental research contribute to the improved design of the recovery furnace.

The objective of this study is to develop a computer model simulating the combustion of black liquor in a kraft recovery furnace. The coupling of the spray model with the gas-phase model should allow for a detailed analysis of the different stages of the combustion process. The black liquor spray is simulated using a statistical method; one computational droplet represents number of real droplets. Each computational droplet is tracked from the time of injection until the combustion and chemical reactions are completed. The evaporation of water and volatile release are assumed to be heat transfer controlled. The char burning rate is considered to be mass transfer dependent. The exchange of mass, momentum and

energy between the droplet phase and the gas phase is accounted for by source terms. The Magnussen model is used to compute the combustion rate of volatiles in the gas phase.

Some of the problems that are addressed by the computer simulation of the black liquor combustion are:

- carryover and fouling (mostly due to small diameter droplets and high velocity central core flow),
- incomplete combustion/reduction of the black liquor on the bed,
- high levels of the CO, CH4 and H2 in the exit gases,
- nonuniform distribution of temperature and velocity at the superheater entry.

Chapter 2

Black Liquor Combustion

2.1 Mathematical Model

Mathematical modeling and computer simulation of the kraft recovery boiler involve mathematical representation of the physical and chemical processes occurring in the boiler and obtaining a solution to the resulting conservation equations of the mass, momentum, energy and gas species concentration. The turbulent flow inside the boiler is modeled using the k-ϵ model [14]. A log normal distribution is assumed for the liquor droplet diameters. The black liquor spray is simulated using a method proposed by Walsh, Frederick and Grace [1, 2]. Each droplet is tracked from the time of injection until it lands on the bed or is carried over. The exchange of mass and energy between the droplet phase and the gas phase are taken into account. The gas combustion rate is computed using the Magnussen model [9]. The gas radiation heat transfer is calculated using the discrete-ordinates method [10].

The governing differential equations with the boundary conditions for the flow, heat transfer, and combustion are discretized using the control volume method and the Power Law differentiation scheme [6]. A block structured segmented grid is used. The grid in each segment is completely independent of the grid at the other segments, and is based on the requirements for the local flow resolution and the air port geometry. Since the grid in each segment is independent, the control volume faces at the segment interfaces do not necessarily match. The segmentation feature of the mathematical model allows for a representation of the details of the flow in critical zones of the recovery boiler, for example where jet interaction

takes place at the air port level. It also allows for a more accurate representation of the air ports, as the grid at each segment is designed specifically to take into account the air port sizes and locations in that segment. The grid distribution is optimized using this technique, as over 80 % of the grid nodes can be concentrated in regions of interest. The importance of this capability is critical as a realistic representation of the jet interaction is needed to provide information for the computation of the droplet trajectories and the chemistry. It should be noted that the complexity of the computer code increases significantly to provide such flexibility in defining the grid.

The solution method has been developed from a technique proposed originally by Vanka [19]. This technique has been extensively modified to make rapid computation of recovery boiler flows possible. The modifications include additional terms in the momentum equations, such that overall mass conservation is satisfied, even in the initial iterations. In addition, several terms in the momentum and turbulence equations are damped to prevent divergence. UBC has run several test cases in which the more classical methods [11] do not converge at all, while the new method shows good convergence. Further details of of the numerical techniques are presented elsewhere [18].

2.2 Elemental Analysis

Typical black liquor contains about 35% water and 65% solids (BLS). An elemental analysis of a black liquor solids sample provides a detailed elemental composition. An example of black liquor solids composition is presented in the Table 2.1. Using the elemental composition of black liquor solids and making some assumption about the percentage of the elements that go into the creation of the volatiles, one can compute the composition of the black liquor solids in terms of chemical compounds. An example of such a calculation is presented in Appendix A. The volatile gases may consist of CO, CH4, H2, H2S and CO2. The smelt usually contains Na2CO3, Na2S, Na2SO4, K2CO3 and NaCl.

The higher heating value (HHV) of black liquor is measured in an oxygen bomb calorimeter. Typical HHV is about 15 MJ/kgBLS. The net heating value (NHV) that is actually available in the boiler is lower due to the fact that the reduction process is endothermic and the water in the furnace is in the gas-state. The HHV and the elemental composition of

Carbon C	39.0% wt.
Hydrogen H	3.8% wt.
Oxygen O	33.0% wt.
Sodium Na	18.6% wt.
Potassium K	1.2% wt.
Sulfur S	3.6% wt.
Chloride Cl	0.6% wt.
Inerts	0.2% wt.

Table 2.1: Elemental composition of black liquor solids.

BLS is used to analyze the energy balance during the black liquor combustion. The value of the total heat release computed by adding up the energy contribution of each reaction is usually different from the HHV. This difference is attributed to the pyrolysis process that can be either endothermic or exothermic. A sample analysis of the projected heat release is presented in Appendix B.

2.3 Spray System

The common types of spray nozzles used in recovery boilers are the splash plate, V-jet and helical cone. The mass fraction of the black liquor spray can be related to the droplet diameter through a distribution function. The log-normal distribution function is often used to represent the black liquor spray:

$$f(D) = \frac{1}{D\sigma\sqrt{2\pi}} exp - (\frac{\ln(D/D_m)}{2\sigma^2})$$

where

D - the droplet diameter

D_m - the mean droplet diameter

σ - the standard deviation

In an average size recovery boiler about 20 kg of black liquor is sprayed per second, this results in millions of droplets suspended in the furnace cavity at any given moment.

However, due to the limited computer resources only a relatively small number of droplets can be represented in the model. Therefore, a statistical method is used to simulate the spray. Each computational particle is assumed to represent a number of real particles that have the same location, velocity, chemical composition and physical properties. The droplets diameters are computed in a following way. First, a distribution function is assumed. The log-normal or square root log-normal distribution is considered to be a good representation of a splash plate nozzle distribution. A typical mean diameter for black liquor spray is about 2.5-5 mm. The range of droplet diameter to be simulated is defined by a lower and upper limits; the range 0.1-6.0 mm represents over 95 % of the total mass of the distribution. The number of computational droplets is selected as an optimum between available computer resources and the required accuracy of the simulation, for example 10000. The diameter range is subdivided into 10000 intervals, and for each interval a mean interval diameter is computed. Once the droplet diameter, the value of the distribution function and the interval step are known, one can compute how much mass and how many real droplets are represented by one computational droplet. The real-to-computational ratio does not have to be and integer, and can be adjusted in a continuous way by changing the length of each interval. This method allows to control the computational representation of the different diameter ranges. For example, if carryover is of special interest, one can insist on lower real-to-computational ratio, and better representation in the small droplet diameter range.

The black liquor is introduced into the furnace through a number of liquor guns, located few meters above the furnace floor. The spray created by a splash plate is defined by the horizontal spread angle, and the vertical angle (due to the plate oscillation). Typically, the droplets are spread about 150 deg in horizontal plane and 30 deg in vertical plane (e.g., between 0 deg "top position" and -30 deg "down position"). A random method is used to distribute the droplets among the nozzles and ranges of possible injection directions defined by the horizontal and vertical angles. Once the nozzle location, and the initial droplet velocity magnitude and direction are known, the velocity components u, v, w can be computed. A number of droplets is injected at the same time and their positions, changes in mass and chemical composition are tracked and recorded until the droplets/particle leave the computational domain.

The bed shape curvature is approximated by a staircase grid arrangement. A droplet/particle

that lands on the bed is assumed to complete its remaining combustion stages on the bed surface. Mass and energy are exchanged between spray and gas within the first adjacent to the bed gas phase cell. The instantaneous rates of mass and energy release/absorption, that are required for the in-flight combustion, are not required for the steady state bed treatment. A droplet/particle that impinge on wall is assumed to stick to the wall surface and exchange mass and energy within the first neighboring gas phase cell.

The results of the spray simulation can be sensitive to the random number generator seed number when a relatively small number of computational droplets is used (e.g. 100). The sensitivity subsides as the number of droplets increases. In a typical test case 10000 droplets are usually used to represent spray, and the results are almost independent (i.e. differences are smaller than 1-2%) of a chosen seed number.

2.4 Black Liquor Combustion Stages

After the black liquor droplets are injected into the high temperature furnace environment the combustion process begins ([2, 5, 3]). The droplets evaporate water, pyrolysis gases are released and char carbon reacts with surrounding gases

2.4.1 Drying

Drying starts immediately after the injection. The temperature of the droplet increases up to approx. 150 C and stays constant thereafter until the end of the drying phase. Drying is described mathematically by the following set of equations.

$$\frac{dm}{dT} = \frac{Q_t}{h_v}$$

where

m the droplet mass

T the droplet temperature

Q_t - the total heat transfer to the droplet

h_v - the evaporation enthalpy

The total heat transfer consists of convective and radiative heat transfer.

$$Q_t = Q_c + Q_r$$

The convective heat transfer Q_c is a function of the heat transfer coefficient h, the droplets surface area S and the temperature difference between the droplet and the surrounding gas $(T_g - T_d)$.

$$Q_c = hS(T_g - T_d)$$

The heat transfer coefficient is dependent on the heat conduction coefficient for the gas, k, the Nusselt number , Nu, and the droplet diameter D.

$$h = k\frac{Nu}{D}$$

The Nusselt number for a droplet can be correlated with the Reynolds and Prandtl numbers by the following empirical formula

$$Nu = 2 + 0.6Re^{0.5}Pr^{0.33}$$

The radiative heat transfer is due to the radiation between the droplet and the surrounding gas Q_{rg}, smelt bed Q_{rb} and furnace walls Q_{rw}.

$$Q_r = Q_{rg} + Q_{rb} + Q_{rw}$$

The three radiative components can be computed as follows:
the radiation from the gas
$Q_{rg} = \epsilon S\sigma(T_g^4 - T_d^4)$
the radiation from the smelt bed
$Q_{rb} = (1 - \epsilon)S\sigma F_b(T_b^4 - T_d^4)$
the radiation from the furnace walls
$Q_{rw} = (1 - \epsilon)S\sigma(1 - F_b)(T_w^4 - T_d^4)$
where
ϵ the emission coefficient of the gas,

σ the radiation constant,

F_b the smelt bed view factor,

S the droplet surface area,

T_b the smelt bed temperature,

T_w the average furnace walls temperature

From the experimental data it is known that the droplet swelling occurs almost immediately after the injection, and stays constant during the rest of the drying phase. The diameter increase can be described by the swelling factor. A typical value of the drying phase swelling factor is 1.6 . The droplet diameter can be computed as:

$$D = \Theta_{dr} D_i$$

where

Θ_{dr} swelling factor during the drying phase

2.4.2 Devolatilization

The total energy required for the droplet devolatilization, Q_{tot}, can be calculated as

$$Q_{tot} = \frac{m_0 s_0}{s_{ig}} (c_P (T_{max} - T_{ig}) + H_{vw}(1 - s_{ig}))$$

where m_0 - the initial droplet mass

s_0 - the initial solid content

s_{ig} - the solid content at ignition (start of devolatilization)

c_P - the droplet heat capacity

T_{max} - the maximum temperature of the droplet

T_{ig} the droplet temperature at ignition

H_{vw} - the enthalpy of evaporation for water

The total heat consists of the heat necessary to evaporate the remaining water (if $s_{ig} < 1$), and the heat necessary to increase the temperature of the droplet from T_{ig} to T_{max}.

The total mass loss during the pyrolysis includes the evaporation of the remaining water and the release of volatile gases, and can be computed as

$$M_{tot} = \frac{m_0 s_0}{s_{ig}}(1 - s_{ig}) + m_0 s_0 \frac{c_v}{c_s}$$

The heat transfer rate to the particle, $Q(t)$, and heat transfer during one time step, dQ, can be calculated in the same way as for the drying phase. The droplet mass loss, $M(t)$, can be computed as being proportional to the heat transfer

$$M(t) = \frac{m_0 s_0}{s_{ig}}(1 - \frac{M_{tot} s_{ig} Q(t)}{m_0 s_0 Q_{tot}})$$

The change of droplet diameter is assumed to be proportional to the mass loss and heat transfer

$$D(t) = \sqrt{A/\pi}$$

where droplet area, A,

$$A = \pi D_0^2 (D_{dr} + (D_{max} - D_{dr})\frac{dQ}{Q_{tot}})^2$$

2.4.3 Char Combustion

For the calculation of the char burning rate the concentration of oxygen O2, carbon dioxide CO2 and water vapor H2O have to be known. First the mass transfer rates to the particle surface for the reacting gases are computed ([16]), i.e. :

Oxygen transfer rate

Sherwood number: $Sh = 2 + 0.5 Re^{0.5} Sc^{0.33}$

Oxygen mass transfer coefficient $k_{O2} = Sh\ D_{O2}/D$

Oxygen molar flux $R_{O2} = k_{O2} x_{O_2}/(82.1\ T_g)$

Water vapor transfer rate

Sherwood number: $Sh = 2 + 0.5 Re^{0.5} Sc^{0.33}$

Mass transfer coefficient $k_{H2O} = Sh\ D_{H2O}/D$

Molar flux $R = k_{H2O} x_{H2O}/(82.1\ T_g)$

The kinetic limitation $R_k = const.\ exp(-24000/T_g)$

The resulting molar flux of water $R_{H2O} = 1/(1/R + 1/R_k)$

Carbon-dioxide transfer rate

Sherwood number: $Sh = 2 + 0.5Re^{0.5}Sc^{0.33}$

Mass transfer coefficient $k_{H2O} = Sh\ D_{H2O}/D$

Molar flux $R = k_{H2O}x_{H2O}/(82.1\ T_g)$

The kinetic limitation $R_k = const.\ exp(-24000/T_g)$

The resulting molar flux $R_{CO2} = 1/(1/R + 1/R_k)$

where

x_{O_2}, x_{CO_2}, x_{H_2O} are the molar gas concentrations

Re is the Reynolds number

Sc is the Schmidt number

D_{O_2}, D_{CO_2}, D_{H_2O} are the gas diffusion coefficients

D is the particle diameter

T_g is the gas temperature

The relatively high furnace gas temperature makes the kinetic reaction rate limitation insignificant, and the char-carbon gasification rate is controlled by the mass transfer of the reactants.

The carbon loss due to reaction depends on the ratio between the transfer rate of oxygen and the transfer rate of steam and carbon-dioxide.

If $R_{O2} > (R_{H2O} + R_{CO2})$ then $R_C = R_{O2}$

If $R_{O2} < (R_{H2O} + R_{CO2})$ then $R_C = (R_{H2O} + R_{CO2})$

After the molar carbon loss rate is computed the carbon loss during one time step can be computed as

$$dm = 12R_C\pi D^2 dt$$

and the droplet diameter as

$$D = (6/\pi \frac{X_{ash}}{\rho_{smelt}} m_o s_o)^{1/3}$$

where

X_{ash} is the mass fraction of ash

ρ_{smelt} is the smelt density

2.4.4 Char Combustion with Reduction

The following reactions are considered ([17]):

$$C + O_2 = CO_2$$

$$C + CO_2 = 2CO$$

$$C + H_2O = CO + H_2$$

$$C + (2 - f)/4Na_2SO_4 = (2 - f)/4Na_2S + fCO + (1 - f)CO_2$$

$$Na_2S + 2O_2$$

The net oxygen transfer rate to the smelt/char is

$$R'_{O_2} = R_{O_2} - R_{CO_2} - R_{H_2O} - 2f/(2 - f)R_{SO4}$$

The overall smelt reduction efficiency

$$SxIxdE/dt = R_{SO4} - R_S = R_{SO4} - (1 - p)/2R'_O2$$

where

$$E = [Na_2S]/([Na_2S] + [Na_2SO_4])$$

is the smelt reduction

The carbon rate equation has the following form:

$$R_C = MAX(R_{CO_2} - R_{H_2O} + 4/(2 - f)SI(dE/dt), R_{O_2} + 2SIdE/dt)$$

The rate equations that are necessary to to solve the above equations are:

$$R_{CO_2} = 6.3E - 10 * [C]P_{CO_2}/(P_{CO_2} + 3.4P_{CO}) * exp(-30070/T)$$

$$R_{H_2O} = 2.56 - 9 * [C]P_{H_2O}/(P_{H_2O} + 1.42P_{H_2}) * exp(-25300/T)$$

$$R_{SO4} = 1310 * [SO4]/(0.011([C] + [S]) + [SO4]) * [C]exp(-14700/T)$$

or

$$R_{SO4} = 3790[C][SO4]^{1.4}exp(-18700/T) \quad .$$

2.5 Droplet Trajectory

The droplet location and velocity as a function of time is found after solving the equation of motion for a particle. For z-coordinate the equation has form

$$m\frac{dw}{dt} = \frac{1}{2}\rho C_D A U_{rel}^2 + mg$$

where m is the droplet mass

t is the time

w is the velocity component along z-axis

C_D is the drag coefficient

ρ is the gas density

A is the area of the droplet cross section

U_{rel} is the relative velocity between the droplet and the gas

g is the gravitational constant

Similar equations can be written for the x and y coordinates. The drag coefficient is a function of the Reynolds number. The correlations for different Reynolds number ranges can be taken from literature:

$C_D = 28Re^{-3/4}$ for $0.5 < Re < 30$

$C_D = 12Re^{-1/2}$ for $30 < Re < 700$

2.6 Turbulent Dispersion

The gas flow in a recovery boiler is highly turbulent. The turbulent quantities characterizing the turbulence (e.g., k, ϵ, l_{sc}) vary widely throughout the boiler. Relatively small length scales can be encountered around the jets, and larger structures are present in the upper

boiler around the bullnose. The computation of droplet/particles trajectories based solely on the mean flow data does not take into account the turbulent character of the flow. One of the most important objectives of the boiler simulation is to predict the mechanical carryover that contributes to the plugging problem. The mechanical carryover occurs when particles are entrained into the fast moving upward flow that is often present in the center of the boiler. The best chance of being carried over have small smelt particles (i.e. smaller than 1.5 mm), and larger particles that are in the swollen state and have very low specific density.

The turbulent dispersion model should account for the turbulence of the flow and modify the trajectory of the particles accordingly. The turbulent dispersion model used is based on the typical turbulent quantities that are available from $k - \epsilon$ model.

turbulent length scale

$$l_{sc} = C_{\mu}^{3/4} \frac{k^{3/2}}{\epsilon}$$

and turbulent time scale or eddy disspation rate

$$t_{turb} = k/\epsilon$$

The turbulent time scale can be interpreted as the time required to dissipate an eddy. The turbulent length scale is correlated with the size of an eddy. The particle residence time in an eddy or the time a particle needs to traverse an eddy of the size given by the turbulent length scale can be computed as

$$t_{res} = \frac{l_{sc}}{u + u' - u_p}$$

A typical time step used for the particle trajectory computation is of an order 0.01 sec. If the time step is larger than t_{res} or t_{turb} than one assumes that there is no significant interaction between particle and turbulent eddy, and particle trajectory is computed only from the mean flow velocity. However, if the opposite is true one assumes that the particle will be influenced by the local turbulence structures. The time of the interaction is taken as the smaller of the time needed to traverse the eddy and the time needed to dissipate the eddy. Typical values for t_{res} and t_{turb} in a recovery boiler are of an order 1 sec.

The additional turbulent/fluctuating velocity component is assumed to follow Gaussian distribution with the variance $var = 2/3k$, and standard deviation $\sigma = u' = \sqrt{2/3k}$.

Using the reverse error function and the random number generator one can pick a velocity component following the Gaussian distribution. The fluctuating component u' is added to the mean flow value of the u-component and the total velocity of the flow is used in the calculation of the particle trajectory.

Practically, it means that a droplet traversing a gas-volume characterized by the large turbulent structures and long eddy dissipation times is subject to the additional "turbulent drag force". The trajectories computed only from the mean flow data are usually relatively smooth (Fig 2.1a). The turbulent trajectories can differ considerably from the mean flow trajectories (Fig 2.1b). The simulation that includes the turbulent dispersion predicts smaller carryover than the simulation based solely on the mean flow data. For example, for the flow characterized by the strong central core there can be approximately 30-50% reduction in carryover prediction. A particle has alaways a better chance of being moved away or ejected from the central core due to the local turbulence than to be moved back into the central core.

There are some model simplifications that could cause the overprediction of the turbulence dispersion. For example, the model does not take into account the change in the value and direction of the eddy-particle relative velocity as the particle traverses the eddy and at the same time the eddy dissipates its energy.

2.7 Volatiles Combustion Model

Methane CH4, carbon monoxide CO and hydrogen H2 are the combustible gases that are reacting with oxygen in the gas phase following a single step reactions.

METHANE

$$CH_4 + 2O_2 -> CO_2 + 2H_2O$$

or in mass units

$$16kgCH_4 + 64kgO_2 -> 44kgCO_2 + 36kgH_2O$$

CARBON MONOXIDE

$$CO + 0.5O_2 -> CO_2$$

or in mass units

$$28kgCO + 16kgO_2 -- > 44kgCO_2$$

HYDROGEN

$$H_2 + 0.5O_2 -- > H_2O$$

or in mass units

$$2kgH_2 + 16kgO_2 -- > 18kgH_2O$$

If the combustion process is assumed to be chemical-kinetically controlled, the reaction rate can be calculated from the Arrhenius expression e.g.,

$$R = [CH_4]^a[O_2]^b c_f exp(E_f/T)$$

This approach includes the assumption that the chemical reaction time is much longer than the time scale of turbulent fluctuations. However, in the kraft recovery boilers this is not the case. The average temperature in a typical furnace is usually about 1000 C (1273 K) which means that the combustion rate computed from the Arrhenius expression is very high and is not limiting/controlling the combustion rate in the furnace. The mixing between combustible gases and oxygen is the process that controls the combustion rate in the gas phase.

In the present study the combustion model due to Magnussen [9] has been implemented. This model explicitly takes into account the turbulent kinetic energy and its rate of dissipation during the premixed or mixing phase of combustion.

In the mixing controlled combustion, fuel and oxygen are assumed to be initially located in separate eddies. Since the temperature is very high, the combustion rate is assumed to be determined by the micro-mixing rate. A correlation between the reaction and the turbulence quantities and the fuel concentration is expressed as

$$R_f = A(\epsilon/k)\rho_f$$

where

A is a reaction dependent constant

k is the local turbulence kinetic energy

ϵ is the dissipation rate of k

ρ_f partial density of fuel

The units of combustion rate are $kgfuel/s$. The term (ϵ/k) has units of $1/s$ and represents the eddy dissipation rate which is correlated with mixing at the micro-level and the combustion rate. There can be volumes of the gas where the local time mean oxygen concentration is low. In this case the dissipation of oxygen containing eddies is assumed to be limiting the combustion rate.

$$R_f = A(\epsilon/k)\frac{\rho_{O_2}}{r_f}$$

where r_f is the stoichiometric oxygen requirement to burn one unit of the fuel.

In the premixed turbulent combustion, fuel and oxygen are found in the same eddies. The reaction rate is determined by the dissipation rate of the structures containing the hot reaction products that provide the premixed structures with activation energy needed for combustion initiation. The following equation takes this into account

$$R_f = A(\epsilon/k)B\frac{\rho_p}{(1+r_f)}$$

where

B is a constant

ρ_p is the local time-mean concentration of reaction products. In a typical recovery boiler the premixed combustion does not take place.

All three cases can be summerized in

$$R_f = A(\epsilon/k)\ MIN(\rho_f, \frac{\rho_{O_2}}{r_f}, B\frac{\rho_p}{(1+r_f)})$$

2.8 Spray and Gas Phase Coupling

The black liquor spray model is coupled with the gas phase model. The gas-phase variables (u, v, w, p, k, ϵ, T, c_i) are solved in a fixed Eulerian coordinate system, for a steady state case and are only functions of position. The properties of black liquor phase are calculated in a moving frame of reference and are function of time and location. The gas-phase and

spray-phase exchange mass, momentum and energy. The interaction is taken into account via source/sink terms added to the gas phase cells. For example, if water evaporates from the droplet while crossing a cell the water vapor mass is added to the cell mass balance through the source term. The amount of thermal energy exchanged between the droplet and the surrounding gas is accounted for by the source/sink terms in the gas-phase energy equation.

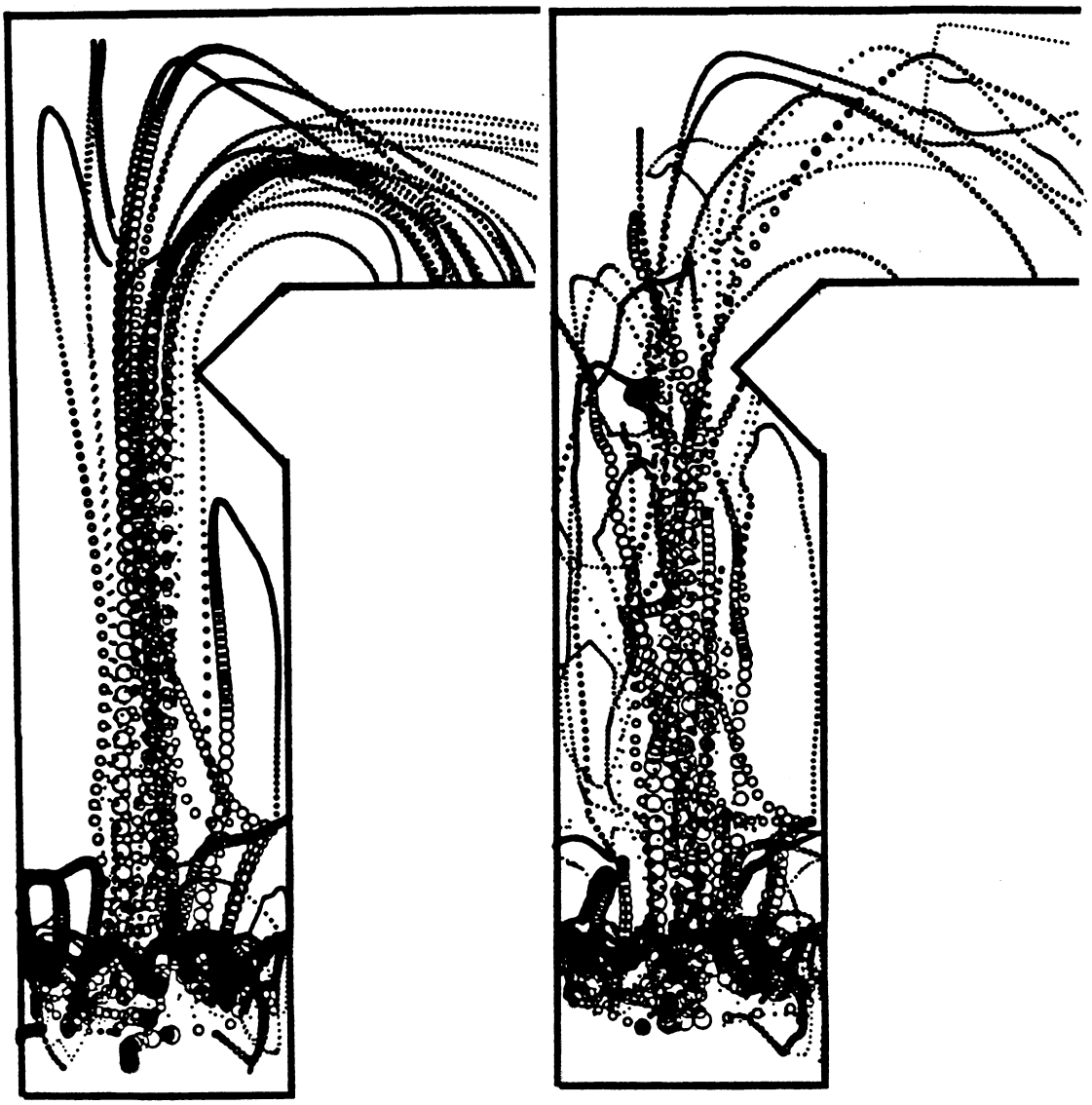

(a) (b)

Figure 2.1: Typical particle trajectories in a recovery boiler: a) based on the mean flow data only b) with turbulent dispersion

Chapter 3

Results

Three air systems and six black liquor spray strategies are evaluated for a generic recovery boiler using mathematical modeling and computer simulation techniques. The presence of a central upward flowing core and the associated mechanical carryover are used as criteria for the evaluation. The air system in the base case features four wall primary, four wall secondary and two wall tertiary air ports. Modifications to the base case include a two wall secondary system and an interlaced tertiary system. The liquor spray configuration in the base case features four liquor guns, 2.8 mm mean droplet diameter, 150° horizontal spread and 0 to -30° vertical oscillation. Modifications to spray conditions include 8 liquor guns, 4 mm mean diameter droplets, stationary firing, 40° wedge and a combination of these. The results indicate that mechanical carryover can be reduced by manipulation of the secondary and tertiary air systems, and the liquor spray conditions. The study shows that mathematical modeling and computer simulation techniques can be effectively used for improving the performance of kraft recovery boilers.

In this study, the use of the model as an optimization tool is demonstrated by investigating three different air firing strategies and six different black liquor spray configurations for a generic recovery boiler. The study demonstrates that the carryover can be reduced by manipulating air and liquor delivery, and that the mathematical model and computer simulation techniques can be effectively used for improving the performance of a kraft recovery boiler.

3.1 Boundary Conditions

A generic recovery boiler is investigated in this study. The boiler has a 10 m square base, and is 40 m high. The bull nose is located 26.5 m from the floor. The boiler features three levels of air: four wall primary (1.2 m above the floor), four wall secondary (3 m above the floor) and two wall tertiary (10 m above the floor).

3.1.1 Air Systems

The boiler operates with an air split of 48% primary, 32% secondary and 20% tertiary.

The three air systems investigated are (a) base case, (b) two wall secondary, and (c) interlaced tertiary, as shown in Fig. 3.1. The jet locations are indicated by arrows. In all three cases, the size and shape of the air ports and the total air injected at each level are the same. The base case has five secondary ports on each wall and seven tertiary ports on the front and rear walls. In case (b), the two wall secondary case, the secondary level configuration has been modified. The side wall jet velocities have been increased, and the front and rear wall jet velocities have been decreased, respectively, by 24% so that the total air input remains unchanged. The primary and tertiary levels are the same as in the base case. In case (c), the interlaced tertiary case, the tertiary level configuration has been changed. The velocities of the opposing jets pairs have been either increased or decreased by 38% to create interlaced tertiary pattern. The primary and secondary level jets are the same as in the base case.

3.1.2 Liquor Systems

The boiler operates at a load of 17.67 kg/s (3.37 X 10^6 lbs/day) of black liquor solids with liquor guns at 7 m above the floor. The six different liquor spray configurations considered in this study are shown in Fig. 3.2. In the base liquor spray configuration, the spray has a mean droplet diameter of 2.8 mm and a horizontal spray angle of 150°, and the nozzles oscillate vertically from 0 to -30°. All liquor spray configurations except case (d) have 4 liquor guns, one at the center of each wall. The liquor spray configuration (d) has 8 liquor guns, 2 on each wall at 3.3 m away from the corners. The spray configuration (e) is similar to the base

configuration except that the mean droplet diameter is 4 mm. In the spray configuration (f), the nozzles are stationary and are fixed at -30°. Otherwise this configuration is similar to the base configuration. The spray configuration (g) differs from the base configuration only in the horizontal spread due to the presence of a 40° wedge in the center. The spray configuration (h) incorporates all the modifications of the configurations (e), (f) and (g).

3.2 Discussion of Results

For the evaluation of air systems, the base case liquor spray configuration shown in Fig. 3.2 with 4 liquor guns, 2.8 mm mean droplet diameter, 150° horizontal spread and oscillating nozzles was used.

Fig. 3.3 shows the vertical velocity contours in the front-rear central plane for the three different air systems. Each case shows central upward flow and downward flow close to the walls. The central upward flow core is narrower in the base case, and is of a higher velocity in the two wall secondary case. For example, the 15 m/s upward velocity contour extends above the bull nose for the two wall secondary case, and terminates below the bull nose in the other two cases. For the interlaced tertiary case, the upward flow region is pushed farther away from the bull nose, resulting in a large recirculation region under the bull nose. The gas temperature is higher in the center, lower near the walls and higher just above the bed (Fig. 3.4). Above the tertiary level, the isotherms have shapes similar to the vertical velocity contours. Similar trends are also observed in the vertical velocity contours and the isotherms (not shown) in the side-side central plane.

Fig. 3.5 compares the velocity distributions in a horizontal plane through the secondary level for the three cases. The secondary air enters the boiler symmetrically from all four sides in the base case and in the interlaced tertiary case, and converges to the central region. This creates a higher pressure in the central region, resulting in a narrow high velocity upward flowing core, and strong downward flow to the bed. Although some downward flow to the bed is required to maintain high bed temperatures, excessive central downward flow can cause bed control problems and erode the bed to the extent that floor tubes become exposed. The high velocity central upward flow can result in flow instabilities because of the high pressure gradients. For the two wall secondary case, the secondary jet interaction takes place over

a larger region spanning the width of the boiler. therefore distributed over a larger region, resulting in lower velocities. In the two wall configuration considered here, there is still some flow through the secondary ports on the front and rear walls. This flow is necessary to cool the port openings, and also to control the bed shape. It should be noted that if lowering of the secondary air flow along the front and rear walls causes bed control problems, then some of the primary air can be shifted from the side wall primary ports to the front and rear wall primary ports to help with bed control.

Fig. 3.6 compares the velocity distributions in a horizontal plane through the tertiary level for the three cases. The tertiary jet penetration is low for the base case and for the two wall secondary case, since the tertiary jets do not have the necessary momentum to penetrate the high velocity upward flowing core. This is especially true for the central tertiary jets. The tertiary jets close to the side walls penetrate somewhat deeper, but are then pushed toward the side walls by the central upward flow. For the interlaced tertiary case, the penetration of the higher velocity tertiary jets is improved considerably. These deeply penetrating jets are quite successful in breaking up the core, resulting in lower vertical velocities in the central region at higher elevations.

Fig. 3.7 compares the upward velocity contours below the bullnose. The upward flow is more uniform for the interlaced tertiary case (c). Fig. 3.8 shows the distribution of carryover particles at the superheater entry plane, a vertical plane stretching from the tip of the bullnose to the top of the boiler. Most of the carryover particles consist of smelt, however, some of the larger particles are still in the char burning stage of combustion. The size of the particles range from about 0.01 mm to about 10 mm. The base case has the highest total carryover of about 12% of the total black liquor mass flow. The distribution of the carryover particles is similar to the shape of the central core contours that are shown on Fig. 3.7. In the base case the central core is narrow and stretched between the left and right walls. The resulting carryover distribution shows a similar crescent-like pattern. The central core of the two wall secondary case is almost circular and slightly shifted to the left wall. The carryover distribution is mostly located in the left half of the superheater entry plane. The total carryover in this case is about 11%. The interlaced jets of the tertiary level form a serpent-shaped contours of the upward velocity. The carryover distribution follows the shape of the upward velocity contours. The total carryover in the interlaced tertiary case

is about 9%.

For the evaluation of liquor delivery systems, only the base case air system shown in Fig. 3.1(a) with four wall secondary and two wall tertiary jets was considered. Since the total black liquor spray was constant, the total heat source is nearly the same in all the spray configurations. However, the heat source distribution is different due to the change in spray conditions. It was found that the vertical velocity contours were similar to those shown previously (Fig. 3.3a) for all the liquor spray configurations. Comparison of the isotherms (not shown) with those shown in Fig. 3.4a indicated that the furnace gas is slightly hotter near the bed and cooler in the upper furnace for cases (e) to (h). This is due to a larger part of the total heat being released near the bed in these cases.

The different air configurations investigated in this study were aimed at making the upward velocity profile more uniform, with the hope of reducing the carryover. This velocity distribution was modified in one case by the the secondary air flow, and in another case at the tertiary air flow. Different liquor spray configurations were investigated next with the aim of reducing the carryover by increasing the mean droplet diameter, spraying liquor away from the central high velocity upward flow and directing the spray downward.

Table I summarizes the fate of the constituents of the black liquor spray and combustion. In all cases, most of the carryover mass consists of smelt. This indicates that most of the char combustion is completed before the char/smelt particles reach the convective sections. Modifications of air systems (Table I: cases b and c) indicate that char carryover for the two wall secondary and the interlaced tertiary configurations are lower than that for the base case. Compared to the base case, the total carryover is nearly the same in the two wall secondary case and, is lower by about 25% in the interlaced tertiary case; the deposition of the smelt on the walls is increased by about 10% in the two wall secondary case and, by about 20% in the interlaced tertiary case. The deposition on the bed is approximately the same in the three configurations.

Modifications to the liquor spray characteristics indicate that the carryover is reduced by increasing the mean droplet diameter (Table I: case e), directing the liquor downwards (case f) and spraying with a wedge (case g). The carryover can be minimized by combining these changes in the liquor spray configurations (case h). However, in this case, the amount of wet liquor landing on the bed also increases. Increasing the number of liquor guns does

not seem to reduce the carryover significantly (case d). When the mean droplet diameter is 4mm and/or the liquor is directed downward, more spray lands on the bed (cases e, f and h). When 8 liquor guns are used or a wedge is present, more spray lands on the walls (cases d and g).

The study has shown that modifying the secondary and tertiary air input or the spray characteristics can produce changes in the mechanical carryover. Many other variations in the secondary and tertiary air input are possible and even in the air split between the different levels. Additional variations in the liquor spray configuration are also possible.

(a) Base Case

%	IN FLIGHT	BED	WALL	CARRY OVER	TOTAL
WATER	29.39	4.99	0.63	0.00	35.00
VOLAT.	13.74	9.96	0.66	0.00	24.36
CHAR	5.56	5.86	1.21	0.28	12.90
SMELT	0.00	13.36	4.97	9.41	27.74
TOTAL	48.69	34.17	7.46	9.68	100.00

(b) Two Wall Secondary

%	IN FLIGHT	BED	WALL	CARRY OVER	TOTAL
WATER	29.57	4.71	0.72	0.00	35.00
VOLAT.	13.12	10.02	1.22	0.00	24.36
CHAR	4.75	6.18	1.87	0.10	12.90
SMELT	0.00	14.48	7.36	5.90	27.74
TOTAL	47.44	35.39	11.17	6.00	100.00

(c) Interlaced Tertiary

%	IN FLIGHT	BED	WALL	CARRY OVER	TOTAL
WATER	29.41	4.93	0.66	0.00	35.00
VOLAT.	13.63	10.04	0.69	0.00	24.36
CHAR	5.39	5.85	1.51	0.16	12.90
SMELT	0.00	13.88	7.28	6.58	27.74
TOTAL	48.43	34.70	10.14	6.74	100.00

Table 3.1: Summary of black liquor combustion

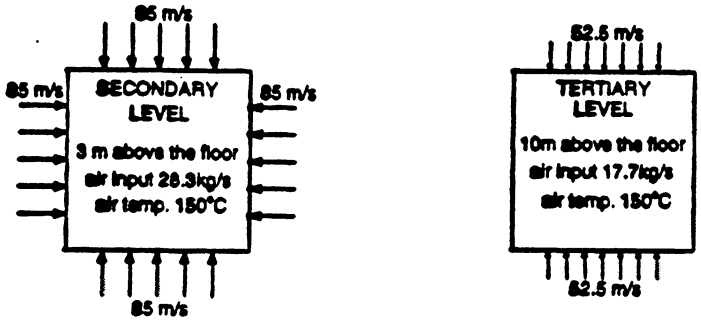

(a)

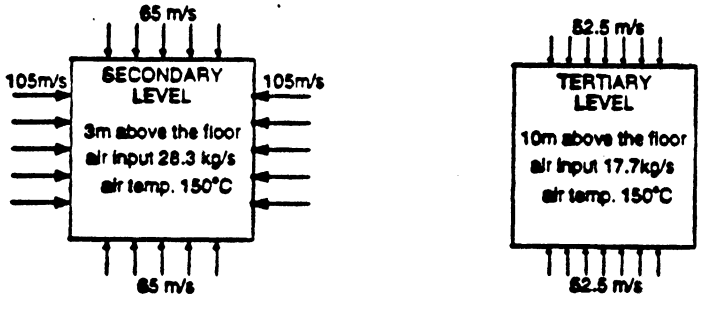

(b)

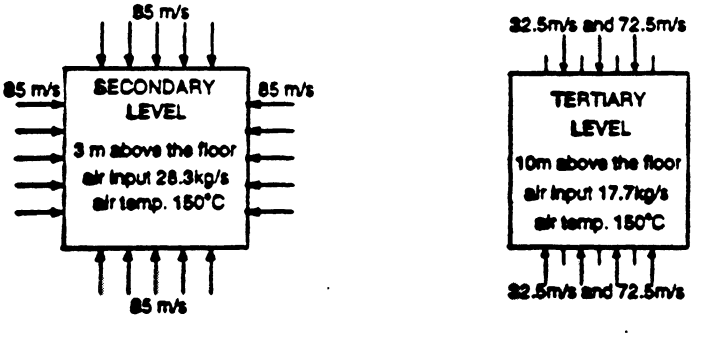

(c)

Figure 3.1: Air systems: (a) Base Case, (b) Two Wall Secondary, and (c) Interlaced Tertiary

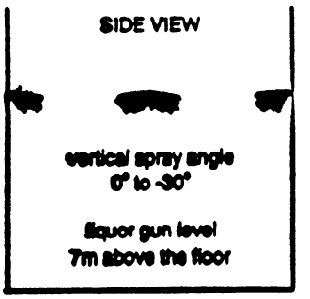

Liquor Spray Configuration Used With Air System Cases (a), (b) and (c)

8 Liquor Guns: Case (d)

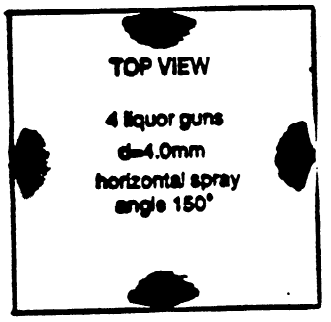

Larger Mean Droplet Diameter: Case (e)

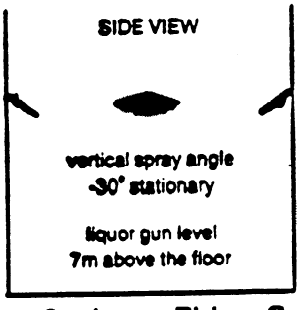

Stationary Firing: Case (f)

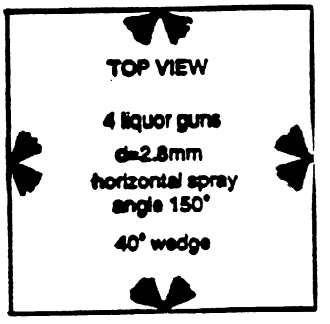

Wedge Firing: Case (g)

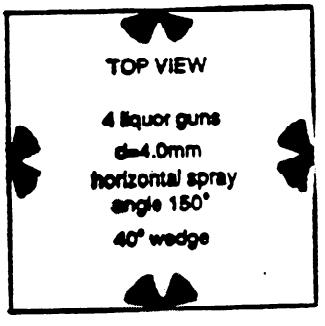

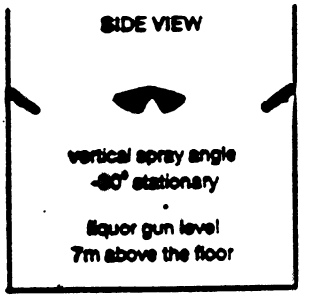

Case (h): Combination of Cases (e), (f) and (g)

Figure 3.2: Liquor Systems

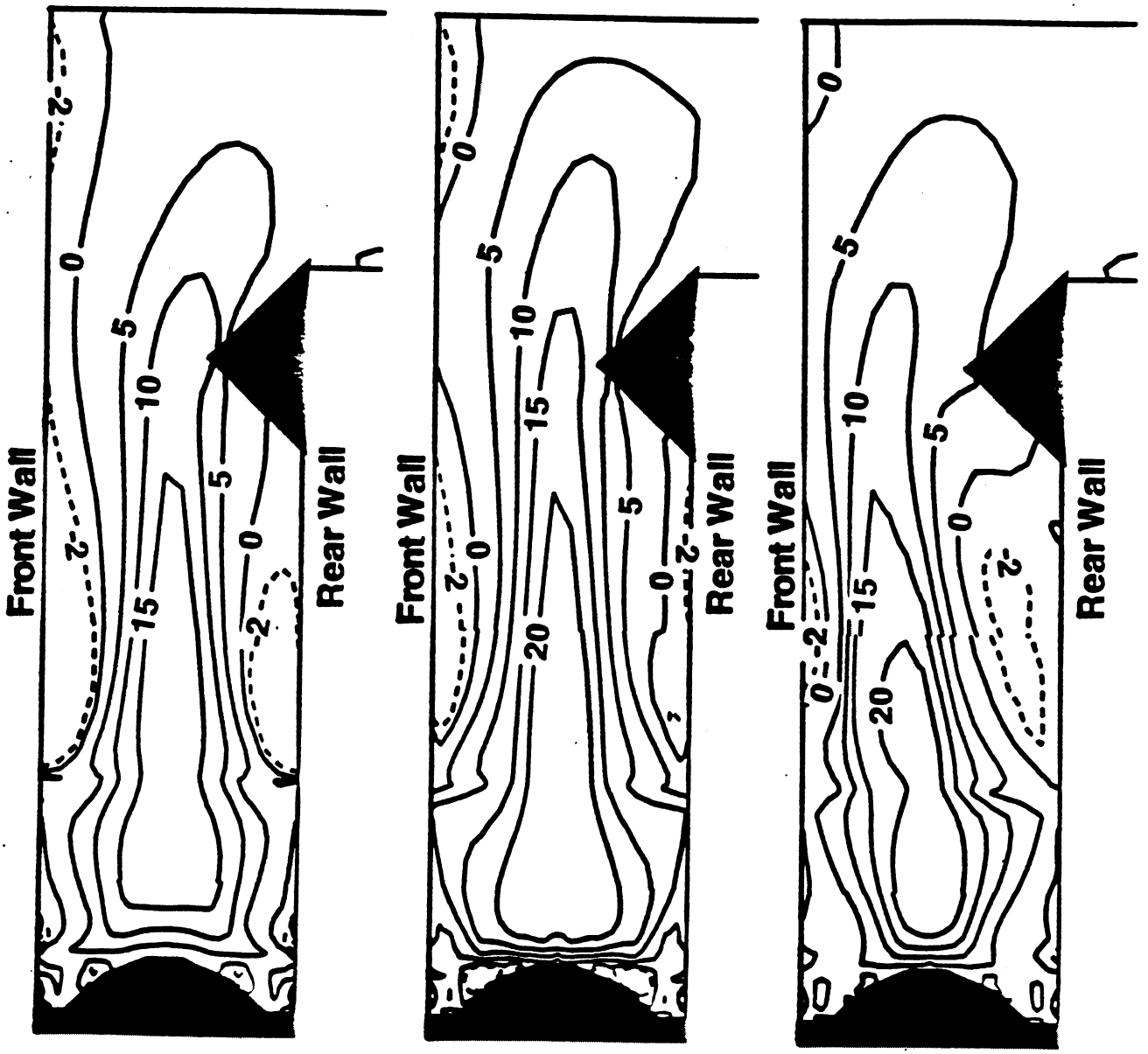

(a) (b) (c)

Figure 3.3: Upward velocity contours (in m/s) in the front-rear vertical central plane: (a) Base Case, (b) Two Wall Secondary, (c) Interlaced Tertiary

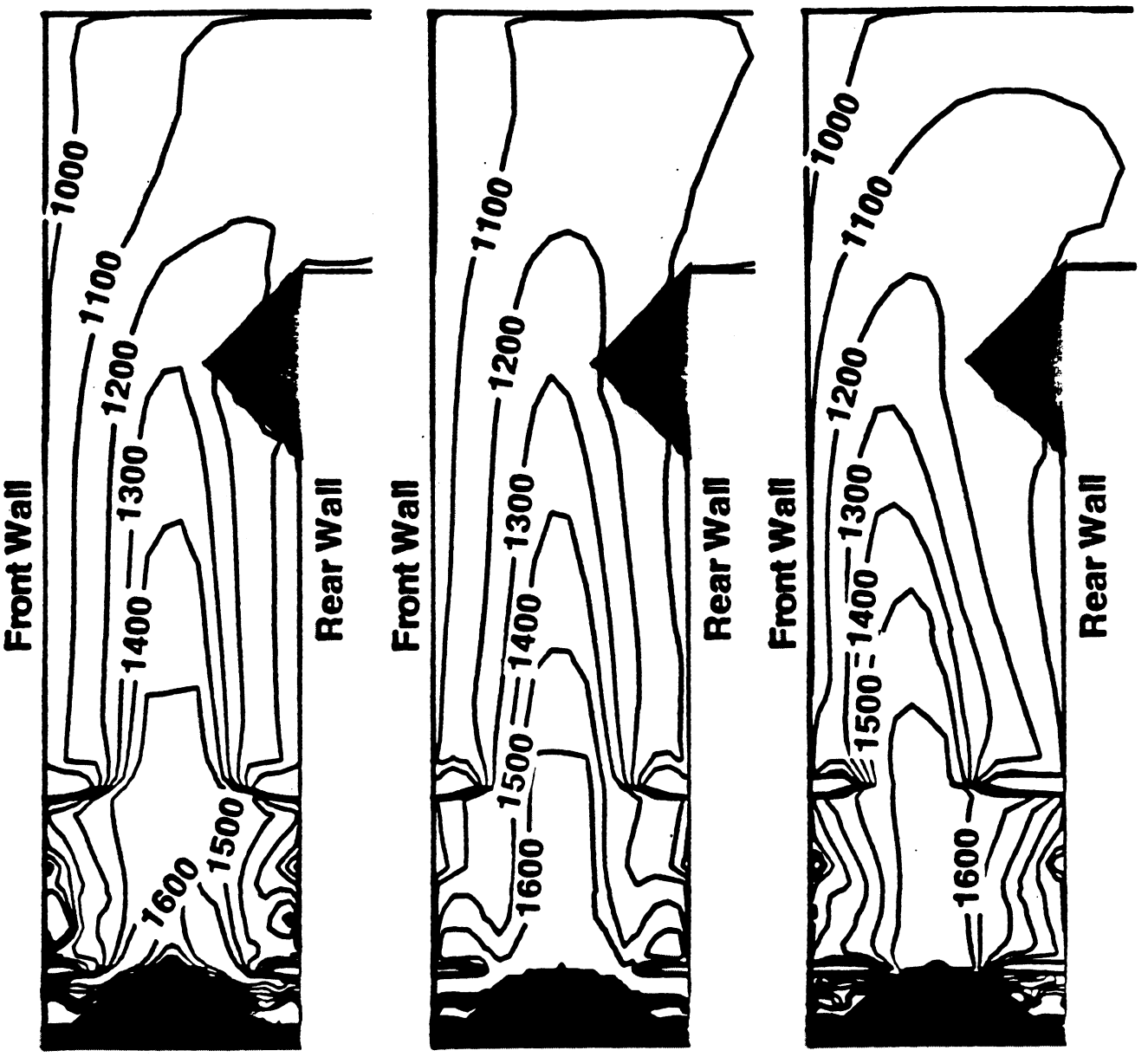

(a) (b) (c)

Figure 3.4: Isotherms (in C) in the front-rear vertical central plane: (a) Base Case, (b) Two Wall Secondary, and (c) Interlaced Tertiary

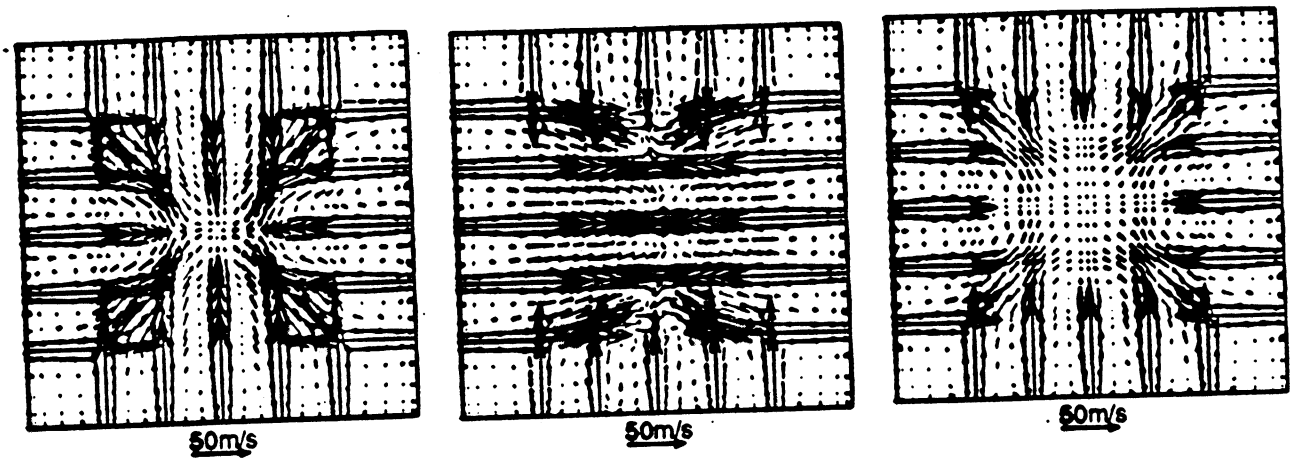

(a) (b) (c)

Figure 3.5: Flow field in a horizontal plane at the secondary level: (a) Base Case, (b) Two Wall Secondary, and (c) Interlaced Tertiary

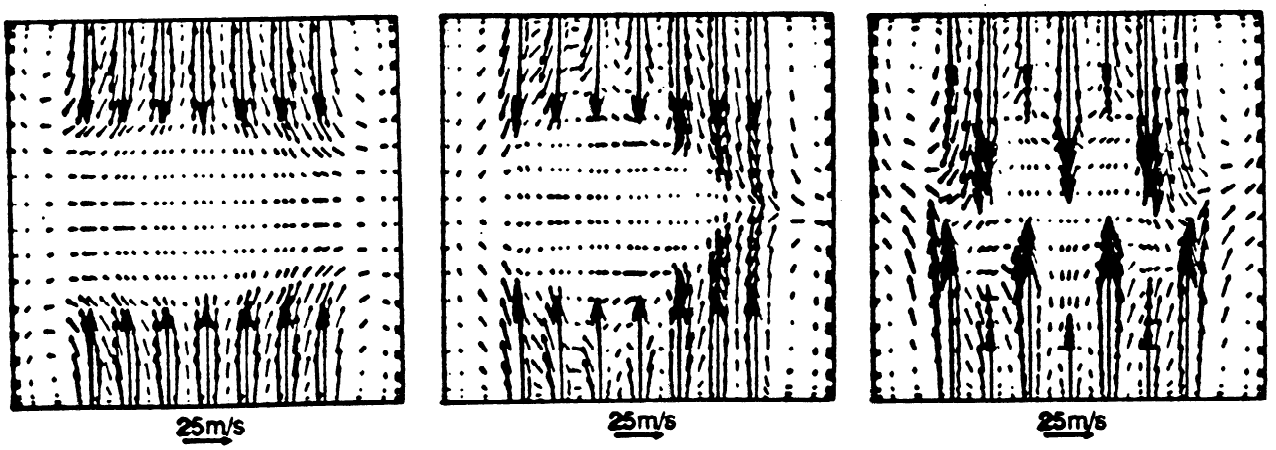

(a) (b) (c)

Figure 3.6: Flow field in a horizontal plane at the tertiary level: (a) Base Case, (b) Two Wall Secondary, and (c) Interlaced Tertiary

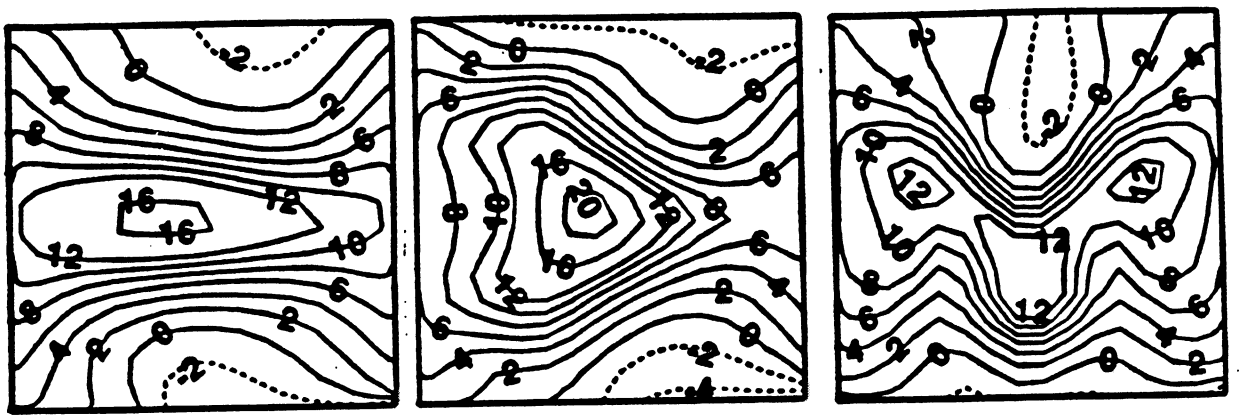

(a) (b) (c)

Figure 3.7: Upward velocity contours in a horizontal plane 6.5 m below the bullnose: (a) Base Case, (b) Two Wall Secondary, and (c) Interlaced Tertiary

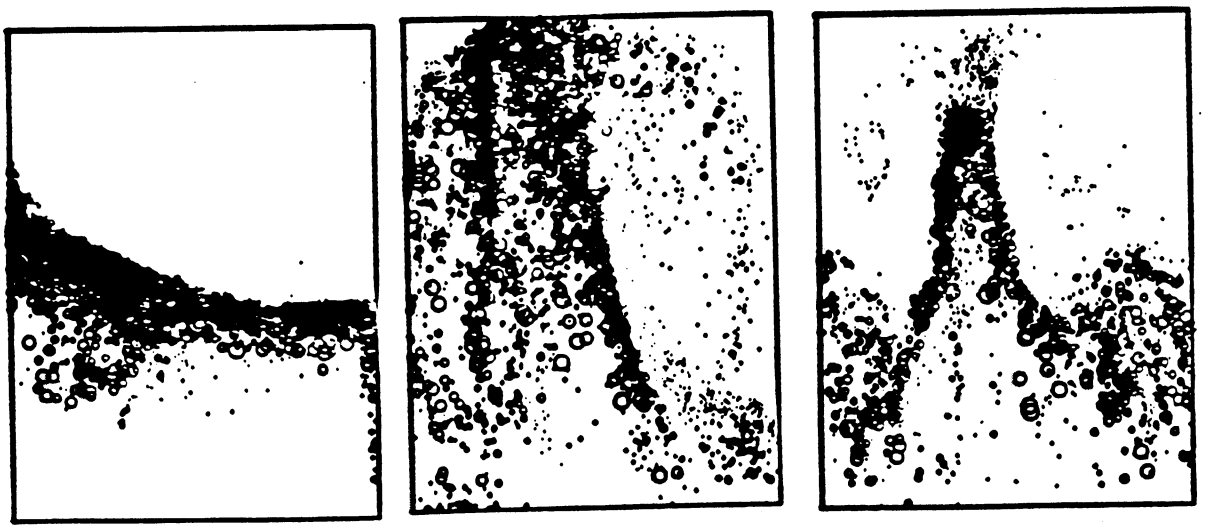

(a) (b) (c)

Figure 3.8: Carryover distribution at the superheater entry plane (vertical plane from the tip of the bullnose to the top): (a) Base Case, (b) Two Wall Secondary, and (c) Interlaced Tertiary

Chapter 4

Conclusions

Three air systems and six black liquor spray strategies are evaluated for a generic recovery boiler using mathematical modeling and computer simulation techniques. The presence of a central upward flowing core and the associated mechanical carryover are used as criteria for the evaluation. The air system in the base case features four wall primary, four wall secondary and two wall tertiary air ports. Modifications to the base case include a two wall secondary system and an interlaced tertiary system. The liquor spray configuration in the base case features four liquor guns, 2.8 mm mean droplet diameter, 150° horizontal spread and 0 to -30° vertical oscillation. Modifications to spray conditions include 8 liquor guns, 4 mm mean diameter droplets, stationary firing, 40° wedge and a combination of these.

The carryover is mostly caused by the relatively small particles that are entrained in the central core upflow. The carried over mass constitutes in some case up to about 10.0 % of the sprayed black liquor. The evaporation of the water occurs mostly in-flight, however, larger droplets (i.e., 4-6mm) that land on the bed still contain water. Approximately 50% of volatile gases are released in flight. The combustion of char-carbon occurs partially in-flight (about 30%) and is completed on the smelt bed and walls. The molar concentration of the oxygen over the bed and in the lower part of the furnace is much lower than the concentration of the gasification gases CO2 and H2O. Because of that less than 1% of the char-carbon reacts directly with oxygen, and more than 99% of char-carbon reacts with the gasification gases CO2 and H2O, and produces combustible gases CO and H2. The gas-phase results show that the strong secondary level air jets define the flow field in the furnace, and

are mostly responsible for the creation of the central core flow. The best conditions for combustion are present in the mixing layers between air jets and combustible gases, where the high concentration of the reactants is coupled with the high rate of eddy dissipation. The spotty-characteristic of the mass and energy sources originating from the spray model may cause in some cases convergence problems, and can lead to very high gas temperature (over 2000 k) in some computational cells.

The present three-dimensional computer model of the black liquor combustion contributes to the better understanding of the operation of the kraft recovery furnace. The model allows to study the dependence between the main design parameters, e.g., air delivery system, spray system, black liquor physical properties, and the boiler's performance parameters, e.g., reduction efficiency, combustion efficiency, carryover, pollution, furnace capacity. This work demonstrates that mathematical modeling can be used as a predictive tool to improve the operation of the recovery boiler.

Acknowledgements

Financial support for the work has been provided by DOE-IPST (USA), NSERC (Canada), EMR (Canada), IC (Canada) and Weyerhaeuser.

Appendix A

INPUT DATA
****

BLACK LIQUOR ELEMENTAL COMPOSITION
C := 39 %
H := 3.8 %
O := 33 %
Na := 18.6 %
S := 3.6 %
K := 1.2 %
Cl := 0.8 %
Total := C + H + O + Na + S + K + Cl Total = 100 %

ASSUMED PARAMETERS

Na_vof := 20 %	% of Na sodium that goes to volatiles
K_vof := 20 %	% of K potassium that goes to volatiles
S_vof := 35 %	% of S-sulfur that goes to volatiles
C_vof := 40 %	% of C-carbon that goes to volatiles
R := 90 %	% of S-sulfur that remains in char as Na2S

CALCULATIONS
****

NON-VOLATILES (CHAR) ELEMENTAL COMPOSITION

C_char := C - C C_vof	C_char = 23.4 %
H_char := 0.0	H_char = 0 %
O_char - oxygen see below	
Na_char := (1 - Na_vof) Na	Na_char = 14.88 %
S_char := (1 - S_vof) S	S_char = 2.34 %
K_char := (1 - K_vof) K	K_char = 0.96 %
Cl_char := Cl	Cl_char = 0.8 %

VOLATILES ELEMENTAL COMPOSITION

C_vo := C C_vof	C_vo = 15.6 %
H_vo := H	H_vo = 3.8 %
O_vo see below	
Na_vo := Na - Na_char	Na_vo = 3.72 %
S_vo := S - S_char	S_vo = 1.26 %
K_vo := K - K_char	K_vo = 0.24 %
Cl_vo := 0.0	Cl_vo = 0 %

ELEMENTAL COMPOSITION OF SPECIES

Na2SO4 - SULFATE ELEMENTAL COMPOSITION

$S_na2so4 := (1 - R) \cdot S_char$ $\quad S_na2so4 = 0.234\ \%$

$Na_na2so4 := S_na2so4 \cdot \left[\frac{46}{32}\right]$ $\quad Na_na2so4 = 0.336\ \%$

$O_na2so4 := S_na2so4 \cdot \left[\frac{4 \cdot 16}{32}\right]$ $\quad O_na2so4 = 0.468\ \%$

Na2S - SULFIDE ELEMENTAL COMPOSITION

$S_na2s := R \cdot S_char$ $\quad S_na2s = 2.106\ \%$

$Na_na2s := S_na2s \cdot \left[\frac{46}{32}\right]$ $\quad Na_na2s = 3.027\ \%$

NaCl - SODIUM CHLORIDE ELEMENTAL COMPOSITION

$Cl_nacl := Cl_char$ $\quad Cl_nacl = 0.8\ \%$

$Na_nacl := Cl_nacl \cdot \left[\frac{23}{35.5}\right]$ $\quad Na_nacl = 0.518\ \%$

K2CO3 - POTASSIUM CARBONATE ELEMENTAL COMPOSITION

$K_k2co3 := K_char$ $\quad K_char = 0.96\ \%$

$O_k2co3 := K_k2co3 \cdot \left[\frac{3 \cdot 16}{2 \cdot 39.1}\right]$ $\quad O_k2co3 = 0.589\ \%$

$C_k2co3 := K_k2co3 \cdot \left[\frac{12}{2 \cdot 39.1}\right]$ $\quad C_k2co3 = 0.147\ \%$

Na2CO3 - SODIUM CARBONATE ELEMENTAL COMPOSITION

$Na_na2co3 := Na_char - Na_na2so4 - Na_na2s - Na_nacl$

$Na_na2co3 = 10.998\ \%$

$O_na2co3 := Na_na2co3 \cdot \left[\frac{3 \cdot 16}{46}\right]$ $\quad O_na2co3 = 11.476\ \%$

$C_na2co3 := Na_na2co3 \cdot \left[\frac{12}{46}\right]$ $\quad C_na2co3 = 2.869\ \%$

OXYGEN IN IN CHAR (OR NON-VOLATILES)

$O_char := O_na2so4 + O_k2co3 + O_na2co3$

$O_char = 12.533\ \%$

Oxygen in volatiles

$O_vo := O - O_char$ $\quad O_vo = 20.467\ \%$

CHECK MOLAR RATIO BETWEEN CARBON AND OXYGEN IN VOLATILES

$C_mol := \frac{C_vo}{12}$ C_mol = 1.3 %

$O_mol := \frac{O_vo}{16}$ O_mol = 1.279 %

>>> IF C_mol>O_mol then only CO is formed (no CO2) <<<

CO_mol := O_mol

CO_vo := CO_mol·28 CO_vo = 35.817 %

CO2_vo := 0

CH4_vo := (C_mol - O_mol)·16 CH4_vo = 0.333 %

$H2S_vo := S_vo \cdot \left[\frac{34}{32}\right]$ H2S_vo = 1.339 %

$H2_vo := H_vo - CH4_vo \cdot \left[\frac{4}{16}\right] - H2S_vo \cdot \left[\frac{2}{34}\right]$ H2_vo = 3.638 %

>>> IF C_mol<O_mol then CO and CO2 are formed <<<

CO_vo2 := C_mol·28 CO_vo2 = 36.4 %

$CO2_vo2 := (O_mol - C_mol) \cdot \left[\frac{12}{32}\right]$ CO2_vo2 = -0.008 %

CH4_vo2 := 0

$H2S_vo2 := S_vo \cdot \left[\frac{34}{32}\right]$ H2S_vo2 = 1.339 %

Na_vapor := Na_vo Na_vapor = 3.72 %

K_vapor := K_vo K_vapor = 0.24 %

VOLATILES := CO_vo + CO2_vo + H2S_vo + CH4_vo + Na_vapor + K_vapor + H2_vo

VOLATILES = 45.087 %

NON-VOLATILE SPECIES COMPOSITION

C_fix := C_char - C_k2co3 - C_na2co3 C_fix = 20.384 %

Na2S := Na_na2s + S_na2s Na2S = 5.133 %

Na2SO4 := S_na2so4 + O_na2so4 + Na_na2so4

Na2SO4 = 1.038 %

Na2CO3 := C_na2co3 + O_na2co3 + Na_na2co3

Na2CO3 = 25.343 %

O_fix := O_char - O_na2so4 - O_k2co3 - O_na2co3

O_fix = 0 %

K2CO3 := C_k2co3 + O_k2co3 + K_k2co3 K2CO3 = 1.697 %

NaCl := Na_nacl + Cl_nacl NaCl = 1.318 %

SMELT := Na2S + Na2SO4 + Na2CO3 + K2CO3 + NaCl + O_fix

SMELT = 34.53 %

TOTAL := VOLATILES + C_fix + SMELT TOTAL = 100 %

Appendix B

HEAT OF COMBUSTION CALCULATION

****

REACTIONS		HEAT OF COMBUSTION kJ/(kmol of reference specie)	
#1	H2S+Na2CO3+2O2=Na2SO4+H2O+CO2	qr1 := 872.151	H2S
#2	2Na+CO2+0.5O2 = Na2CO3	qr2 := 951.658	Na_vapor
#3	2K+CO2+0.5O2 = K2CO3	qr3 := 934.472	K_vapor
#4	CO+0.5O2 = CO2	qr4 := 283.128	CO
#5	CH4+2O2 = CO2+H2O	qr5 := 802.474	CH4 lower HV
#6	Na2S+2O2 = Na2SO4	qr6 := 1021.716	Na2S
#7	C+O2 = CO2	qr7 := 393.710	CHAR
#8	H2+0.5O2 = H2O	qr8 := 241.8	H2 lower HV

HEAT RELEASED in kJ FOR A SPECIFIED MASS OF BLACK LIQUOR SOLIDS

BLS := 1 gram

$$Q1 := \frac{H2S_vo}{34} \cdot qr1 \cdot BLS \qquad Q1 = 0.343$$

$$Q2 := \frac{Na_vapor}{23} \cdot qr2 \cdot BLS \cdot 0.5 \qquad Q2 = 0.77$$

$$Q3 := \frac{K_vapor}{39.1} \cdot qr3 \cdot BLS \cdot 0.5 \qquad Q3 = 0.029$$

$$Q4 := \frac{CO_vo}{28} \cdot qr4 \cdot BLS \qquad Q4 = 3.622$$

$$Q5 := \frac{CH4_vo}{16} \cdot qr5 \cdot BLS \qquad Q5 = 0.167$$

$$Q6 := \frac{Na2S}{78} \cdot qr6 \cdot BLS \qquad Q6 = 0.672$$

$$Q7 := \frac{C_fix}{12} \cdot qr7 \cdot BLS \qquad Q7 = 6.688$$

$$Q8 := \frac{H2_vo}{2} \cdot qr8 \cdot BLS \qquad Q8 = 4.398$$

TOTAL HEAT RELEASED

Q_TOT := Q1 + Q2 + Q3 + Q4 + Q5 + Q6 + Q7 + Q8

Q_TOT = 16.689 kJ/(BLS MASS)

HIGHER HEATING VALUE OF BLS

HHV := 15.3 kJ/g

Q_HHV := HHV·BLS

Q_HHV = 15.3 kJ/(BLS MASS)

HEAT OF PYROLYSIS

Q_PYR := Q_HHV - Q_TOT

Q_PYR = -1.389 kJ/(BLS MASS)

Bibliography

[1] Walsh A. R., A Computer Model for In-Flight Black Liquor Combustion in a Kraft Recovery Furnace. PhD Thesis, The Institute of Paper Chemistry, January 1989.

[2] Walsh A. R. and Grace T. M., TRAC: A Computer Model to Analyze the Trajectory and Combustion Behavior of Black Liquor Droplets. Journal of Pulp and Paper Science, Vol. 15 No. 3, May 1989.

[3] Frederick W. J., Noopila T. and Hupa M., Swelling of Spent Pulping Liquor Droplets During Combustion. Journal of Pulp and Paper Science, Vol. 17 No. 5, Sep. 1991.

[4] Smoot L.D. and Smith P.J., Coal Combustion and Gasification. Plenum Press, New York, 1985.

[5] Clay D.T. et al, Fundamental Studies of Black Liquor Combustion, DOE Report DOE/CE/40637-T9, March 1990.

[6] Salcudean M., Nowak P., Abdullah Z., Mathematical Modeling of Recovery Furnaces, International Chemical Recovery Conference, Seattle, June 1992.

[7] Jones A. K., A Model of the Kraft Recovery Furnace. Phd Thesis, The Institute of Paper Chemistry, January 1989.

[8] Adams T. N. and Frederick J., *Kraft Recovery Boiler Physical and Chemical Processes* The American Paper Institute, 1988.

[9] Magnussen B.F. , Hjertageer B.H., On Mathematical Modelling of Turbulent Combustion with Special Emphasis on Soot Formation and Combustion., Proc. 16th Symp. on Combust. , pp 719- 729 , 1977.

[10] Fiveland, W. A., "Three Dimensional Radiative Heat Transfer Solutions by the Discrete-Ordinates Method", J. Thermophysics and Heat Transfer, 2: J309-J316 (1988).

[11] Abdullah, Z. et al. "Black Liquor Combustion Validated Recovery Boiler Modeling", Report to U. S. Dept. of Energy (1995).

[12] Grace, T.M., et al. "A Three Dimensional Model of the Kraft Recovery Furnace", *Proc. Int. Chem. Recovery Conf.* 1-8 (1989).

[13] Wessel, R. A., Parker, K. L., and A. Akan-Etuk, A., "Three-Dimensional Flow and Combustion Model of a Recovery Furnace", *TAPPI Engineering Conf.*, Orlando, Florida, Sept. 20-25 (1993).

[14] Launder, B.E. and Spalding, D.B., "The numerical computation of turbulent flow", *Comp. Meth. App. Mech. Eng.* 3: J269-J289 (1974).

[15] Frederick, W.J., Noopila, T., Hupa, M., "Combustion behavior of black liquor at high solids firing", *TAPPI J.*, 74(12): (1991).

[16] Grace, T. M., Personal communications.

Grace, T M., Wag, K J. , Horton, R R. , Frederick, W J.

[17] "Recovery Boiler Modeling: An Improved Char Burning Model Inlcuding Sulfate Reduction and Carbon Removal", Proceedings of 16th National Industrial Energy Technology Conference, Houston, Texas, April 1994.

[18] Patankar, S. V., *Numerical Heat Transfer and Fluid Flow*, Washington, DC: Hemisphere Pub. Co. (1980).

[19] Vanka, S. P., "Block-Implicit Multigrid Solution of Navier-Stokes Equations in Primitive Variables", J. Computational Physics 65:J138-J158 (1986).

Investigation of Turbulence Models and Prediction of Swirling Flows for Kraft Recovery Furnaces

Daniel Tse

Department of Mechanical Engineering
University of British Columbia
Vancouver, B.C., Canada

March 1996

This report presents an examination of three eddy viscosity based two-equation turbulence models for the prediction of flows in a kraft recovery furnace. The models chosen are the standard $k-\epsilon$ model by Jones and Launder (1972) and Hanjalić and Launder (1972), the renormalization group $k-\epsilon$ model by Yakhot and Smith (1992) and Yakhot et al. (1992), and the $k-\omega$ model by Wilcox (1988). These models are selected because of their computational efficiency and robustness characters, which are especially important for the prediction of industrial turbulent flows. The accuracy of the models is assessed through comparison with experimental results for flow conditions ranging from a simple two-dimensional flow with separation and reattachment to a complex three-dimensional swirling flow in a furnace model. A recommendation is given concerning the suitable choice of a turbulence model for predicting furnace flows.

Contents

1 Introduction **2**

1.1 Prediction of Turbulent flows 2

1.2 Eddy Viscosity Models 4

1.3 Advantages and Limitations of Eddy Viscosity Models 5

1.4 Renormalizaiton Group (RNG) Models 7

2 Standard $k-e$ Model **8**

2.1 Modeling Equations 9

2.2 Versatility of the Model 10

3 Wilcox's $k-w$ Model **11**

3.1 Modeling Equations 12

3.2 Versatility of the Model 12

4 Renormalization Group $k-e$ Model **14**

4.1 Form of the Model 14

4.2 Versatility of the Model 15

5 Test Case 1: Flow over a Backward-Facing Step **16**

5.1 Description of the Problem 16

5.2 Results and Discussion 18

6 Test Case 2: Multiple Jets in a Crossflow **19**

6.1 Experimental and Numerical Investigation 19

6.2 Results and Discussion 20

7 Test Case 3: Swirling flow Predictions for a Recovery Furnace Water Model **21**

7.1 Experimental Modeling of Recovery Boiler flows 22

7.2 Numerical Predictions and Analysis 23

8 Summary and Conclusion **25**

References **26**

Figures **30**

1 Introduction

The flow in a recovery furnace is highly turbulent due to the interaction of high speed jets. The prediction of such a flow requires the use of a turbulence model. The ability of a turbulence model to predict three-dimensional flows characterized by extensive recirculation and swirls is an important consideration for its suitability for use in the numerical modeling of furnace flows. Other important requirements for the turbulence model are its ease of implementation and computational efficiency. It is the purpose of this report to examine the suitability of several popular turbulence models for the simulation of flows in a furnace.

1.1 Prediction of Turbulent Flows

A common practice for the prediction of turbulent flows is to perform time-averaging operation on the Navier-Stokes equations to isolate the quantities that characterize the mean flow and those that characterize the effect of turbulent fluctuations. The time-averaged conservation equations for mass, momentum and a scalar tracer for an incompressible flow are

$$\frac{\partial U_i}{\partial x_i} = 0 \tag{1}$$

$$\rho\frac{\partial U_i}{\partial t} + \rho\frac{\partial}{\partial x_j}\left(U_iU_j + \overline{u_i'u_j'}\right) = -\frac{\partial P}{\partial x_i} + \frac{\partial}{\partial x_j}(2\mu S_{ij}) \tag{2}$$

$$\rho\frac{\partial \Phi}{\partial t} + \rho\frac{\partial}{\partial x_j}(\Phi U_j + \overline{\phi u_j'}) = \frac{\partial}{\partial x_j}\left[\lambda\left(\frac{\partial \Phi}{\partial x_j}\right)\right] \tag{3}$$

In the above system of equations,

$$S_{ij} = \frac{1}{2}\left(\frac{\partial U_i}{\partial x_j} + \frac{\partial U_j}{\partial x_i}\right) \tag{4}$$

is the time-averaged strain-rate tensor, while $-\rho\overline{u_i'u_j'}$, and $-\rho\overline{\phi u_j'}$ are known respectively as Reynolds stresses and turbulent scalar fluxes. They consist of mean products of fluctuating components and arise from the averaging of nonlinear convective terms. Physically, these terms represent diffusion of momentum and scalar quantities due to

turbulent motion. The correlation of fluctuating velocity components is commonly represented by the Reynolds stress tensor τ_{ij}:

$$\tau_{ij} = -\rho\overline{u_i' u_j'} \tag{5}$$

The aim of turbulence modeling is to establish a reasonable representation of τ_{ij} and $-\rho\overline{\phi u_j'}$ in terms of mean flow quantities.

The evolution of various techniques for modeling turbulent flows during the past two decades has been described in a number of review papers and monograph (Hanjalić (1989,1994), Wilcox (1993), Launder (1991), Leschziner (1989)). Turbulence models exhibit a wide range of complexity: from the conventional two-equation eddy viscosity models and differential second-moment Reynolds stress models to spectral approach and partial field models such as subgrid modeling. In present engineering calculations, eddy viscosity models and Reynolds stress models are the only types that are computationally feasible.

In differential Reynolds stress models, each component of the Reynolds stress tensor τ_{ij} is obtained from the solution of a full transport equation derived from the Navier-Stokes equation with modeling assumptions. In addition to the solution of equations for each Reynolds stress component, solution to a turbulence time- or length-scale supplying equation is needed to complete the modeling process. Thus, a total of ten differential equations need to be solved in addition to the hydrodynamical equation system and other scalar transport equations.

In basic eddy viscosity models, Boussinesq assumption is invoked to represent the Reynolds stress tensor as the product of an eddy viscosity μ_t and the mean strain-rate tensor S_{ij} as follows:

$$\tau_{ij} = 2\mu_t S_{ij} - \frac{2}{3}\rho k\delta_{ij} \tag{6}$$

The above definition for τ_{ij} mimics the linear stress and rate-of-strain relationship that describes the molecular momentum transfer in a Newtonian fluid. The quantity $k = -\frac{1}{2\rho}\tau_{ii}$ has the physical interpretation of the kinetic energy per unit mass of the turbulent fluctuations. Thus, each component of τ_{ij} is determined once μ_t and k are

known. For the modeling of turbulent scalar flux, a standard approach within the eddy viscosity modeling framework is to apply the linear gradient transport hypothesis. In analogy to molecular transport processes, it is assumed that

$$-\rho\overline{\phi u_j'} = \frac{\mu_t}{\sigma_\phi}\frac{\partial \Phi}{\partial x_j} \tag{7}$$

The quantity σ_ϕ is called the turbulent Prandtl or Schmidt number and is used to relate the heat/mass transfer process to the momentum transfer process. It is usually assigned a value close to unity throughout the entire flow field.

For eddy viscosity models, two differential equations are usually solved to determine the distributions of μ_t and k and consequently τ_{ij}. This is a substantial reduction in computational effort compared to that for Reynolds stress models. Regarding suitability for recovery furnace simulations, a model with a smaller number of equations is advantageous because in addition to hydrodynamic equations and turbulence modeling equations, equations governing the transport of heat and chemical species need to be solved in conjunction. Aside from the concerns of having to solve a large number of equations, another issue that needs attention is the level of accuracy in the modeling of various physical and chemical processes in a recovery furnace. At present, understanding of the detailed combustion properties of black liquor droplets is still incomplete, and modeling of radiative heat transfer in a furnace involves many simplifying assumptions (see De Michele et al. (1989)). Thus, the use of turbulence models that are computationally more demanding than basic two-equation eddy viscosity type models is not justified in most cases, both in view of the computational requirement and the approximate nature in the modeling of other physical and chemical processes. The focus of the following study will be on three variants of two-equation eddy viscosity models to examine their suitability for use in recovery furnace modeling.

1.2 Eddy Viscosity Models

By assuming the redistribution of momentum due to turbulent transport is similar to that by molecular transport, and by virtue of dimensional reasoning, the eddy viscosity

is written as

$$\mu_t = \text{constant} \cdot \rho k^{1/2} l \tag{8}$$

where l is a length scale of turbulence. This formulation suggests that the prediction of a turbulent flow depends on a knowledge of k and l in the flow field, and the two quantities together provide a means for specifying characteristic turbulence time-, length- and velocity scales for describing various turbulence interactions. The kinetic energy of turbulent fluctuations k has been employed almost universally as one of the two variables since it has proved to be the best defined and most readily obtainable turbulence parameter. The other scale-supplying variable is usually defined based on the power-law form $k^a l^b$ for some rational numbers a and b.

Of the many possible choices for a and b, two choices have received continual popularity. The choice $a = \frac{3}{2}$ and $b = -1$ gives the dependent variable ϵ, the rate of turbulent energy dissipation, while the choice $a = \frac{1}{2}$ and $b = -1$ gives the dependent variable ω, which has the physical interpretation of being the characteristic frequency of the large eddy structure or as the specific dissipation rate per unit of kinetic energy since $\omega \sim \epsilon/k$.

The transport equations for k, ϵ and ω are derived based on the Navier-Stokes equations with modeling approximations. The above $k-\epsilon$ and $k-\omega$ models are two of the most popular examples of two-equation eddy viscosity models and are used often in present day engineering calculations.

1.3 Advantages and Limitations of Eddy Viscosity Models

Two-equation eddy viscosity models offer advantages in reducing the computational requirement in turbulent flow simulations. The simplicity with which Reynolds stresses τ_{ij} are computed is remarkable. In addition, these models offer satisfactory computational stability since the molecular viscosity is augmented by the turbulent viscosity and consequently the overall ellipticity measure of the equation system is increased (Brandt and Dinar (1979)). Such is an important consideration when the system of equations is to be solved by iterative numerical means.

Limitations of the eddy viscosity models for the predictions of isothermal flows are well known. The following list is taken from Hanjalić (1994):

- linear stress-strain relationship
- scalar isotropic character of eddy viscosity (insensitivity to the orientation of the turbulence structure and its transporting and mixing mechanisms)
- inability to reproduce stress anisotropy and its consequence (e.g., prediction of stress-induced secondary motion);
- scalar character of turbulence scales – insensitivity to eddy anisotropy;
- limitations to define only one time- or length scale of turbulence for characterizing all turbulence interactions;
- inadequate incorporation of viscosity damping effects on turbulence structure (low Reynolds number models);
- frequent inadequate treatment of boundary conditions, in particular at the solid wall.

The standard $k-\epsilon$ model is also not adequate for hot flows where it fails to predict accurately the effects of thermal expansion and those due to variation in density. Hanjalić remarked that although Reynolds stress models overcome the first three deficiencies, all the others remain to a greater or lesser extent. In addition, this class of models involves further uncertainties in the modeling of various terms in $\overline{u_i' u_j'}$-differential equations. This gives further reasons for Reynolds stress models not being considered in the present discussion.

Regarding suitability for simulating flow phenomena in a recovery furnace, the above weaknesses have the following major implication: eddy viscosity models are inherently unable to accurately predict flows that experience extra rates of strain caused by rapid dilation, out of plane straining, or significant streamline curvature, all of

which give rise to unequal normal Reynolds stresses. Thus, for flows that experience strong swirls and exhibit significant three-dimensionality, predictions by Boussinesq approximation become suspect. Nevertheless, the use of turbulence models to predict complex industrial flows has important merits, as the uncertainties in modeling other phenomena involved may be much higher than those implied in the model of flow hydrodynamics.

1.4 Renormalization Group (RNG) Models

New methods for better efficiency and accuracy in the modeling of turbulence are continuously being pursued. The Renormalization Group (RNG) theory of Yakhot and Orszag (1986), Yakhot and Smith (1992) and Yakhot et al. (1992) offers a promising methodology for deriving accurate and efficient turbulence models. The RNG procedure was originally applied in the study of critical phenomena such as phase transition. In such an approach, dynamical equations for the large-scale field are obtained by averaging over an infinitesimal band of small scales in order to remove them from consideration. The removal procedure is iterated until the corrections add up to finite changes. When applied to fluid dynamical problems, this systematic removal of the smallest scales of turbulence is continued to a point where the remaining scales are resolvable with available computer capacities. The removal of only the smallest scales gives rise to subgrid scale models for large-eddy simulations whereas in the limit as successively large scales are removed, Reynolds stress models are recovered.

The application of renormalization group theory to turbulence is described briefly as follows. First, the assumption is made that the small-scale velocity fluctuations are generated by hydrodynamic instability which strongly depends on large-scale flow features. Hence, the average effect of the large-scale features of the flow is represented by a universal random force that drives the small-scale velocity fluctuations. Then an elimination procedure is carried out for small scale structures by transforming the flow equations in frequency domain and evaluating all quantities in the large-scale limit by allowing the wave-number to approach zero. In this procedure, equations are derived

for large-scale flow properties while the effects of small-scale fluctuations are described by an effective or renormalized coupling constant and viscosity.

This RNG principle offers a theoretically sound basis for the derivation of two-equation eddy viscosity type models. In particular, a form of $k-\epsilon$ model is obtained from the theory. This RNG $k-\epsilon$ model, together with the standard $k-\epsilon$ model and the Wilcox's $k-\omega$ models, are presented in the following sections for assessing their suitability for use in recovery furnace modeling.

2 Standard $k-\epsilon$ Model

In this model, the turbulent kinetic energy k and its dissipation rate ϵ are used for the specification of the eddy viscosity μ_t. The derivation of the equation for k is obtained by taking moments of the Navier-Stokes equation – multiplying the Navier-Stokes equation by a fluctuating property and time average the product. The resulting transport equation for the turbulence kinetic energy has the following form:

$$\rho\frac{\partial k}{\partial t}+\rho U_j\frac{\partial k}{\partial x_j}=\tau_{ij}\frac{\partial U_i}{\partial x_j}-\rho\epsilon+\frac{\partial}{\partial x_j}\left[\mu\frac{\partial k}{\partial x_j}-\frac{1}{2}\rho\overline{u_i'u_i'u_j'}-\overline{p'u_j'}\right] \tag{9}$$

where $\epsilon=\nu\overline{\frac{\partial u_i'}{\partial x_k}\frac{\partial u_i'}{\partial x_k}}$ actually represents the homogeneous part of the rate of energy dissipation. The application of gradient-diffusion hypothesis to represent the dual effect of turbulent transport of scalar quantities and pressure diffusion leads to the expression:

$$\frac{1}{2}\rho\overline{u_i'u_i'u_j'}+\overline{p'u_j'}=-\frac{\mu_t}{\sigma_k}\frac{\partial k}{\partial x_j} \tag{10}$$

where σ_k is a closure coefficient, and the hope is that the model is realistic enough that σ_k can be chosen to be constant. Combining Eqs.(9) and (10) yields the following transport equation for k:

$$\rho\frac{\partial k}{\partial t}+\rho U_j\frac{\partial k}{\partial x_j}=\tau_{ij}\frac{\partial U_i}{\partial x_j}-\rho\epsilon+\frac{\partial}{\partial x_j}\left[(\mu+\mu_t/\sigma_k)\frac{\partial k}{\partial x_j}\right] \tag{11}$$

The terms in the above transport equation model the following physical processes commonly observed in the motion of a fluid: the first two terms on the left model

the unsteadiness and convection of k following a fluid particle, the terms on the right model respectively the production of k, the dissipation of k, and diffusion of k within the fluid. The production of k represents the rate at which kinetic energy is transferred from the mean flow to the turbulence, while the dissipation of k represents the rate at which turbulent kinetic energy is converted into thermal internal energy. The diffusion consists of two parts, one due to molecular transport process and the other due to the combined effect of turbulent fluctuations and pressure diffusion.

The transport equation for the turbulent energy dissipation rate ϵ may similarly be obtained by taking appropriate moment of the Navier-Stokes equations and modeling of various physical processes. Unfortunately, due to a lack of data available, the transport process for ϵ is not well understood. Thus, the derivation of the ϵ equation is more empirical and the modeling equation attempts to account for various physical processes that include unsteadiness and convection, molecular diffusion, turbulent transport, production and dissipation.

2.1 Modeling Equations

The standard $k-\epsilon$ model has the following form:

Eddy Viscosity:

$$\mu_t = \rho C_\mu k^2/\epsilon \tag{12}$$

Turbulent Kinetic Energy:

$$\rho\frac{\partial k}{\partial t} + \rho U_j\frac{\partial k}{\partial x_j} = \tau_{ij}\frac{\partial U_i}{\partial x_j} - \rho\epsilon + \frac{\partial}{\partial x_j}\left[(\mu + \mu_t/\sigma_k)\frac{\partial k}{\partial x_j}\right] \tag{13}$$

Specific Dissipation Rate:

$$\rho\frac{\partial \epsilon}{\partial t} + \rho U_j\frac{\partial \epsilon}{\partial x_j} = C_{\epsilon 1}\frac{\epsilon}{k}\tau_{ij}\frac{\partial U_i}{\partial x_j} - C_{\epsilon 2}\rho\frac{\epsilon^2}{k} + \frac{\partial}{\partial x_j}\left[(\mu + \mu_t/\sigma_\epsilon)\frac{\partial \epsilon}{\partial x_j}\right] \tag{14}$$

Closure Coefficients:

$$C_\mu = 0.09 \quad C_{\epsilon 1} = 1.44 \quad C_{\epsilon 2} = 1.92 \quad \sigma_k = 1.0 \quad \sigma_\epsilon = 1.3 \tag{15}$$

The closure coefficients listed above are valid at high Reynolds numbers and are obtained from benchmark experiments for equilibrium turbulent boundary layers and

isotropic turbulence (Hanjalić and Launder (1972)): C_μ is fixed by the requirement that in a constant stress layer $\tau_w/\rho k = C_\mu^{1/2}$; $C_{\epsilon 1}$ is chosen so that the von Karman constant equals 0.42, $C_{\epsilon 2}$ is determined by reference to the decay of grid turbulence, and the diffusion coefficients σ_k and σ_ϵ are fixed by computer optimization.

2.2 Versatility of the Model

The standard $k-\epsilon$ model enjoys wide usage for the following reasons: first, ϵ itself appears in the k-equation and is amendable to physical interpretation; second, compared to other two-equation models that use kl or k/l^2 as the scale-supplying variables, the $k-\epsilon$ model predicts a more accurate level of energy dissipation for boundary layer type flows, and third, the model exhibits robust numerical stability characteristics and can be solved conveniently with other conservation equations by iterative methods.

For boundary conditions at a wall surface, perturbation analysis shows that, in close proximity to the surface, the $k-\epsilon$ modeling equations do not reproduce the law-of-the-wall velocity profile

$$U = u_\tau \left[\frac{1}{\kappa}\ln\left(\frac{u_\tau y}{\nu}\right) + B\right] \tag{16}$$

in a boundary layer under zero pressure gradient. In the above equation, U is the tangential velocity component at a position y above the wall surface, $\kappa = 0.4$ is the von Karman coefficient, $u_\tau = \sqrt{\tau_w/\rho}$ is the friction velocity with τ_w being the wall shear stress, and $B = 5.0$ is obtained experimentally for smooth walls. An implication is that simple no-slip boundary condition cannot be applied for the tangential velocity components. Instead, either viscous damping functions need to be introduced or the wall function method be applied for which the solution is required to match the above log-layer law-of-the-wall solution at the grid node adjacent to the wall. In this wall function method, Eq.(16) is solved as a transcendental equation for u_τ. Once u_τ is determined, corresponding values for k and ϵ are obtained through

$$k = \frac{u_\tau^2}{\sqrt{C_\mu}} \qquad \epsilon = \frac{u_\tau^3}{\kappa y} \tag{17}$$

To summarize past research experience, the standard $k-\epsilon$ model gives satisfactory predictions for two-dimensional shear flows with mild streamline curvature and body force effects. For more complex flows, the model provides qualitatively reasonable information but fails in matching detailed phenomena.

3 Wilcox's $k-\omega$ Model

In addition to the standard $k-\epsilon$ model, other two-equations models have been developed with the hope that some of the deficiency of the standard $k-\epsilon$ model would be overcome. The $k-\omega$ model as developed by Wilcox (1988) is one such results. The model is developed with specific attention to applications in aerodynamics where flow separation under an adverse pressure gradient needs to be predicted accurately.

The standard $k-\epsilon$ model has a deficiency that for flows approaching separation, the ϵ-equation significantly underpredicts the near-wall levels of ϵ. A consequence is the significant overprediction of the shear-stress levels and thereby a delay of separation. Specific *ad hoc* corrections have been proposed such as including a secondary source term to the ϵ-equation but the modification is usually valid only for simple flat-plate type geometries.

Another deficiency of the $k-\epsilon$ model in the prediction of aerodynamic flows is that when a low Reynolds number $k-\epsilon$ model is used for integration through the turbulent and viscous sublayers, numerical stiffness problems may be encountered. This problem is caused by the use of highly nonlinear functions of dependent variables like $k^2/\epsilon\nu$ in the damping functions in most low Reynolds number $k-\epsilon$ models.

Wilcox's $k-\omega$ model employs $\omega \sim \epsilon/k$ as the scale-supplying variable. As noted in Hanjalić (1994), the resulting system of differential equations is similar to the $k-\epsilon$ model as the two models can be mathematically transformed from one to the other. The only difference is how the diffusion term is modeled in the equation for the scale-supplying variable.

3.1 Modeling Equations

The $k-\omega$ model derived by Wilcox (1988) has the following form:

Eddy Viscosity:

$$\mu_t = \rho k/\omega \tag{18}$$

Turbulent Kinetic Energy:

$$\rho\frac{\partial k}{\partial t} + \rho U_j\frac{\partial k}{\partial x_j} = \tau_{ij}\frac{\partial U_i}{\partial x_j} - \beta^*\rho k\omega + \frac{\partial}{\partial x_j}\left[(\mu + \sigma^*\mu_t)\frac{\partial k}{\partial x_j}\right] \tag{19}$$

Specific Dissipation Rate:

$$\rho\frac{\partial \omega}{\partial t} + \rho U_j\frac{\partial \omega}{\partial x_j} = \alpha\frac{\omega}{k}\tau_{ij}\frac{\partial U_i}{\partial x_j} - \beta\rho\omega^2 + \frac{\partial}{\partial x_j}\left[(\mu + \sigma\mu_t)\frac{\partial \omega}{\partial x_j}\right] \tag{20}$$

Closure Coefficients:

$$\alpha = 5/9, \quad \beta = 3/40, \quad \beta^* = 9/100, \quad \sigma = 1/2, \quad \sigma^* = 1/2 \tag{21}$$

3.2 Versatility of the Model

The model was demonstrated by Menter (1992b) to be superior to the standard $k-\epsilon$ model for boundary layer flows under adverse pressure gradient conditions. The reason for its better performance is that the $k-\omega$ model predicts a more accurate level of turbulence length scales $l = k^{1/2}/\omega$ near a wall and consequently more accurate prediction for the shear stress levels within the boundary layer.

An asymptotic analysis carried out by Wilcox (1988) shows that the $k-\omega$ model equations gives the value of $B = 5.1$ in Eq.(16) in the near wall region. This value agrees closely with the experimental observed value of $B = 5.0$ and compares significantly better than the values obtained from other two-equation models (Wilcox (1993), p.123). An important implication is that, unlike other two-equation models, the $k-\omega$ model can be used with no additional viscous modifications in the near wall region. Hence, simple no-slip boundary condition can be imposed and integrating through the turbulent and viscous sublayers can yield satisfactory results.

The fact that the $k-\omega$ model can be integrated directly to a wall surface is an important advantage over the $k-\epsilon$ model since Dirichlet-type boundary conditions can be used at a wall leading to better numerical stability (Menter (1992b)). At a wall surface, specification of the no-slip boundary condition leads to $\mathbf{V}=\mathbf{0}$ and $k=0$. As for the value of ω at the wall surface, denoted as ω_w, the following asymptotic expression holds:

$$\omega \rightarrow \frac{6\nu}{\beta y^2} \quad \text{as} \quad y \rightarrow 0 \tag{22}$$

For ease of implementation, Menter (1992b) suggested the following boundary condition for smooth walls:

$$\omega_w = f_\omega \frac{6\nu}{\beta(\Delta y)^2} \quad \text{at} \quad y=0 \tag{23}$$

where Δy is the distance to the grid point adjacent to the wall, and $f_\omega = 10$ was recommended for use by Menter who claimed that the results would not be sensitive to the factor used, as long as the value of ω_w was made large enough. Wilcox (1988) gave suggestions as to the meaning of assigning different values of ω as boundary condition at a wall surface. He showed that large values of ω_w gives best agreement to the law-of-the-wall prediction for smooth walls, while small values of ω_w simulates the situation where there is substantial surface roughness.

The most significant noted drawback of the $k-\omega$ model is its dependence on the free stream value of ω, designated as ω_f, in the prediction for free shear flows (Menter(1992a)). As a result, the spreading rates for many types of free shear flows such as mixing layer, plane jet and round jet are predicted incorrectly. The problem was identified to be caused by the diffusion of the free stream value of ω across the shear layer as the value of k decreases approaching the shear layer edge (Wilcox (1993)).

To circumvent this problem of ω_f dependency, Menter (1992b) modified the ω-equation by adding a cross-diffusion term as follows:

$$\rho\frac{\partial \omega}{\partial t} + \rho U_j \frac{\partial \omega}{\partial x_j} = \alpha \frac{\omega}{k}\tau_{ij}\frac{\partial U_i}{\partial x_j} - \beta\rho\omega^2 + \frac{\partial}{\partial x_j}\left[(\mu+\sigma\mu_t)\frac{\partial \omega}{\partial x_j}\right] + \sigma_d \frac{\rho}{\omega}\frac{\partial k}{\partial x_j}\frac{\partial \omega}{\partial x_j} \tag{24}$$

The form of Eq.(24) is obtained by formally transforming the ϵ-equation using the relationship $\omega \approx \epsilon/k$. The effect of adding the cross-diffusion term $\frac{\partial k}{\partial x_j}\frac{\partial \omega}{\partial x_j}$ is to prevent

the value of ω_f from diffusing from the non-turbulent region into the turbulent region. For the value of σ_d, Wilcox (1993, p.101) suggested the following:

$$\sigma_d = \begin{cases} 0, & \frac{\partial k}{\partial x_j}\frac{\partial \omega}{\partial x_j} \leq 0 \\ \sigma, & \frac{\partial k}{\partial x_j}\frac{\partial \omega}{\partial x_j} > 0 \end{cases} \tag{25}$$

However, the above modification still yields shear layer spreading rate that is farther from measurements than those predicted by the $k-\epsilon$ model. Research effort is still on-going to establish an optimum set of parameters for the $k-\omega$ model.

4 Renormalization Group $k-\epsilon$ Model

As mentioned earlier, the development of the RNG $k-\epsilon$ model is an attempt to derive rigorously a two-equation $k-\epsilon$ model from the Navier-Stokes equations. Using the concept of renormalization groups, the equations for turbulence parameters k and ϵ were obtained by averaging the basic 'microscopic' Navier-Stokes equations over the fluctuating velocity field.

4.1 Form of the Model

When applied to derive a two-equation eddy viscosity model in the variables k and ϵ, the RNG theory gives a set of modeling equations that has the same characteristic form as the standard $k-\epsilon$ model (Eqs.(12-14)), with the exception that the modeling parameters are different. In the standard $k-\epsilon$ model, the modeling parameters are derived based on empirical fitting to benchmark experimental results. In the RNG $k-\epsilon$ model, the parameters are explicitly computed and assume the following values:

$$C_\mu = 0.085, \quad C_{\epsilon 1} = 1.42 - R, \quad C_{\epsilon 2} = 1.68, \quad \sigma_k = 0.7179, \quad \sigma_\epsilon = 0.7179 \tag{26}$$

where

$$R = \frac{\eta(1-\eta/\eta_o)}{1+\beta\eta^3} \tag{27}$$

In the above expression,

$$\eta = Sk/\epsilon \tag{28}$$

is interpreted as the ratio of turbulence to mean strain time scale, with $S = (2S_{ij}S_{ij})^{1/2}$ being the norm of the mean rate of strain tensor S_{ij} given in Eq.(4). The values of η_o and β are taken to be 4.38 and 0.015, respectively.

For viscosity dominated flow regions near a wall, the standard renormalization group theory cannot be applied directly. The reason is that the primarily viscous scales of motion are removed by the ultraviolet cutoff of the RNG procedure. Orszag et al. (1993) claimed to have developed low Reynolds number modifications based on the RNG theory that allows direct integration of the equation system across the viscous sublayer, but apparently such modifications have not been presented in the literature. Speziale and Thangam (1992) applied a wall function to bridge the gap between the fully turbulent region and the viscous sublayer.

4.2 Versatility of the Model

The form of the modeling equation for the turbulent energy dissipation rate ϵ (Eq.(14)) has been the subject of suspicion due to its empirical origin that relies mainly on dimensional reasoning. The renormalization group theory offers a theoretical support to the basic form of the ϵ-equation, and also perspectives to better account for the effects of extra strain rates. The value of η given in Eq.(28) reflects the degree of isotropy in the flow field. When η is small, deviation from the isotropic condition is small, and vice versa. The extra fractional term R shown in Eq.(27) in the expression for $C_{\epsilon 1}$ has been found to be significant in regions of large strain rate. The improvement of the RNG $k-\epsilon$ model for predicting flow phenomena that contain separation and turbulence anisotropy has been attributed to the inclusion of such a term and deserves attention.

Note that the sign of R depends on the difference $1-\eta/\eta_o$ where $\eta_o = 4.38$ represents a typical value for the turbulence to mean strain time scale in homogeneous shear flows. The difference changes sign depending on whether the time-scale ratio η is greater or smaller than the homogeneous value η_o, distinguishing in such a way the small from the large strain rates. This feature has probably contributed more than other modifications

to an apparent success of the model to predict the appropriate length of recirculating zones of several separating flows, as compared with other two-equation models (Speziale and Thangam (1992)).

Although the theory yields the same form of the dissipation rate equation for high Reynolds numbers, and produces numerical values of the coefficients that are considerably different from the standard values, without employing any experimental results, it was pointed out by Hanjalić (1994) that the coefficients had to be brought closer to the conventional values to reproduce some simple flows. The RNG $k-\epsilon$ model, although substantiated by seemingly very convincing physical arguments, has not been able to bring about expected improvements in a uniform manner for a variety of engineering relevant flows. Hanjalić (1994) noted that the model brought only marginal improvement of the velocity field in a flow through a staggered tube bank, and no improvement in the badly predicted shear stress field. As well, for impinging jets, the RNG based ϵ-equation did not seem to give more accurate results.

5 Test Case 1: Flow over a Backward-Facing Step

The flow over a backward-facing step is examined to compare the performance of the three turbulence models considered. Data for this flow field are widely used to test the accuracy of turbulence models because the specification of flow conditions is straightforward and the flow field exhibits separation and reattachment features which test the predictive performance of turbulence models.

5.1 Description of the Problem

The experimental results by Driver and Seegmiller (1985) are considered because of available data for wall shear stress which can be used to infer the location of the flow reattachment point. The geometry and flow conditions are given in Figure 1.

For both the standard and RNG $k-\epsilon$ models, the standard wall function treatment (Eqs.(16,17)) is applied to simulate the viscous damping effect of the wall. Although

wall functions do not formally apply to separated flows, but for this specific flow, it was postulated by Speziale and Thangam (1992) that a large portion of the turbulent kinetic energy is not associated with the separated zone. Therefore, wall functions should not give rise to major errors in this problem. The inlet values of k and ϵ are set to be $k_f = 0.005 \times U_o^2$ and $\epsilon_f = k_f^{3/2}/0.05Y_o$, respectively. A 120×120 grid is used for the simulation.

For the $k-\omega$ model, attention is on the specification of boundary values for k and ω. The same value for k_f is used as for the $k-\epsilon$ models. At solid walls, the practice by Menter (1992b) is followed here that the governing equations are integrated directly across the viscous sub-layer and the wall value of k, denoted as k_w, is set to zero as with the velocity components. As for ω, different choices for the free stream values ω_f and wall values ω_w are possible and several cases are studied.

	$\omega_f(s^{-1})$	$\omega_w(s^{-1})$
Case 1	600	10^5
Case 2	6000	10^5
Case 3	600	10^6
Case 4	600	10^7

In case 1, ω_f is chosen based on its definition to be the specific dissipation rate of turbulent energy. Then on dimensional grounds, $\omega \sim \epsilon/k$, and simple equality is assumed so that $\omega_f = \epsilon_f/k_f$ with values of k_f and ϵ_f taken from those used in the $k-\epsilon$ models calculation. The value of ω_w is chosen according to Eq.(23) with $f_\omega = 10$. In case 2, ω_f is calculated according to the formal relationship given by Wilcox (1993): $\omega = k/(C_\mu \epsilon)$, which causes ω_f to increase by one order of magnitude. This case is considered to examine how sensitive will the results be dependent on the free stream value of ω. In cases 3 and 4, the values of ω_w are increased by one and two orders of magnitude respectively over that of case 1 to examine the claim made by Menter that the results are not sensitive to the value of f_ω in Eq.(23).

5.2 Results and Discussion

The reattachment length is the most prominent feature of the flow field and this length can be estimated by observing the location where the wall shear stress τ_w vanishes. The law-of-the-wall is used to estimate the wall shear stress using values of k and U at nodes closest to the wall. In an equilibrium layer where turbulence energy generation balances dissipation, the law-of-the-wall gives

$$\tau_w = \rho C_\mu^{1/4} k^{1/2} \kappa U / (\ln(E y^+)), \qquad y^+ > 11.63 \tag{29}$$

where y^+ is given by

$$y^+ = y \rho C_\mu^{1/4} k^{1/2} / \mu \tag{30}$$

with y being the normal distance from the wall. The value of E is correlated to be 9.8 for smooth walls. The computed values of τ_w behind the step for the various cases are shown in Figure 2, together with the experimental data.

A number of remarks can be drawn from the results. First, comparing the two $k-\epsilon$ models, the RNG model gives better prediction for the reattachment length than the standard model. Both models give good predictions for the magnitude of the most negative τ_w just after the step, but the location is predicted incorrectly. The prediction for the overall wall shear stress distribution by the standard model is not good, and the RNG model does not give much improvement. Second, comparing the results for the four cases of the $k-\omega$ model shows that there is sensitivity of the results on the boundary data for ω. Differences in the results between cases 1 and 2 show the dependence on ω_f. The differences, though noticeable, are not very significant. The dependence of the results on ω_w is more noticeable. Comparing the results of cases 1, 3 and 4 shows that the reattachment length increases as ω_w incraeases. This observation contrasts the statements forwarded by Menter (1992b) that the simulated flow field is not sensitive to the choice of ω_w as long as its value is large.

The prediction of the overall wall shear stress distribution by the $k-\omega$ model is not good. Menter (1992b) reported very good agreement between the same experimental

data and results from the unmodified $k-\omega$ model by Wilcox (1988), however, such good agreement cannot be repeated here. The difference is not likely caused by the grid used since the grid here has approximately the same density as that used by Menter. The observation that the $k-\omega$ model gives results which depend strongly on the prescription of ω close to the wall surface is a concern since there is no obvious means for choosing a suitable value for f_ω in Eq.(23).

6 Test Case 2: Multiple Jets in a Crossflow

The problem of multiple jets injecting into a confined crossflow is of importance in the study of air jet interactions in a recovery furnace since the upward flowing flue gas channel acts like a crossflow to jets at secondary and tertiary levels. Accurate prediction of this flow is thus vital to the prediction of flows in a recovery furnace.

6.1 Experimental and Numerical Investigation

An experiment was carried out at the University of British Columbia to investigate jet penetration into a cross-flowing stream. The experiment was performed in a wind tunnel facility where an array of square jet orifices was positioned laterally across the base of the test section (see Figure 3). The jet air is mixed with a small amount of propane for monitoring the distribution of jet fluid. Details of the experimental conditions are given in Tse et al. (1996b).

The crossflow speed is $U_{cf} = 1.5$ m/s and the jet speed is $V_{jet} = 19.3$ m/s. The concentration of propane, which is normalized by the concentration at the jet exit, is measured in the jet symmetry plane at the two downstream positions $x/D = 6$ and 12 using a flame ionization detector. The experimental condition is to be simulated by the standard $k-\epsilon$, RNG $k-\epsilon$ and Wilcox's $k-\omega$ models. A uniform $120 \times 60 \times 12$ grid is used in the simulations.

For the two $k-\epsilon$ models, boundary conditions are specified as follows: symmetry conditions at the two lateral planes bounding a jet so that only half of a jet is simulated;

zero-gradient condition for all dependent variables at the exit plane of the domain; wall function model to simulate the presence of a solid wall; at the crossflow inlet, $U = U_{cf}$, $V = W = \Phi = 0$, $k = 0.005U_{cf}^2$ and $\epsilon = k^{3/2}/0.06H$, while at the jet exit, $V = V_{jet}$, $U = W = 0$, $\Phi = 1$, $k = 0.005V_{jet}^2$ and $\epsilon = k^{3/2}/0.5D$. For the $k - \omega$ model, same values of k are prescribed at the crossflow inlet and the jet exit, while values of ω are set according to $\omega = k/\epsilon$. At the solid surface, k is set to be zero while ω_w is chosen according to Eq.(23). Three values of ω_w are considered by choosing $f_\omega = 10$, $f_\omega = 100$ and $f_\omega = 1$. These cases are studied to observe the dependence of the flow field on the value of ω_w.

6.2 Results and Discussion

The computed jet fluid distribution in the jet symmetry plane for various cases are shown in Figure 4. The results for the two $k - \epsilon$ models are similar, indicating that the eddy viscosity are similarly predicted. The $k - \omega$ model results, however, show differences both from the predictions by the $k - \epsilon$ models and among the three values of f_ω. It is seen that changing the value of ω_w affects the flow field prediction in a significant way. The jet penetrates significantly deeper across the crossflow channel for larger values of f_ω (ω_w) than for smaller values. The case $f_\omega = 1$ gives the unrealistic result that the jet fluid lies close to the injection wall with very little mixing with the crossflow fluid.

Detailed numerical and experimental results for the jet fluid concentration at the two downstream locations $x/D = 6$ and 12 in the jet symmetry plane are shown in Figure 5. The predictions by the two $k - \epsilon$ models are indeed very similar, with both slightly underpredicting the jet penetration while slightly overpredicting the jet fluid concentration. The $k - \omega$ results with $f_\omega = 10$ do not match the experimental data well at positions near the injection wall. It appears that the mixing of the jet fluid with the crossflow fluid is incorrectly predicted by the $k - \omega$ model for any choice of f_ω. It is not clear whether a viscous correction for the $k - \omega$ model near a wall will lead to better prediction.

7 Test Case 3: Swirling Flow Predictions for a Recovery Furnace Water Model

In many recovery furnace operations, swirling flows are generated intentionally to promote mixing of air with combustibles. These swirling flows are usually created by a specific air admission practice for which the windboxes at the secondary or tertiary level are injecting air in specific directions so as to impart a rotation pattern for the flow within the furnace cavity. In many operations, this practice has demonstrated to achieve good mixing and high combustion efficiencies at moderate jet velocities and low fan power requirements (see Lefebvre and Burelle (1988)). However, it may contribute to unacceptable gas side temperature variations at the furnace outlet plane. As a result, accurate predictions of such swirling flows in a recovery furnace can yield information to optimize the air system.

Sloan et al. (1986) discussed the shortcomings regarding the prediction of swirls by two-equation eddy viscosity based models. The standard $k-\epsilon$ model has been accused of failing to reproduce, even qualitatively, several important features of swirling flows such as velocity component decay, jet spreading or diffusion rate, degree of entrainment, and Reynolds stress levels. The deficiencies are associated with the limitations of eddy viscosity models discussed earlier in Section 1.3. In particular, the source terms in the dissipation rate equation (ϵ or ω) control, to a significant degree, the magnitude of the turbulent kinetic energy, the mean velocity decay, and the jet spreading rates. However, the modeling of the source terms has not yet been satisfactorily extended to rotating flows. Since the dissipation equation is common to both two-equation models and higher-order closure schemes, the implication is that little predictive improvement may be gained by resorting to a more refined stress closure model.

Attempts at improving the prediction of swirling flows by the standard $k-\epsilon$ model through modifications to C_μ and the source terms in the ϵ equation based on Richardson number corrections have been discussed in Sloan et al. (1986). They also discussed the possibility of using Reynolds stress models which were not sufficiently proven in applied

studies for swirling flows. The following conclusion was reached:

- predictive accuracy was found to be a partial function of inlet boundary conditions and numerical diffusion;
- corrections which serve to modify the turbulence intensity by altering the isotropic eddy viscosity or the source terms in the dissipation rate equation are generally inadequate;
- standard $k-\epsilon$ model performs competitively with the other model modifications and in some instances is judged to be superior than the modified treatments;
- higher closure models can only claim marginal superiority in the prediction of swirling flows, but the substantial increase in computational complexity and calculation time does not justify their use.

In view of these observations, Sloan et al. recommended that the present generation of combustion code calculations retain the standard $k-\epsilon$ model. Such a recommendation is still followed in many CFD codes designed for furnace simulations (Nowak et al. (1995), Hill and Smoot (1993), Wessel et al. (1993)). The purpose of the present study is to test the prediction performance of the standard $k-\epsilon$, RNG $k-\epsilon$ and $k-\omega$ models for a swirling flow generated within a recovery furnace water model. Details of the experiment and numerical procedure are described next.

7.1 Experimental Modeling of Recovery Boiler Flows

An experiment was conducted at the University of British Columbia in an isothermal scale water model shown in Figure 6 of a Combustion Engineering recovery boiler design. Particle image velocimetry (PIV) is used as a quantitative flow visualization technique to provide two-dimensional velocity information on the liquid flow field through optical recording and analysis of motion of small tracer particles added to the flow. A laser light sheet is used to illuminate a two-dimensional region within the experimental apparatus, in which the motion of the particles is recorded using digital videotape

for high resolution. The recordings are then analyzed using correlation techniques to obtain a time series of two-dimensional velocity vectors. Details of the experimental set-up and analysis techniques are given in Ketler et al. (1994).

There are four starting burners located just above the primary orifices in the front and rear faces at elevation $z = 0.05$ m. The burners are angled in a horizontal plane towards the center at 25° from the perpendicular. Jets from these burners cause a swirling flow in the model. In the experiment, jets from the primary level, the starting burners, the secondary level, and load burners are in operation. The resulting flow field is examined by particle image velocimetry at three horizontal levels shown in Figure 6: level 1, $z = 0.26$ m; level 2, $z = 0.55$ m, and level 3, $z = 0.70$ m. The results are compared to numerical predictions described next.

7.2 Numerical Predictions and Analysis

Numerical predictions of the furnace flow field are carried out using the standard $k-\epsilon$, RNG $k-\epsilon$ and Wilcox's $k-\omega$ models. For the two $k-\epsilon$ models, the wall function is used to simulate the viscous damping effect due to the presence of solid walls. Zero gradient condition is imposed for all flow variables at the furnace exit plane. At jet inlets, velocity values V_{jet} are prescribed according to the experimentally measured flow rate data, while turbulence quantities are specified according to the formulae:

$$k_{jet} = I \times V_{jet}^2 \tag{31}$$

$$\epsilon_{jet} = k_{jet}^{3/2}/L_d \tag{32}$$

where I denotes the turbulence intensity and L_d is a characteristic turbulence dissipation length scale at the jet exit. Jets at the secondary level are modeled individually, with I and L_d for the jet turbulence parameters chosen to be 0.01 and 0.5 times the orifice width, respectively. The rows of primary jets are modeled as slot jets because of close orifice spacings. Following the study done by Tse et al. (1996a), the values for both I and L_d need to increase for the slot jets to compensate for the neglect of

interaction between neighboring jets. The values chosen for I and L_d for the primary slot jets are 0.1 and ($10^{3/2} \times 0.5 \times$ original primary orifice width), respectively.

For the $k-\omega$ model, values of ω specified at the jet exits are obtained through $\omega_{jet} = k_{jet}^{1/2}/L_d$. When values of ω_w are chosen according to Eq.(23) with $f_\omega = 10$, preliminary viewing of the prediction suggested that the results were not realistic when compared to experimental data and to results given by the two $k-\epsilon$ models. Satisfactory results were obtained only after f_ω was increased to 1000.

Figure 7 shows the interaction of the four jets from the starting burners that causes the swirling flow. The predictions given by the standard and RNG $k-\epsilon$ models are compared to the $k-\omega$ model results with $f_\omega = 100$ and 1000. The results from the standard and RNG $k-\epsilon$ models are very similar, whereas the results generated by using $f_\omega = 100$ appear to underpredict the swirl intensity. The results with $f_\omega = 1000$ are similar to those obtained by either $k-\epsilon$ model.

Figures 8 through 10 show a comparison of numerical and experimental results at the three elevations where the PIV data are taken. Portion of the experimentally obtained velocity field in each plane is blanked out due to either obstruction by the bullnose or high noise level in the data. The predictions by the RNG $k-\epsilon$ model are visually almost indistinguishable from those by the standard $k-\epsilon$ model. The predictions by the $k-\omega$ model with $f_\omega = 1000$ are also very similar to the standard$k-\epsilon$ results for both the magnitude of the velocity vectors around the swirl core and the position of the core. The numerical results appear to predict the position of the swirling core at each elevation quite well. It is significant to note that the magnitudes of the velocity vectors around the swirl core predicted by any of the three models are generally higher than the experimental values at the lowest elevation level 1, while the opposite is true at the two higher levels. This observation confirms the suspicion that two-equation eddy viscosity type models predict too rapid a swirl decay rate (Sloan et al. (1986)) and are unable to produce quantitatively accurate results for swirling flows.

8 Summary and Conclusion

The main attractiveness of eddy viscosity based two-equation turbulence models is their efficient and robust numerical performance. These models have only demonstrated satisfactory predictions for two-dimensional shear flows with mild streamline curvatures and body force effects. For more complicated flows that involve rotation, buoyancy, and three-dimensional effects, the models yield results that can only be judged to be qualitatively reasonable, and much care is needed to apply the results to solve engineering problems.

The standard $k - \epsilon$ model continues to enjoy wide usage in the solution of applied problems. An important reason is that no other two-equation models has yet proven to be significantly better for general engineering fluid dynamical problems in terms of either accuracy or efficiency. Modifications to the basic $k - \epsilon$ model may be made through suitable adjustment to the modeling coefficients or to the source terms in the ϵ-equation to give better predictions for flows with strong curvature or other specific effects. However, such modifications are *ad hoc* in nature and none has yet gained universal acceptance.

The RNG $k - \epsilon$ model appears to rest on a firmer theoretical basis. However, as noted by Hanjalić (1994), the modeling parameters need to be adjusted to more conventional values before good comparison with experimental data can be achieved. Although the model promises to give better prediction for flows with separation and anisotropy, our numerical results for flow over a backward-facing step and a row of jets in a crossflow show that the improvement over the standard $k - \epsilon$ model is not very significant. For the more complex swirling flow found in a recovery furnace model, the RNG $k - \epsilon$ model does not yield any noticeable improvement over the standard model.

For certain classes of shear flows in adverse pressure gradient conditions, Wilcox's $k - \omega$ model performs better than many other two-equation models (Wilcox (1993), Menter (1992b)). However, the model has not yet gained wide acceptance and its superior performance over variances of the $k - \epsilon$ model was not established by the

numerical experiments performed in this study. Instead, it was found that the solution to the $k-\omega$ model exhibits dependence not only on the free stream value of ω but also on the value of ω specified near a wall. The guidance given by Menter (1992b) for determining ω_w as given in Eq.(23) is of little use since our calculation for simple shear flows shows that the results change significantly for different choices of f_ω. Resolution to this problem may lie in the use of some viscous damping functions in conjunction with the model near a wall.

The present study reveals that the standard $k-\epsilon$ model yields the same performance as two other state-of-the-art two-equation models, the RNG $k-\epsilon$ and Wilcox's $k-\omega$ models, for the prediction of complex flows that are found in recovery furnaces. In view of the uncertainty in the modeling of the many other physical and chemical processes in a kraft recovery furnace, the standard $k-\epsilon$ model is recommended for use for general simulation purposes. Despite its noted weaknesses, the model yields qualitatively accurate results as shown in our study of furnace swirling flows. The results are therefore useful in guiding design development. Hence, the immediate focus should be to develop more efficient and robust methods to solve the $k-\epsilon$ modeling equations. Such numerical methods will remain useful while waiting for further progress in turbulence modeling and computing speed.

References

Brandt, A. and Dinar, N. (1979), "Multigrid Solutions to Elliptic Flow Problems", in S.V. Parter (ed.), *Numerical Methods for Partial Differential Equations*, pp.53-147, Academic Press, New York.

De Michele, G., Ghiribelli, L., Pasini, S. and Tozzi, A. (1989), "A 3-D Code for Predicting Radiative and Convective Heat Transfer in Boilers", ASME HTD-Vol.106, Heat Transfer Phenomena in Radiation, Combustion and Fires, pp.275-286.

Driver, D.M. and Seegmiller, H.L. (1985), "Features of a Reattaching Turbulent

Shear Layer in Divergent Channel Flow", *AIAA Journal*, Vol.23, No.2, pp.163-171.

Hanjalić, K. (1994), "Advanced turbulence closure models: a view of current status and future prospects", *Int. J. Heat and Fluid Flow*, Vol.15, No.3, pp.178-203.

Hanjalić, K. (1989), "Practical Predictions by Single-Point Closure Methods – Twenty Years of Experience", Proc. Z. Zaric Memorial Symp. on Near Wall Turbulence, S.J. Kline (ed.), Hemisphere, Washington, DC, pp.762-781.

Hanjalić, K. and Launder, B.E. (1972), "A Reynolds stress model of turbulence and its application to thin shear flows", *J. Fluid Mech.*, Vol.52, pp.609.

Hill, S.C. and Smoot, L.D. (1993), "A Comprehensive Three-Dimensional Model for Simulation of Combustion Systems: PCGC-3", *Energy & Fuel*, Vol.7, pp.874-883.

Jones, W.P. and Launder. B.E. (1972), "The Prediction of Laminarization with a Two-Equation Model of Turbulence", *International Journal of Heat and Mass Transfer*, Vol.15, pp.301-314.

Ketler, S.P., Ajersch, P. and Gartshore, I.S. (1994), "Particle Image Velocimetry Investigation of Recovery Boiler Flows", Proceedings TAPPI Engineering Conference, pp.215-224.

Launder, B.E. (1991), "Current capabilities for modelling turbulence in industrial flows", *Applied Scientific Research*, Vol.48, pp.247-269.

Lefebvre, B.E. and Burelle, R. (1988), "The Chemical Recovery Boiler Optimized Air System", TAPPI Notes, Kraft Recovery Operations Seminar, pp.237-244.

Leschziner, M.A. (1989), "Modeling turbulent recirculating flows by finite-volume methods – current status and future directions", *Int. J. Heat and Fluid Flow*, Vol.10, No.3, pp.186-202.

Menter, F.R. (1992a), "Influence of Freestream Values on $k-\omega$ Turbulence Model Predictions", *AIAA Journal*, Vol.30, No.6, pp.1657-1659.

Menter, F.R. (1992b), "Improved Two-Equation $k-\omega$ Turbulence Models for Aerodynamic Flows", NASA TM-103975.

Nowak, P., Matys, P., Sabhapathy, P., Abdullah, Z., and Salcudean, M. (1995), "Numerical Study of a Kraft Recovery Furnace", TAPPI International Chemical Recovery Conference, Toronto, pp.A149-A159.

Orszag, S.A., Yakhot, V., Flannery, W.S., Boysan, F., Choudhury, D., Maruzewski, J. and Patel, B. (1993), "Renormalization Group Modeling and Turbulence Simulations", in R.M.C. So et al. (eds.), *Near-Wall Turbulent Flows*, Elsevier Science Publishers B.V., pp.1031-1046.

Saffman, P.G. (1970), "A Model for Inhomogeneous Turbulent Flow", *Proc. Roy. Soc., Lond.*, Vol.A317, pp.417-433.

Sloan, D.G., Smith, P.J. and Smoot, L.D. (1986), "Modeling of Swirl in Turbulent Flow Systems", *Prog. Energy Combust. Sci.*, Vol.12, pp.163-250.

Speziale, C.G. and Thangam, S. (1992), "Analysis of an RNG Based Turbulence Model for Separated Flows", *Int. J. Engng. Sci.*, Vol.30, No.10, pp.1379-1388.

Tse, D., Abdullah, Z., Nowak, P., Salcudean, M. and Gartshore, I. (1996a), "Evaluation of Boundary Conditions and Calculation of Jet Flows in Recovery Furnaces", *Journal of Pulp and Paper Science*, Vol.22, No.1, pp.J8-J16.

Tse, D., Salcudean, M. and Gartshore, I. (1996b), "A Numerical and Experimental Study of Mixing between a Row of Jets and a Confined Crossflow", Proceedings for the 2nd European Thermal-Sciences Conference.

Wessel, R.A., Parker, K.L., and Aniefiok, A.-E. (1993), "Three-Dimensional Flow

and Combustion Model of a Kraft Recovery Furnace", Proceedings TAPPI Engineering Conference, pp.651-664.

Wilcox, D.C. (1988), "Reassessment of the Scale Determining Equation for Advanced Turbulence Models", *AIAA Journal*, Vol.26, No.11, pp.1299-1310.

Wilcox, D.C. (1993), *Turbulence Modeling for CFD*, DCW Industries, Inc., La Cañada, California.

Yakhot, V. and Orszag, S.A. (1986), "Renormalization group analysis of turbulence. I. Basic theory", *J. Sci. Comput.*, Vol.1, pp.3-51.

Yakhot, V. and Smith, L.M. (1992), "The Renormalization Group, the ϵ—Expansion and Derivation of Turbulence Models", *J. Sci. Comput.*, Vol.7, pp.35-61.

Yakhot, V., Orszag, S.A., Thangam, S., Gatski, T.B. and Speziale, C.G. (1992), "Development of turbulence models for shear flows by a double expansion technique", *Phys. Fluids A*, Vol.4, No.7, pp.1510-1520.

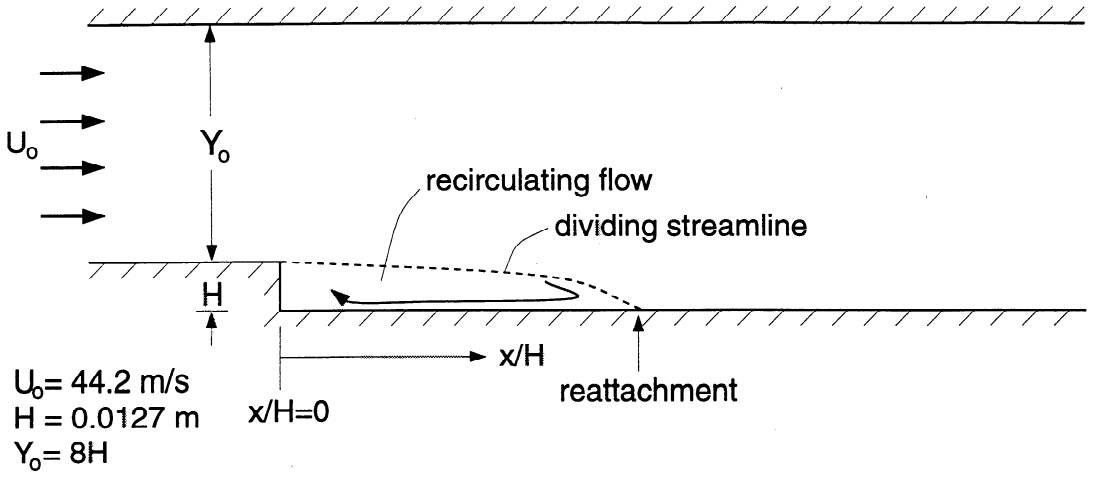

Figure 1: Flow over a backward-facing step, experimental geometry and inlet conditions.

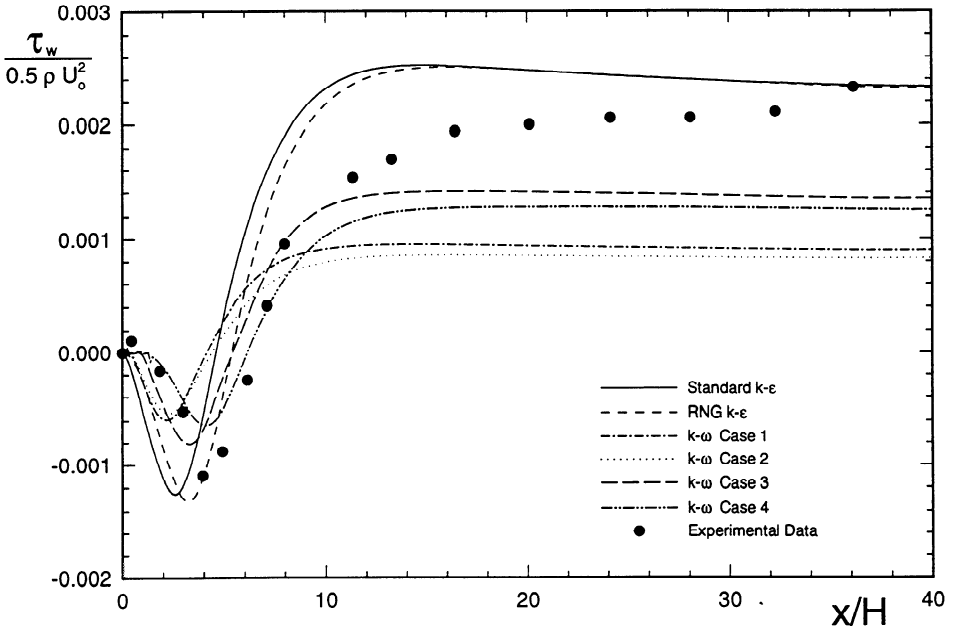

Figure 2: Wall shear stress distribution for backward-facing step flow.

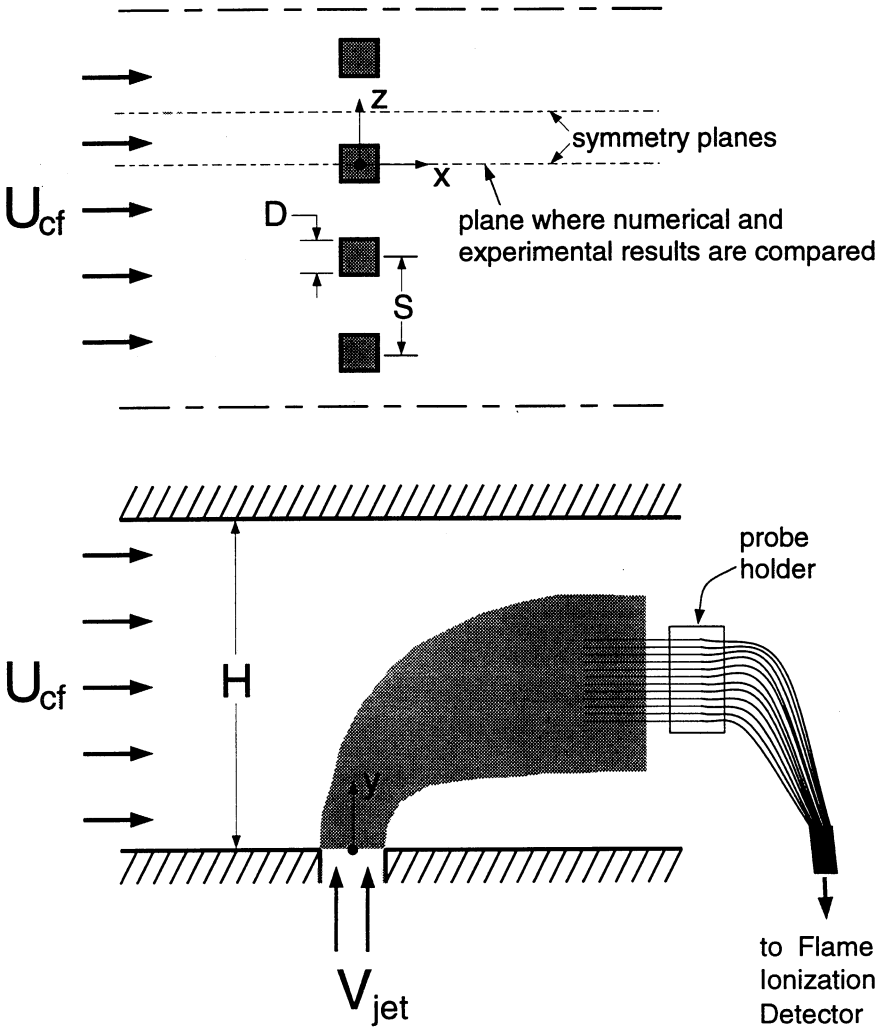

Figure 3: A schematic representation of the flow configuration. Top: plan view; bottom: side view.

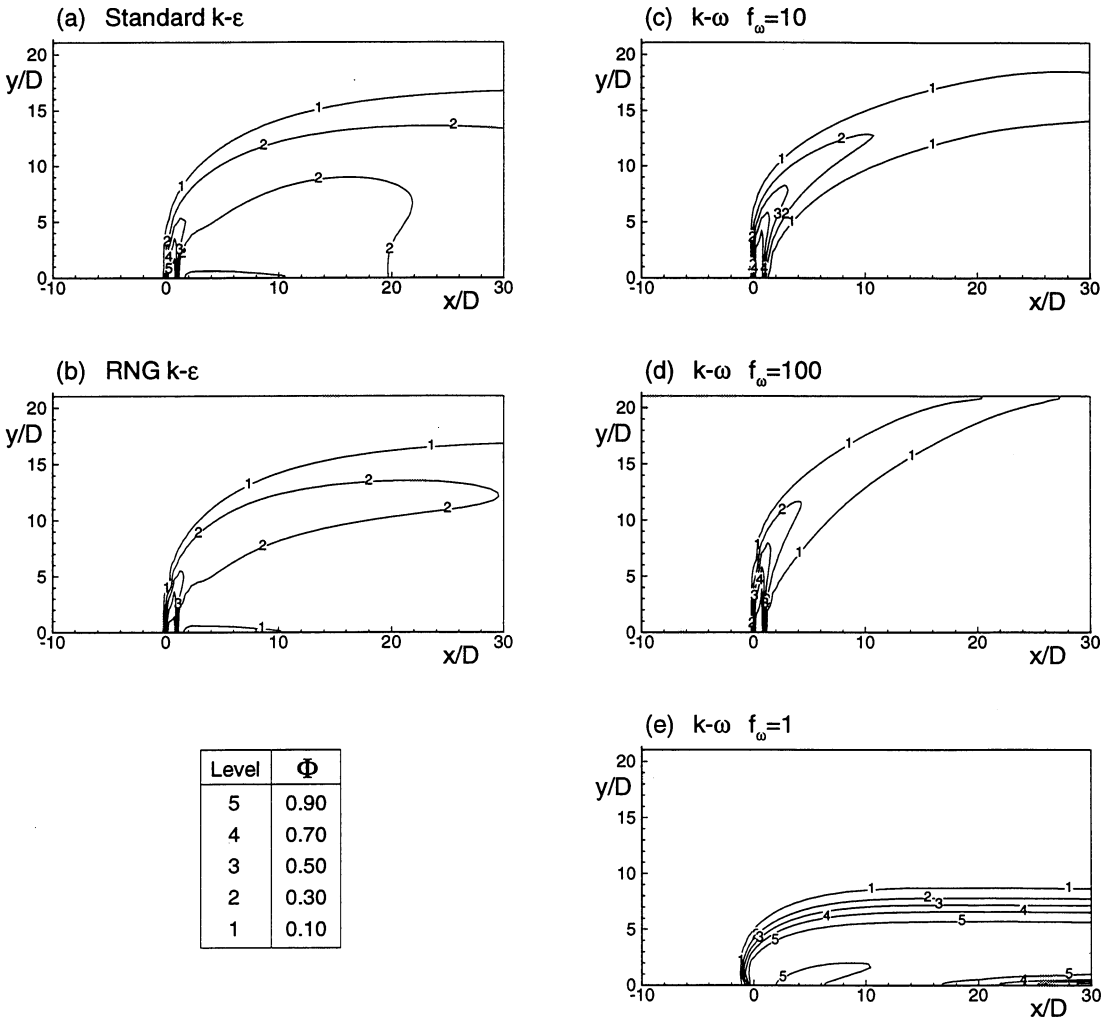

Level	Φ
5	0.90
4	0.70
3	0.50
2	0.30
1	0.10

Figure 4: Distributions of jet fluid in the jet symmetry plane obtained from different models.

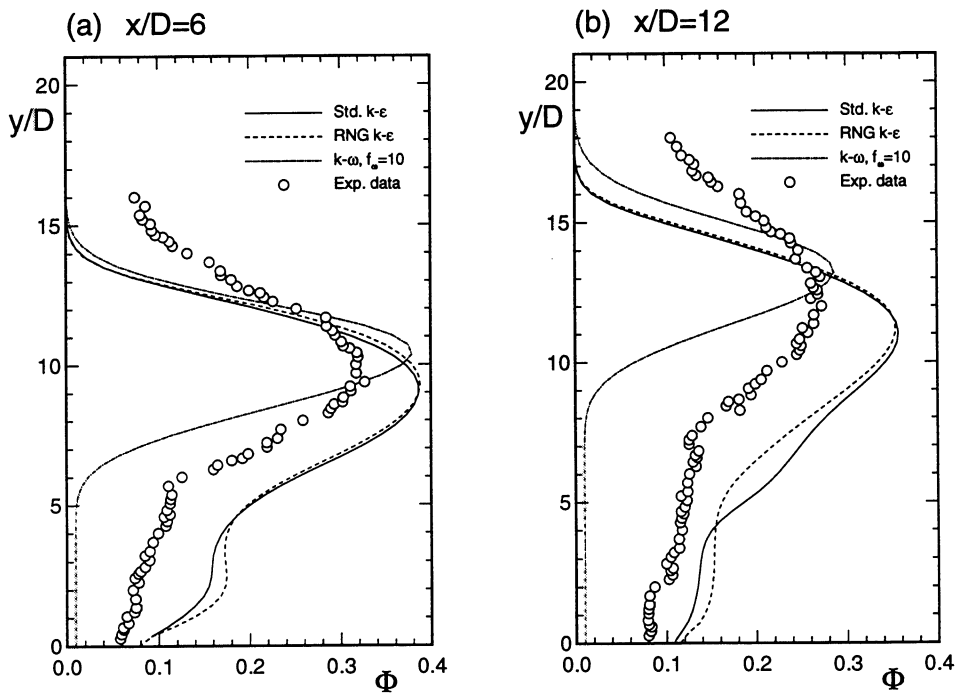

Figure 5: Numerical and experimental results for the jet fluid concentration at two downstream positions.

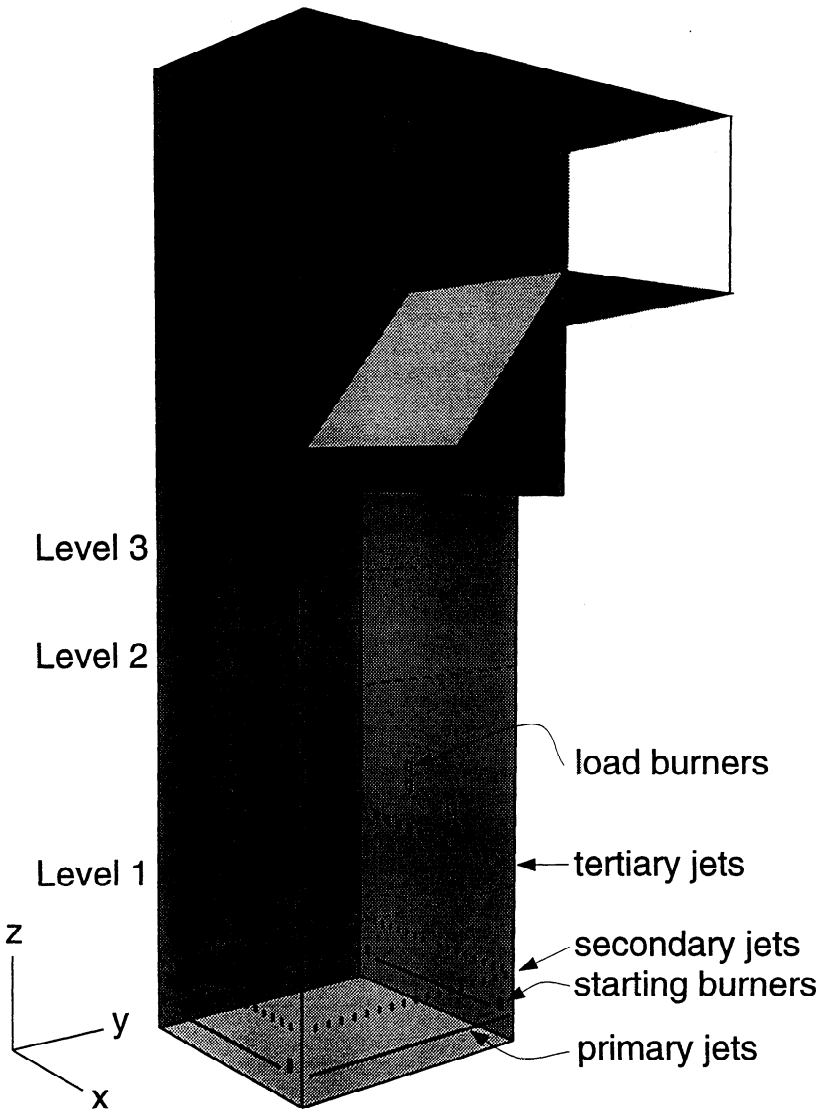

Figure 6: A schematic drawing of a kraft recovery furnace water model.

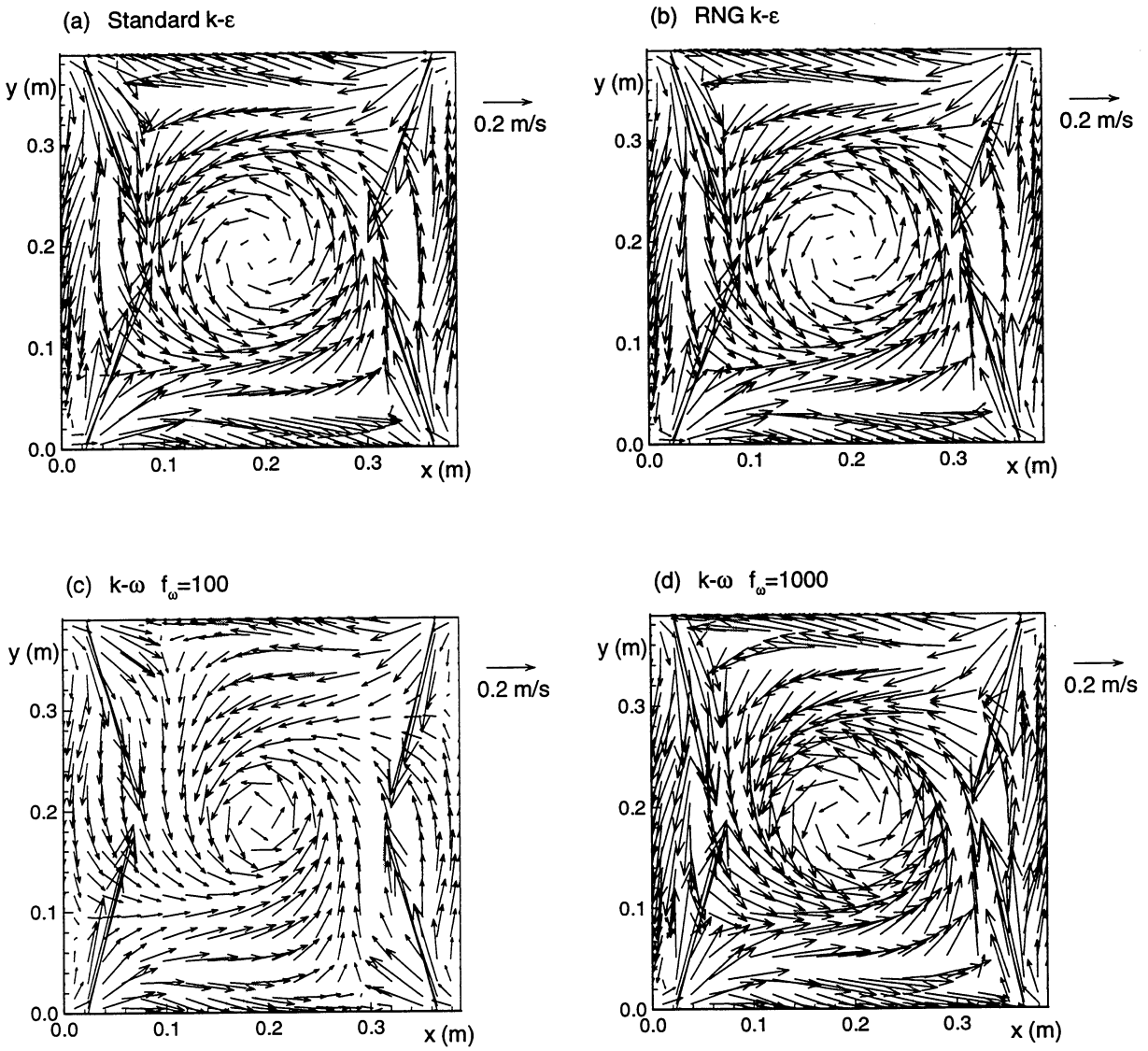

Figure 7: Velocity distribution at the starting burners level.

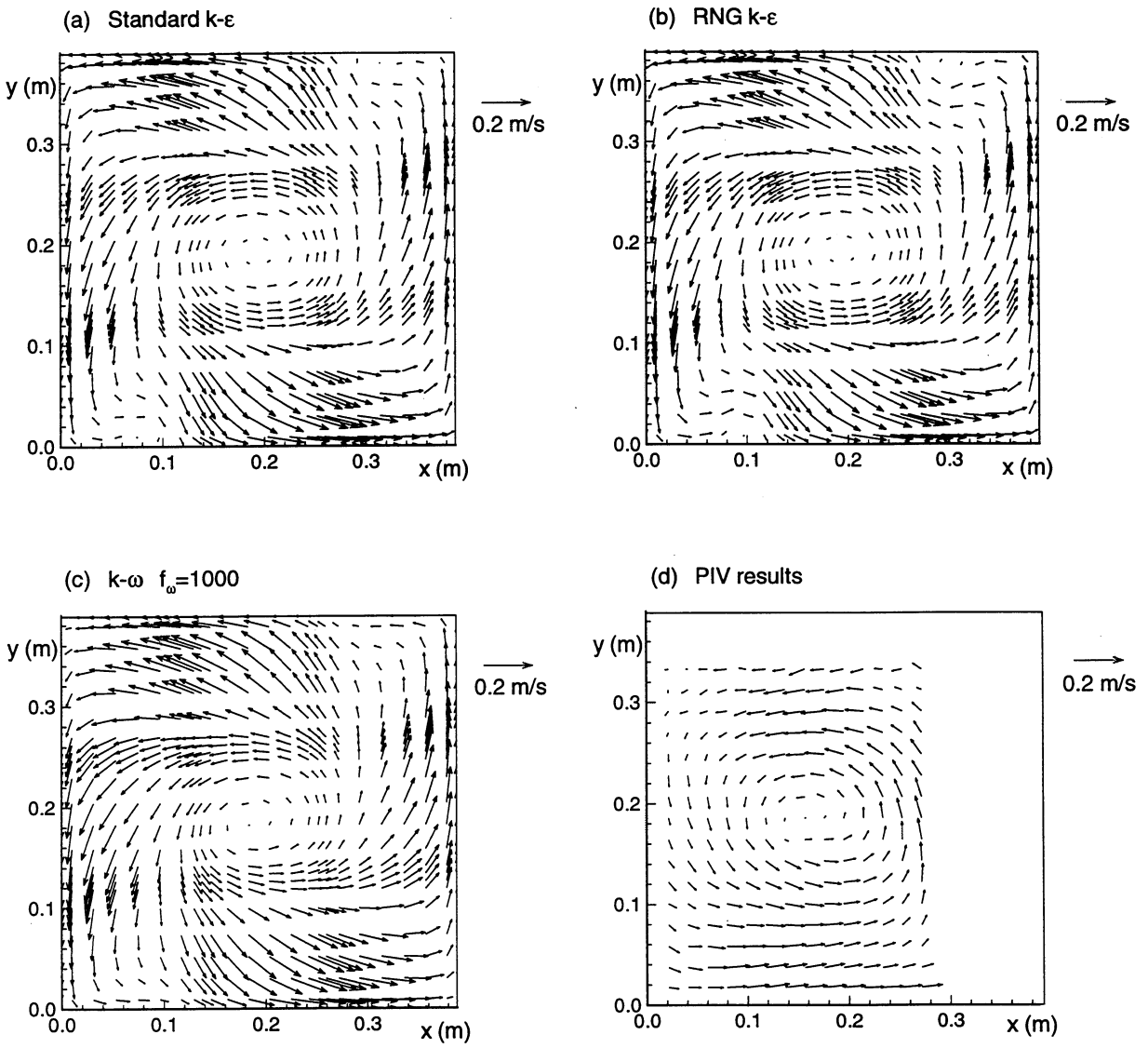

Figure 8: Velocity distribution at level 1, numerical and experimental results.

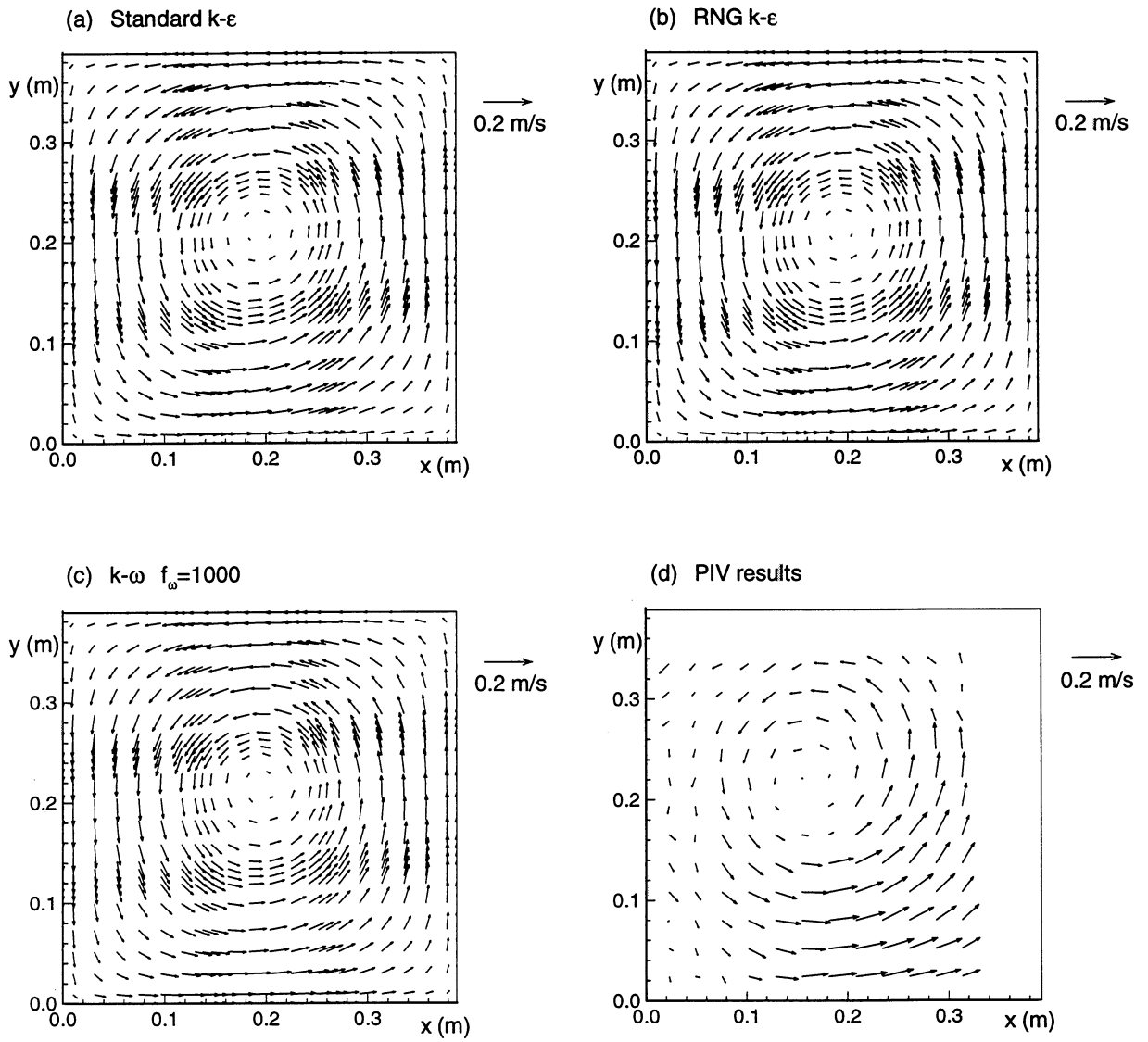

Figure 9: Velocity distribution at level 2, numerical and experimental results.

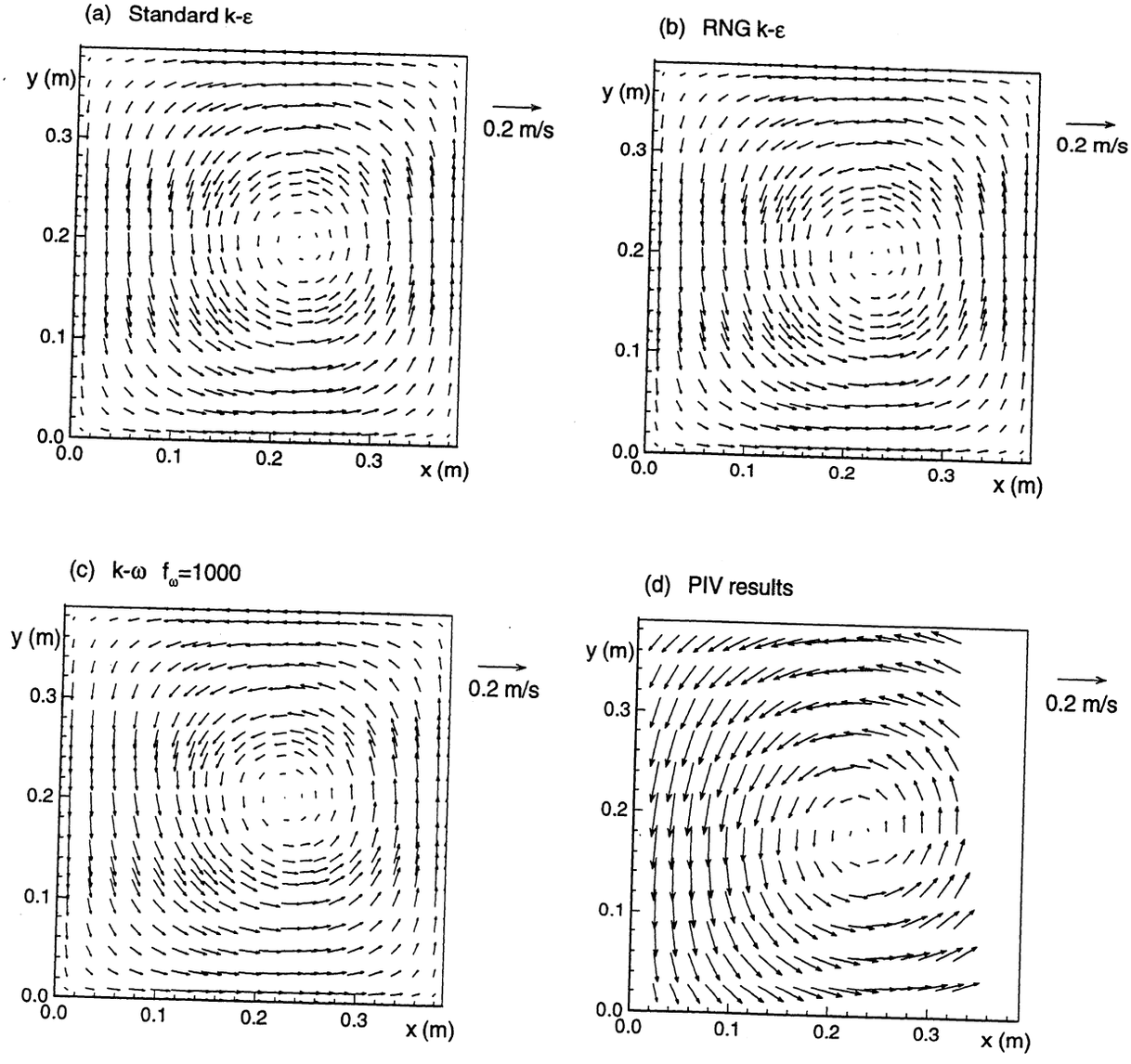

Figure 10: Velocity distribution at level 3, numerical and experimental results.